THE DISCOVERY OF A NOVEL SERIES OF AMYLOID-β ANTIAGGREGANTS BASED ON THE STRUCTURE OF 3-HYDROXYANTHRANILIC ACID: A DETAILED ANALYSIS OF THE MECHANISM OF ACTION UNDERPINNING ANTIAGGREGANT ACTIVITY

By

Gordon A. Simms

Submitted in partial fulfilment of the requirements
for the degree of Doctor of Philosophy

at

Dalhousie University
Halifax, Nova Scotia
April 2015

For my father.

You are the man I admire most in this world. Your lessons on the importance of education and hard work got me here, and your unflinching support continues to inspire me. If not for you I would not have the drive, determination or confidence to pursue my dreams.

Table of Contents

List of Tables

List of Figures

Abstract

Alzheimer's disease (AD) is the fourth leading cause of death in the industrialized nations, yet there are no disease-stabilizing therapies currently in use. The amyloid hypothesis suggests that oligomeric species of the amyloidogenic protein amyloid-β (Aβ) are the principle neurotoxic species in Alzheimer's disease brain; therefore compounds which inhibit the self-association of Aβ may serve as putative therapeutics which address the underlying pathogenesis of AD. 3-hydroxyanthranilic acid (3HAA) is a compound endogenous to the brain which previous work has determined is a modulator of Aβ secondary structure. The thioflavin T (ThT) fibrillogenesis assay has confirmed that 3HAA is a potent inhibitor of amyloid-β fibril formation, and a comparison of its antifibrillogenic to several known polyphenol antiaggregants has confirmed that 3HAA is among the most potent small-molecule inhibitors of Aβ fibril formation known.

Here, 3HAA was assessed as a platform for the development of a novel series of antiaggregant compounds. Analyses of several analogues of 3HAA confirm that the *o*-aminophenol motif underlies the observed antifibrillogenic activity of the compound that has led to the development of a serious of *o*-aminophenol-containing compounds which are novel inhibitors of Aβ aggregation. These compounds, as well as a series of plant-derived polyphenol-containing antiaggregants, were assessed *in vitro* for antifibrillogenic activity using the ThT fibrillogenesis assay and antioligomeric activity using a modified sandwich enzyme-linked immunosorbent assay (ELISA); results from these assays suggest that disparate mechanism underlie their observed antifibrillogenic activity.

Here, *in vitro* assessments of antiaggregant activity were supplemented with both molecular modeling studies of compound binding to monomeric Aβ and nuclear magnetic resonance studies to assess compound binding *in situ*. Taken together these studies indicate that multiple mechanisms of action underlie the observed antiaggregant activity of these compounds – all of which involve the stabilization of fibrillogenically inactive monomeric forms of Aβ. These studies have clarified the mechanism of action of both *o*-aminophenol-containing antiaggregants and polyphenol-containing antiaggregants and provide a framework for the development of future antiaggregants with putative clinical application in the treatment of AD.

List of Abbreviations and Symbols Used

82E1	Anti-human mouse immunoglobulin G monoclonal antibody
%Dev	Percent deviation from Aβ control in the absence of compound
%Fib	The percentage of observed amyloid-β fibril formation relative to a control in the absence of compound
$[M+H]^+$	Singly-charged parent ion formed by incorporation of a hydronium ion
$[M+Na]^+$	Singly-charged parent ion formed by incorporation of a sodium ion
[x]	The concentration of compound, x
1D	One-dimensional
2D	Two-dimensional
3D	Three-dimensional
3HAA	3-Hydroxyanthranilic acid
Å	Angstrom
A	Absorbance
A11	An epitope specific polyclonal antibody for detection of amyloid-β oligomers
AA	Amino acid
AnA	Anthranilic acid
AChE	Acetylcholine Esterase
AD	Alzheimer's disease
ADAM	A disintegrin and metalloproteinase
ApoE	Apolipoprotein E
APP	Amyloid precursor protein
APPs-α	α-Secretase-generated large soluble ectodomain
APPs-β	β-Secretase-generated large soluble ectodomain
Aβ	Amyloid β-peptide
$Aβ_{1-10}$	The 10-amino acid peptide corresponding to residues 1-10 of amyloid-β
$Aβ_{12-21}$	The 10-amino acid peptide corresponding to residues 12-21 of amyloid-β
$Aβ_{1-40}$	Amyloid β-peptide (40 amino acid isoform)
$Aβ_{1-42}$	Amyloid β-peptide (42 amino acid isoform)

$A\beta_{21-30}$	The 10-amino acid peptide corresponding to residues 21-30 of amyloid-β
b	The hill coefficient
BBB	Blood-brain barrier
Bio-82E1	N-terminally biotinylated anti-human mouse immunoglobulin G monoclonal antibody
Bn	Benzyl
BSA	Bovine serum albumin
C83	83-amino acid C-terminal domain of the amyloid precursor protein
C99	9-amino acid C-terminal domain of the amyloid precursor protein
CA	California
CD	Circular Dichroism
$CDCl_3$	Deuterated Chloroform
CSF	Cerebrospinal fluid
d	doublet
D_2O	Deuterated water
D_{APP}	Apparent diffusion coefficient
DCM	Dichloromethane
DHB	Dihydroxybenzoic acid
DMF	Dimethylformamide
DMSO	Dimethyl sulfoxide
DMSO-*d6*	Deuterated dimethyl sulfoxide
DOSY	Diffusion spectroscopy
EGCG	Epigallocatechin gallate
ELISA	Enzyme-linked immunosorbent assay
EM	Electron microscopy
ESI	Electrospray ionization
ESI +	Electrospray ionization in positive ion mode
ES-MS	Electrospray mass spectrometry
Et	Ethyl
EtOAc	Ethyl acetate

EtOH	Ethanol
Exp.	Experiment
F	Fluorescence
fAβ	Insoluble fibrils of amyloid β-Peptide
F_{MAX}	The maximum observed ThT fluorescence
F'_{MAX}	The maximum rate of fluorescence change
F''_{MAX}	The maximum value for the derivative of the fluorescence change
F''_{MAX}	The minimum value for the derivative of the fluorescence change
Fmoc	Fluorenylmethyloxycarbonyl
F_{MIN}	The minimum observed ThT fluorescence
F_t	The observed ThT fluorescence at time, t
g	Grams
g_z	Applied gradient in the z-direction
h	Hours
H_2O	Water
H^A	Hydrogen-acceptance
HBTU	O-(Benzotriazol-1-yl)-N,N,N’,N’-tetramethyluronium hexafluorophosphate
H^D	Hydrogen-donation
Hex	Hexanes
HFIP	Hexafluoroisopropanol
HIV	Human immunodeficiency virus
HMG-CoA	3-Hydroxy-3-methylglutaryl-coenzyme A
HOBt	Hydroxybenzotriazole
HPLC	High-pressure liquid chromatography
HRMS	High-resolution mass spectrometry
HTS	High-throughput screen
Hz	Hertz
H-π	hydrogen-pi
I	Signal intensity in the absence of a applied gradient
IC50	The half-maximal inhibitory concentration
I_o	Signal intensity in the presence of a applied gradient

IR	Infrared
J	Coupling constant in Hertz
k_b	Boltzmann's constant
kDa	Kilodaltons
m	multiplet
MA	Massachusetts
mAβ	Soluble monomers of amyloid β-peptide
Me	Methyl
MeCN	Acetonitrile
MeOD	Deuterated methanol
MeOH	Methanol
mg	Milligrams
MHz	Megahertz
min	Minutes
mL	Millilitres
MM	Molecular mechanics
mM	Millimolar
mm	Millimeter
MoA	Mechanism of action
ms	Millisecond
mV	Millivolts
MW	Molecular weight
NA	Nicotinic acid
Na_2SO_4	Sodium sulfate
NaCl	Sodium chloride
$NaHCO_3$	Sodium bicarbonate
NaOH	Sodium Hydroxide
nM	Nanomolar
nm	Nanometer
NME	New molecular entity
NMDA	N-methyl-D-aspartate
NMR	Nuclear magnetic resonance spectroscopy

NSAID	Non-steroidal anti-inflammatory drug
oAβ	Soluble oligomers of amyloid β-peptide
OC	A rabbit-derived epitope specific polyclonal antibody for detection of amyloid-β oligomers
ON	Ontario
p3	The small peptide generated by γ-secretase cleavage of the C83 peptide
PBS	Phosphate Buffered Saline
PFG	Pulsed-field gradient
Ph	Phenyl
pH	Power of the hydrogen ion
PS1	Presenilin 1
PS2	Presenilin 2
QM	Quantum Mechanics
r	Stokes' radius
R & D	Research and development
rpm	Revolutions-per-minute
rt	Room temperature
s	Second
s	singlet
S.D.	Standard Deviation
s/n	signal-to-noise
SALA	Selective $A\beta_{1-42}$-lowering agent
SDS	Sodium dodecyl Sulfate
STD	Saturation transfer difference
STRP-HRP	Streptavidin-horse radish peroxidase conjugate
t	Time
T	Temperature
t	triplet
TEM	Transmission electron microscopy
TFA	Trifluoroacetic acid
$t_{F'MAX}$	Time at which the rate of *f*Aβ formation is a maximum

$t_{F''MAX}$	Time at which the maximum value for the derivative of the fluorescence change is reached
$t_{F'MAX(1)}$	Time at which the rate of *f*Aβ formation is a maximum for the first iteration of curve fitting
$t_{F'MAX(2)}$	Time at which the rate of *f*Aβ formation is a maximum for the second iteration of curve fitting
$t_{F''MAX(2)}$	Time at which the maximum value for the derivative of the fluorescence change is reached for the second iteration of curve fitting
$t_{F''MIN}$	Time at which the minimum value for the derivative of the fluorescence change is reached
$t_{F''MIN(2)}$	Time at which the minimum value for the derivative of the fluorescence change is reached for the second iteration of curve fitting
ThT	Thioflavin T
TMB	3,3',5,5'-Tetramethylbenzidine
TMB	3,3',5,5'-Tetramethylbenzidine diimine
Tris	Tris(hydroxymethyl)ammoniamethane
USA	United States of America
USD	United States Dollars
ν	Frequency
v/v	Volume concentration
vdw	van der Waals
w/v	Mass concentration
γ	Gyromagnetic ratio
δ	Gradient application time
Δ	Diffusion time
$\Delta F_{(-)compound}$	The change of ThT fluorescence due to amyloid-β in the absence of compound
$\Delta F_{(+)compound}$	The change of ThT fluorescence due to amyloid-β in the presence of compound
$\Delta F_{(+)compound[x]}$	The change of ThT fluorescence due to amyloid-β in the presence of compound at concentration, x
FC	Flash Chromatography
$\Delta F_{COMPLETE}$	The change of ThT fluorescence due to complete amyloid-β fibril

	formation
ΔF_t	The change in fluorescence at time, t
ΔG	Gibbs' free energy
$\Delta t_{(1)}$	Time range used for the second iteration of curve fitting
$\Delta t_{(2)}$	Time range used for the final iteration of curve fitting
η	Viscosity
μM	Micromolar
μs	Microsecond
ξ	The activity ratio of a compound and control as per the Thioflavin T fibrillogenesis assay
λ_{MAX}	Wavelength of maximum absorbance
$\pi/2$	90-degree
π-H	pi-hydrogen
π-π	pi-pi stacking
.moe	MOE molecule file extension
.pdb	Protein databank file extension

Acknowledgments

Over the last 7 years the following exercise in the application of medicinal chemistry has morphed into a multidisciplinary approach to gain insight into a tremendously complicated process. Were it not for the valued input of several friends and colleagues this project would not have been possible. I would first like to express my sincerest gratitude to my co-supervisors, Dr. Donald Weaver and Dr. Mark Stradiotto. Don, you are a visionary and I truly believe that your research programme will lead to a breakthrough in fighting this debilitating disease. I would also like to thank my committee members Dr. Alan Doucette, Dr. Peng Zhang and Dr. Norman Schepp as well as Dr. Peter Wentzell – without your insights and guidance this thesis would not have been achievable in its current form.

This project has brought together several areas of chemistry and biology and I would be remiss not to thank the many people whose guidance and support have allowed me to undertake such a complex project. I would like to extend sincerest thanks to Dr. Mark Reed, Dr. Scott Banfield, Dr. Shengguo Sun and Dr. Arun Yadav for your help in everything synthetic organic from arrow pushing to perfecting experimental technique; Dr. Felix Meier-Stephenson for teaching me the ins and outs of automated peptide synthesis; Dr. Autumn Meek and Dr. Chris Barden for helpful discussions surround the applications of molecular modeling and Amanda Saoud for her volunteer work in aspects of data collection during molecular modeling studies; Dr. Mike Lumsden, Dr. Ray Syviski and Nadine Merkely for their input and support during NMR studies; Dr. Michael Carter, Pamela Gallant and Rose Chen for tips, tricks and proper technique during biological assay work.

I also need to thank the wonderful support staff in the department of chemistry – without your support, immense talent and attention to detail my own research and the impeccable work of many others in the department would not be impossible. A huge thank you to Giselle Andrews in particular as well as Deanna Wentzell, Cheryl Stanton, Cheryl Coolen, Sean Hartwell and Cheryl Weaver for their efforts in helping me navigate the administrative side of graduate school; also thank you to Mike Boutilier, Xaio Feng, Todd Carter, Juergen Mueller, Barry Moore and Cathy Ryan for their behind the scenes work that makes research in the department possible.

Finally I wish to thank all of my family and friends for their overwhelming support throughout this endeavour. First and foremost thank you to my love, Jeanne Egar, who has had the resilience to support a perpetually frenzied grad student in the final years of his thesis. The last two years have felt like unyielding sprint towards the finish, but you have been nothing short of amazing. You've always been there making sure I'm healthy, happy and that my worries are kept in perspective. I'll always admire your strength and passion; you are the person that pushed me the hardest and I'll always owe you for that. Thank you.

My family has been overwhelming supportive of their "permanent student." Thank you to my father Gordon, my step-mother Ange, my brother Shane and of course Oma and Opa. It has been hard for me to maintain the work-life balance I desire, but your constant phone calls have kept me happy (and sane); I treasure every moment we get to spend together – even if only on the phone. While on the topic of family I need to extend my sincerest gratitude to David, Shelagh and Susie – all of you have treated me as your own kin from the first day we've met and not a day goes by where I don't think of your constant love, support and overwhelming generosity. My sincerest thanks and love to all of you whom I have the privilege of calling family.

Lastly thank you too ALL of my wonderful friends; although there are too many of you who have helped me to mention everyone by name there are a few people I would like to explicitly thank. Special thanks to (in no particular order) Emile Colpron, Drew Pelley and Laura Conrad, Kris Osmond, David Beckwith and Chantelle Brown, Nick Charman and Lyndsay Belair, Jordan Turner, and Drew Vinson. You have always been there for me and are always good for a hot meal (or a sandwich, at the least), a good chat and most importantly keeping my worries in perspective. Were it not for your continued support and guidance I don't think I'd have the guts to finish.

Chapter 1: Introduction

1.1 Alzheimer's Disease

1.1.1 A Global Epidemic

Few topics in biomedical research have aroused as much interest in both the scientific and lay communities as Alzheimer's disease (AD). AD is a chronic and progressive neurological disorder which first manifests with decreased cognitive function, altered behaviour, progressive memory impairment, and a decline in language function.[1] The symptom onset is gradual – typically spanning a decade – however, in their final years all patients afflicted with the disorder will succumb to profound dementia and ultimately death. Typically AD onset commences in the seventh to ninth decades of life; the risk of developing AD increases almost exponentially with age. As a consequence of the significant increase in life expectancy in the industrialized nations the incidence of AD has achieved epidemic proportions.[1] AD is the fourth leading cause of death in industrialized societies, preceded only by heart disease, cancer, and stroke.[2]

It is estimated that 44 million persons are afflicted worldwide, and this number will likely triple by 2050 – with 1 in 85 persons living with AD.[1] The socioeconomic ramifications are staggering – not only in terms of the emotional duress faced by and ever-increasing population of AD patients and their families, but in terms of the burden placed on the global economy. In the United States alone AD accounts for 65,000 deaths at a direct cost of 48.6 billion USD annually.[3] There are no disease-stabilizing therapies for AD. Drugs in the current therapeutic landscape provide only modest symptomatic relief and do not address the underlying pathology of the disorder. Needed are new drugs that delay, or ideally, halt the progression of the disease. It has been estimated that a therapeutic which delayed the onset of AD by an average of two years would decrease the worldwide prevalence of AD in 2050 by 22.8 million cases.[4]

1.1.2 A Brief History

Alois Alzheimer – after whom the disorder is named – first defined the clinicopathological symptom in a meeting in Munich in 1907.[5] The significance of this discovery may have been lost both on his audience and on Alzheimer himself; it was not until the work of Blessed, Tomlinson and Roth in the late 1960s that AD became accepted as the most common

basis of common senile dementia.[6] In 1976, Robert Katzman further demonstrated that AD was indeed an epidemic.[6]

In his first description of AD Alzheimer noted the presence of interneuronal tangles and extracellular "amyloid" plaque deposits in disease-damaged brains.[5] Along with reduction of several neurotransmitters (including serotonin, noradrenaline, dopamine, glutamate, and especially acetylcholine) plaques and tangles are the defining hallmarks of the disease and their identification post-mortem remains the only way to conclusively diagnose AD.[2,7] At the time of his discovery Alzheimer was unable to ascertain whether interneuronal tangles or neuritic plaques were causative of AD or were merely markers of disease progression. In 1984 the chief component of the neuritic plaque was sequenced and identified.[8,9] The peptide, known now as amyloid β-peptide, or Aβ, was also shown to be the main constituent of neuritic plaques common to patients with trisomy 21 – the most common form of Down syndrome.[9] The aptly named amyloid precursor protein (APP)– from which Aβ is derived – was subsequently cloned and localized to chromosome 21;[10,11] this discovery, along with the recognition that aged individuals with trisomy 21 develop AD neuropathology in a progressive age dependent manner, would form a basis of the amyloid hypothesis of AD.[2]

1.1.3 Amyloid Precursor Protein

Amyloid plaque from AD brain is primarily composed of Aβ.[8] Due to variability in processing, the length of the ~4.5 kDa peptide ranges from 39-43 amino acid (AA) residues. Aβ occurs predominately in two isoforms, either 40 or 42 AA in length (more commonly referred to as $A\beta_{1-40}$ and $A\beta_{1-42}$, respectively). Aβ – especially $A\beta_{1-42}$ – is prone to aggregation, a process characterized by a drastic conformational change. Prior to aggregation the structure of Aβ is α-helical whereas extraneuronal aggregates have a fibrillar β-pleated structure.[7] Prior to liberation via enzymatic processing Aβ is fully contained within APP (**Figure 1.1**) – a 695-770-AA transmembrane protein found in virtually all peripheral and brain cells. The liberation of Aβ from APP is dependent on the action of three enzymes, namely α-, β-, and γ-secretase.

During secretory processing the majority of APP molecules are initially cleaved by α-secretase. This cleavage occurs nearly central to the Aβ sequence and results in the release of APPs-α, a large soluble ectodomain. The remaining 83-AA, membrane-retained, C-terminal domain, C83, is then cleaved by γ-secretase generating the small p3 peptide (**Figure 1.2B**).

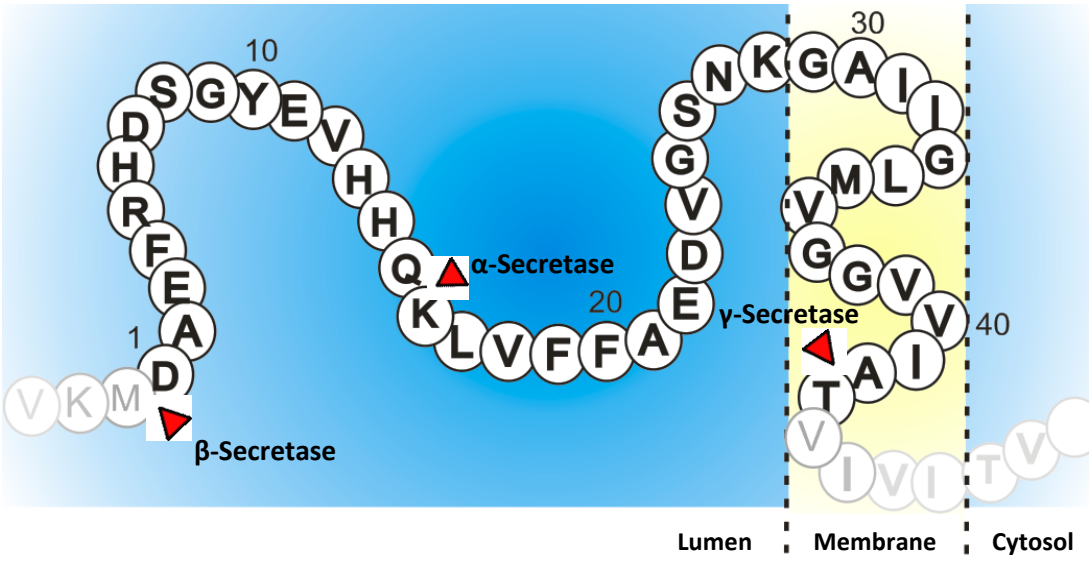

Figure 1.1 The sequence of $A\beta_{1-42}$ contained within APP as well as the sites of action of the α-, β-, and γ-secretase enzymes.

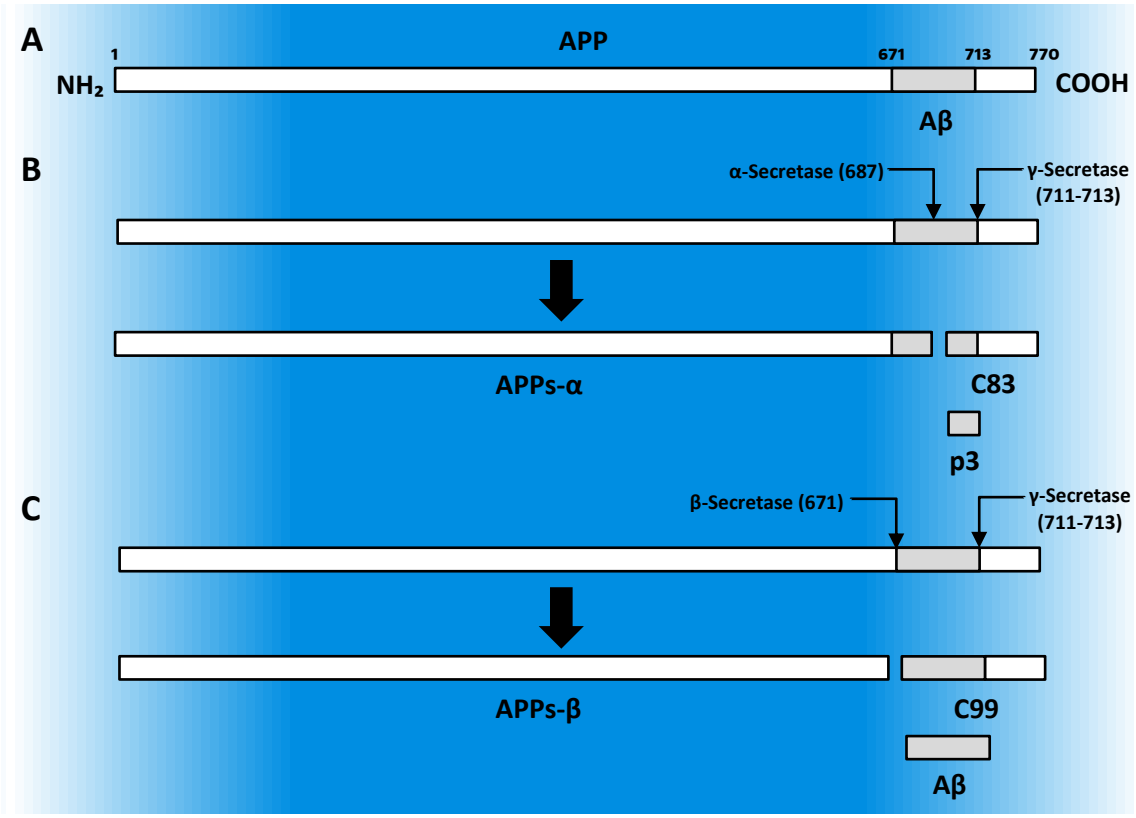

Figure 1.2 A schematic of the membrane-retained APP accompanied by its alternative processing pathways.

Successive action by α- and γ-secretase results in the release of APPs-α and C83 but not Aβ. Alternatively APP may be initially processed by β-secretase resulting in the release of another large soluble ectodomain, APPs-β, resulting in the retention of membrane-bound C99, the 99-AA, membrane retained C-terminal domain. Subsequent processing of C99 by γ-secretase results in the release of $A\beta_{1-40}$ or $A\beta_{1-42}$ into the cell (**Figure 1.2C**). Upon excretion from the cell, the peptide is able to participate in extracellular aggregation and become incorporated into growing plaques. The apparent lack of specificity of γ-secretase is a result of numerous discrete mutations in the genes encoding APP, presenilin 1 and presenilin 2 (PS1 and PS2, respectively) – the latter two being constituents of γ-secretase.[12,13] Numerous mutations about APP (especially those on or near the γ-secretase cleavage sites) have been shown to alter the processing of C99, resulting in increased cellular production of $A\beta_{1-42}$. Because of its increased propensity to aggregate (relative to $A\beta_{1-40}$) $A\beta_{1-42}$ is far more neurotoxic; as a result, the overproduction of the $A\beta_{1-42}$ isoform is thought to be a major contributing factor in early-onset AD. Many γ-secretase mutations have been implicated in the propagation of the early onset form of AD – a hereditary autosomal dominant form of the disease which constitute approximately 5% of all cases.[14,15]

1.1.4 The Amyloid Hypothesis

Biochemical and morphological studies have indicated that the clinical impairment observed in AD involves early synaptic dysfunction which, in turn, is followed by synaptic loss, widespread neuritic dystrophy, neurofibrillary tangles and ultimately neuron death.[16] Aβ is believed to be the chief mediator of these neurotoxic effects and as such it is believed that the age-dependent accumulation of the peptide initiates the pathology of AD; however, Aβ is a naturally occurring peptide and is present in both the brains and cerebrospinal fluid (CSF) of healthy humans.[17] This was initially considered to be a stumbling block of the amyloid hypothesis, but it has been since shown that Aβ itself does not exhibit neurotoxicity – its deleterious effects are a consequence of self-association into higher order oligomers. [17]

Ongoing is the debate as to what level of aggregation is responsible for the observed neurotoxicity. Initially it was assumed that large aggregates – readily observable with electron microscopy (EM) – were the mediators of Aβ toxicity; yet it has since been recognized that amyloid plaque deposition precedes cognitive decline in dementia. Again, this had been frequently cited as a critical inconsistency in the amyloid hypothesis. More recent research shows a robust correlation between soluble Aβ oligomer (*o*Aβ) levels and the extent of synaptic

loss and severity of cognitive impairment.[17] Soluble Aβ refers to any form of *o*Aβ (as well as monomeric Aβ, *m*Aβ) that is soluble in a buffered solution and remains in solution following high-speed centrifugation. More recently *o*Aβs have been implicated as the chief mediators of neurotoxicity;[17–19] research into these assemblies have implicated Aβ trimers[20] and dodecomers[21] among the principle neurotoxic species.

If lower-order *o*Aβs are indeed the pathologic species in AD then insoluble Aβ fibrils, *f*Aβs, may still significantly contribute to neurotoxicity by acting as peptide reservoirs for toxic *o*Aβ formation. Aβ dimers and trimers have been isolated in extracts of amyloid plaques, and suggest that *o*Aβs are indeed the fundamental building blocks of insoluble amyloid deposits.[22,23] Regardless of whether it is soluble Aβ species or larger insoluble aggregates that are of greatest detriment to neurons preventing the self-assembly of Aβ would be expected to mitigate neuronal damage.

1.2 Strategies for Therapeutic Intervention of AD

1.2.1 Current Treatments are largely Symptomatic

To date no therapeutics for AD have been clinically proven to modify disease progression in a way that prevents, or even slows, the progression of the illness. Current therapies provide symptomatic relief – they work to ameliorate or suppress certain symptoms, but do not address the underlying pathology. Generally, the current treatment options are limited to two categories: drugs that modify behavioural symptoms and neurotransmitter-based therapies.

1.2.1.1 Neurotransmitter-Based Therapies

Acetylcholine augmentation is the mechanism of action for all but one of the drugs currently prescribed for AD: tacrine, donepezil, rivastigmine, and galantamine (**Figure 1.3**).[24–26] These agents act by inhibiting acetylcholinesterase (AChE) and thereby raising levels of acetylcholine the brain. The other commonly prescribed drug, memantine, also acts via neurotransmitter modulation, albeit in a different manner. As an uncompetitive antagonist of N-methyl-D-aspartate (NMDA) receptors it blocks the overstimulation by glutamate, and

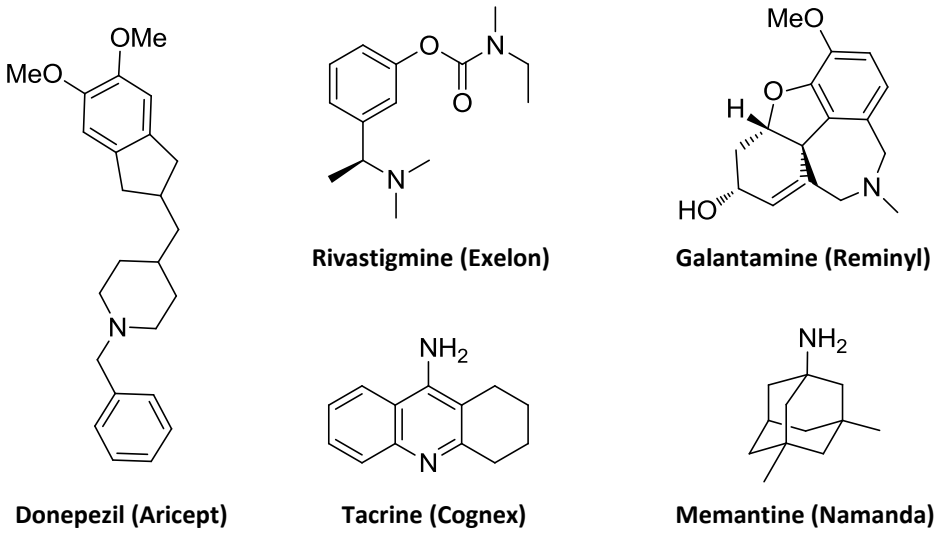

Figure 1.3 Drugs that are the currently prescribed for AD. Donepezil, tacrine, rivastigmine and galanamine are AChE inhibitors; memantine is primarily a NMDA receptor antagonist.

attenuates its excitotoxicity (although some of its efficacy in AD has been attributed to action as an uncompetitive antagonist at serotonergic 5-HT3 and nicotinic acetylcholine receptors).[27] While neurotransmitter therapies do indeed slow the progression of cognitive decline, improvements are often modest and of temporary duration.[24] This is a consequence anticipated for drugs which do not address the underlying pathogenesis of AD.

1.2.1.2 Drugs that Modify Behavioral Symptoms

Patients with AD undergo a myriad of behavioural disturbances which include: anxiety, apathy, agitation, aggressiveness, depression, delusions and hallucinations.[26] These symptoms can be emotionally debilitating for both patients and their caregivers. Non-phenothiazine antipsychotic agents such as risperidone, olanzapine, haloperidol and quetiapine in low-to moderate doses may blunt some of these symptoms. Methylphenidate can be prescribed for marked apathy and anticonvulsants such as divalproex sodium or carbamazepine for agitation and anxiety. Indeed the administration of one or more of these agents can significantly improve behavioral symptoms in AD patients.[25] The behavioral aberration for which these agents are administered may only be significant for a relatively short period of time; as dementia worsens these symptoms are lost and patients become more apathetic.[25]

1.2.2 Overview of Therapeutic Approaches in Development

Current approaches to the treatment of AD generally have two targets: interneuronal tangles of tau protein, and extraneuronal Aβ. Strategies which inhibit tau toxicity are actively being pursued; however, the focus of this review will be approaches which directly target Aβ formation and address the amyloid hypothesis of AD. The majority of therapeutic strategies which are actively address the role of Aβ in AD pathology fall into three broad categories:

1) inhibition of Aβ production;

2) upregulation of Aβ degradation and clearance;

3) and inhibition of Aβ aggregation/deposition.

Given the inherent complexity of AD a multitude of therapeutic targets have been postulated and rigorously examined which may be modulated in hopes of mitigating disease progression. The following discussion will give a general overview of the approaches as well as their successes and failures in working towards a cure for AD.

1.2.2.1 Inhibition of Aβ Production

The first approach to be discussed looks to address the aetiology of AD by altogether eliminating Aβ production *in vivo*. To date it has been the most thoroughly examined putative therapeutic approach. Release of Aβ from APP is dependent on the successive action of the proteolytic enzymes β-secretase and γ-secretase (**Figure 1.2**); selective inhibition of either would reduce Aβ production and therefore preclude the formation of toxic *o*Aβs. Alternatively, upregulation of α-secretase would increase scission of APP within the sequence of Aβ – and this too would decrease Aβ production. Over the past 25 years the secretases have been a primary target in the development of putative AD therapeutics and will be discussed further.

1.2.2.1.1 β-Secretase Inhibitors

As β-Secretase is the catalyst of the initial, rate-limiting, step of Aβ production it has been deemed an attractive therapeutic target for inhibition of Aβ production. β-Secretase knockout mice do not generate $A\beta^{28}$ and furthermore these mice appear healthy and do not show developmental, neurological or behavioural abnormalities (although some mice exhibit

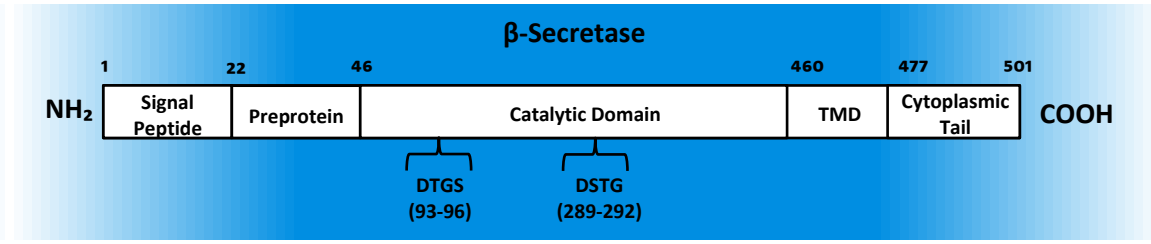

Figure 1.4 A schematic representation of β-secretase.

hypomyelination of peripheral nerves).[29] These observations support the notion that inhibition of β-secretase reduces Aβ production and therefore could alter AD progression with minimal side effects.

β-Secretase is a novel 501-AA aspartyl protease that selectively cleaves APP between residues 671 and 672 to form APPs-β and membrane bound C99.[2] The sequence of β-secretase is comprised of an N-terminal signal peptide followed sequentially by preprotein, catalytic and transmembrane domains, with the sequence concluding with a cytoplasmic tail (**Figure 1.4**).[30] Central to the protease are two conserved aspartyl protease active sites (DTGS and DSGT at AA residues 93-96 and 289-292, respectively). The mechanism of the aspartyl proteases has been thoroughly investigated by kinetic methods, affinity labeling, and x-ray crystallography.[31] These investigations are consistent with a general acid-base mechanism in which a nucleophilic water molecule is held between the two catalytic aspartic acid residues.[32] For activation of the water molecule, one of the two aspartic acids must be deprotonated; this is congruent with the optimal pH range for aspartyl proteases ($4 \geq pH \geq 4.5$). On deprotonation (activation) by the aspartate anion the water molecule it is able to attack the carbonyl of the scissile amide bond, resulting in the formation of an oxyanion tetrahedral intermediate. Subsequent protonation of the amide nitrogen atom, and the resultant rearrangement about the tetrahedral center, leads to the formation of the hydrolysis products and cleavage of the amide bond. β-Secretase cleavage of APP is highly sequence specific with the scission occurring at the N-terminus of Aβ by recognition of the sequence $V_{669}K_{670}M_{671}{*}D_{672}A_{673}$.

Aspartyl proteases are a well-characterized class of protein and include pepsin, renin, cathepsins D and E, and napsin A. β-secretase does share significant sequence homology with these enzymes and therefore its crystal structure displays the conserved general folding of aspartyl proteases.[33] Structural differences of β-secretase relative to other aspartyl proteases

have been observed via co-crystallization with peptidomimetic inhibitors. The active site is more open and solvent accessible and has subsites that are relatively hydrophilic compared to other aspartyl proteases. The inhibition mechanism of aspartyl proteases is well known and as such the design of transition-state mimetics has been thoroughly investigated.[30] Inhibitors of other aspartic proteases such as renin and the retroviral human immunodeficiency virus (HIV) protease have been developed and are currently in therapeutic use.[30] The successful development of inhibitors of renin and HIV protease has in some ways facilitated the search for β-secretase inhibitors.

Over the last decade, several β-secretase inhibitors have been described,[25] the majority of which are peptidomimetic and are based on the AA sequence at the cleavage site of APP.[34] Reports of synthetic small-molecule inhibitors have been scarce. Naturally occurring small-molecule non-competitive inhibitors such as hispidin and the catechins have only μM potency and poor specificity.[35] Thus far it has been difficult to design small-molecule inhibitors which avidly bind the large catalytic site domain of β-secretase, however larger peptidomimetic inhibitors have been developed which show blood-brain barrier (BBB) permeability.[33] The recently developed GRL-8234 has been shown to be a potent and highly selective inhibitor of Aβ production both *in vitro* and *in vivo*. GRL-8234 has shown excellent inhibitory activity in Chinese hamster ovary cells and intraperitoneal administration to Tg2575 mice (a triple transgenic murine model of AD progression) facilitates a 65% reduction of $A\beta_{1-40}$ formation – a result that the authors indicate confirms β-secretase inhibition is viable target for putative AD therapeutics.[36] The promise of β-secretase inhibition was further bolstered by completion of CTS-21166 (a potent and selective β-secretase inhibitor) in a phase I study assessing the drug's safety and tolerability in healthy adults.[34] In the dose-escalation study plasma levels of Aβ and the drug were monitored. CTS-21166 was shown to have good BBB permeability and a single-dose administration of compound produced a 60% reduction in Aβ. Despite the success of phase I assessment CTS-21166 was abandoned prior to further clinical assessment.

Overall, the progression of small-molecule inhibitors of β-secretase to clinical assessment has been slow. The structural similarity of the active site of β-secretase to other aspartyl proteases has presented a daunting hurtle in the development of selective inhibitors with high affinity – although this has been achieved with peptidomimetic inhibitors. Developing small-molecule inhibitors with both specificity and BBB permeability remains a challenge given

the relatively large active site of β-secretase; to this end, research programmes developing γ-secretase inhibitors have been more successful and have gained favour in the pursuit for a putative AD therapeutic.

1.2.2.1.2 γ-Secretase Inhibitors

The proteolytic scission that ultimately generates Aβ is mediated by γ-secretase. Due to a lack of specificity in the proteolytic processing of APP by γ-secretase multiple isoforms of Aβ are produced *in vivo*; as such the ratio of $A\beta_{1-40}$ to $A\beta_{1-42}$ (the latter of which has a higher propensity to aggregate and is generally recognized as being more neurotoxic) generated is directly mediated by γ-secretase. Given the role of γ-secretase in Aβ production (and moreover its role in the formation of isoforms of varying neurotoxicity) compounds which alter proteolytic processing via this enzyme are actively pursued.

Although γ-secretase displays the pharmacologic characteristics of an aspartyl protease, it shares little or no sequence homology with known members of the aspartyl protease family.[37] Over the last 20 years a concerted effort has been centered on determining the structure and function of γ-secretase, a multi-protein complex with at least four membrane-spanning constituents (presenilin, nicastrin, anterior pharynx-1, and presenilin enhancer-2) (**Figure 1.5**). The catalytic component of the γ-secretase complex is presenilin where two aspartate residues form the active site. There are two presenilin genes, PS1 and PS2, mutations of which are associated with early-onset forms of AD.[38] Over 100 missense mutations have been identified in

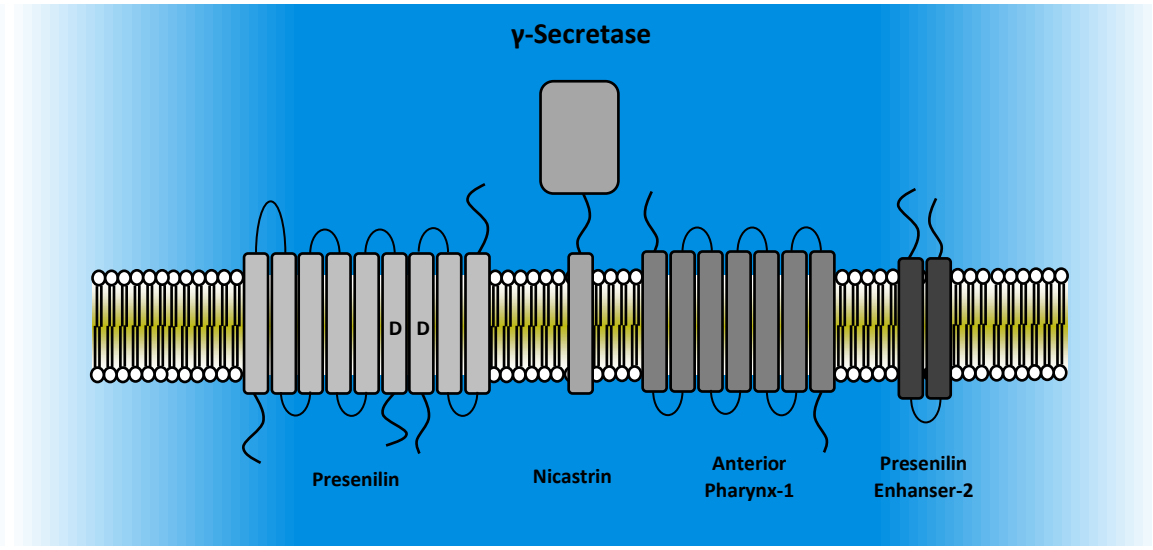

Figure 1.5 A schematic representation of γ-secretase.

PS1 alone and the majority of these mutations skew the proportion of Aβ toward the more aggregation-prone $A\beta_{1-42}$ (accounting for > 50% of cases of familial early-onset AD);[13,25,39] mutations about the γ-secretase cleavage site of APP have also been shown to increase the proportion of $A\beta_{1-42}$ and also confer a genetic predisposition to early-onset AD.[40]

In vivo levels of Aβ are markedly decreased in PS1 knockout mice wherein Aβ production decreases as much as 80% compared to wild-type littermates;[41] furthermore, cells from PS1/PS2 double-knockout mice are completely devoid of γ-secretase activity.[42] Although gene knockout studies of murine models implicate γ-secretase as a putative target, the deletion of PS1 in mice is lethal *in utero* (or shortly after birth) and indicate that γ-secretase inhibition may have significant safety drawbacks.[41] Toxicity concerns surrounding γ-secretase inhibitors are due to alteration of the Notch signaling pathway which plays a significant role in cell differentiation during *in utero* development (and into adulthood).[41] γ-Secretase alters Notch signaling by blocking proteolysis of Notch-1 which like APP is a substrate of γ-Secretase.

Despite safety concerns surrounding Notch signaling the progression of γ-secretase inhibitors remains steadfast. Several nonpeptidic, orally available, γ-secretase inhibitors have been developed which are shown to lower Aβ load in CSF.[43] To date, γ-secretase inhibitors have had the most success in terms of progression to clinical human trials.[25] Currently there are two γ-secretase inhibitors undergoing clinical assessment (BMS-708163 and GSI-953 have proceeded to Phase II trials).[44–46] Five other compounds (BMS-299897, MK-0752, RO4929097, LY-450139 and PF-3084014) did proceed to clinical testing but have since been abandoned.[47,48] Thus far, LY-450139 is the most well documented γ-secretase inhibitor and the results of its trials have been fully published. In Phase I and II studies patients given LY-450139 showed a transient period of plasma Aβ reduction, followed by a period of significantly elevated plasma Aβ which eventually dropped to baseline; however, central nervous system (CNS) levels of Aβ remained unaltered in both studies. In 2011 phase III trials were abruptly halted due to an increased risk of skin cancer and infections in trial participants; it was found, notably, that LY-450139 did not improve cognition of trial participants relative to a control.[49]

1.2.2.1.3 γ-Secretase Modulators

Although a number of highly potent γ-secretase inhibitors have been identified, but their interference with Notch signaling may preclude their use clinical use in the treatment of

AD;[48,50] consequently γ-secretase modulators (as opposed to outright inhibitors) are also being evaluated as potential therapeutic agents.[51] Selective $A\beta_{1-42}$-lowering agents, or SALAs, are being developed as potential disease-modifying therapeutics agents. SALAs allosterically modulate γ-secretase and affect the site of action about the sequence of APP, and in doing so may potentially decrease the proportion of $A\beta_{1-42}$ released (relative to $A\beta_{1-40}$).

Non-steroidal anti-inflammatory drugs (NSAIDs) were the first class of molecules that exhibited potential as SALAs.[52] Epidemiological studies have shown that chronic use of some NSAIDs has been associated with a significantly lower risk of developing AD.[53] Treatment of Aβ-secreting cells with the sulindac sulfate, ibuprofen or indomethacin selectively reduces $A\beta_{1-42}$ production while concurrently increasing $A\beta_{1-38}$ production. Promising *in vitro* results aside, there remain serious safety concerns surround the use of NSAIDs as SALAs due to the toxicity associated with high doses of NSAIDs (especially in the elderly); still the NSAID-related compound (R)-Flurbiprofen has undergone a clinical assessment. (R)-Flurbiprofen was shown to reduce the concentration of $A\beta_{1-42}$ in mouse brain and long-term dosing of this compound prevented defects in memory and learning.[54] Although the results from a Phase II study were encouraging a large Phase III study of 18 months' duration yielded completely negative results.

Several other γ-secretase modulators are being developed and have reached or are approaching clinical testing. E2012, a diarylcinnamide derivative, has been claimed to lower Aβ by γ-secretase modulation without interfering with Notch processing.[47] Another promising SALA in development is CHF5074, which has been shown to preferentially lower $A\beta_{1-42}$ secretion in human neuroglioma cells overexpressing the Swedish mutated APP.[55] Long-term dosing of CHF5074 in an aggressive murine AD model has also been shown to attenuate brain Aβ pathology and the associated behavioural deficits. By only modulating γ-secretase activity SALAs may exert a beneficial effect without affecting Notch processing *in vivo*.[25] This is an attractive alternative to γ-secretase inhibitors, which have a tendency of gastrointestinal and immunological side effects. Although selective lowering of $A\beta_{1-42}$ has been shown to attenuate plaque formation and behavioural deficits in AD murine models, it remains to be seen if these beneficial effects will be translated to humans.

1.2.2.1.4 α-Secretase Activators

α-Secretase activation may serve as an alternative to therapeutics which inhibit the amyloidogenic enzymes β- and γ-secretase. α-Secretase processing occurs within the Aβ domain of APP and thereby precludes the formation of neurotoxic Aβ; as such compounds that potentiate the α-secretase pathway of APP processing may be and attractive alternative to inhibitors of β- and γ-secretase. It is generally thought that potentiating α-secretase cleavage is more difficult than inhibiting β- and γ-secretase.[25] The identity of α-secretase is still somewhat elusive, although the general consensus is that the enzyme is a member of the ADAM (a disintegrin and metalloprotease) family of proteases.[25] It has been suggested that ADAM10 is in fact α-secretase, as overexpression of ADAM10 in transgenic murine models of AD has been show to decrease in amyloid pathology.[56] Conversely, expression of a catalytic inactive form of ADAM10 results in an increase in amyloid pathology.[57]

Statins are a class of approved agents which have shown to increase APPs-α via α-secretase activation. The shift from amyloidogenic to non-amyloidogenic processing of APP may account for epidemiological studies that show an association between statin use and reduced risk of developing AD. *In vitro* studies have shown that lovastatin, atorvastatin, simvastatin and rosuvastatin stimulate APPs-α shedding from human cell lines.[58–61] Prospective clinical trials of statins for the treatment of patients who already have AD have been negative thus far but remain ongoing. Although statin use has been epidemiologically associated with a reduction in risk of developing AD the mechanism(s) by which these effects propagate are poorly understood. Statin use may indeed increase α-secretase activation, but other mechanisms (such as alterations in cholesterol homeostasis) have been implicated.

1.2.2.1.5 Shortcomings of Secretase-Based Approaches

Inhibitors of APP processing have been shown to be effective in reducing Aβ production *in vitro* and *in vivo*, although promising bench-top results have yet to translate to clinical success. There remain several major hurdles in developing agents which alter amyloidogenic processing of APP. Ultimately the challenge is developing a molecule with high specificity for the targeted secretase which possesses an adequate absorption and pharmacokinetic profile while maintain a low toxicity and sufficient BBB penetration.

1.2.2.2 Upregulation of Aβ Degradation and Clearance

The next therapeutic approach to be discussed looks to address the aetiology of AD by upregulating Aβ clearance from the brain; these methods target various species of Aβ along the aggregation pathway of the peptide – from *m*Aβ to higher order *o*Aβs and *f*Aβs. These approaches are more recently developed that those which target the secretases and are quickly gaining favour in the drug development community.

1.2.2.2.1 Cholesterol Homeostasis

Several lines of evidence have been uncovered that increasingly supports the idea that cholesterol homeostasis is intrinsically connected to the deposition of amyloidogenic plaques *in vivo*. Although many of the mechanistic details remain unsettled it has become increasingly clear that the many proteins tasked with regulating cholesterol homeostasis, and cholesterol itself, significantly contribute to the production, degradation and clearance of Aβ *in vivo*.

The identification of the apolipoprotein ε (ApoE) genotype as a genetic risk factor in late-onset AD was the first clue that cholesterol homeostasis indeed played a significant role in AD pathology. ApoE is the predominant protein constituent of lipoproteins found in the brain. Lipoproteins are the main transporters by which dietary fats and other water insoluble molecules (fat-soluble vitamins and cholesterol for example) are transported throughout the body. In humans, ApoE exists in three allelic isoforms: ε2, ε3 and ε4. Inheritance of the ε4 allele increases the risk and reduces the age of AD onset, whereas inheritance of the ε2 allele confers neuroprotection – both reducing risk and increasing the age of AD onset.[62,63] ApoE is colocalized in cerebral amyloid deposits and has been suggested as a molecular chaperone that modulates Aβ deposition and clearance.[64] Several early studies have shown isoform-dependent differences in ApoE-Aβ binding affinity.[65] The role of ApoE in AD pathogenesis is a complex one; it has become increasingly apparent that both protein isoform and lipidation status affect ApoE-Aβ binding, and presumably, Aβ clearance and degradation.

Exactly how ApoE isoform and lipidation status contribute to Aβ homeostasis is by no means clearly defined. Lipidation of ApoE affects Aβ clearance via two major pathways: the first being regulation of Aβ transport across the BBB; the second being regulation of Aβ degradation.[66,67] Major inconsistencies between these discrete pathways have arisen, and when taken together, the evidence supporting each pathway is confounding.[68] Although much

progress has been made in defining the role of ApoE in Aβ clearance and degradation in recent years, many questions remain unanswered. The relative contributions of these two pathways to Aβ clearance *in vivo* is not yet known, nor are the pathways themselves clearly understood. Questions such as these need be addressed before drugs which modify cholesterol-homeostasis can be rationally developed as AD-modifying therapeutics.

Although no cholesterol-lowering agents have been approved for use as AD-modifying therapeutics considerable evidence has been amassed that suggests drugs which lower CNS cholesterol significantly reduce systemic Aβ and amyloid plaque burden. An increased risk of developing AD has been associated with high dietary intake of fat and cholesterol. In an investigation on the effect of cholesterol intake Aβ burden, the administration of a high fat/high cholesterol diet to a double mutant PS1/APP mouse line was shown to increase in total brain Aβ levels by 50%. It was found that these Aβ levels correlated strongly with plasma and brain total cholesterol content. Moreover, the treatment of this mouse line for five weeks with the cholesterol lowering drug BM15.766 decreased total brain Aβ levels and plaque burden by approximately 50%.[66]

Statins are inhibitors of HMG Co-A reductase, the rate-limiting enzyme of the mevalonate pathway of cholesterol synthesis, and are effective as cholesterol-lowering agents. Lovastatin has been shown to inhibit cholesterol levels in hippocampal neurons, and markedly decrease Aβ formation, although some debate as to the mechanism of action remains.[58,69] Similarly, *in vivo* experiments have demonstrated that a three-week administration of simvastatin to guinea pigs decreased *de novo* brain cholesterol synthesis and lowered CSF levels of $A\beta_{1-40}$ and $A\beta_{1-42}$, by 50% and 40%, respectively.[70] Although, statins have been shown to affect CNS cholesterol metabolism, clinical trials evaluating their efficacy to lower Aβ or decrease AD prevalence have been mixed.[67,71] Some studies show a modest neuroprotective effect in patients with mild AD but others find no correlation between statin use, cognition deficits, and risk of dementia.[69,72,73] Several retrospective epidemiological studies of cholesterol-lowering agents and AD have been reported as well. In the majority of these studies daily use of statins was shown to drastically reduce the likelihood of developing AD or dementia.

1.2.2.2.2 Aβ Immunization

Another approach to eliminating Aβ from the brain is to stimulate an autoimmune response against the peptide. Aβ immunization is being attempted using both active and passive immunization techniques. Active immunity requires the introduction of an antigen to which antibodies are produced and these, in turn, flag Aβ for clearance from the CNS. Passive immunization is conferred by giving preformed antibodies (either specific or pooled/nonspecific) interperitoneally; unlike active immunization, regular and frequent administration of antibodies is needed to carry on immune-mediated clearance of antigen by the host. Mice that are "immunized" with fibrillar $A\beta_{1-42}$ show reduced levels of soluble Aβ and increased clearance of pre-formed amyloid plaques.[74] Aβ immunized mice also performing better than their littermates in maze tests, suggesting that increased cognition is due to diminished Aβ levels.[75] Inoculation with unaggregated Aβ significantly decreases the hosts immune response indicating that the fibrillar form of the peptide is a more effective immunogen.[76] No adverse effects of $A\beta_{1-42}$ immunization have been observed in the treated mice, and other research groups have also reported positive results in transgenic murine models of AD (either as reduced AD pathology or improved cognitive function) after active or passive immunization against Aβ.[76–78]

Current research is aimed at elucidating the mechanism by which the immune response decreases Aβ burden in brain. Antibodies generated by Aβ injection could primarily act by crossing the BBB and binding directly to plaques and oligomers.[76] Alternatively, the antibodies may predominantly bind to peripheral Aβ and prevent it from crossing the BBB. This "peripheral sink" phenomenon could alter the dynamic equilibrium of Aβ between CNS and systemic plasma and allow for a net efflux of Aβ from the brain.[79]

Phase I studies have found that vaccination with $A\beta_{1-42}$ paired with an adjuvant (AN-1792) was well tolerated in individuals with moderate AD, with a subset of patients developing an immunological response.[80] Following the promising initial clinical assessments AN-1792 was moved to phase II studies in the United States and Europe, although these were eventually halted due to a low, but unacceptable, incidence of aseptic meningoencephalitis.[81] The inflammation of brain caused in patients treated with AN-1792 was unexpected given the safe profile of the drug during Phase I testing (and further considering encephalitis was not observed in any of the five animal species used in pre-clinical testing). The adverse reaction has been suggested to be a result of excessive inflammation from an autoimmune attack directed at APP

rather than Aβ, a scenario that would explain why animals injected with the human form of Aβ did not experience similar autoimmune toxicity. Nevertheless, three participants of the AN-1792 trial were shown to have reduced CNS Aβ burden (upon autopsy); this result along with the numerous successes *in vivo* using murine models of AD have solidified a continued interest Aβ immunization therapy.

Current development efforts focus on activating highly specific antibody responses to Aβ, thus minimizing the adverse effects that were observed in the AN-1792 Phase II study.[51] ACC-001 is an active immunoconjugate which has been designed to induce an antibody response specific to Aβ (and not APP) thereby minimizing the incidence of aseptic meningoencephalitis as was seen with AN-1792 – however as of August 2013 ACC-001 was no longer in Pfizer's pipeline. No meningoencephalitis was observed in during phase II clinical assessment of another immunoconjugate, CAD106, wherein continued safety was observed after seven injections and at follow-up (after two and a half years).[82] Other active vaccines are in or nearing clinical trials, but are proprietary and as such their structures and modes of action have not been disclosed.[83] Several passive immunotherapy techniques have made it to clinical testing although, again with disappointing outcomes. Ponezumab was halted after failure to meet specified outcomes in phase II clinical trials due to a lack of BBB permeability. Soluenzumab and bapineuzumab had similarly disappointing outcomes after phase III testing as neither where shown to decrease plague load or increase cognitive ability in patients with mild to moderate AD.[84,85] Indeed, much progress has been made in the last 5 years in developing passive and active immunization strategies but still no immunotherapies have been successful in clinical testing to date.

1.2.2.2.3 Beyond Traditional Targets: Inhibitors of Aβ Aggregation

To date the vast majority of compounds that have progressed to clinical trials have been either small-molecule modulators of the secretases or immunotherapies that target liberated Aβ. High-throughput screening (HTS) has in large part been the driving force behind research efforts towards effectors of the amyloid secretases, wherein libraries of small-molecules are screened against well-established targets. Secretases are considered traditional targets which have (for the most part) well defined receptors. Here molecule development is pushed forth according to the 'hand-in-glove' or 'lock-in-key' ideology of drug development (these are the targets that the pharmaceutical industry has become accustomed to). Time and again efforts to

affect disease progression through traditional targets have come up short, and this is not unique to the development of AD therapeutics. In 2010, despite global research and development (R & D) spending having escalated to 60 billion USD worldwide only 2 new molecular entities (NME) entered the market.[86] It is obvious that working within the traditional paradigm has resulted in a significant lack of productivity from the pharmaceutical community – a shift is needed.

Aβ antiaggregants are compounds that interact with Aβ directly and thereby alter its aggregation. Many novel classes of compounds have been identified that inhibit the formation of *f*Aβs. These compounds too show promising *in vitro* and *in vivo* activity. Unlike small-molecule modulators of the secretases or immunotherapies, the development of Aβ antiaggregants has been driven in large part by the academic community. Indeed, uncertainties about the mechanism of action and a lack of understanding of the molecular properties underpinning antiaggregant activity have somewhat stigmatized antiaggregant development as putative AD therapeutics. Often these research endeavors are considered academic research by the drug development community, but nevertheless antiaggregant development has gained popularity in the last two decades. A fundamental understanding of the mechanism by which Aβ self-associates has been driven (in large part) by the development of Aβ peptidomimetic antiaggregants; subsequently, small-molecule antiaggregants have been developed which retain (or improve) on the activity of their peptidomimetic counterparts, and many of these compounds are well suited for development into BBB-permeable compounds. Compounds which inhibit the aggregation and deposition of Aβ may well be an alternative to the approaches discussed thus far.

1.2.2.3 Aβ Antiaggregants

1.2.2.3.1 Aggregation of Amyloidogenic Proteins

Protein aggregation – the conversion of soluble *m*Aβ into large, insoluble, multimeric protein complexes (*o*Aβs and *f*Aβs) – is a stepwise progression of three key processes: conformational interconversion, oligomerization and fibrillization. Conformational interconversion is an intramolecular process; oligomerization and fibrillization are intermolecular processes. The formation of *f*Aβs is complex process and is yet to be fully understood (**Figure 1.6**). Upon the structural interconversion of *m*Aβ an α-helical to a random

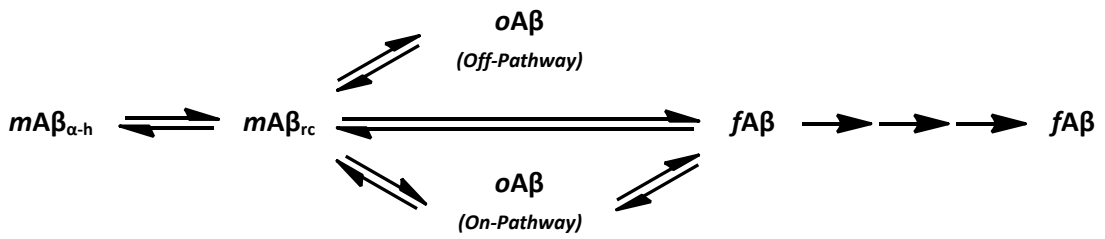

Figure 1.6 Multiple pathways of Aβ assembly.

coil conformation *m*Aβ may self-associate (or oligomerize) into soluble *o*Aβs comprised of multiple units of *m*Aβ.[87] These may be on- or off-pathway to full *f*Aβ formation but oligomers of both types are neurotoxic.[19,88] On-pathway *o*Aβs retain a β-sheet conformation and form β-pleated sheets where each pleat (or strand) is a unit of protein non-covalently bound to its neighbors.[89] These are intermediates of aggregation; they are extremely stable, and resist denaturation in the presence of the reagents (such as urea and SDS) and harsh solvent conditions typically used to disrupt protein quaternary structure.[90] The inherent stability of amyloidogenic oligomers is a result of their β-pleated structure, wherein adjacent strands of protein are non-covalently bound by an extensive hydrogen-bonding network along the protein backbone.[89] On-pathway *o*Aβs are structurally analogous to *f*Aβs – both are rich in β-sheet conformation – they are generally recognized by antibodies as different from both *m*Aβs and *f*Aβs.

The intrinsic stability of β-pleated oligomers drives their growth.[91] Monomeric protein may incorporate into soluble oligomers, or alternatively oligomers may self-associate, thereby forming larger oligomers; this continuous process results in the formation of oligomers with ever-increasing molecular weight (MW). The low solubility of high MW oligomers in aqueous solution limits their growth, and eventually they fall from solution as insoluble protein fibrils; this, the final phase of aggregation is known as fibrillization. Once insoluble fibrils are formed, monomers and oligomers may then incorporate themselves into the ends of the fibrils – resulting in fibril elongation and conservation of the β-pleated structure.[92]

1.2.2.3.2 Inhibitors of Aβ Aggregation and Deposition

Because of the inherent complexity of Aβ aggregation the search for inhibitors of its aggregation has been erratic and remains somewhat confused.[90] In spite of this hundreds of novel antiaggregants have been identified and presented in the literature.[93] Aβ antiaggregants

can be broadly categorized as peptidomimetic inhibitors or small-molecule inhibitors of aggregation – both will be discussed further.

1.2.2.3.2.1 Peptidomimetic Inhibitors

Early studies on peptidomimetic antiaggregants focussed on the elucidation of the "recognition sequence" sequence of Aβ aggregation – the motif responsible for *m*Aβ self-association. Using ^{125}I-radiolabled $A\beta_{1-40}$ Tjernberg and co-workers were able to elucidate the central recognition sequence of *m*Aβ by detecting ^{125}I- $A\beta_{1-40}$ binding to various cellulose membrane-bound 10-AA segments using autoradiography and densitrometry.[94] ^{125}I- $A\beta_{1-40}$ binding was detected to all membrane-bound peptides containing the sequence KLVFFA, AA residues 16-20 of Aβ; The authors then showed that the acylated peptide Ac-QKLVFF-NH_2 was able to inhibit *f*Aβ formation.[95]

Efforts in developing antiaggregant peptides have been focused on developing modified peptides with Aβ sequence homology.[96–98] These peptides are designed to bind to Aβ and disrupt its normal assembly into toxic aggregates and generally involves synthesizing peptides of 5-11 AA in length that contain a portion of the KLVFFA sequence (to facilitate molecular recognition). Generally peptides that contain this sequence, but have no further structural modifications, will delay but not abrogate *f*Aβ formation;[96] however peptides which contain a bulky "disrupter" group (attached to either the peptide *N*- or *C*-terminus) such as a cholyl group will inhibit *f*Aβ formation.[96] In this case the antiaggregant peptide associates with Aβ and the disrupter group then prevents further association of Aβ by destabilizing β-sheet formation in *o*Aβs. The disrupter group may also lie directly within the recognition sequence, as is the case with the peptide LPFFD (iAβ5) wherein a proline incorporated directly into the sequence of the antiaggregant peptide is used as the disrupter.[98,99] iAβ5 was shown to reduce plaque load by 51% in the amygdala of rats when co-injected with $A\beta_{1-42}$ (as compared to control rats injected with $A\beta_{1-42}$ alone). In both cases the disrupter group acts to prevent Aβ incorporating into aggregates, thereby arresting their growth.

Abrogation of *f*Aβ formation can also be achieved using peptidomimetic inhibitors which incorporate methylated amide nitrogens.[96,100–103] Here incorporation of methylated amide nitrogens about every second AA residue allows the inhibitor to incorporate into the β-sheet structure of growing *o*Aβs through amide H-bonding. Further incorporation of Aβ into inhibitor-

bound *o*Aβs is prevented due to an inability to hydrogen-bond to the methylated amides of the inhibitor. Alternatively inhibition of *f*Aβ can be achieved by substituting D-enantiomers in the place of naturally occurring L-amino acids;[79,96,104] again these achieve a therapeutic effect by inhibiting *m*Aβ incorporation into growing *o*Aβs. The all-D form of the peptidic inhibitor methyl-LVFFL-NH_2, known as PPI-1019 or Apan, has completed phase I and II human clinical trials.[103] It was found to be safe, well tolerated, and able to cross the BBB. Furthermore, administration of the compound led to increased levels of $Aβ_{1-40}$ in CSF, suggesting it may enhance clearance of Aβ from the brain into the CSF. Further studies showed that peptides such as the all-D-enantiomeric lflrr and yfllr were shown to completely inhibit *f*$Aβ_{1-40}$ formation and showed that: first, peptides consisting of non-natural amino acids have the capability of binding Aβ and preventing its assembly into amyloid fibrils; and second, that incorporation of a recognition sequence element was not essential to antifibrillogenic activity. This was the first indication that pharmacologically useful organic non-peptidomimetic molecules (with similar functional properties as peptidomimetic inhibitors) could potentially be developed as Aβ antiaggregants.[104]

1.2.2.3.2.2 Small-Molecule Inhibitors

In recent years a large number of structurally diverse small-molecule inhibitors of *f*Aβ formation have been added to the compendium of known antiaggregants – both naturally occurring compounds as well as a wide variety of synthetically derived compound can inhibit Aβ aggregation. Many structurally diverse plant-derived polyphenolic compounds which inhibit *f*Aβ formation are known and included various flavonoids (myricetin, morin, quercetin, kampferol, catechin, epicatechin, and epigallocatechin gallate),[105,106] benzoic acid derivatives (2,3-dihydroxybenzoic acid, 3,5-dihydroxybenzoic acid, gentisic acid and gallic acid),[107] tannic acid,[108] rosmarinic acid,[109] nordihydroquiaretic acid,[109,110] ferulic acid,[111] curcumin[109] and resveratrol;[112] Other natural products include melatonin,[113] nicotine,[114,115] β-carotene,[116] vitamin A (retinol, retinal and retinoic acid),[116,117] α-lipolic acid,[118] various tetracyclines[119] and anthrancyclines,[120] analogues of apomorphine,[53] dopamine,[53] norepinephrine,[53] glycosaminoglycans[121] and proteins

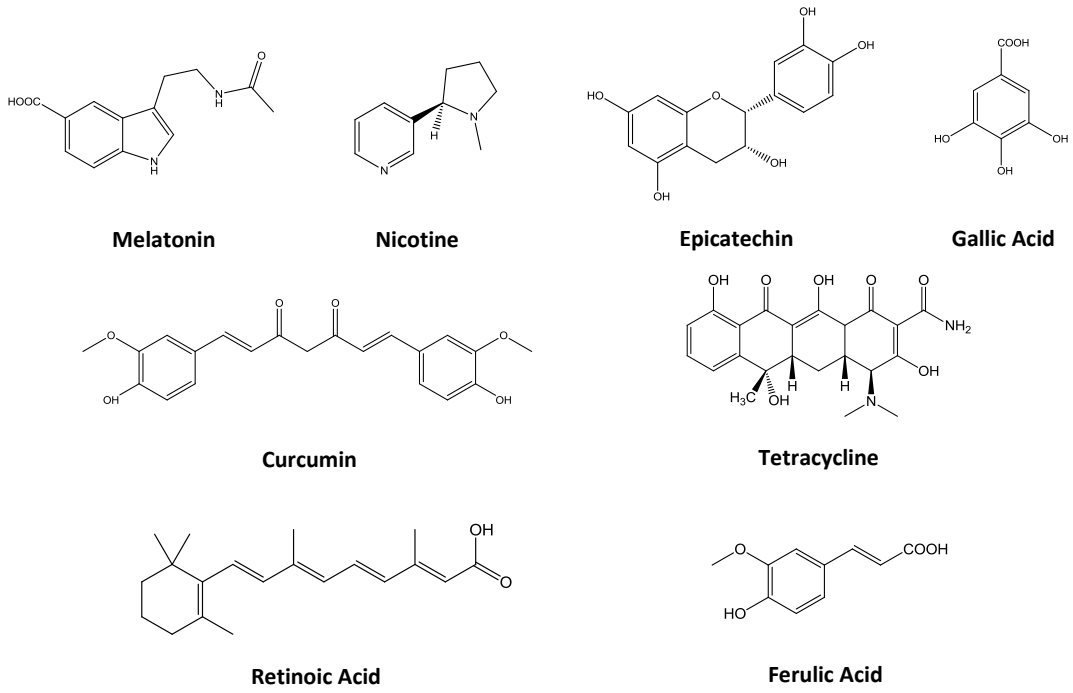

Figure 1.7 Natural product inhibitors of *f*Aβ formation.

such as apolipoprotein E[65,122,123] and laminin 1.[124,125] Some representative structures are presented in **Figure 1.7** and show the structural diversity of these naturally occurring antiaggregants.

Many synthetically derived inhibitors of *f*Aβ formation are also known and include drugs such as aspirin and other NSAIDs (celecoxib, rofecoxib, naproxen, ibuprofen and diclofenac – to name a few),[126–128] histological dyes and their derivatives such as RS-0406,[129] congo red,[130,131] chrysamine-G[130] and thioflavin T,[132] and a variety of imaging agents.[133,134] A large proportion of the synthetic antiaggregants are indole-based and include RO-7501,[135] indole 3-propionoic acid (Oxygon),[136,137] a variety of hydroxyindoles,[138] imidazopyridoindoles[139] and organofluorines;[140] other synthetic analogues include hexadecyl-N-methyl piperidinium bromide[141] 7-hydroxyquinolines analogues (including cliquinol),[142] N-phenyl anthranilic acid analogues[143] and acylated 3-aminopyrazoles[144,145]

Two small-molecule antiaggregants have made it to clinical trials: *scyllo*-inositol (AZD-103)[146] and 3-aminopropane-1-sulfonic acid (Alzhemed).[147] Both *scyllo*-inositol and Alzhemed have been shown to reduce Aβ plaque load and circulating Aβ levels in transgenic AD mice expressing human Aβ. *Scyllo*-inositol has been further shown to rescue memory deficits in

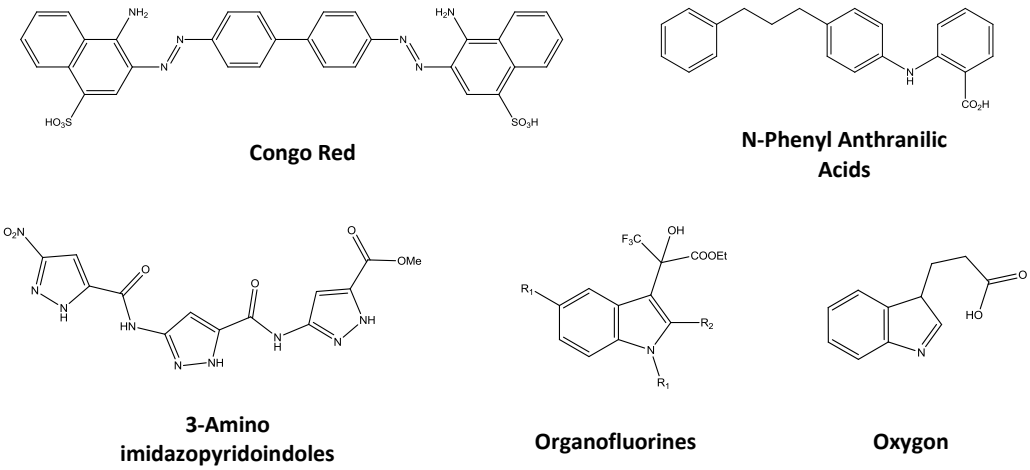

Figure 1.8 Some synthetic inhibitors of *f*Aβ formation.[130,136,140,143,144]

transgenic mice and in wild type mice following cerebroventricular injection of neurotoxic Aβ oligomers. Human clinical trials of *scyllo*-inositol continue, however a Phase III trial of Alzhemed planned in Europe was halted after the FDA deemed that an 18-month Phase III trial in the United States failed to demonstrate efficacy.

1. 3 Objectives Moving Forward

What form of Aβ is bound by these antiaggregants has yet to be seen. Aβ species exist *in vitro* and *in vivo* as a dynamic mixture of *m*Aβ, small *o*Aβs (dimers, trimers), large *o*Aβs (10-mers, 12-mers), protofibrils and *f*Aβs.[90] Antiaggregants may bind to all of these structures. However, it is possible that binding only occurs to a subset of these species. Although a variety of antiaggregants have shown excellent activity *in vitro* and *in vivo* uncertainty in their mechanism of action have impeded their further development as putative AD therapeutics; it is because of these uncertainties that the pharmaceutical industry has approached these compounds with much trepidation. Without a concise mechanism of action Aβ antiaggregants are well outside the comfort zone of most pharmaceutical research programmes. A greater effort is needed to tease out the mechanistic details of antiaggregant inhibition of *f*Aβ formation. A concise mechanism of action allows the use of rational drug design – without one medicinal chemistry programmes developing antiaggregants are doing so blindly. Only with a clear mechanistic picture will pharmaceutical research programs take notice of the potential of Aβ antiaggregants; considering this, a thorough analysis of the MoA for several classes of antiaggregant will be conducted here, in an effort to gain insight into the MoA of these potential therapeutic agents.

Chapter 2: An Assessment of 3-Hydroxyanthranilic Acid

2.1 Background

2.1.1 Aβ Conformation Confers Toxicity

Post mortem analysis of brain reveals a significant increase in amyloidogenic plaque in those individuals afflicted with severe cognitive impairment. Although Aβ plaque burden is one of the hallmarks of AD there is no definitive correlation between total CNS levels of monomeric Aβ and cognitive impairment. [17–21] Levels of soluble Aβ are virtually indistinguishable in those who are cognitively healthy from individuals with moderate and severe cognitive impairment, and the majority of epidemiological evidence suggests that the *m*Aβ alone is not responsible for neurotoxicity – a finding that is corroborated with substantial *in vitro* experimentation. [17–21] *m*$A\beta_{1\text{-}42}$ is devoid of toxicity in a number of studies;[148] furthermore, both *m*$A\beta_{1\text{-}40}$ and *m*$A\beta_{1\text{-}42}$ have been shown to be neuroprotective via several mechanisms.[148] Aβ may well be an immunogen of the innate immune system.[149] *o*Aβs are intermediates of fibril formation and are the suspected etiological agents in AD.[17–21] Given: first, the limited variability in soluble *m*Aβ levels in cognitively health individuals compared to those afflicted with AD; second, the correlation between *o*Aβs and AD progression; and finally, that β-sheet formation is requisite for Aβ toxicity, it was postulated by Weaver and co-workers that there may exist compounds, endogenous to the brain, that interfere with the self-association of Aβ. Endogenous compounds that interfere with Aβ self-association may address the underlying aetiology of AD progression directly, preventing the neurotoxic cascade associated with the disease and thereby mitigating disease progression and cognitive decline.

2.1.2 The "Promiscuous Drug" Concept

Although the amyloid β-peptide has been the focus of the discussion herein, a multitude of other structurally and functionally diverse proteins have likewise been implicated in themolecular pathogenesis of AD.[8] Indeed, Aβ is the main constituent but several unique proteins are found in amyloid plaques; considering this, Stephenson and co-workers identified a structural motif common to many proteins implicated in pathogenesis of AD.[150] It was postulated that a common receptor could then be exploited for the design of a "promiscuous drug," thereby enabling a "one-drug-multiple-receptors" therapeutic strategy for AD. The

common motif was deemed to be a BBXB peptide motif (where B is a basic residue and X is any other amino acid), which was identified in 27 of the 43 proteins investigated.[150] In Aβ the BBXB motif is HHQK (AA residues 13-16 of Aβ) and *in silico* simulations have suggested the HHQK motif may act as a receptor for small-molecule antiaggregants. Curcumin and resveratrol – both of which are known to be potent antiaggregants – show strong affinity for HHQK in *in silico* studies; these experiments predicting favorable HHQK-ligand interactions suggest that this potential mode of interaction for some antiaggregants may indeed be correct.[150]

2.1.3 In Silico Screening: BBXB-HHQK and CCM

Within the Weaver group, molecules with potential Aβ antiaggregant activity are identified via an *in silico* screen which has become an important aspect of rational drug design, particularly in academia and small biotechs as it is an excellent alternative to costly and laborious HTS efforts. *In silico* studies utilize models of *m*Aβ and *o*Aβ referred to as HHQK-BBXB and CCM, respectively. These models serve to identify targets that may potentially prevent or interrupt the aggregation process.

2.1.4 Indoleamine Metabolites Inhibit Aβ Aggregation

In previous work conducted by Claire and co-workers within the Weaver group, a library of 1109 compounds (endogenous to the human brain) was screened against HHQK-BBXB and CCM using manual docking. Initial screens identified the amino acid tryptophan as a preferred HHQK "hit" in both models. The observed binding energy of tryptophan to HHQK in the CCM model was comparable to those calculated for curcumin and resveratrol. Subsequent to *in silico* identification functional *in vitro* assays were used to experimentally evaluate the ability of tryptophan and selected metabolites to inhibit Aβ aggregation. Circular dichroism (CD) has been used extensively to monitor the changing secondary structure of *m*Aβ during aggregation.[90] In aggregating conditions α-helical *m*Aβ progresses to structures comprised primarily of β-sheets.[91] Nicotinic acid and 3-hydroxyanthranilic acid (3-HAA) were identified as modulators of Aβ aggregation, as coincubation of *m*Aβ with these compounds reduced the formation of β-sheet containing structures. NA and 3HAA are metabolites of Tryptophan via the kynurenine-nicotinamide adenine dinucleotide metabolic pathway (**Figure 2.1**), and it is interesting to note that both melatonin and nicotine (*in vivo* derivatives of tryptophan metabolism) have been previously described as inhibitors of Aβ aggregation.[113,114]

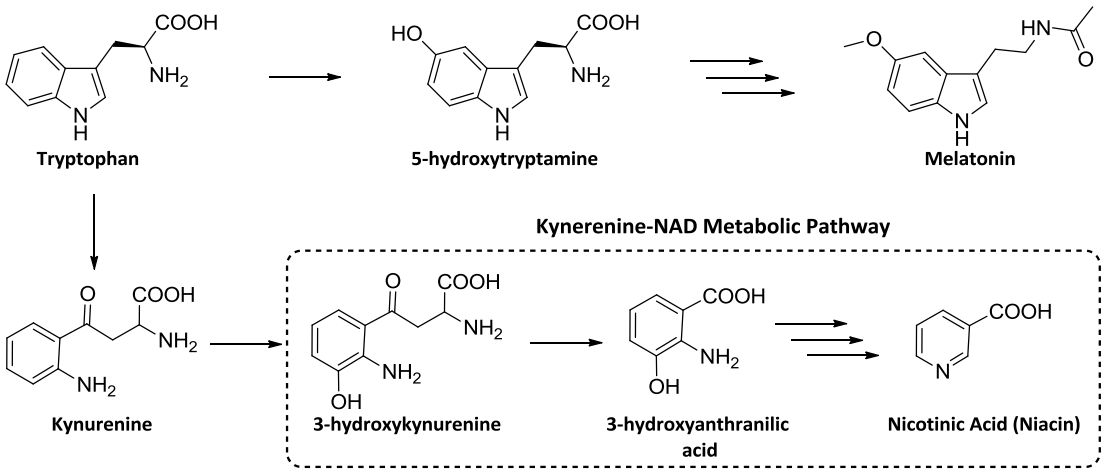

Figure 2.1 3HAA and nicotinic acid derived via the kynurenine-nicotinamide adenine dinucleotide metabolic pathway.

2.1.5 3-Hydroxyanthranilc Acid: a Platform for Drug Development

The objective of the research described herein is threefold: first, to identify a motif which confers antiaggregant activity; second, to develop novel class of compounds which will inhibit the aggregation of Aβ thereby decreasing or eliminating the formation of neurotoxic multimeric protein complexes; and finally, to gain insight into the mechanism of action of the developed antiaggregants. Previous studies have indicated that 3HAA may have the capacity to inhibit Aβ protein misfolding (a potentially disease-modifying action) and thus may be a biochemical platform for the design of a putative AD therapeutic. 3HAA is a small-molecule with a simple structure: an aromatic center consisting of a single benzene ring, functionalized at positions 1, 2, and 3 at by a carboxylic acid, an amine and a hydroxyl, respectively (**Figure 2.1**). 3HAA is significantly smaller than most antiaggregants described in the literature – it lacks the structural complexity of other classes of antiaggregants (such as histological dyes, peptides, vitamins and hormones). Given the simple structure of 3HAA analogues are easily selected

Table 2.1 A comparison of the molecular properties of 3HAA and with the criteria of druglike and leadlike compounds.

Property	Druglikeness	Leadlikeness	3HAA
MW (g/mol)	≤500	≤300	153.14
Log P	≤5	≤3	1.15
# H-bond Acceptors	≤10	≤3	4
# H-bond Donors	≤5	≤3	3

which differ in functional group composition (and position), and testing the relative activity of these compounds is a simple method to determine structural motif responsible for antiaggregant activity. 3HAA may be a well-suited lead in the development of novel Aβ antiaggregants as it satisfies the criteria of druglikeness proposed by Lipinski and co-workers;[151] furthermore, with the exception of H-bond acceptors, 3HAA meets most of the more stringent requirements of leadlikeness (**Table 2.1**).[152] Given its antifibrillogenic activity and structural simplicity, 3HAA certainly is a reasonable starting point in developing compounds with putative antiaggregant activity. Further studies will explore the diversity space of 3HAA as a platform for drug design. Analogues developed during lead optimization of 3HAA will be assessed for antifibrillogenic Aβ activity in an effort to develop a novel class of antiaggregants. With a series of structurally similar antiaggregants biological data from *in vitro* assays will be used to assess potency and *in silico* studies conducted to better understand the mechanism of action.

2.2 An Assessment of Antifibrillogenic Activity

2.2.1 The Thioflavin T Fibrillogenesis Assay

The ability of 3HAA to interfere with the conversion of *m*Aβ to structures with a β-sheet conformation (the initial step in aggregation) was demonstrated using CD on *m*$A\beta_{1-40}$ incubated with 3HAA. In the literature and in practice, Aβ antiaggregants are further assessed for their ability to interfere with the *f*Aβ formation; to this end the thioflavin T (ThT) fibrillogenesis assay has been developed.[155] ThT is a fluorescent benzothiazole dye commonly used in histological staining of amyloids, as it selectively binds *o*Aβs and *f*Aβs composed of β-sheets.[153,154] Upon binding fAβ, the excitation and emission wavelengths of ThT fluorescence undergo a characteristic shift ($\lambda_{Max(EX)}$=450 nm, $\lambda_{Max(EM)}$=482 nm). By irradiating Aβ incubated with ThT at 401 nm and observing the resulting fluorescence at 482 nm fibrillar protein may be selectively monitored. The methodology employed in the ThT assay will be discussed presently in brief, and a more detailed experimental methodology can be found in **Section 6.4.4** of the methodology chapter.

Aβ aggregation is a process which occurs *in vivo* and therefore it is of utmost importance that *in vitro* assessments of *f*Aβ formation mimic physiological conditions as closely as possible. ThT fibrillogenesis assay is employed at physiological temperature (37°C) and pH (7.4). In order to ensure consistency and reproducibility in the ThT fibrillogenesis assay care

must be taken to ensure that all Aβ is initially present as *m*Aβ. Fluorinated solvents are efficient disaggregators of amyloidogenic proteins and have been shown by CD and NMR spectroscopy to disaggregate *o*Aβs and *f*Aβs and stabilize α-helical *m*Aβ.[93] Before use in the ThT fibrillogenesis assay Aβ was taken up in hexafluoroisopropanol (HFIP), vortexed and sonicated to achieve full dissolution in order to disaggregate preformed oligomers; after disaggregation of Aβ the solvent subsequently was removed with a stream of argon gas prior to used (**Section 6.4.1**).

To assess *f*Aβ formation as a function of time Aβ aggregation was monitored via ThT fluorescence over the course of 72 h. Freshly disaggregated *m*$A\beta_{1\text{-}40}$ was taken up in tris(hydroxymethyl)aminomethane (Tris) buffer, adjusted to physiological pH and diluted with Tris buffer containing ThT (pH 7.4) – the resulting solution was ready for analysis and contained *m*$A\beta_{1\text{-}40}$ and ThT at concentrations of 20 μM and 4 μM, respectively. The tris-buffered *m*$A\beta_{1\text{-}40}$-ThT solution was separated into 3 aliquots and ThT fluorescence measured independently for each. Fluorescence measurements of ThT alone, in the absence of protein were taken concurrently to verify that change in fluorescence was due to *f*Aβ formation (**Figure 2.2**).

In the sample of containing *m*$A\beta_{1\text{-}40}$ the observed ThT fluorescence increases over the course of the experiment due to *f*Aβ formation. The minimum value of ThT fluorescence, F_{MIN}, is the observed ThT fluorescence in the absence of *f*Aβ (at this point only *m*Aβ is present in solution). At 12 h an increase in fluorescence is the first indication of *f*Aβ formation; by 72 h ThT fluorescence has reached a maximum value, F_{MAX}, indicating *f*Aβ formation is complete. ThT fluorescence remains constant throughout the course of the control experiment indicating that

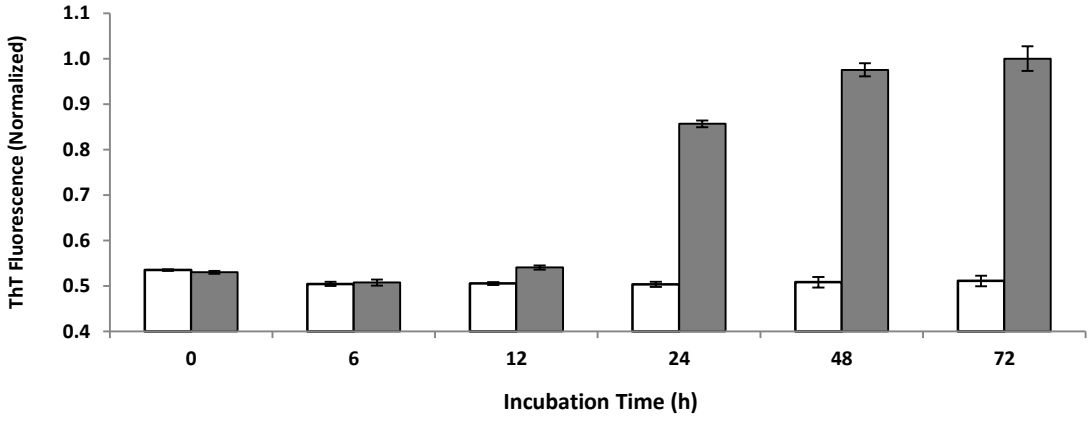

Figure 2.2 Time-course of ThT fluorescence of 4 μM ThT in the absence (white bars) and presence (grey bars) of 20 μM *m*$A\beta_{1\text{-}40}$ (± S.D. , n=3).

the increase in ThT fluorescence is due only to *f*Aβ formation. The change in the observed ThT fluorescence at completion of *f*Aβ formation, $\Delta F_{COMPLETE}$, is the difference of F_{MAX} and F_{MIN}:

$$F_{MAX} - F_{MIN} = \Delta F_{COMPLETE}$$

Equation 2.1 The total change in ThT fluorescence due to Aβ fibrillogenesis.

The ThT fluorescence at any time, *t*, (F_t) can be used to determine how far *f*Aβ formation has progressed. The change in ThT fluorescence at a given time, ΔF_t, is given by the difference of F_t and F_{MIN}:

$$F_t - F_{MIN} = \Delta F_t$$

Equation 2.2 The change in ThT Fluorescence due to Aβ fibrillogenesis at time, t.

Since ThT fluorescence is proportional to the amount of *f*Aβ present the ratio of ΔF_t and $\Delta F_{COMPLETE}$ gives the percent completion of *f*Aβ formation:

$$\frac{\Delta F_t}{\Delta F_{COMPLETE}} \times 100\% = Percentage\ of\ fA\beta\ completion$$

Equation 2.3 Percent completion of Aβ fibrillization at time, *t*.

The values for percent completion of *f*Aβ formation can thusly by calculated at each time point during *f*Aβ formation (using ThT fluorescence at 6 h and 72 h as F_{MAX} and F_{MIN}, respectively).

To assess the antifibrillogenic activity of 3HAA the ThT assay was conducted on freshly disaggregated $A\beta_{1\text{-}40}$ (prepared to a concentration of 20 μM) in the presence and absence of 50 μM 3HAA (**Figure 2.3**). After 48 h an increase in ThT fluorescence is observed in the sample of $A\beta_{1\text{-}40}$ incubated alone due to *f*Aβ. ThT fluorescence is reduced substantially in the $A\beta_{1\text{-}40}$ solution containing 50 μM 3HAA indicating a reduction in *f*Aβ formation. A significant change in ThT fluorescence was not observed for solutions containing 4 μM ThT, 50 μM 3HAA or 20 μM Aβ incubated alone; taken together, these results show that 3HAA readily inhibits Aβ fibrillogenesis.

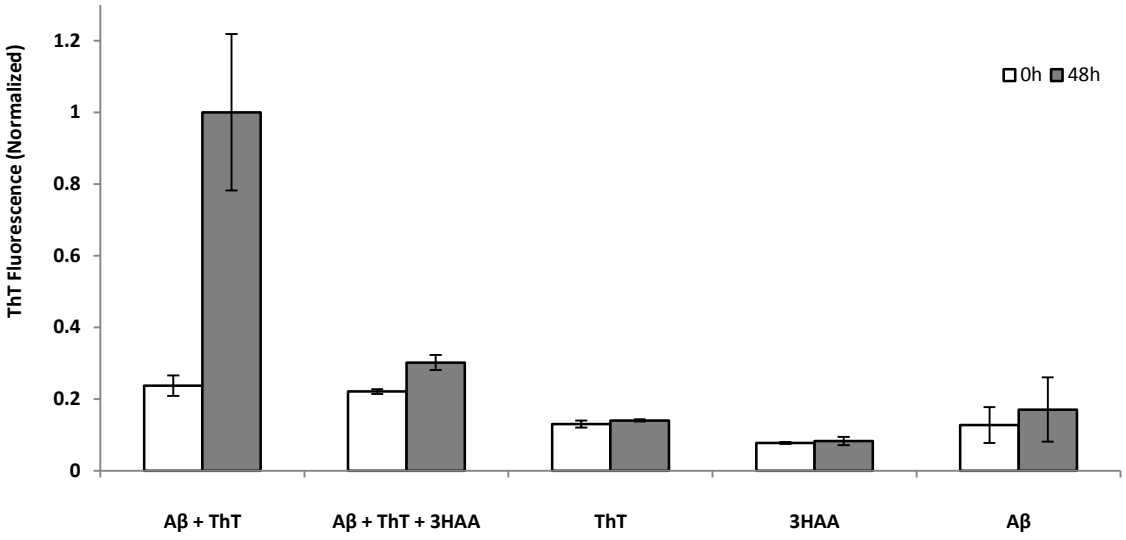

Figure 2.3 ThT Fluorescence of $A\beta_{1\text{-}40}$ incubated with ThT (Aβ + ThT); $A\beta_{1\text{-}40}$ incubated with 3HAA and ThT (Aβ + ThT + 3HAA); 3HAA alone (3HAA); ThT alone (ThT); and Aβ alone (Aβ). Initial fluorescence measurements (white bars) and fluorescence measurements at 48 h (grey bars) are given (± S.D., n=3).

The percentage of *f*Aβ formation in the $A\beta_{1\text{-}40}$ solution containing 3HAA (relative to the solution of $A\beta_{1\text{-}40}$ in the absence of compound) is determined by the ratio of the change in ThT fluorescence due to of *f*Aβ formation in the absence ($\Delta F_{(-)compound}$) and presence ($\Delta F_{(+)compound}$) of compound:

$$\frac{\Delta F_{(+)compound}}{\Delta F_{(-)compound}} \times 100\% = Percentage\ of\ fA\beta\ formation\ (\%fib)$$

Equation 2.4 The percentage of *f*Aβ formation in the presence of compound.

ThT fluorescence is generally assumed to be proportional to the amount of fibrillogenic material present.[155] By comparing the relative change in ThT fluorescence due to *f*Aβ formation in the absence and presence of 3HAA, it is calculated that at an incubation concentration of 50 µM 3HAA inhibits *f*Aβ formation in a solution of 20 µM $A\beta_{1\text{-}40}$ here by approximately 90%.

2.2.2 Dose Dependency of 3HAA inhibition of Aβ fibrillogenesis

By conducting the ThT fibrillogenesis assay at multiple concentrations the observed antifibrillogenic activity may be assessed as a function of compound concentration, so called dose dependency. The antifibrillogenic activity of 3HAA was assessed via the ThT fibrillogenesis

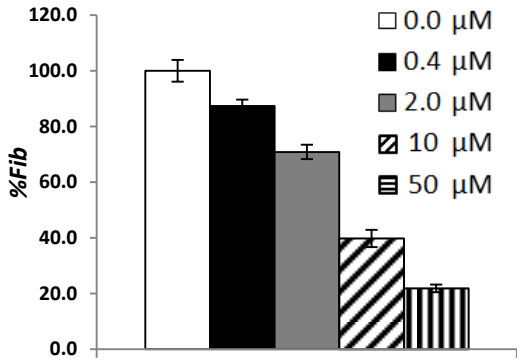

Figure 2.4 Values of *%Fib* (determined via the ThT fibrillogenesis assay) for the 20 µM $A\beta_{1\text{-}40}$ incubated alone and with 3HAA at various concentrations. (± S.D., n=3).

assay at four concentrations (0.4 µM, 2 µM, 10 µM and 50 µM) using 20 µM $A\beta_{1\text{-}40}$. The observed change in ThT fluorescence in the absence of compound (at 72h), $\Delta F_{(-)compound}$, corresponds to the change in fluorescence due to unimpeded *f*Aβ formation (100% *f*Aβ formation). The *%Fib* of the various $A\beta_{1\text{-}40}$ solutions are calculated from the $\Delta F_{(+)compound}$ at each concentration, and show that increasing the incubation concentration of 3HAA decreases the extent of the observed *f*Aβ formation in a dose dependent manner (**Figure 2.4**). At the highest incubation concentration, 50 µM, 3HAA inhibited *f*Aβ formation by 87.4%. 3HAA remained an efficacious antifibrillogenic compound even at the lowest concentration investigated, 0.4 µM, inhibiting *f*Aβ formation by 21.9% relative to the control.

2.2.3 Quantitation of Antifibrillogenic Activity

To better assess the relative antifibrillogenic potency of the compounds for comparison, their antifibrillogenic activity should be monitored at several concentrations. By plotting values for *%Fib* as a function of compound concentration (in µM) a dose response curve may be generated. Taking *%Fib* presented in **Figure 2.4** a dose response curve may be generated (**Figure 2.5**) by fitting with a sigmoid of the following form:

$$\%Fib_{(+)compound_{[x]}} = \frac{\%Fib_{(-)compound}}{1 + \left(\frac{[x_{(\mu M)}]}{IC_{50}}\right)^{b}}$$

Equation 2.5 The form of the sigmoidal function used to generate dose response curves from concentration dependent *%Fib* data generated using the ThT assay.

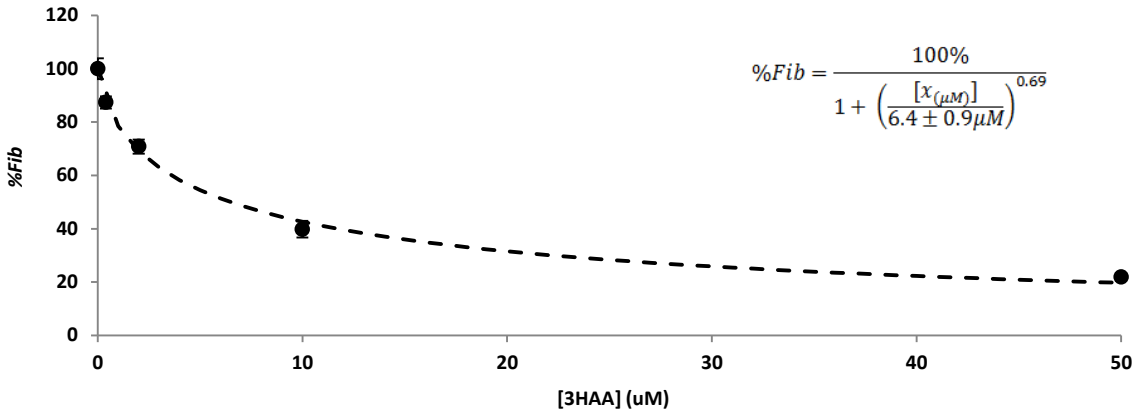

Figure 2.5 Dose response curve of 3HAA inhibition of *f*Aβ formation.

Here the *%Fib* of *f*Aβ formation in the presence of a compound at concentration, $[x_{(\mu M)}]$ (in units of μM) is denoted $\%\boldsymbol{Fib}_{(+)\boldsymbol{compound}_{[x]}}$, and is given as a function of the *%Fib* of Aβ in the absence of compound ($\%\boldsymbol{Fib}_{(-)\boldsymbol{compound}}$), the hill coefficient b (which determines that maximum slope of the sigmoid), $[x]$ and the half-maximal inhibitor concentration of complete *f*Aβ formation, or IC_{50}. The IC_{50} of a compound is the concentration at which it will reduce *f*Aβ formation by 50% as compared to a control in the absence of compound. Both b and the compounds IC_{50} are determined from the curve fit of dose response data. Fitting the %*Fib* data of Aβ in **Figure 2.4** it can be determined that 3HAA inhibits the formation of *f*Aβ with an IC_{50} of 6.4 ± 0.9 μM in this experiment.

2.2.4 IC_{50} as a Function of Aβ Concentration

The calculated values of IC_{50} for inhibition of *f*Aβ formation are sensitive to Aβ concentration. In **Figure 2.6** the IC_{50} for 3HAA inhibition of *f*Aβ formation (at 72h) is presented as a function of $A\beta_{1\text{-}40}$ concentration (μM). In order to directly compare determined IC_{50}'s from different assays great care must be taken in ensuring that experimental conditions are consistent experiment to experiment; this is somewhat problematic for Aβ. In our experience supplier estimations of peptide content are often inaccurate. Further confounding this issue is the fickle nature of Aβ solubility. Indeed, aliquots of Aβ from the same lot may behave differently when following an identical procedure. Solutions of disaggregated Aβ in aqueous buffer are sometimes cloudy due to the presence of insolubilized peptide; As such, solutions of Aβ are always filtered to ensure only solubilized Aβ is present during an assay. Consequently, the concentration of Aβ may be close to the desired concentration but may vary.

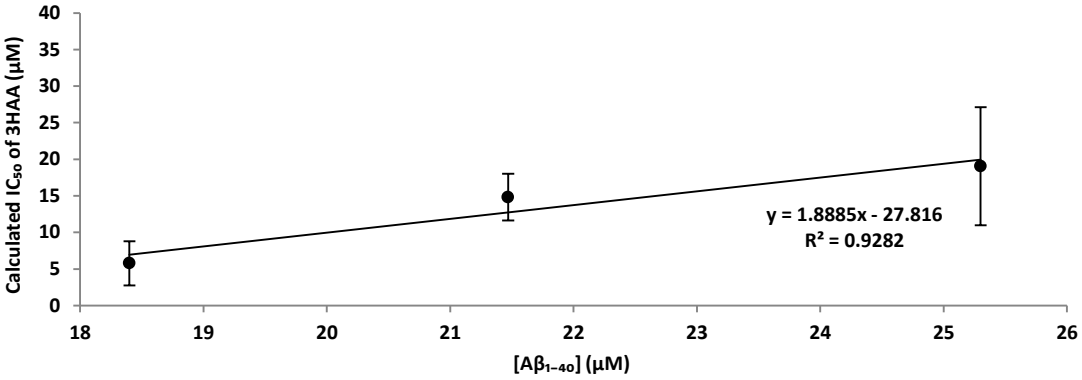

Figure 2.6 IC_{50} values (and their errors from curve fitting) of 3HAA inhibition of *f*Aβ formation as a function of $A\beta_{1\text{-}40}$ concentration.

In **Figure 2.6** all of the Aβ solutions were prepared from the same aliquot of $A\beta_{1\text{-}40}$, where dilution of $A\beta_{1\text{-}40}$ to the stated concentration was conducted after Aβ was disaggregated and filtered in preparation for the assay, in this way relative concentrations of $A\beta_{1\text{-}40}$ in each experiment are well known. The determined IC_{50} of 3HAA inhibition of *f*Aβ formation increases with $A\beta_{1\text{-}40}$ concentration. The relationship is roughly linear over the concentrations of $A\beta_{1\text{-}40}$ investigated (R^2=0.928) (**Figure 2.6**).

2.2.5 Reproducibility of IC_{50} Values of *f*Aβ Inhibition

Despite concerns of variability in $A\beta_{1\text{-}40}$ concentration during the ThT fibrillogenesis assay the determined IC_{50} of 3HAA inhibition of *f*Aβ typically varies only modestly between assays. In **Table 2.2** the calculated IC_{50} values (and their estimated errors from dose response fitting) of 3HAA inhibition of *f*Aβ formation after 75h are presented for 12 separate experiments. In each experiment $A\beta_{1\text{-}40}$ is at a concentration of 20 μM; again, this assumes that supplier estimations of peptide content are accurate and 100% of the peptide was solubilized and is present during the assay. The lowest observed IC_{50} was 3.3 ± 1.4 μM and 7.5 ± 3.3 μM the highest; the average observed IC_{50} is 5.3 ± 1.5 μM, where the presented error is the S.D. of the 12 averaged IC_{50} measurements. For the purpose of the work presented herein, this is taken as the IC_{50} of 3HAA inhibition of *f*Aβ formation in 20 μM $A\beta_{1\text{-}40}$.

Table 2.2 IC_{50} values of 3HAA inhibition of *f*Aβ formation from 20μM $Aβ_{1-40}$ solution for 12 experiments.

Run	IC_{50} (μM)
1	3.6 ± 0.3
2	3.3 ± 1.4
3	7.5 ± 3.2
4	4.6 ± 1.4
5	6.2 ± 2.4
6	6.4 ± 0.9
7	3.7 ± 1.9
8	4.1 ± 2.3
9	7.2 ± 0.9
10	5.7 ± 0.5
11	4.2 ± 2.0
12	6.7 ± 1.7

2.2.6 Normalization of IC_{50} Values of *f*Aβ Inhibition

As the measured IC_{50} value of inhibition of *f*Aβ formation varies from experiment to experiment a method to normalize the observed activities of antifibrillogenic compounds is needed. This will allow for a direct comparison of the antifibrillogenic activity of compounds determined from different runs of the ThT fibrillogenesis assay. Although absolute values of IC_{50} may change between assay runs, the relative activity of analyte compounds remains unchanged. Take for example IC_{50} values calculated for 3HAA and *o*-aminophenol from two separate runs of the ThT fibrillogenesis assay (**Table 2.3**). Although the absolute values of IC_{50} differ for both 3HAA and *o*-aminophenol when comparing runs, in both assays the relative activities of these compounds remains the same. In both runs the ratios of the determined IC_{50} for 3HAA and *o*-aminophenol are identical. By running 3HAA as a control during ThT analysis the obtained

Table 2.3 Comparison of the IC_{50} values for *f*Aβ inhibition by 3HAA and *o*-aminophenol determined from two separate runs of the ThT fibrillogenesis assay.

Run #	IC50 (μM)		$\frac{IC_{50}\ (o\text{-aminophenol})}{IC_{50}\ (3HAA)}$
	3HAA	*o*-aminophenol	
1	5.72 ± 0.50	5.51 ± 3.17	0.96 ± 0.56
2	7.47 ± 3.23	7.19 ± 4.03	0.96 ± 0.69

IC_{50} values may be normalized, and in this way the corrected IC_{50} values may be compared from separate experiments. To normalize the observed IC_{50} values the calculated IC_{50} of any compound is divided by the IC_{50} of 3HAA (concurrently run as a control)

$$\frac{Analyte\ IC_{50}}{3HAA\ IC_{50}} = \xi$$

Equation 2.6 The ratio of the determined IC_{50} values of inhibition of *f*Aβ formation of a compound of interest and the 3HAA control to give the activity ratio, ξ.

giving the ratio of activities, denoted here as ξ; multiplying ξ calculated for the analyte compound by the averaged value of IC_{50} for 3HAA (**Section 2.2.5**):

$$\xi\ x\ 5.3 \pm 1.5\ \mu M = Corrected\ IC_{50}$$

Equation 2.7 Correction of IC_{50} values for inhibition of *f*Aβ formation by multiplying the activity ratio by the averaged IC_{50} of 3HAA (*n*=12).

allows for a corrected IC_{50} to be determined, thereby allowing for direct comparison of IC_{50} values as determined in disparate runs of the ThT fibrillogenesis assay.

2.2.7 Comparison of 3HAA Antifibrillogenic Activity to Other Compounds

Above it is determined that 3HAA inhibits *f*Aβ formation with an IC_{50} value of 5.3 ± 1.2 µM; Taken at face value, this corresponds to a 40-fold decrease in activity compared to the most active compounds described in the literature.[110,156] However, one must be cautious when comparing measured IC_{50} values determined via the ThT assay to literature compounds.[93] The ThT fibrillogenesis assay has become a staple in antiaggregant development – it has become widely adopted and is a standard assay method for assessing inhibition of *f*Aβ formation,[90] but experimental conditions vary from one study to the next. Temperature, pH, buffer selection and Aβ concentration are but a few conditions that may be varied – and variations in assay format will invariability lead to differences in measured IC_{50} values (considering alone the large effect of Aβ concentration on the values of IC_{50} determined via the ThT fibrillogenic assay presented here); as such one should take care when making comparisons to literature assessments of antifibrillogenic activity. To better assess the relative potency of 3HAA to other compounds

described in the literature known antiaggregants were analyzed via the ThT fibrillogenesis assay (using 3HAA as a control to allow for direct comparison of activity).

2.2.7.1 Antifibrillogenic Polyphenols

Ono and coworkers have conducted detailed analyses of a vast array of polyphenolic compounds.[105,106,109] These surveys of antiaggregant activity include thorough analyses of Aβ antifibrillogenic activity using the ThT fibrillogenesis assay. The potency of 3HAA against *f*Aβ formation was directly compared to 8 of the most active compounds described by Ono and coworkers: rosmarinic acid, curcumin, resveratrol, epicatechin, quercetin, myricetin, kaempferol and epigallocatechin gallate (EGCG) (**Figure 2.7**). Each compound was incubated with solubilized $A\beta_{1\text{-}40}$ (prepared to a concentration of 20 μM) at four concentrations (0.4 μM, 2 μM, 10 μM and 50 μM) to allow IC_{50} values of *f*Aβ inhibition to be determined. To control, 20 μM $A\beta_{1\text{-}40}$ in the absence of compound was used. 3HAA was run concurrently at four concentrations (0.4 μM, 2 μM, 10 μM and 50 μM) with all compounds to allow for normalization of the determined IC_{50} values. All incubations were run in triplicate. F_{MIN} and F_{MAX} were taken at 1 h and 72 h after

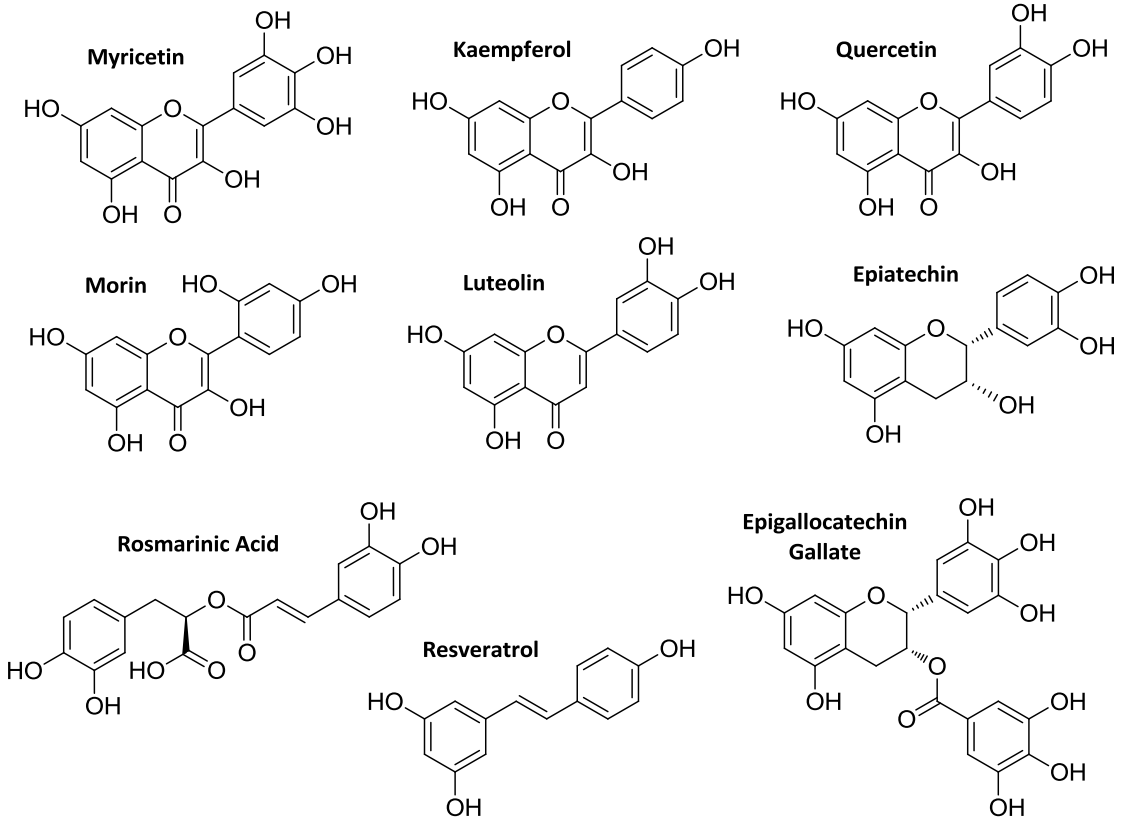

Figure 2.7 The structures of 9 polyphenolic antiaggregants analyzed via ThT.

Table 2.4 *%Fib* of 20 μM $A\beta_{1\text{-}40}$ incubated with various polyphenols as determined via the ThT fibrillogenesis assay (± S.D., *n*=3).

Exp.	Compound	*%Fib*											
		0.4μM			2.0μM			10μM			50μM		
1	**3HAA Control**	**88.6**	**±**	**13.9**	**68.6**	**±**	**8.1**	**42.5**	**±**	**5.0**	**9.3**	**±**	**3.3**
	Rosmarinic Acid	84.5	±	14.0	52.8	±	16.7	18.1	±	5.7	5.3	±	5.3
	Epicatechin	91.3	±	18.1	64.1	±	19.7	19.9	±	4.0	20.9	±	4.0
	EGCG	85.0	±	3.9	48.9	±	7.4	10.3	±	2.3	0.1	±	4.0
2	**3HAA Control**	**96.9**	**±**	**13.4**	**83.5**	**±**	**30.8**	**46.7**	**±**	**7.4**	**24.2**	**±**	**4.1**
	Quercetin	70.3	±	11.1	67.1	±	16.5	36.8	±	4.2	19.6	±	7.3
	Resveratrol	89.2	±	4.5	73.0	±	3.0	35.2	±	4.5	8.7	±	3.7
	Myricetin	93.1	±	29.1	63.8	±	6.2	20.7	±	3.1	4.9	±	3.2
3	**3HAA Control**	**56.5**	**±**	**11.5**	**49.6**	**±**	**4.4**	**21.0**	**±**	**3.7**	**16.9**	**±**	**4.7**
	curcumin	51.3	±	6.5	55.1	±	16.0	28.0	±	3.7	8.1	±	11.0
	Kaempferol	83.1	±	7.8	78.0	±	4.8	47.9	±	4.3	15.3	±	4.8
3	**3HAA Control**	**86.0**	**±**	**23.5**	**69.3**	**±**	**12.8**	**40.0**	**±**	**15.3**	**13.5**	**±**	**4.6**
	Luteolin	95.0	±	32.3	45.4	±	1.3	16.1	±	4.9	8.0	±	4.2
	Morin	70.0	±	29.0	62.7	±	18.5	32.7	±	4.8	14.6	±	0.2

incubation at 37°C, respectively and are the averages of fluorescence measurements taken in triplicate. The values of $\%Fib_{(+)compound_{[x]}}$ observed in the $A\beta_{1\text{-}40}$ incubations with each compound (as determined via **Equation 2.4**) is presented in **Table 2.4**.

All of the polyphenols investigated inhibited *f*Aβ formation in a dose-dependent manner (**Figure 2.8**). IC_{50} values for inhibition of *f*Aβ formation were calculated for all polyphenols and their respective 3HAA controls. Absolute and corrected values for IC_{50} of *f*Aβ inhibition are presented in **Table 2.5**. The order of observed activities is in good agreement with literature values for the polyphenols analyzed, although the activities as determined in the work herein are of an order of magnitude larger than those determined in the work of Ono and coworkers.[105,106,109] The difference in the observed magnitude of activity underscores the notion that making direct comparison of antifibrillogenic activities with literature is not good practice. Nevertheless, by running 3HAA concurrently with the polyphenols of investigation it is determined that the antifibrillogenic activity of 3HAA is of the same order of magnitude to the polyphenols analyzed; these are among the most potent small-molecule inhibitors of *f*Aβ

Table 2.5 IC_{50} values for *f*Aβ inhibition by polyphenol antiaggregants as determined via the ThT fibrillogenesis assay on 20μM $A\beta_{1\text{-}40}$.

Compound	IC_{50} (μM)	IC_{50} (3HAA Control) (uM)	ξ	Corrected IC_{50} (μM)
3HAA	-	-	-	**5.3 ± 1.5**
Rosmarinic Acid	2.2 ± 0.6	5.8 ± 1.2	0.4 ± 0.2	**2.0 ± 1.2**
Epicatechin	3.4 ± 1.6	5.8 ± 1.2	0.6 ± 0.4	**3.0 ± 2.2**
Epigallocatechin Gallate	1.8 ± 0.1	5.8 ± 1.2	0.31 ± 0.07	**1.6 ± 0.6**
Quercetin	4.4 ± 2.1	10.0 ± 2.0	0.4 ± 0.3	**2.3 ± 1.7**
Resveratrol	5.5 ± 0.5	10.0 ± 2.0	0.5 ± 0.2	**2.9 ± 1.6**
Myrecetin	3.2 ± 0.1	10.0 ± 2.0	0.3 ± 0.1	**1.7 ± 0.9**
Curcumin	1.1 ± 1.0	1.0 ± 0.6	1.1 ± 1.3	**5.6 ± 7.0**
Kaempferol	9.2 ± 2.7	1.0 ± 0.6	9.2 ± 7.3	**49 ± 41**
Luteolin	2.0 ± 0.4	5.5 ± 0.4	0.4 ± 0.1	**1.9 ± 0.8**
Morin	3.0 ± 0.7	5.5 ± 0.4	0.5 ± 0.1	**2.9 ± 1.0**

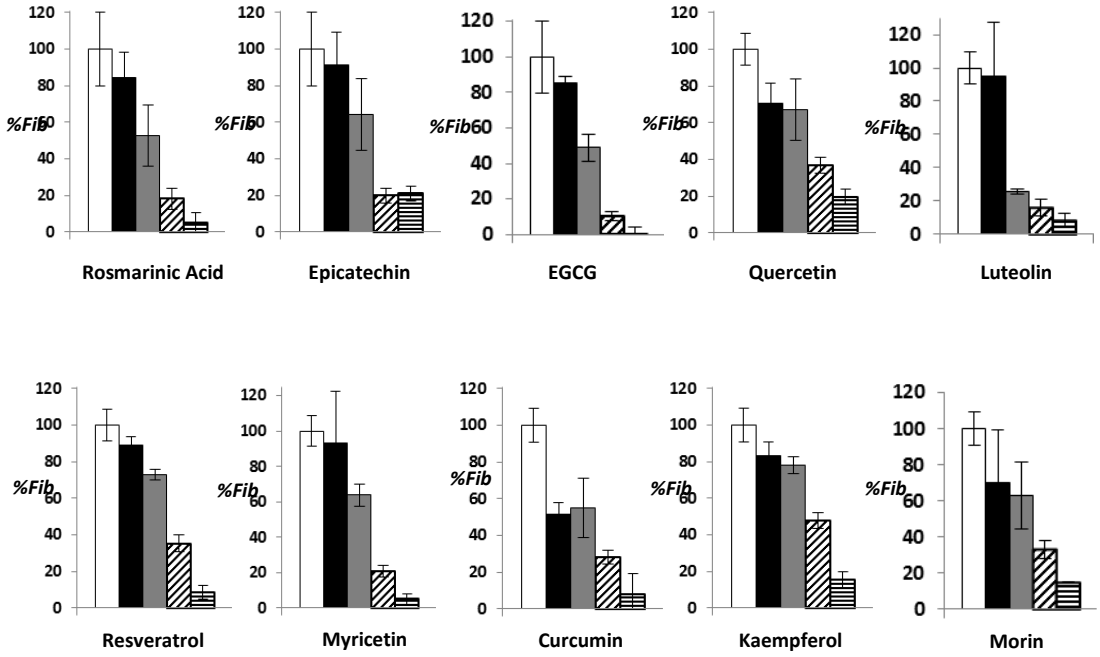

Figure 2.8 *%Fib* of 20 μM $A\beta_{1\text{-}40}$ incubated alone (what bars) and in the presence of various polyphenols at 0.4 μM (black bars), 2 μM (grey bars), 10 μM (diagonally stripped) and 50 μM (horizontally striped) as determined via the ThT fibrillogenesis assay (± S.D., *n*=3).

discussed in the literature. Although less potent than the majority of the polyphenols analyzed, 3HAA confers excellent activity in inhibiting *f*Aβ formation, and such further investigation of 3HAA as a potential platform for antiaggregant development is warranted.

2.3 An Assessment of Antioligomeric Activity

3HAA is a potent inhibitor of *f*Aβ formation, having an activity of the same order of magnitude as a series of plant-derived polyphenols – known high-potency inhibitors of *f*Aβ formation. Although the ThT fibrillogenesis assay has allowed for a determination of antifibrillogenic activity this assay alone gives little insight into the mechanism of action underlying the observed activity. Is 3HAA interacting with oligomeric precursors to *f*Aβ formation, or does it interfere with fibrillogenesis via interactions with elongating *f*Aβs directly? To address this question an assay is needed in which a quantitative assessment of oligomers of Aβ (*o*Aβ) is possible. A quantitative assessment of *o*Aβ may be achieved by a sandwich enzyme-linked immunosorbent assay (ELISA) developed by Levine and coworkers;[107] using this modified ELISA protocol the effect of 3HAA on preformed *o*Aβ may be investigated.

2.3.1 Sandwich ELISA

All compounds analyzed herein were assessed on their ability to dissociate preformed oligomers of $A\beta_{1\text{-}42}$; as with ThT fibrillogenesis assay all experiments are conducted in triplicate. Compounds were incubated overnight with preformed *o*$A\beta_{1\text{-}42}$ and were subsequently pipetted into a 96-well clear ELISA plate coated with Aβ-82E1 anti-human mouse immunoglobulin G monoclonal antibody (82E1). During the overnight incubation active compounds may dissociate preformed *o*Aβ into *m*Aβs. 82E1 binding is specific to amino acid residues 1-16 about the *N*-terminus of Aβ (DAEFRHDSGYEVHHQK) and will recognize and bind *m*Aβ and *o*Aβs. Once the various forms of Aβ have been captured via the plate-bound 82E1 capture antibody a detection antibody facilitates selective visualization of *o*Aβ. The detection antibody used here is *N*-terminally biotinylated Aβ-82E1 anti-human mouse immunoglobulin G monoclonal antibody (*bio*-82E1). Because 82E1 and *bio*-82E1 bind the same epitope about Aβ *bio*-82E1 is unable to interact with captured *m*Aβ as residues 1-16 are already bound to the capture antibody, 82E1. *o*Aβs possess unoccupied binding sites which are free to interact with *bio*-82E1. Detection of the capture antibody is facilitated with a streptavidin-horseradish peroxidase conjugate (STP-HRP). Streptavidin binding of the biotin tag affixed to the detection antibody ensures that HRP is

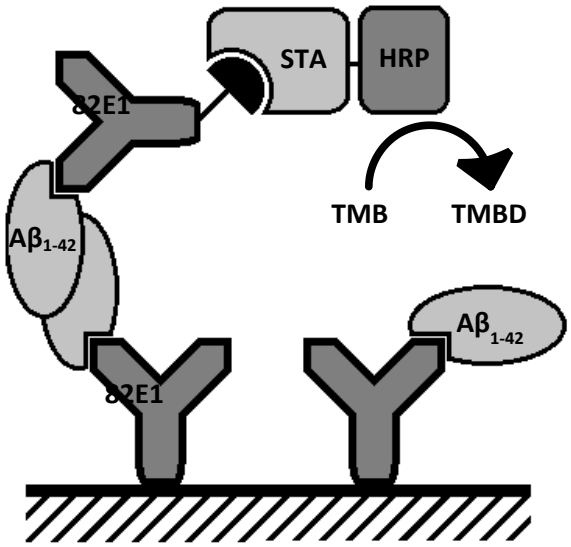

Figure 2.9 A schematic of the modified sandwich ELISA used to detect *o*Aβ.

secured only to captured *o*Aβs. Selective visualization of *o*Aβs is achieved via the addition of a substrate solution containing 3,3',5'5'-tetramethylbenzidine (TMB), which in turn is oxidized by HRP into 3,3',5,5'-tetramethylbenzidine diamine (TMBD). Addition of acid halts HSP oxidation of TMB to the oxidation product, TMBD, and the solution adopts an intense yellow colour (λ_{MAX}=450nm).[157] By selectively monitoring absorbance at a wavelength of 450nm the relative concentration of TMBD can be determined in each experiment and is directly related to the presence of *o*Aβ – the higher the concentration of *o*Aβ the higher the absorbance observed (at 450 nm) due to TMBD.

2.3.1.1 Assessment of 3HAA with Sandwich ELISA

Oligomers of $A\beta_{1-42}$ were prepared as described in **Section 6.4.3.1** and diluted to a final analysis concentration of 10 nM, and were incubated with a 10 µM of each 3HAA, anthranilic acid (AA) and 3 positional isomers of dihydroxybenzoic acid (DHB) overnight in a 96-well clear ELISA plate. Incubated solutions of *o*$A\beta_{1-42}$ with compound were then pipetted to another plate pre-adsorbed with 82E1 antibody for capture. Detection of *o*$A\beta_{1-42}$ was achieved by the addition of a *bio*-82E1 detection antibody followed by STP-HRP. TMB oxidation by HRP allowed for visualization of *o*$A\beta_{1-42}$. Due to the single-site assay format *o*$A\beta_{1-42}$ was selectively visualized by monitoring TMBD absorbance at 450 nm. The reported absorbances are the average of the three separate measurements conducted on incubations run in triplicate. For a more detail protocol used in the sandwich ELISA refer to **Section 6.4.3**. Compared to the control

Table 2.6 Absorbance (450nm) due to captured *o*Aβ_{1-42} from oligomer solutions incubated overnight with 3HAA and other acids at a concentration of 10 µM (S.D., *n*=3).

Compound	Absorbance (450nm)	Absorbance (450nm) as % of Control
Blank	0.066 ± 0.001	-
Control	0.38 ± 0.01	**100 ± 3**
3HAA	0.21 ± 0.01	**44 ± 4**
AA	0.36 ± 0.03	**92 ± 9**
2,5-DHB	0.14 ± 0.01	**24 ± 3**
2,3-DHB	0.23 ± 0.02	**52 ± 6**
3,5-DHB	0.39 ± 0.01	**102 ± 3**

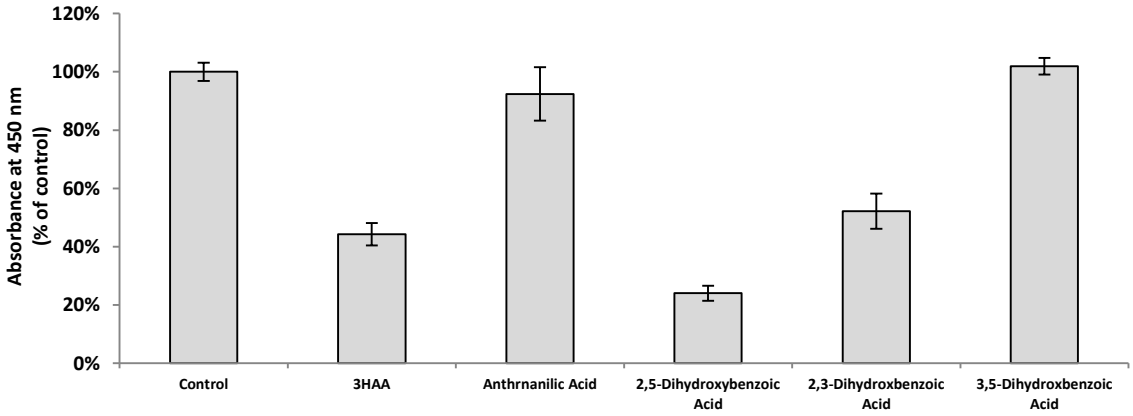

Figure 2.10 Absorbance (450 nm) due to captured *o*Aβ_{1-42} from oligomer solutions incubated overnight with 3HAA and other acids at a concentration of 10 µM (S.D., *n*=3).

(*o*Aβ_{1-42} incubated in the absence of compound) incubation with 3HAA caused a 65% decrease in the observed absorbance at 450 nm (**Table 2.6** and **Figure 2.10**) as compared to anthranilic acid which only decreased absorbance by 8%. To ensure these results were accurate three positional isomers of dihydroxybenzoic acid (DHB) were run concurrently for comparison to work described by Levine and coworkers. [107] The antioligomeric activity of the three isomers was determined to be 2,5-DHB > 2,3-DHB > 3,5-DHB (the latter being completely inactive) and is in complete agreement with the published results.[107]

2.3.1.2 Comparison of 3HAA to Polyphenols

The antioligomeric activity of the several polyphenols was measured via a sandwich ELISA for comparison to 3HAA. Activity of *o*Aβ disassembly was determined for the

Table 2.7 Absorbance (450 nm) due to captured *o*A$\beta_{1\text{-}42}$ from oligomer solutions incubated overnight with various polyphenols at a concentration of 10 µM (S.D., *n*=3).

Compound	Absorbance (450nm)	Absorbance as % of Control
Control	0.38 ± 0.01	**100 ± 3**
3HAA	0.21 ± 0.01	**44 ± 4**
Kaempherol	0.11 ± 0.01	**12 ± 3**
Quercetin	0.21 ± 0.03	**44 ± 11**
Epigallocatechin Gallate	0.23 ± 0.01	**53 ± 3**
Morin	0.24 ± 0.01	**54 ± 2**
Rosmarinic Acid	0.24 ± 0.11	**55 ± 35**
Resveratrol	0.32 ± 0.04	**79 ± 12**
Apigenin	0.32 ± 0.02	**80 ± 5**
Myricetin	0.35 ± 0.01	**89 ± 3**
Luteolin	0.39 ± 0.03	**104 ± 9**
Epicatechin	0.45 ± 0.03	**122 ± 9**
Naringenin	0.56 ± 0.03	**155 ± 9**
Hesperitin	0.59 ± 0.03	**166 ± 11**
Curcumin	0.83 ± 0.04	**242 ± 12**

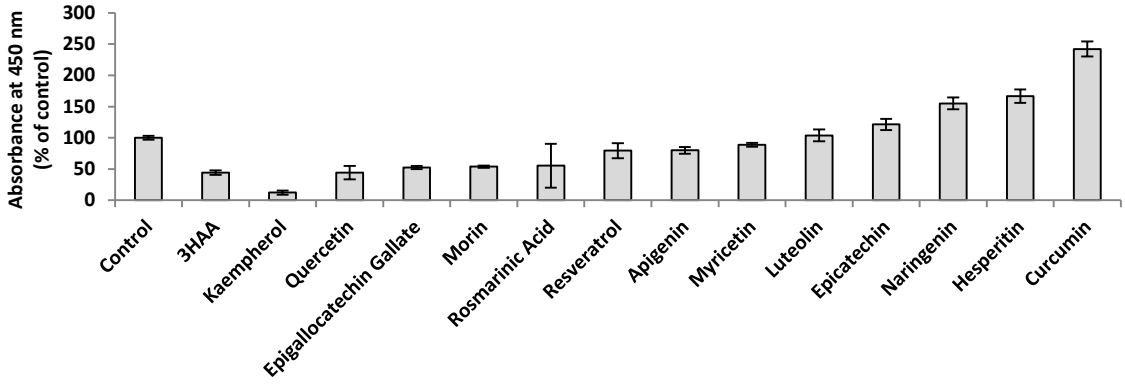

Figure 2.11 Absorbance (450 nm) due to captured *o*A$\beta_{1\text{-}42}$ from oligomer solutions incubated overnight with various polyphenols at a concentration of 10 µM (S.D., *n*=3).

aforementioned polyphenols as well as morin, hesperetin, naringenin, luteolin and apigenin following the same procedure as presented in **Section 2.3.1.1**.

Of the polyphenols analyzed kaempferol most actively dissociated *o*A$\beta_{1\text{-}42}$ with a measured absorbance of only 12 ± 3% that of the control; with a measured absorbance of 44 ± 11%, quercetin dissociation of *o*A$\beta_{1\text{-}42}$ was equivalent to 3HAA. Interestingly, all of the other polyphenols analyzed via the sandwich ELISA conferred less activity in dissociating *o*A$\beta_{1\text{-}42}$ than 3HAA (**Table 2.7** and **Figure 2.11**). With a measured absorbance of 104 ± 9% the flavanol

Luteolin was ineffective against *o*A$\beta_{1\text{-}42}$ dissociation; epicatechin, naringenin, hesperitin and curcumin all had measured absorbances significantly greater than the control, a result consistent with increasing the relative abundance of *o*A$\beta_{1\text{-}42}$ (as compared to the control). This effect was particularly significant in the case of curcumin whose measured absorbance was nearly 2.5-fold larger than the control.

2.4 Validation of 3HAA for Further Development

3HAA was assessed both for its effect on *f*Aβ formation as well as its effect on preformed *o*Aβs using the ThT fibrillogenesis assay and sandwich ELISA assay, respectively. With an IC_{50} value of 5.3 ± 1.5 μM for inhibition of *f*Aβ formation, 3HAA possesses activity similar to several known plant-derived polyphenol antiaggregants, which were also assessed here using the ThT fibrillogenesis assay; although 3HAA is slightly less active than these compounds, its activity is of the same order of magnitude, making it one of the most potent endogenous antifibrillogenic agents known, with respect to Aβ. Additionally, 3HAA is a potent disassembler of *o*Aβs as determined from overnight incubations of 3HAA with preformed *o*Aβs analyzed using a sandwich ELISA assay; in this regard, 3HAA was more active than all of the polyphenols assessed here with the exception of kaempferol. Taken together, the potent antifibrillogenic and antioligomeric activity of 3HAA observed here has served to validate 3HAA as an excellent scaffold for further development in an effort to create novel Aβ antiaggregants.

Chapter 3: Optimization of 3HAA

3.1 Defining an Antiaggregant Motif

Unlike most antiaggregants found in the literature 3HAA has a very simple scaffold; as such its potent antifibrillogenic activity must an artifact of its functional groups and their substitution pattern about the benzene ring. In working towards defining a potential antiaggregant motif first the minimal functional group requirements that confer antiaggregant activity must be investigated. The three functional groups about 3HAA – namely the carboxylic acid, amine and hydroxyl group – may all be required for activity. Alternatively, the underlying activity may be due to the presence of a single functional group, or a combination of two of 3HAAs three functional groups. The minimal functional requirements for antiaggregant activity can be probed by running 3HAA analogues with one or more of these groups removed (**Figure 3.1**). Benzoic acid, aniline and phenol each possess one of the functional groups about 3HAA; AnA, *o*-aminophenol and *m*-hydroxybenzoic acid each possess two of the three functional groups of 3HAA substituted about the phenyl ring as in 3HAA. The relative activities of the six functional analogues of 3HAA were assessed via a ThT fibrillogenesis assay, thereby providing insight into the functionality which confer the observed activity of 3HAA. By conducting the ThT fibrillogenesis assay at multiple concentrations the observed activity of antifibrillogenic compounds may be assessed as a function of compound concentration.

Each compound was incubated with solubilized $A\beta_{1\text{-}40}$ (prepared to a concentration of 20 μM) at four concentrations (0.4 μM, 2 μM, 10 μM and 50 μM) to assess the dose dependency of inhibition of *f*Aβ formation. 20 μM $A\beta_{1\text{-}40}$ in the absence of compound served as the control. 3HAA was run concurrently at four concentrations (0.4 μM, 2 μM, 10 μM and 50 μM) with all compounds to allow for comparison. All incubations were run in triplicate. F_{MIN} and F_{MAX} were taken at 1 h and 72 h after incubation at 37°C, respectively and are the averages of fluorescence

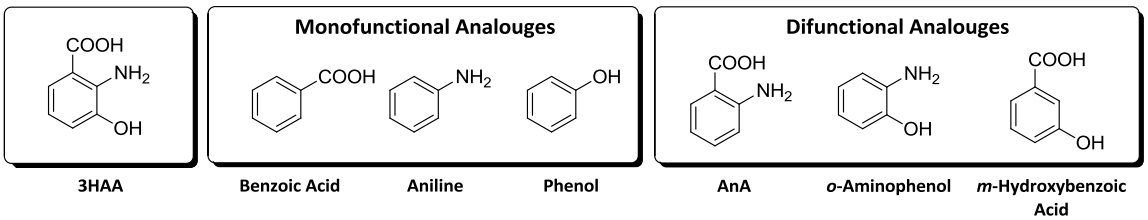

Figure 3.1 3HAA shown in comparison to functionally simplified analogues thereof.

Table 3.1 *%Fib* of 20 µM $A\beta_{1\text{-}40}$ after 72 h incubations with 3HAA, its 3 monofunctionalized analogues (benzoic acid, aniline and phenol) and its 3 difunctionalized analogues (*m*-hydroxybenzoic acid, anthranilic acid, and *o*-aminophenol) (± S.D., *n*=3).

Compound	*%Fib* (± S.D.)			
	0.4 µM	2.0µM	10 µM	50 µM
3-Hydroxyanthranilic Acid	92 ± 4	59 ± 3	35 ± 4	19 ± 3
Benzoic Acid	99 ± 14	103 ± 14	102 ± 2	87 ± 17
Aniline	104 ± 12	103 ± 2	110 ± 4	105 ± 9
Phenol	90 ± 5	95 ± 7	98 ± 14	91 ± 4
m-Hydroxybenzoic Acid	102 ± 20	87 ± 3	82 ± 5	84 ± 4
Anthranilic Acid	77 ± 3	87 ± 14	87 ± 14	86 ± 10
o-aminophenol	74 ± 4	67 ± 2	42 ± 13	4 ± 2

measurements taken in triplicate. The values of $\%Fib$ observed in the $A\beta_{1\text{-}40}$ incubated with each compound was calculated at all ligand incubation concentrations (**Table 3.1**).

3HAA prevented the formation of *f*Aβ in a dose dependent manner (**Figure 3.2**). The three monofunctionalized analogues (benzoic acid, aniline and phenol) were mostly inactive although at a concentration of 50 µM benzoic acid and phenol slightly inhibit *f*Aβ formation (87% and 91%, respectively), this same activity was achieved by 3HAA at a concentration of 0.4 µM (a 125 x decrease in concentration). The comparatively negative result of all three monofunctionalized analogues suggests that, on their own, none of the three functionalities about 3HAA confer significant antifibrillogenic activity. The three difunctionalized analogues – AnA, *o*-aminophenol and *m*-hydroxybenzoic acid – were subsequently analyzed for antifibrillogenic activity. At all concentrations (with the exception of 0.4 µM *m*-hydroxybenzoic acid) both *m*-Hydroxybenzoic acid and AnA showed a slight decrease in *f*Aβ relative to the control, although the decrease in *f*Aβ formation did not change with increasing dose. Dose dependent inhibition of fibrillogenesis was achieved by incubating Aβ with *o*-aminophenol.

Incubation of $A\beta_{1\text{-}40}$ with *o*-aminophenol at a concentration of 50 µM results in an almost complete abrogation of *f*Aβ formation (4%, relative to control), an improvement over 3HAA at the same concentration; even at a concentration as low as 0.4 µM *o*-aminophenol inhibits fibrillogenesis by 24%. The increased antifibrillogenic activity of *o*-aminophenol relative to the 5 other functional analogues of 3-HAA is an indication of the importance of the aminophenol motif in the observed activity of 3HAA.

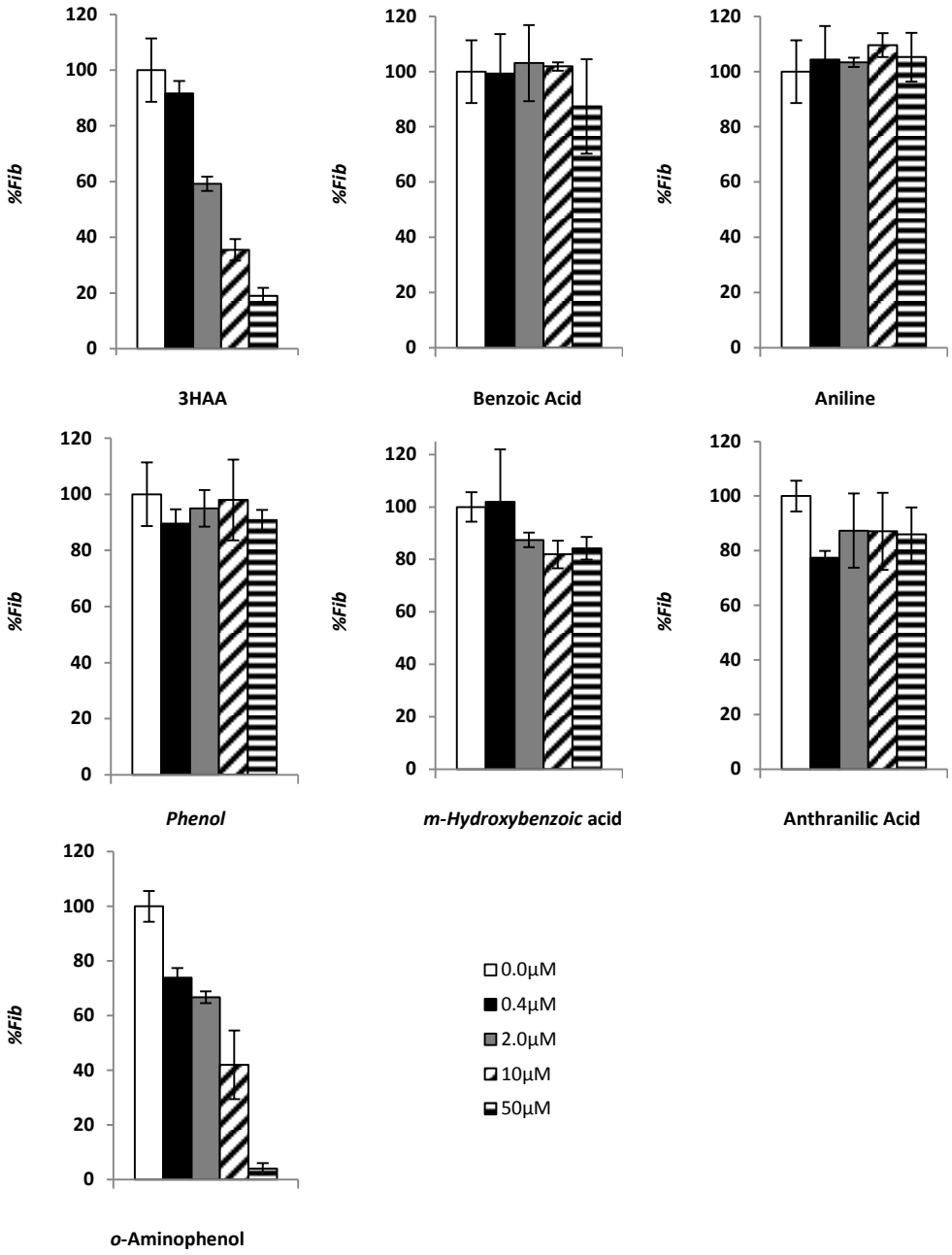

Figure 3.2 *%Fib* of 20 µM $A\beta_{1\text{-}40}$ incubated in the absence (white bars) and presence of 3HAA or simplified analogues at 0.4 µM (black bars), 2 µM (grey bars), 10 µM (diagonally stripped) and 50 µM (horizontally striped) (± S.D., *n*=3).

3.1.1 Assessment of *o*-Aminophenol

3.1.1.1 Substitutions of the Hydroxyl Group

Of the 6 functional analogues of 3HAA tested via the fibrillogenesis assay only *o*-aminophenol showed significant dose dependent antifibrillogenic activity. To further assess the antifibrillogenic activity conferred by the aminophenol motif the role of the hydroxyl was probed by assessing analogues of *o*-aminophenol in which the hydroxyl was outright substituted by another functional group or modified by alkylation or arylation (**Figure 3.3**). All of the analogues tested were commercially available and were assessed for antifibrillogenic activity via the ThT fibrillogenesis assay at a concentration of 10 μM and their $\%Fib$ relative to $A\beta_{1\text{-}40}$ in the absence of compound calculated (**Table 3.2**). At 10 μM *o*-aminophenol inhibits *f*Aβ formation by 58%, but replacement of the hydroxyl group by a carboxylic acid (as with AnA) resulted in poor activity – an indication that antifibrillogenic activity is sensitive to outright replacement of the hydroxyl. Replacement of the hydroxyl group by chlorine, bromine, ethyl, or amine resulted in a complete abrogation of antifibrillogenic activity ($\%Fib$ for *o*-bromoaniline, *o*-chloroaniline, *o*-ethylaniline and *o*-phenylenediamine of 90%, 103%, 95%, and 84% respectively) and is a further indication of the importance of the hydroxyl in the aminophenol motif.

o-Anisidine, *o*-phenetidine and *o*-phenoxyaniline are analogues of *o*-aminophenol in which the hydroxyl hydrogen has been replaced by a methyl group, ethyl group and phenyl ring, respectively. Of the three analogues with hydroxyl hydrogen replacements *o*-phenetidine was the only compound which was completely inactive when compared to the control (**Figure 3.4**). *o*- Anisidine and *o*-phenoxyaniline with a $\%Fib_{(+)compound}$ of 78% and 71%, respectively, show

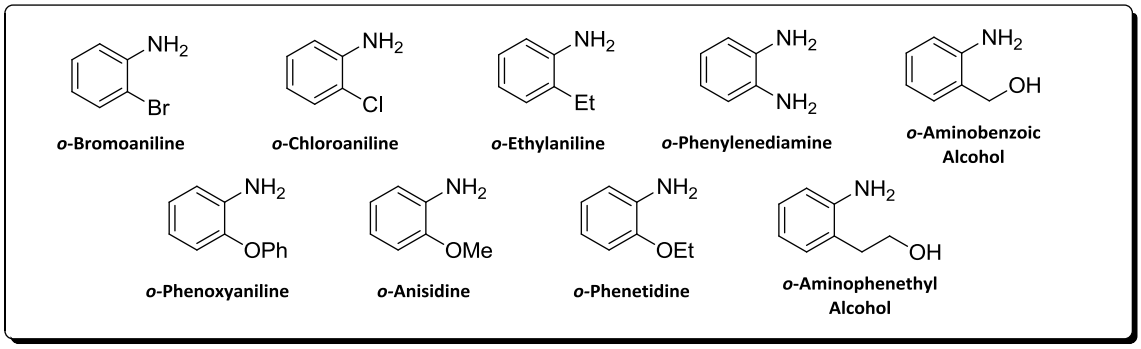

Figure 3.3 Structures of *o*-aminophenol analogues with hydroxyl replacement.

Table 3.2 The *%Fib* of 20 μM $A\beta_{1-40}$ incubated with *o*-aminophenol analogues (with hydroxyl replacement) (±S.D., *n*=3).

Compound	*%Fib*		
***o*-Aminophenol**	***42***	***±***	***13***
Anthranilic acid	***87***	***±***	***14***
o-Chloroaniline	103	±	14
o-Bromoaniline	90	±	3
o-Ethylaniline	95	±	21
o-Phenylenediamine	84	±	17
o-Anisidine	78	±	6
o-Phenetidine	121	±	6
o-Phenoxyaniline	71	±	11
o-Aminobenzoic alcohol	85	±	18
o-Aminophenethyl alcohol	100	±	14

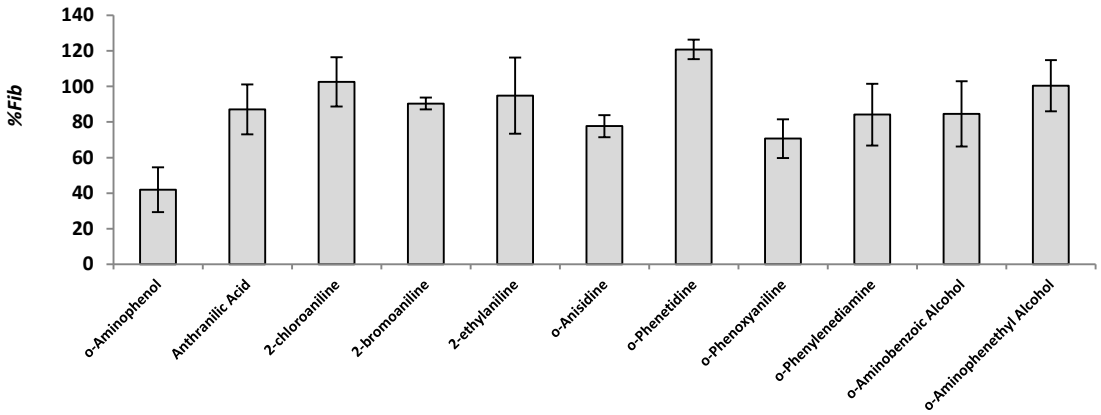

Figure 3.4 The *%Fib* of 20 μM $A\beta_{1-40}$ incubated with *o*-aminophenol analogues (with hydroxyl replacement) (±S.D., *n*=3).

moderate activity and suggest that perhaps replacement of the hyroxyl hydrogen may indeed produce analogues which maintain some antifibrillogenic activity. *o*-Aminobenzoic alcohol and *o*-aminophenethyl alcohol are analogues of *o*-aminophenol wherein the hydroxyl group is extended from the central ring using a carbon linker containing one and two methylene subunits, respectively. Both *o*-Aminobenzoic alcohol and *o*-aminophenethyl alcohol are inactive, indicating that the alcohol must be directly affixed to the ring to maintain antifibrillogenic activity.

Taken together the analogues of *o*-aminophenol tested here show antiaggregant activity is sensitive to modifications to, or outright replacement of, the hydroxyl and give further insight

into the nature of the aminophenol motif. Hydroxyls are excellent hydrogen-bond donors and hydrogen-bond acceptors, which may be key contributors and allow the aminophenol motif to interact non-covalently with Aβ. Replacement of the hydroxyl with groups which are weakly hydrogen-bond accepting (Cl and Br) or do not act as hydrogen-bond acceptors at all (ethyl) results in complete loss of antifibrillogenic activity. In AnA and *o*-phenylenediamine the hydroxyl is replaced with a carboxylic acid and amine, respectively, both of which are able to act as hydrogen-bond acceptors, but both of these compounds are inactive indicating that fibrillogenic activity is not easily predicted based on activity as a hydrogen-bond acceptor.

Analogues of *o*-aminophenol in which the hydroxyl hydrogen has been replaced are unable to interact via hydrogen-bond donation (H^D) interactions. *o*-Phenetidine was completely inactive; however *o*-Anisidine and *o*-phenoxyaniline display moderate activity suggesting that the ability to interact via hydrogen-bond acceptance (H^A) may also serve as an important mechanism of interaction. Finally, the inactivity of *o*-aminobenzoic and *o*-aminophenethyl alcohols suggests that the hydroxyl must be directly affixed to the central ring. With a better understanding of hydroxyl's role in the aminophenol motif, analogues which explore the role of amine were subsequently investigated.

3.1.1.2 Substitutions of the Amine

To further assess the antifibrillogenic activity conferred by the aminophenol motif the role of the amine was probed by assessing analogues of *o*-aminophenol in which the amine was outright substituted by another functional group or modified by alkylation or arylation (**Figure 3.5**). A few of the analogues of interest were commercially available; however some of the analogues to be tested were synthesized, purified and characterized using standard synthetic organic methods. Compounds which were synthesized for analysis are identified by a unique alphanumerical code ('GS-' followed by a four-digit numeric code). Detailed synthetic methods are found in **section 6.2** of the methodology chapter. As with the hydroxyl replacement analogues of aminophenol all amine replacement analogues were assessed for antifibrillogenic activity via the ThT fibrillogenesis assay at a concentration of 10 μM and their percent fibrillization relative to Aβ in the absence of compound calculated (**Table 3.3**).

Analogues in which the amine has been replaced by a carboxylic acid, a methyl group, or chlorine (salicylic acid, *o*-methylphenol, and *o*-chlorophenol, respectively) were devoid of antifibrillogenic activity – these groups were also unable to be substituted for a hydroxyl in the analogues tested above. Replacement of the amine by a nitro group also resulted in abrogation of activity. GS-1019, wherein the amine is extended from the central ring of aminophenol (analogous to hydroxyl replacement analogues *o*-aminobenzoic alcohol and *o*-aminophenethyl alcohol) was also inactive. Catechol – the analogue in which the amine is replaced by a hydroxyl – maintains antifibrillogenic potency, making hydroxyl the only functional group tested that was a suitable replacement for the amine. The methyl and benzyl esters of catechol, GS-1031 and GS-1033, were substantially less active than catechol, but did maintain partial activity (91% and 81%, respectively).

The hydroxyl analogues discussed above provided some insight into the role of H^D and H^A interactions. The final three analogues – GS-1044, GS-1047 and GS-1048 – were not outright substitutions of the amine, but were modifications thereof to probe the effect of modifying the amine's ability to act through H^D and H^A interactions. The N-methyl (GS-1047) and N,N-dimethyl (GS-1048) analogues of *o*-aminophenol contain an amine, which is still able to act through H^A interactions, but replacement of amine protons with methyl groups would limit their H^D ability; even so, both GS-1047 and GS-1048 maintain antifibrillogenic potency compared to *o*-aminophenol – suggesting that an amine's ability to interact via H^D is not requisite for *f*Aβ inhibition. The lone pair about the amine is still able to form strong H^A interactions, but the lone pair about the nitrogen in the formamide found in GS-1044 will not act as strongly through H^D interactions because of resonance with the adjacent carbonyl. Although GS-1044 does retain

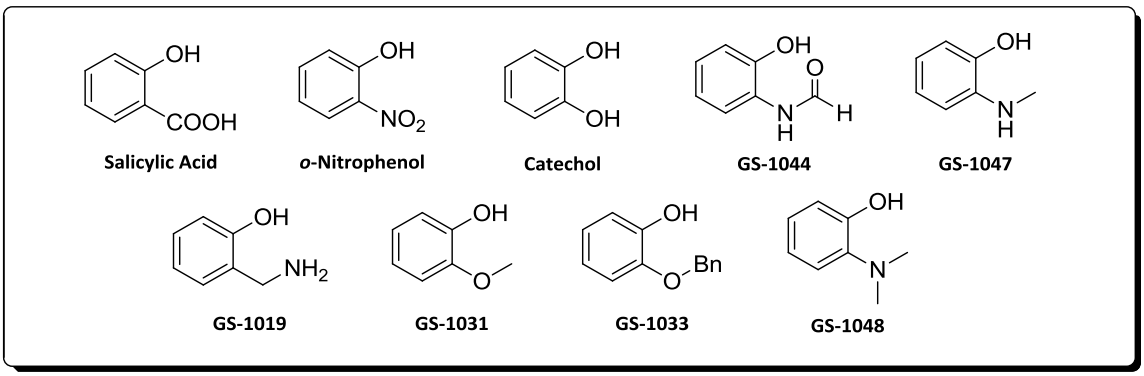

Figure 3.5 Structures of *o*-aminophenol analogues with amine replacement.

Table 3.3 The *%Fib* of 20 μM $A\beta_{1-40}$ incubated with *o*-aminophenol analogues (with amine replacement) (±S.D., *n*=3).

Compound	*%Fib*		
o-Aminophenol	***42***	***±***	***13***
Salicylic acid	114	±	17
o-Nitrophenol	111	±	18
Catechol	38	±	8
GS-1019	96	±	5
GS-1031	91	±	4
GS-1033	81	±	3
GS-1044	81	±	1
GS-1047	38	±	3
GS-1048	40	±	2

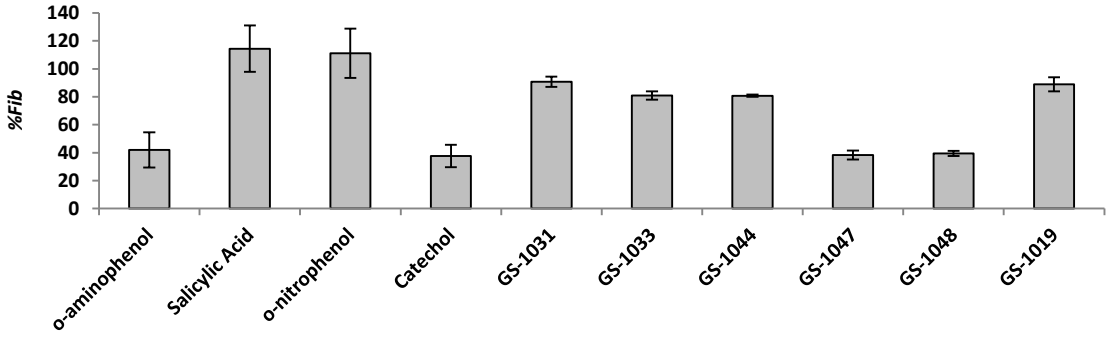

Figure 3.6 The *%Fib* of 20 μM $A\beta_{1-40}$ incubated with *o*-aminophenol analogues (with amine replacement) (±S.D., *n*=3).

activity (81% compared to control), it failed to maintain potency at levels observed in *o*-aminophenol, GS-1047, and GS-1048. The disparate antifibrillogenic activity of GS-1044 compared to *o*-aminophenol, GS-1047, and GS-1048 suggest that amine H^A interactions may potentially have a role in mediating activity.

3.1.1.3 Analogues Containing the Catechol/Aminophenol Motif

Of the analogues of 3HAA investigated with ThT antifibrilogenisis assay, catechol and *o*-aminophenol-based compounds are the most active in inhibiting Aβ fibrillogenesis – displaying similar activity to that of 3HAA – *o*-Anisidine also prevented fibrillization, albeit to a lesser extent. Catechol and *o*-aminophenol are structurally similar – they possess two functional

groups in an *ortho*-arrangement that are able to act either via H^D and H^A interactions. A survey of the antiaggregant literature shows that the *ortho*-substituted dihydroxy motif (here forth called the catechol motif) is found in several known antiaggregants including: catechin,[106] apomorphine,[53] dopamine,[158] and 2,3-dihydroxybenzoic acid[107] (**Figure 3.7**). The aminophenol motif, however, is not a commonly found in antiaggregants. The only mention of aminophenol antiaggregants that could be found was in comprehensive review by Török and co-workers, although no structure or specific comment on activity was given.[93] It is clear that catechol and *o*-aminophenol are structurally very similar, and their shared antifibrillogenic activity may be due to a similar mechanism of action.

The catechol/aminophenol motif(s) confer antifibrillogenic activity. The relative antifibrillogenic activities of catechol, *o*-aminophenol and analogues thereof have given some insight into the structure-activity relationship compounds that inhibit *f*Aβ foramtion. Alkyl or aryl substitutions of the hydroxyl hydrogen result in a substantial decrease in antifibrillogenic activity, but conversely similar modifications to amine have no effect on activity. To probe further the structural limitations about the catechol/aminophenol motif additional analogues of catechol, *o*-aminophenol and *o*-anisidine were prepared and analyzed via the ThT fibrillogenesis assay and the relative antifibrillogenic activity of these analogues compared to the analogues discussed thus far. The structures of all analogues used to assess the catechol/aminophenol motif are presented in **Figure 3.8**. For the sake of simplicity, the analogues are broken down into three analogue series for discussion: analogues of catechol, analogues of aminophenol and analogues of *o*-anisidine; each series will be discussed in turn. Each series contains the three positional isomers of the series namesake but, aside from these, all analogues were the *ortho*-substituted. Taken together, these analogues will allow for a thorough assessment of the catechol/aminophenol motif.

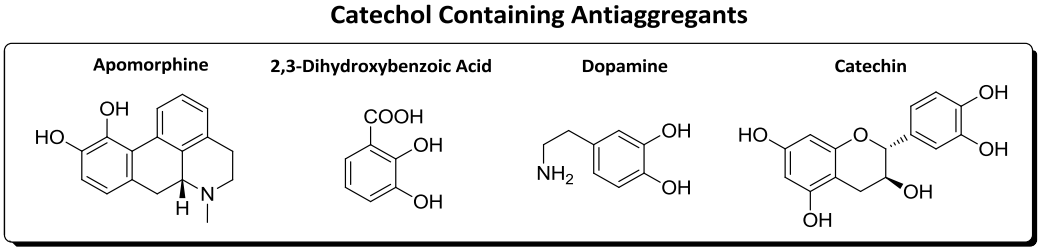

Figure 3.7 The structures of catechin, dopamine, 2,3-dihydroxybenzoic acid, and apomorphine – antiaggregants which contain the catechol motif.

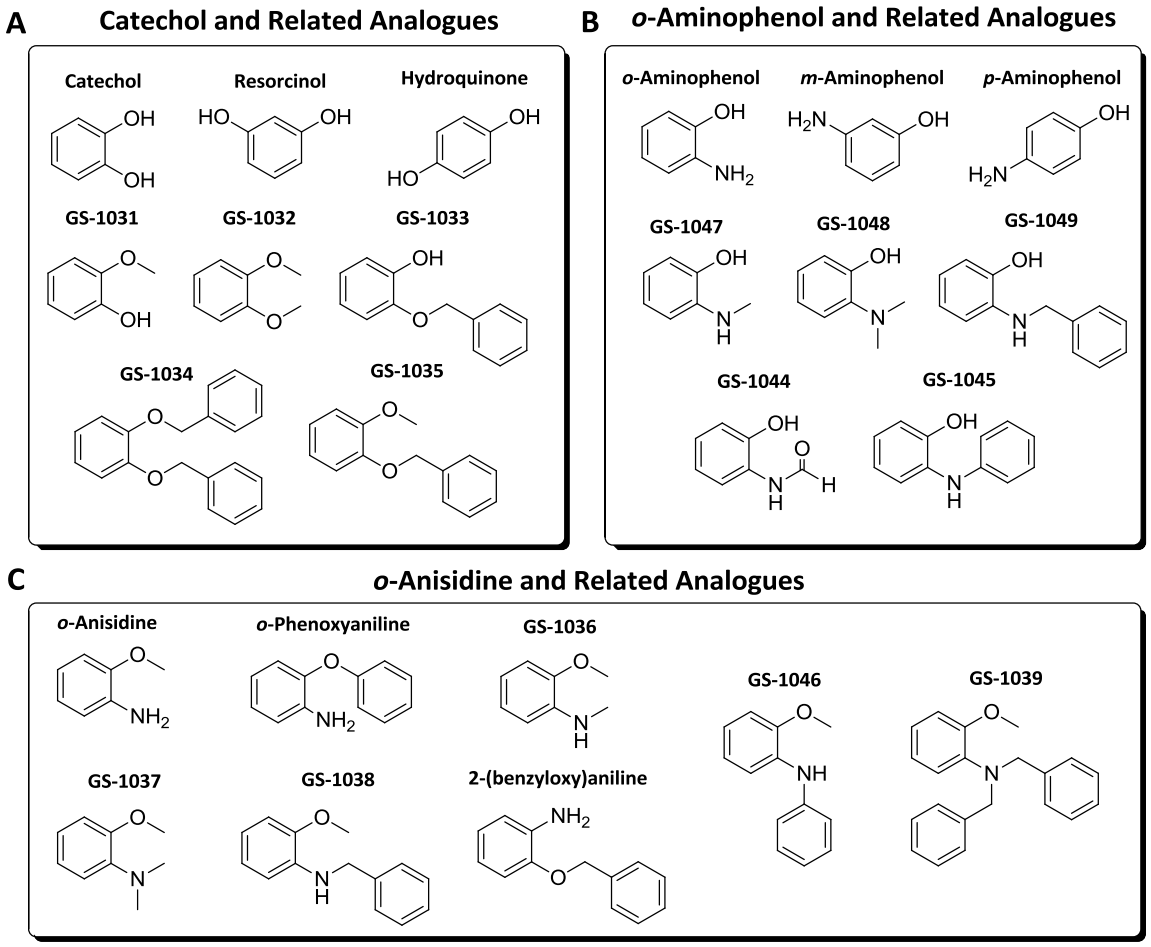

Figure 3.8 Structure of **A**) catechol **B**) *o*-aminophenol and **C**) *o*-anisidine and analogues thereof tested for antifibrillogenic activity via the ThT fibrillogenesis assay.

3.1.1.3.1 Analogues of Catechol

The antifibrillogenic activity of catechol and 7 analogues thereof was determined using the ThT fibrillogenesis assay. Fibril formation of 20 μM $A\beta_{1\text{-}40}$ coincubated with 10 μM of each compound was assessed relative to Aβ in the absence of compound after a 72 h incubation period – the values for *%Fib* are presented in **Table 3.4** and **Figure 3.9** and include *%Fib* values of Aβ coincubated with 10 μM GS-1031 and GS-1033 (presented above) for comparison. At a concentration of 10 μM, catechol inhibited *f*Aβ formation by approximately 50%, however methylation of one or both of the hydroxyls (GS-1031 and GS-1032, respectively) resulted in an loss of potency. Loss of potency is also observed for the mono- and di-benzylated analogues of catechol (GS-1033 and GS-1034, respectively) with *%Fib* values of approximately 81% and 82%, respectively, although these are slightly more active than the corresponding methylated

Table 3.4 The *%Fib* of 20 μM $A\beta_{1\text{-}40}$ incubated with catechol and analogues (±S.D., *n*=3).

Compound	*%Fib*
Catechol	50 ± 5
Resorcinol	85 ± 8
Hydroquinone	59 ± 4
GS-1031	91 ± 4
GS-1032	92 ± 4
GS-1033	81 ± 3
GS-1034	82 ± 2
GS-1035	101 ± 3

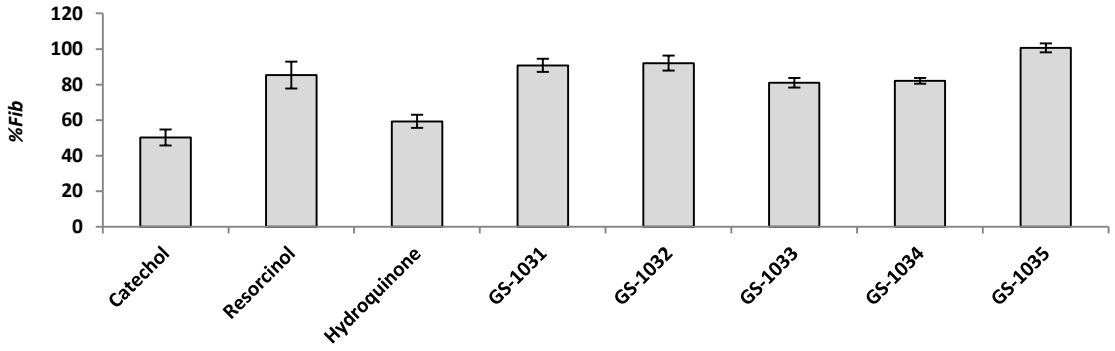

Figure 3.9 The *%Fib* of 20 μM $A\beta_{1\text{-}40}$ incubated with catechol and analogues (±S.D., *n*=3).

analogues. GS-1035 which contains both a methyl and benzyl ester was the least active of all catechol analogues analyzed and did not alter Aβ fibrillogenesis. The two structural isomers of catechol, resorcinol and hydroquinone, inhibited fibrillogenesis to a lesser extent than catechol; however at 59% *f*Aβ formation hydroquinone had a notable effect – almost equivalent to catechol.

3.1.1.3.2 Analogues of o-Aminophenol

The antifibrillogenic activity of *o*-aminophenol and 7 analogues thereof was determined using the ThT fibrillogenesis assay. Fibril formation of 20 μM $A\beta_{1\text{-}40}$ coincubated with 10 μM of each compound was assessed relative to $A\beta_{1\text{-}40}$ in the absence of compound after a 72 h incubation period – the values for *%Fib* are presented in **Table 3.5** and **Figure 3.10** and include *%Fib* values of Aβ coincubated with 10 μM GS-1044, GS-1047 and GS-1048 (presented above) for comparison. At a concentration of 10 μM *o*-aminophenol inhibits *f*Aβ formation by approximately 60%. Methylation of the amine caused a slight decrease in activity, however with

Table 3.5 The *%Fib* of 20 μM $A\beta_{1\text{-}40}$ incubated with *o*-aminophenol and analogues (±S.D., *n*=3).

Compound	*%Fib*
o-Aminophenol	41 ± 2
m-Aminophenol	94 ± 2
p-Aminophenol	34 ± 2
GS-1044	81 ± 1
GS-1045	26 ± 1
GS-1047	45 ± 4
GS-1048	46 ± 2
GS-1049	24 ± 1

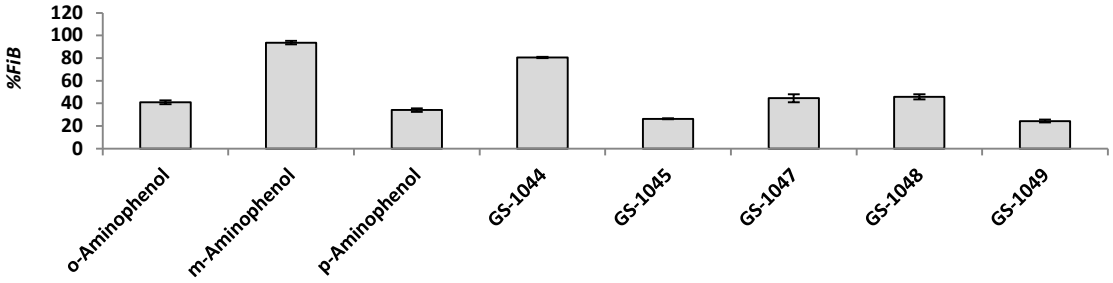

Figure 3.10 The *%Fib* of 20 μM $A\beta_{1\text{-}40}$ incubated with *o*-aminophenol and analogues (±S.D., *n*=3).

percent fibrillization of 45% and 46% respectively, the antifibrillogenic activity of GS-1047 and GS-1048 are comparable to *o*-aminophenol – an indication that aniline is much less sensitive to hydrogen replacement than the hydroxyl; furthermore, by furnishing the amine with either a phenyl or benzyl ring, as in GS-1045 and GS-1049, antifibrillogenic activity is significantly improved. With *%Fib* values of 26% and 24% respectively, GS-1045 and GS-1049 are the most active antifibrillogenic compounds observed thus far. Activity varied among the three structural isomers of aminophenol – following a similar trend to that of the catechol and isomers thereof. At 96% *f*Aβ formation (relative to the control) *m*-aminophenol was the least active of the aminophenol analogues analyzed but p-aminophenol with 34% *f*Aβ formation has improved potency relative to *o*-aminophenol. Taken together, the aminophenol analogues demonstrate that amine is far less sensitive to structural modification.

3.1.1.3.3 Analogues of *o*-Anisidine

The antifibrillogenic activity of *o*-anisidine and 9 analogues thereof was determined using the ThT fibrillogenesis assay. Fibril formation of 20 µM $A\beta_{1\text{-}40}$ coincubated with 10 µM of each compound was assessed relative to Aβ in the absence of compound after a 72 h incubation period – the values for *%Fib* are presented in **Table 3.6** and **Figure 3.11**. At a concentration of 10 µM, *o*-anisidine moderately inhibits fibrillization (*%Fib* of 79%). *o*-Anisidine is structurally similar to *o*-aminophenol the only difference being methylation of the hydroxyl hydrogen, a so-called methyl ether. By replacing the alcohol of *o*-aminophenol with the methyl ether potency is lost, and *f*Aβ formation increases by approximately 30%. With a *%Fib* of 70%, *o*-phenoxyaniline is more active than *o*-anisidine, but is still much less potent than *o*-aminophenol. GS-1040 which contains benzyl ether has no effect on *f*Aβ formation. GS-1036, GS-1037, GS-1038 and GS-1046 are the methyl ethers of GS-1047, GS-1048, GS-1049 and GS-1045, respectively; in all cases the methyl ether analogues are significantly less active than the corresponding aminophenols, highlighting the importance of the hydroxylic hydrogen in conferring antifibrillogenic activity (**Figure 3.12**).

Table 3.6 The *%Fib* of 20 µM $A\beta_{1\text{-}40}$ incubated with *o*-anisidine and analogues (±S.D., *n*=3).

Compound	*%Fib*		
o-Anisidine	79	±	6
o-Phenoxyaniline	70	±	10
2-(benzyloxy)aniline	99	±	3
GS-1036	96	±	6
GS-1037	87	±	4
GS-1038	99	±	5
GS-1039	84	±	3
GS-1046	104	±	9

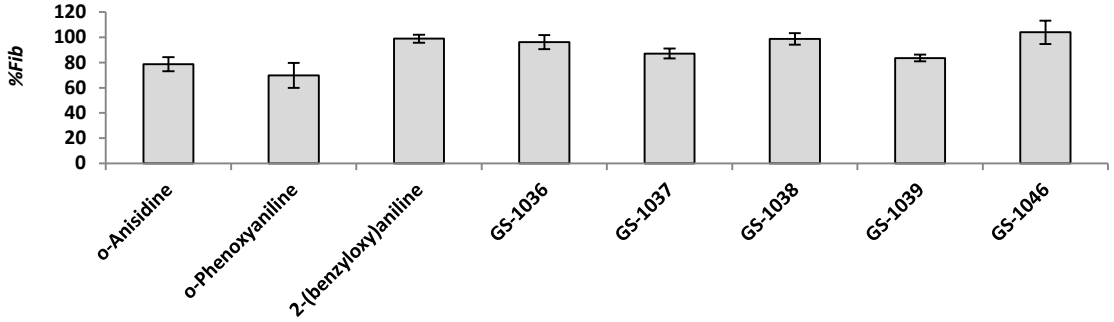

Figure 3.11 The *%Fib* of 20 µM $A\beta_{1\text{-}40}$ incubated with *o*-anisidine and analogues (±S.D., *n*=3).

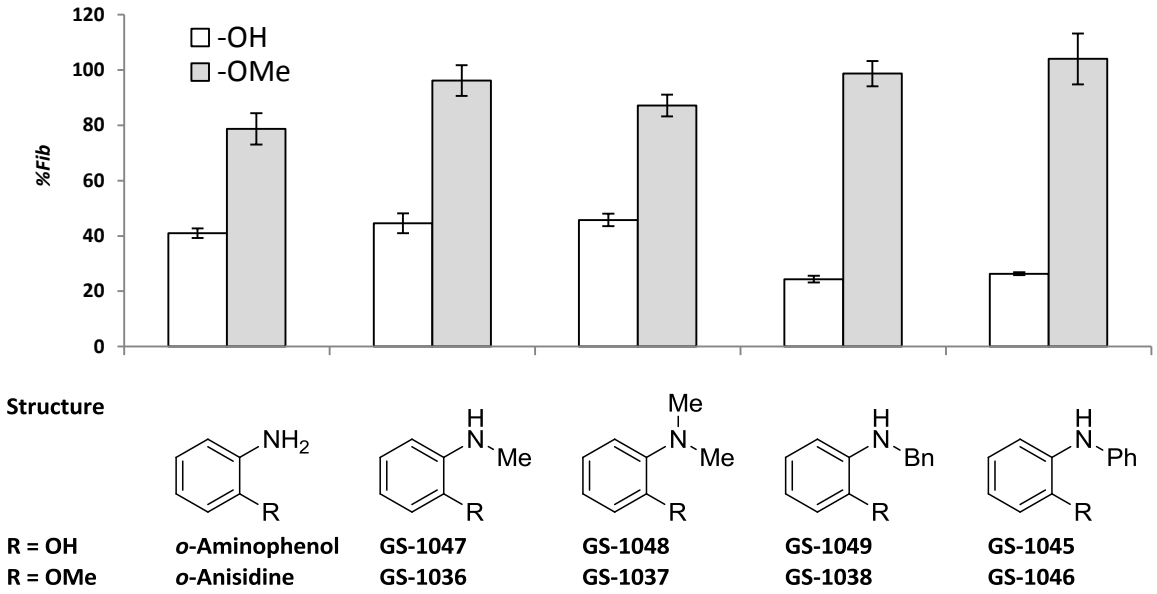

Figure 3.12 Comparison of *%Fib* of 20 μM $A\beta_{1-40}$ incubated with o-aminophenols (white bars) and their corresponding methyl ether analogues (grey bars) (±S.D., *n*=3).

3.1.1.3.4 Positional Isomers of Catechol, Aminophenol and Phenylenediamine

The substitution pattern of the positional isomers of catechol, aminophenol and phenylenediamine drastically affects the observed activity in inhibition of *f*Aβ formation. The *ortho*-distributed analogues of catechol and aminophenol are more active than *ortho*-

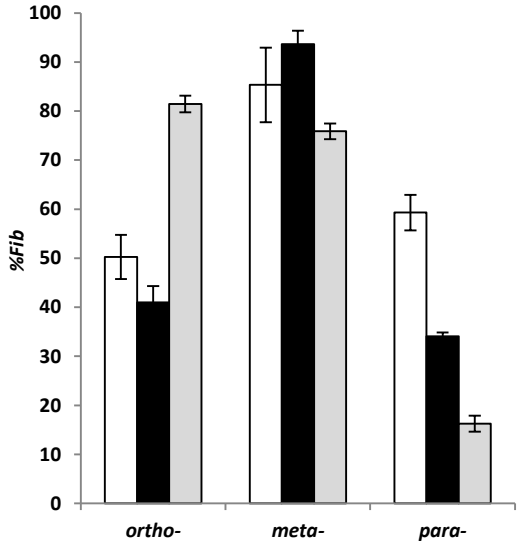

Figure 3.13 Comparison of *%Fib* of 20 μM $A\beta_{1-40}$ incubated with positional isomers of catechol (white bars), aminophenol (black bars), and phenylenediamine (grey bars) (±S.D., *n*=3).

distributed phenylenediamine (%Fib values of 50%, 59% and 80%) respectively, but this trend in activity is reversed in the *meta*-distributed analogues (**Figure 3.13**). Overall, the *meta*-distributed analogues of catechol, aminophenol and phenylenediamine are the least active. Interestingly, the *para*-distributed isomers are all active and an improvement in activity is actually observed for the *para*-distributed isomers of phenylenediamine and aminophenol over their *ortho*-distributed analogues.

3.1.2. The Aminophenol Motif

The analogues of 3HAA surveyed thus far have been analyzed with the ThT antifibrilogenisis assay in an effort to identify a motif that confers antifibrillogenic activity. With a defined motif, the principles of rational drug design may be applied in an effort to design antifibrillogenic agents of increasing potency so as long as the mechanism of action of these compounds is better understood. The structure-activity relationship is a powerful tool in the medicinal chemist's toolkit; by relating structure to function one can gain powerful insight into the elements needed to confer antifibrillogenic activity – hypothesis about the role of functional groups (or modifications) can be made, and analogues can be synthesized and tested.

Although catechol itself confers antiaggregant activity (indeed it is found in a variety of antiaggregants) replacement of either hydroxyl by various ether linked alkyl and aryl groups abrogates antifibrillogenic activity. The activity conferred by the catechol and hydroquinone in inhibiting *f*Aβ formation warrant further investigation. To date compounds containing catechol motifs have been the most studied in the literature. Of all the structural isomers of catechol, aminophenol and phenylenediamine tested here, *p*-phenylenediamine was the most active and therefore may too serve as a platform for the development of novel antifibrillogenic agents. Analogues containing the aminophenol motif not only retain the antifibrillogenic activity of *o*-aminophenol but in all analogues improve on it – these analogues were subsequently studied in more detail.

3.2 Further Assessment of Antifibrillogenic Activity

3.2.1 The Kinetic ThT Fibrillogenesis Assay

In the assessments of antifibrillogenic activity presented thus far, the relative fibrillogenic activity of all analogues has been calculated after a 72 h incubation period. The

approach of using only single measurement for initial and final ThT fluorescence proves useful in identifying compounds which actively prevent fibrillogenesis and has allowed for the aminophenol antifibrillogenic motif to be identified (furthermore it has allowed for the activity of 3HAA to be assessed relative to other literature antiaggregants). Although the methodological approach employed thus far has been fruitful in identifying compounds it provides no mechanistic insight into compound activity.

Aβ aggregation proceeds by a multistep, nucleation-dependent process.[90,91,159] The rate limiting step of *f*Aβ formation is the generation of fibril seeds of Aβ that act as nucleation sites for fibril elongation. In the absence of seeding fibrils there is a lag period for the formation of Aβ fibrils. Once aggregation begins fibril elongation occurs rapidly.[108] In the ThT fibrillogenesis assay the lag period corresponds to an initial plateau in the observed ThT fluorescence. With fibril elongation a sharp increase in ThT fluorescence is observed which again plateaus as the

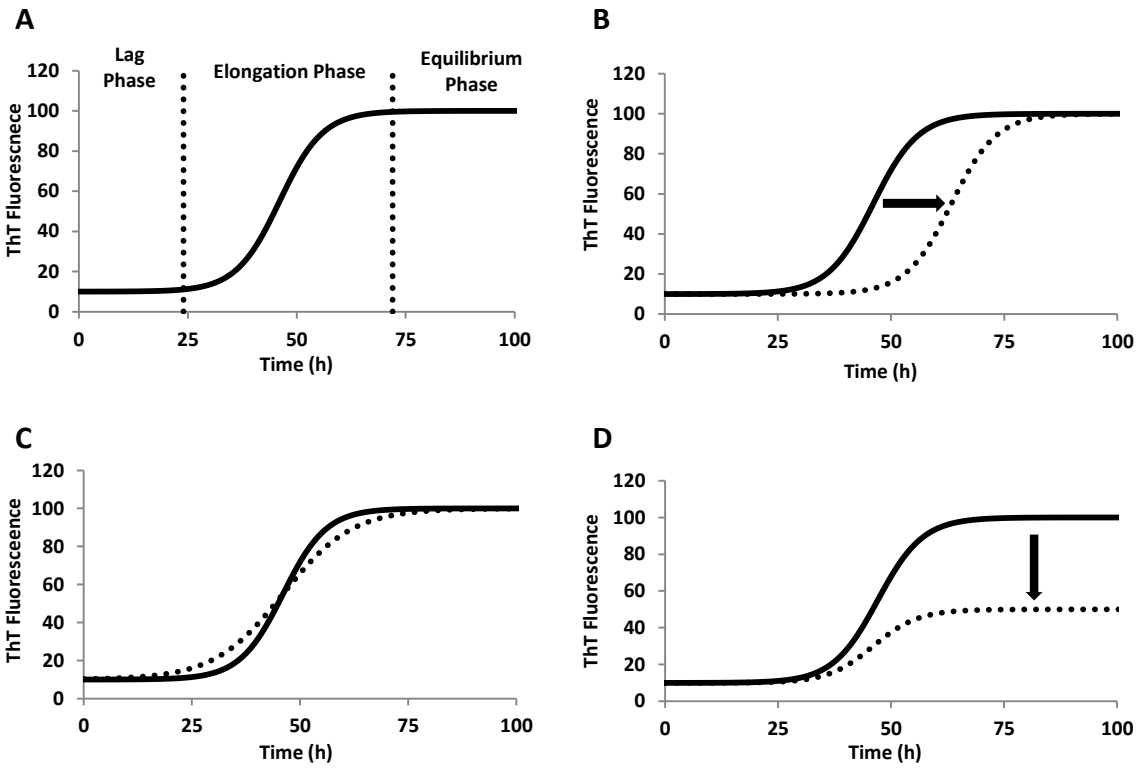

Figure 3.14 **A**) An aggregation curve of Aβ as observed using the ThT antifibrilogenisis assay (with the lag, elongation and equilibrium phases of *f*Aβ formation shown. **B**) ThT curve transformation due to inhibition of nucleation. **C**) ThT curve transformation due to inhibition of monomer addition to nucleating Aβ or Aβ fibrils. **D**) ThT curve transformation due to inhibition of *f*Aβ formation.

supply of *m*Aβ has been exhausted and fibril formation has reached equilibrium. The three phases of fibril formation are presented in **Figure 3.14A**. Antifibrillogenic compounds can affect a variety of transformations to the ThT curve which can be used to garner mechanistic insight into their mode of action. The initial lag phase can be shortened by the addition of preformed fibril seeds to monomer solutions and conversely interfering with *m*Aβ nucleation will increase lag time. Peptidomimetic antiaggregants[96] and certain proteins such as laminin 1[124,125] have been shown to interact directly with Aβ and inhibit nucleation; As a result, the lag phase is prolonged and the increase in ThT fluorescence due to fibril formation is delayed as in **Figure 3.14B**. The rate of monomer incorporation into the growing Aβ fibril increases with both increasing concentration of seed and increasing concentration of monomer.[122] Therefore, the rate of *f*Aβ formation is controlled by both fibril seed concentration and *m*Aβ. The maximum rate of fibril extension is equal to the maximum slope of the ThT curve. Apolipoprotein E non-covalently interacts with *m*Aβs and as a result lowers the rate of fibril extension and as a result decreases the slope of the ThT curve (**Figure 3.14C**).[122] By decreasing the relative amount of *f*Aβ the height of the ThT curve decreases (**Figure 3.14D**). This last transformation is observed for the majority of antiaggregants and is what has been solely monitored in the antifibrillogenic compounds discussed thus far. Further insight into the mechanism of action of these compounds may be gained by monitoring changes in the lag phase and maximum rate of fibril formation (as compared to Aβ in the absence of compound). This may be achieved using ThT fluorescence data from a kinetic assay whereby fluorescence is monitored at short time increments (15 minutes) as to observe *f*Aβ formation.

Since Aβ fibrillization follows a nucleation-dependent polymerization model the kinetic fluorescence data from the elongation phase *f*Aβ formation (generated via the ThT fibrillogenesis assay) can be fit to a sigmoidal function:

$$F(t) = d + \frac{a}{1 + be^{-ct}}$$

Equation 3.1 The general logistic function.

where fluorescence, $F(t)$, is given as a function of t. Here, a and d represent the F_{MAX} and F_{MIN} of the elongation phase, respectively. The variables b and c control the time and rate at which values progress from F_{MIN} to F_{MAX}. The derivative at any point along the logistic equation fitted

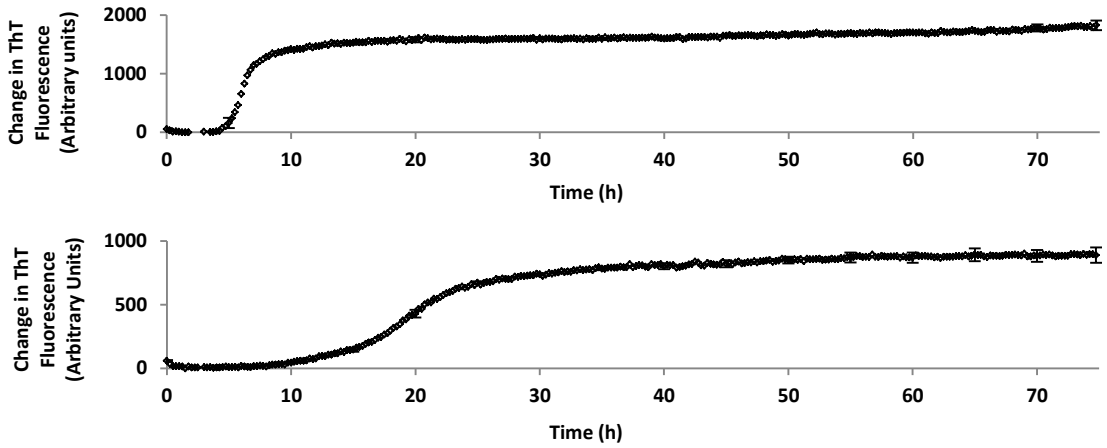

Figure 3.15 Kinetic aggregation curves of 20 µM Aβ generated during separate runs of the ThT fibrillogenesis assay (± S.D., *n*=3, for clarity error bars are only shown every 5 h).

to the kinetic ThT data (**Equation 3.1**) represents the rate of change in ThT fluorescence (and as such the rate of fibril formation) at that point:

$$F'(t) = \frac{abce^{cx}}{(e^{cx} + b)^2}$$

Equation 3.2 The first derivative of the general logistic function.

By fitting kinetic ThT fluorescence data with **Equation 3.1** the time at which the rate of *f*Aβ formation is a maximum, $t_{F'_{MAX}}$, can be calculated using **Equation 3.2** and serves as a point at which *f*Aβ formation data can be compared for Aβ incubated with various compounds. It is of utmost importance that a fitting methodology is robust enough to be applied in a consistent manner to any data set; this is particularly important in the case of the kinetic ThT fibrillogenesis assay as the time of *f*Aβ formation varies from run to run. **Figure 3.15** shows the ThT fluorescence curves for separate runs conducted on 20 µM $A\beta_{1\text{-}40}$; note that both the position and length of the elongation phase may vary. Since determination of $t_{F'_{MAX}}$ is achieved by fitting the elongation phase of *f*Aβ formation (which may vary in position and length) a consistent method to define the range to be fit was developed, in an effort to avoid arbitrarily selecting a time range to define the elongation phase for each curve. In this way analyses are consistent over a range of experimental data sets.

To define the elongation phase of the aggregation curves the second derivative of the original data fit (**Equation 3.1**) is calculated:

$$F''(t) = \frac{abc^2e^{cx}(b - e^{cx})}{(e^{cx} + b)^3}$$

Equation 3.3 The second derivative of the general logistic function.

An example of a general logistic function is plotted in **Figure 3.16** along with plots of its first and second derivatives. The derivative of the general logistic function is symmetric about $t_{F'_{MAX}}$ and consequently the second derivative achieves a maximum ($t_{F''_{MAX}}$) and a minimum ($t_{F''_{MIN}}$) of equal magnitude and opposite sign and flank $t_{F'_{MAX}}$ equidistantly. The region intermittent to $t_{F''_{MAX}}$ and $t_{F''_{MIN}}$ spans the majority of the region corresponding to the elongation phase of *f*Aβ formation. Since the second derivative can be simply determined for the logistic fit (**Equation 3.1**) solving for $t_{F''_{MAX}}$ and $t_{F''_{MIN}}$ provides a simple method to determine an appropriate region for data fitting (for the detailed methodology employed in the fitting procedure please refer to **Section 6.4.4.3** of the methodology chapter).

By fitting the kinetic fluorescence data obtained via the ThT fibrillogenesis assay with **Equation 3.1** both the maximum rate of fluorescence change, F'_{MAX}, and the time at which this maximum occurs $t_{F'_{MAX}}$ may be accurately determined and provides a valuable method of assessing the effect of antifibrillogenic compound dose on delaying *f*Aβ formation. Since ThT

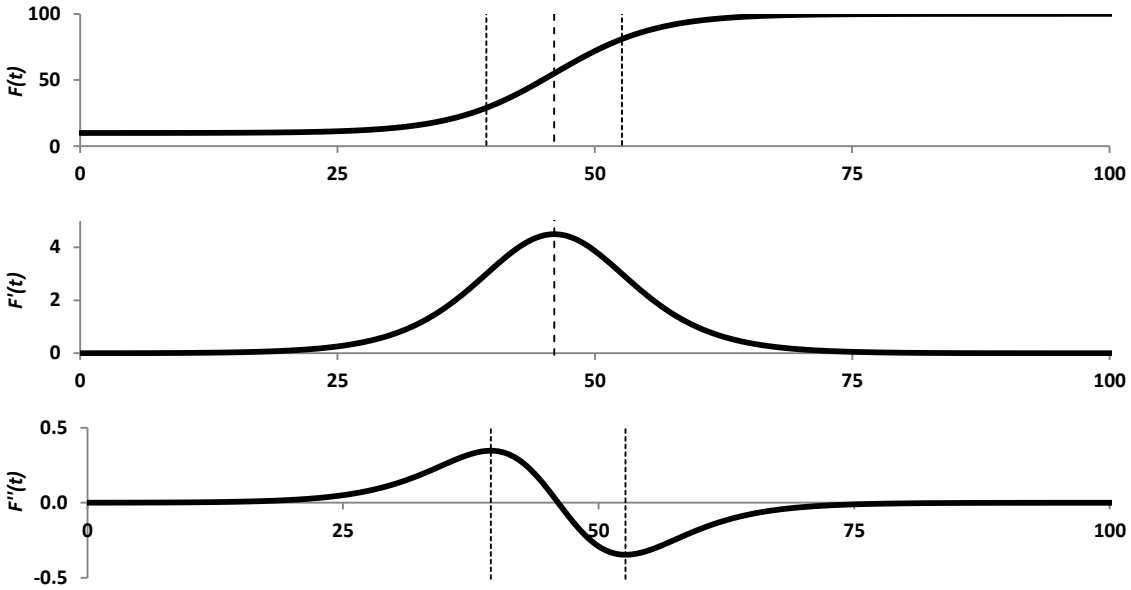

Figure 3.16 An example of a general logistic function is plotted in along with plots of its first and second derivatives, along with hashed lines to represent the maximum (or minimum) values for the first (– – – –) and second (- - - -) derivatives.

fluorescence is proportional to the amount of *f*Aβ present, it follows that the rate of change in fluorescence response, F'_{MAX}, is proportional to the maximum rate of *f*Aβ formation; as such the role of various antiaggregants in preventing of *f*Aβ formation can be quantitatively assessed. Values of F'_{MAX}, and $t_{F'_{MAX}}$ of Aβ in the absence of compound can be compared directly to those values determined in the presence of antiaggregants. Compounds which interfere with *m*Aβ (or *o*Aβ) incorporation into growing *f*Aβs will retard F'_{MAX}. Taken together, measurements of F'_{MAX}, and $t_{F'_{MAX}}$ may provide insight into the mechanism of action of antifibrillogenic compounds – a feat not accomplished by determination of IC_{50} alone.

3.2.2 Kinetic Analysis of Inhibition of *f*Aβ Formation

3.2.2.1 3HAA

3.2.2.1.1 IC_{50} Value for Inhibition of *f*Aβ Formation

The kinetic analysis of inhibition of *f*Aβ fibrillization was conducted for 3HAA. Fibril formation of 20 μM $Aβ_{1-40}$ coincubated with 3HAA at four concentrations, 0.4 μM, 2 μM, 10 μM and 50 μM, was assessed relative to $Aβ_{1-40}$ in the absence of compound. All incubations were done in triplicate in a 96-well plate. Fluorescence measurements were taken every 15 min over the course of 75 h. In **Figure 3.17** the fibrillization curves generated via the kinetic ThT fibrillogenesis assay are presented for 3HAA; these fluorescence curves are the product of averaging fluorescence measurements for each of the triplicate runs at each time point. In **Figure 3.17** the concentration of 3HAA is explicitly shown next to each aggregation curve; this will not be done in subsequent displays of kinetic data for the various antiaggregants investigated as the order of the generated curves is the same in all cases.

For all compounds run via the kinetic ThT the total change in fluorescence due to uninhibited *f*Aβ formation (no compound present), $\Delta F_{COMPLETE}$, is taken as the difference between F_{MAX} and F_{MIN} of the control curve. The change in fluorescence at 75 h, $\Delta F_{75\ h}$, for each curve (including the control) is taken as the difference between the measured fluorescence at 75 h, $F_{75\ h}$, and F_{MAX}. The presented values for *%Fib* for each curve are determined as a ratio of $\Delta F_{75\ h}$ and $\Delta F_{COMPLETE}$ and as such the calculated *%Fib* of the control curve is often (but not always) < 100%. IC_{50} values are determined by fitting the dose response curve (**Equation 2.5**) to

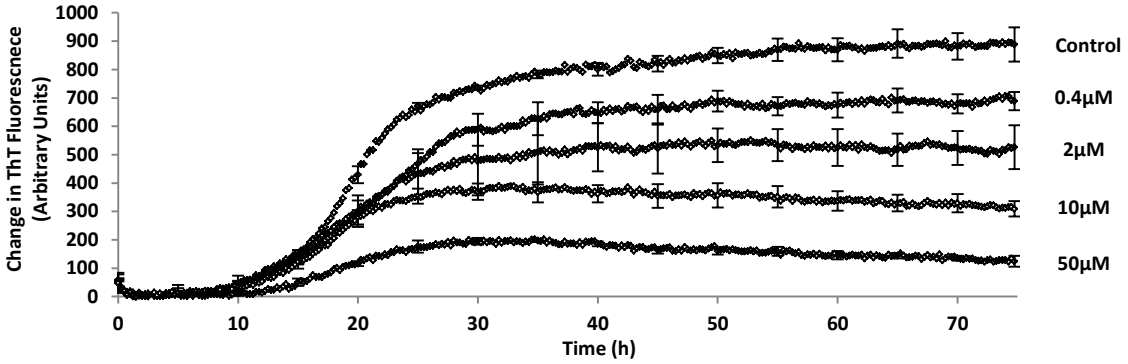

Figure 3.17 Kinetic ThT fluorescence curves of 20 µM $A\beta_{1\text{-}40}$ in the absence (control) and presence of 3HAA (0.4 µM, 2 µM, 10 µM and 50 µM) (± S.D., *n*=3, for clarity error bars are only shown every 5 h).

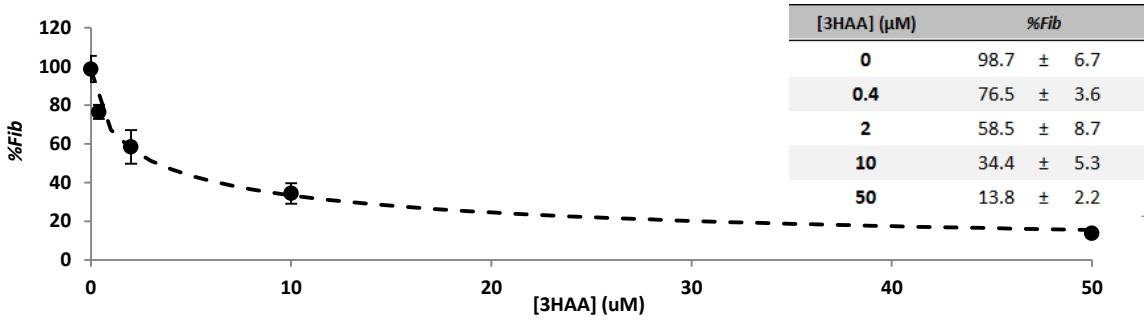

[3HAA] (µM)	%Fib
0	98.7 ± 6.7
0.4	76.5 ± 3.6
2	58.5 ± 8.7
10	34.4 ± 5.3
50	13.8 ± 2.2

Figure 3.18 Fitted dose response curve (hashed line) of 3HAA inhibition of *f*Aβ formation from 20 µM $A\beta_{1\text{-}40}$ as determined from the kinetic ThT fluorescence curves (± S.D., *n*=3).

the values of *%Fib* determined at 75 h for each curve. The dose response curve generated from *the %*Fib values determined from the data in **Figure 3.17** is presented for 3HAA in **Figure 3.18**.

3.2.2.1.2 Values of F'_{MAX} and $t_{F'_{MAX}}$ of *f*Aβ Formation

F'_{MAX} and $t_{F'_{MAX}}$ were determined by fitting the triplicate data for the fibrillization curves presented in **Figure 3.17.** The calculated $t_{F'_{MAX}}$, and calculated F'_{MAX} for each of the three triplicate curves are presented for the control (20 µM $A\beta_{1\text{-}40}$) and incubations of 20 µM $A\beta_{1\text{-}40}$ with 3HAA are presented in **Table 3.7** and **Table 3.8**. The absolute values for the averaged F'_{MAX} and $t_{F'_{MAX}}$ are presented as bar graphs in **Figure 3.19A** and **Figure 3.20A**, respectively. As F'_{MAX} and $t_{F'_{MAX}}$ vary from experiment to experiment the data is presented as percent deviation from values determined from the control curve (*%Dev*) from the control curve, as to allow comparison between ThT runs conducted using different batches of Aβ. Accordingly the

Table 3.7 Values of F'_{MAX} calculated from fitted ThT fluorescence curves for 3HAA (± S.D., *n*=3).

[x] (μM)	F'_{MAX} (ΔF/h)			Average (ΔF/h)	*%Dev*
	Run 1	Run 2	Run 3		
0	59.4	64.7	60.6	61.6 ± 2.8	-
0.4	39.1	44.3	35.1	39.5 ± 4.6	-36 ± 8
2	43	38.1	32.9	38.0 ± 5.1	-38 ± 8
10	29.4	38.8	32.3	33.5 ± 4.8	-46 ± 8
50	17.4	19.6	15.9	17.6 ± 1.9	-71 ± 3

Table 3.8 Values of $t_{F'_{MAX}}$ calculated from fitted ThT fluorescence curves for 3HAA (± S.D., *n*=3).

[x] (μM)	$t_{F'MAX}$ (h)			Average (h)	*%Dev*
	Run 1	Run 2	Run 3		
0	19.4	19.5	18.9	19.3 ± 0.3	-
0.4	19.4	21.3	22.5	21.0 ± 1.6	8.8 ± 0.8
2	18.6	19.1	16.9	18.2 ± 1.2	-5.7 ± 0.6
10	18.2	17.3	16.7	17.4 ± 0.8	-9.8 ± 0.4
50	18.1	18.3	18.6	18.3 ± 0.3	-5.2 ± 0.2

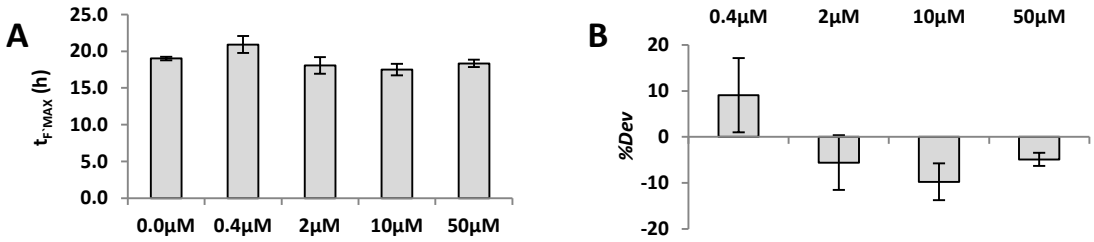

Figure 3.19 **A**) Absolute values of $t_{F'_{MAX}}$ of 3HAA inhibition of *f*Aβ formation and **B**) the data presented as *%Dev* from the control (± S.D., *n*=3).

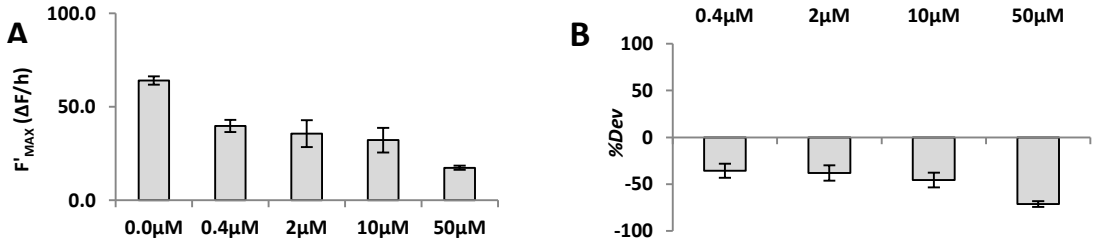

Figure 3.20 **A**) Absolute values for $\boldsymbol{F'_{MAX}}$ of 3HAA inhibition of *f*Aβ formation and **B**) the data presented as *%Dev* from the control (± S.D., *n*=3).

data for F'_{MAX} *and* $t_{F'_{MAX}}$ in terms of *%Dev* from the control are presented as bar graphs in **Figure 3.19B** and **Figure 3.20B**.

Using the method outlined in **Section 6.4.4.3** F'_{MAX} *and* $t_{F'_{MAX}}$ were calculated for each triplicate curve, the averaged values (along with their S.D.) are presented here. Small values of S.D. were observed for all of the calculated values of F'_{MAX} *and* $t_{F'_{MAX}}$ indicating that the triplicate runs for each data set had excellent reproducibility. Increasing the incubation concentration of 3HAA had little effect on the $t_{F'_{MAX}}$ as compared to the control run in the absence of 3HAA; however, F'_{MAX}, changed significantly as a function of 3HAA concentration decreasing (compared to the control) with increasing 3HAA incubation concentration. When incubated with 50 μM 3HAA, rate of *f*Aβ formation from 20 μM $A\beta_{1\text{-}40}$ decreased by 71%.

3.2.2.2 Positional Isomers of Catechol, Aminophenol and Phenylenediamine

3.2.2.2.1 IC_{50} Values for Inhibition of *f*Aβ Formation

Catechol and its *para*-isomer hydroquinone, *o*-aminophenol and *p*-aminophenol and *o*-phenylenediamine were further investigated via the kinetic ThT fibrillogenesis assay. As with the aforementioned kinetic analysis of 3HAA each compound was incubated with 20 μM $A\beta_{1\text{-}40}$ at 4 concentrations (0.4 μM, 2 μM, 10 μM and 50 μM). Again, 20 μM $A\beta_{1\text{-}40}$ in the absence of 3HAA served as the control.

In **Figure 3.21** the fibrillization curves generated via the kinetic ThT fibrillogenesis assay are presented for catechol, hydroquinone, *o*-aminophenol, *p*-aminophenol, and *o*-phenylenediamine. From the kinetic fibrillization curves values for *%Fib* were determined at 75 h (**Table 3.9**) and IC_{50} values for *f*Aβ inhibition were determined from the fitted dose response curves (**Figure 3.22**). From the fitted dose response curves IC_{50} values for inhibition of *f*Aβ formation from 20 μM $A\beta_{1\text{-}40}$ were determined and corrected with concurrently collected 3HAA controls (**Table 3.10**). With corrected IC_{50} values of 8.0 ± 6.7 μM and 15.2 ± 7.5 μM, respectively, catechol and hydroquinone are less active than 3HAA (5.3 ± 1.5 μM); with corrected IC_{50} values of 5.1 ± 3.6 μM, 3.4 ± 61.8 μM and 2.0 ± 0.9 μM *o*-aminophenol, *p*-aminophenol and *p*-phenylenediamine, respectively, all possess improved activity over 3HAA (**Table 3.10**).

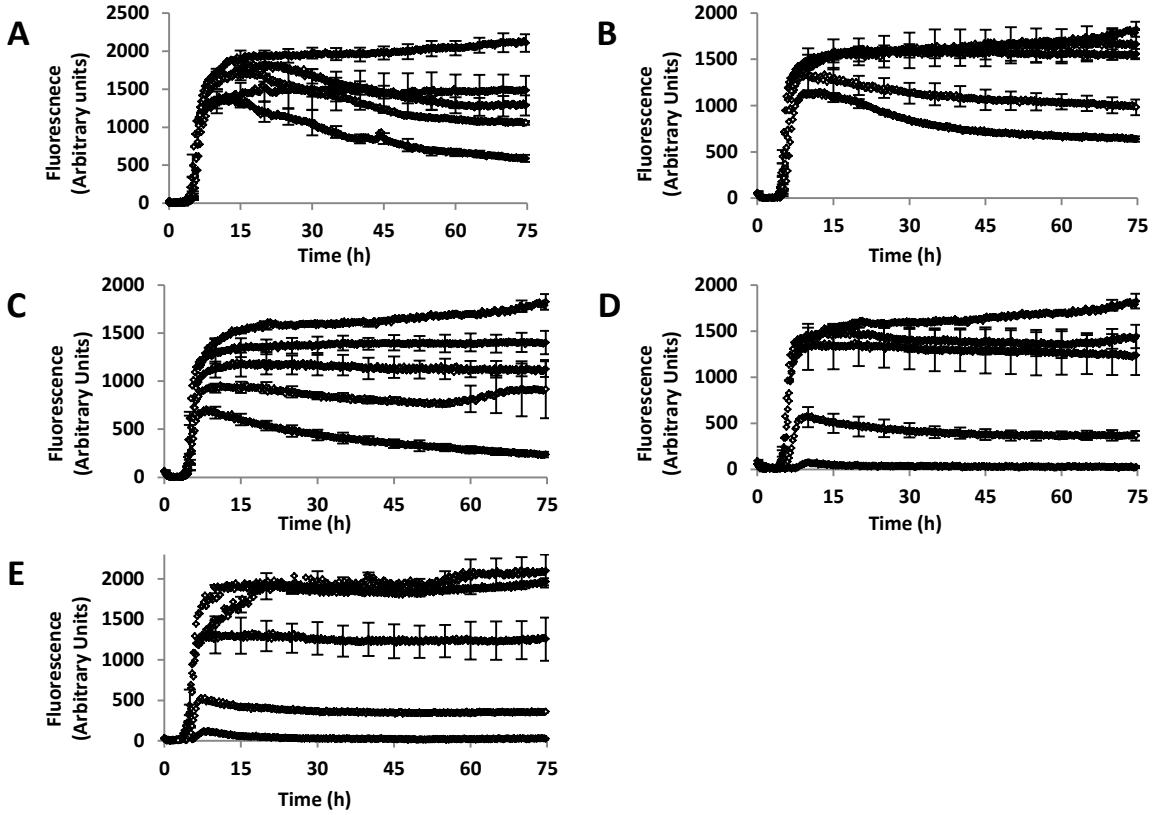

Figure 3.21 75h kinetic ThT fluorescence curves of 20 µM $A\beta_{1-40}$ in the absence (control) and presence of **A**) catechol, **B**) hydroquinone, **C**) *o*-aminophenol, **D**) *p*-aminophenol and **E**) *p*-phenylenediamine (0.4 µM, 2 µM, 10 µM and 50 µM) (± S.D., *n*=3, for clarity error bars are only shown every 5 h).

Table 3.9 Values for *%Fib* as determined from the kinetic ThT curves for 20 µM $A\beta_{1-40}$ incubated with catechol, hydroquinone, *o*-aminophenol, *p*-aminophenol and *p*-phenylenediamine (± S.D., *n*=3).

Concentration (µM)	*%Fib*				
	Catechol	Hydroquinone	*o*-Aminophenol	*p*-Aminophenol	*p*-Phenylenediamine
0	98.9 ± 5.4	100.0 ± 4.5	100.0 ± 4.5	100.0 ± 4.5	99.7 ± 9.6
0.4	69.8 ± 8.9	91.1 ± 8.3	76.8 ± 6.6	79.0 ± 6.9	93.3 ± 2.1
2	60.5 ± 6.3	85.3 ± 3.0	61.6 ± 4.4	67.8 ± 11.8	59.7 ± 12.7
10	49.6 ± 1.2	53.8 ± 4.6	50.2 ± 16.6	20.0 ± 2.9	17.0 ± 0.5
50	27.6 ± 2.3	35.0 ± 1.6	13.0 ± 1.6	0.0 ± 0.8	1.1 ± 0.7

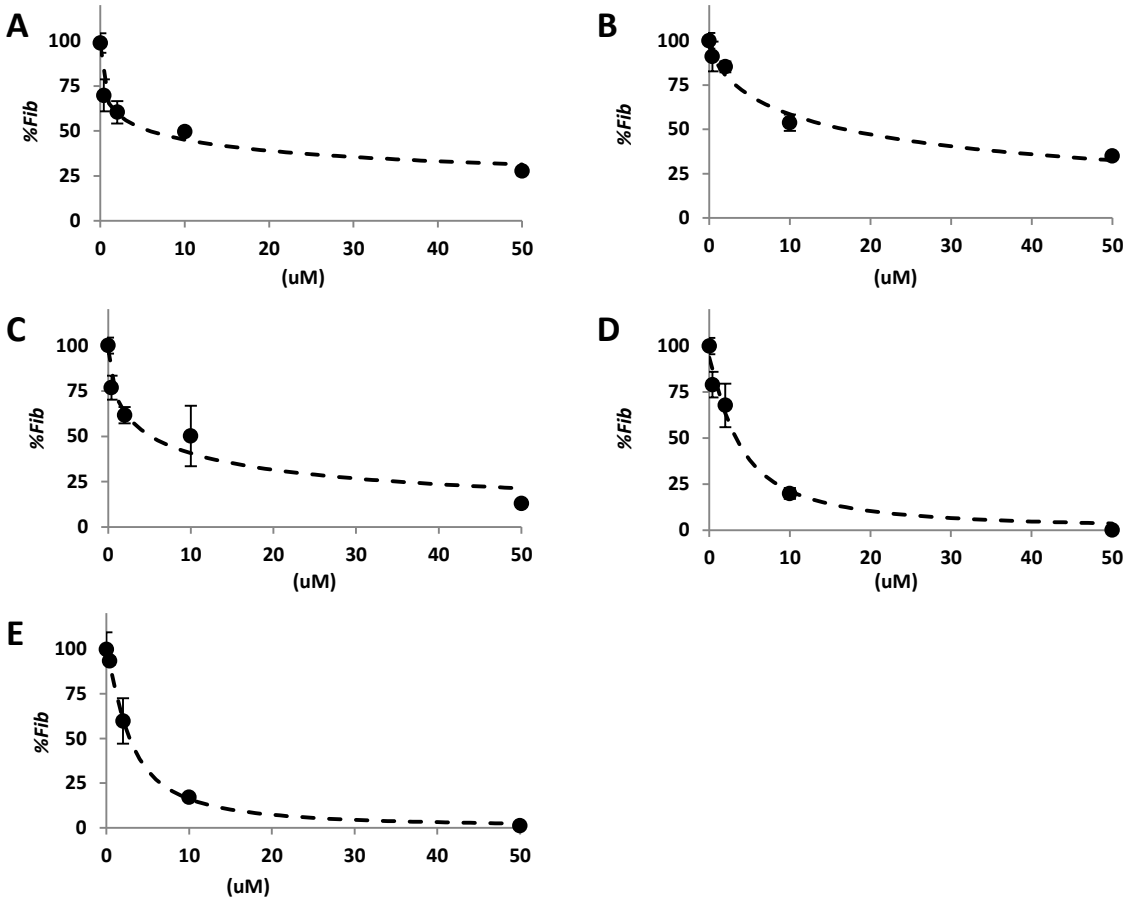

Figure 3.22 Fitted dose response curves (hashed lines) to *%Fib* values determined at 72 h (black circles, ± S.D., *n*=3) for **A**) catechol, **B**) hydroquinone, **C**) *o*-aminophenol, **D**) *p*-aminophenol and **E**) *p*-phenylenediamine from kinetic fluorescence measurements during the ThT fibrillogenesis assay for of 20 µM $A\beta_{1\text{-}40}$.

Table 3.10 IC_{50} values for inhibition of *f*Aβ formation by catechol, hydroquinone, *o*-aminophenol, *p*-aminophenol and *p*-phenylenediamine as determined from kinetic ThT curves.

Compound	IC_{50} (µM)	IC_{50} (3HAA Control) (uM)	ξ	Corrected IC_{50} (µM)
3HAA	-	-	-	**5.3 ± 1.5**
Catechol	6.4 ± 2.5	4.2 ± 2.0	1.5 ± 1.2	**8.0 ± 6.7**
Hydroquinone	16.5 ± 4.4	5.7 ± 0.5	2.9 ± 1.1	**15.2 ± 7.5**
***o*-Aminphenol**	5.5 ± 3.2	5.7 ± 0.5	1.0 ± 0.6	**5.1 ± 3.6**
***p*-Aminophenol**	3.7 ± 1.2	5.7 ± 0.5	0.6 ± 0.3	**3.4 ± 1.8**
***p*-Phenylenediamine**	2.8 ± 0.1	7.2 ± 0.9	0.4 ± 0.1	**2.0 ± 0.9**

3.2.2.2.2 Values of F'_{MAX} and $t_{F'_{MAX}}$ of *f*Aβ Formation

$t_{F'_{MAX}}$, and F'_{MAX}, of *f*Aβ formation of $A\beta_{1\text{-}40}$ was determined for the incubations of 20 μM $A\beta_{1\text{-}40}$ with catechol, hydroquinone, *o*-aminophenol, *p*-aminophenol, and *o*-phenylenediamine by fitting the triplicate data for the fibrillization curves presented in **Figure 3.21**.The calculated values of $t_{F'_{MAX}}$, and F'_{MAX} for incubations of each compound (at all concentrations) as well as their respective controls are presented in **Table 3.11**, **Table 3.12** and

Table 3.11 Values of $t_{F'_{MAX}}$ calculated from fitted ThT fluorescence curves for catechol, hydroquinone, *o*-aminophenol, *p*-aminophenol and *o*-phenylenediamine (± S.D., *n*=3).

Compound	[Compound] (μM)	$t_{F'MAX}$ (h)			Average (h)	%Dev
		Run 1	Run 2	Run 3		
Catechol	0	6	6	5.8	5.9 ± 0.1	-
	0.4	5	5.4	5	5.1 ± 0.2	-13.5 ± 3.8
	2	6	6.4	5.5	5.9 ± 0.5	0.6 ± 7.6
	10	6	5.8	5.9	5.9 ± 0.1	0.2 ± 1.5
	50	6.4	6.4	6	6.3 ± 0.2	6.0 ± 3.6
Hydroquinone	0	5.7	6.2	6	6 ± 0.3	-
	0.4	5.2	5.2	5.1	5.2 ± 0.1	-13.0 ± 1.5
	2	5.5	5.6	5.3	5.5 ± 0.2	-8.5 ± 2.8
	10	5.8	5.8	6	5.9 ± 0.1	-1.5 ± 1.7
	50	6.2	6.5	6.4	6.4 ± 0.1	7.4 ± 2.3
o-Aminophenol	0	5.7	6.2	6	6 ± 0.3	-
	0.4	5.1	5	4.8	5 ± 0.2	-16.5 ± 2.7
	2	4.7	5.9	5.1	5.3 ± 0.6	-11.9 ± 10.5
	10	5.6	5.5	5.4	5.5 ± 0.1	-7.8 ± 2.2
	50	5.7	5.7	5.5	5.7 ± 0.1	-4.9 ± 1.8
p-Aminophenol	0	5.7	6.2	6	6 ± 0.3	-
	0.4	5.5	5.6	5.8	5.6 ± 0.1	-5.3 ± 2.2
	2	5.9	6.3	6.1	6.1 ± 0.2	2.1 ± 3.1
	10	7	7.1	6.3	6.8 ± 0.4	14.1 ± 7.3
	50	8.3	8.4	8.9	8.5 ± 0.3	43.3 ± 5.6
p-Phenylenediamine	0	5.7	5.4	5.6	5.6 ± 0.2	-
	0.4	5.3	5.7	5.2	5.4 ± 0.3	-2.3 ± 4.9
	2	5.5	4.2	5.3	5 ± 0.7	-9.7 ± 12.4
	10	5.7	5.9	5.8	5.8 ± 0.1	4.3 ± 2.0
	50	6.7	6.5	6.2	6.5 ± 0.3	16.2 ± 5.0

Table 3.12 Values of F'_{MAX} calculated from fitted ThT fluorescence curves for catechol, hydroquinone, *o*-aminophenol, *p*-aminophenol and *o*-phenylenediamine (± S.D., *n*=3).

Compound	[Compound] (μM)	F'_{MAX} (ΔF/h)			Average (ΔF/h)			*%Dev*		
		Run 1	Run 2	Run 3						
Catechol	0	1040.5	956.3	1090.2	1029	±	67.7		-	
	0.4	944.9	822.6	819.7	862.4	±	71.4	-16	±	7
	2	799.2	723.2	932.5	818.3	±	105.9	-20	±	10
	10	948.4	851.7	956.2	918.8	±	58.2	-11	±	6
	50	652.4	683.1	689.1	674.9	±	19.7	-34	±	2
Hydroquinone	0	621.2	826	644.6	697.3	±	112.1		-	
	0.4	1040.8	1205.6	834.9	1027.1	±	185.7	47	±	27
	2	953.6	820.1	873.5	882.4	±	67.2	27	±	10
	10	895.5	885.1	774.7	851.8	±	67.0	22	±	10
	50	635.9	656	627	639.6	±	14.9	-8	±	2
o-Aminophenol	0	621.2	826	644.6	697.3	±	112.1		-	
	0.4	868.4	917.4	817.2	867.7	±	50.1	24	±	7
	2	713.8	960.1	911.2	861.7	±	130.4	24	±	19
	10	499.7	673.4	790	654.4	±	146.1	-6	±	21
	50	497.3	501.7	541.2	513.4	±	24.2	-26	±	3
p-Aminophenol	0	621.2	826	644.6	697.3	±	112.1		-	
	0.4	971.3	1042	760.5	924.6	±	146.5	33	±	21
	2	708.5	1121.5	726.7	852.2	±	233.4	22	±	33
	10	375	382.1	125.4	294.1	±	146.2	-58	±	21
	50	32.3	27.6	34	31.3	±	3.4	-95.5	±	0.5
p-Phenylenediamine	0	797.5	837.3	794.8	809.8	±	23.8		-	
	0.4	1127.9	1068.1	1334.9	1177	±	140	45	±	17
	2	943.3	521.6	1158.1	874.3	±	323.8	8	±	40
	10	277.5	380.8	345.7	334.7	±	52.6	-59	±	6
	50	58.5	85.6	47.8	64	±	19.5	-92	±	2

Figure 3.23. Although absolute values of $t_{F'_{MAX}}$ and F'_{MAX} determined for each analogue can be compared to their respective control curves directly (as they are prepared from the same aliquot of $A\beta_{1\text{-}40}$) these values cannot be compared in absolute terms from experiment to experiment. Instead $t_{F'_{MAX}}$ and F'_{MAX} are compared in terms of *%Dev* from their relative controls.

All of the compounds presented in **Figure 3.23** tend to have negative *%Dev* for $t_{F'_{MAX}}$ at low concentrations, meaning that F'_{MAX} is occurring earlier than in the control which may be an indication of a decrease in the lag phase of *f*Aβ formation. Here, a *%Dev* of -15% corresponds to F'_{MAX} occurring 1 h earlier than the control. For all of the analogues investigated, as incubation concentration is increased so too does $t_{F'_{MAX}}$. At the highest incubation concentration investigated, 50 μM, the observed $t_{F'_{MAX}}$ for all compounds (with the exception of *o*-aminophenol) is larger than that of the control resulting in positive values for *%Dev* as compared to the control; this effect is largest for *p*-aminophenol and *p*-phenylenediamine with deviations of 43.3 ± 1.7% and 16.2 ± 0.7%, respectively. For *p*-aminophenol this significant increase corresponds to a ~ 2.5 h delay in F'_{MAX}. These results suggest that the analogues of 3HAA discussed here may indeed modulate nucleation of $A\beta_{1\text{-}40}$, potentiating nucleation at low concentrations (≤ 2.0 μM) but conversely inhibiting it at higher concentrations. Interestingly this effect is more significant for the *para*-distributed analogues.

Catechol decreased the maximum rate of fibril extension, F'_{MAX} at all of the incubation concentrations investigated; as a general trend, increasing catechol concentration decreased the

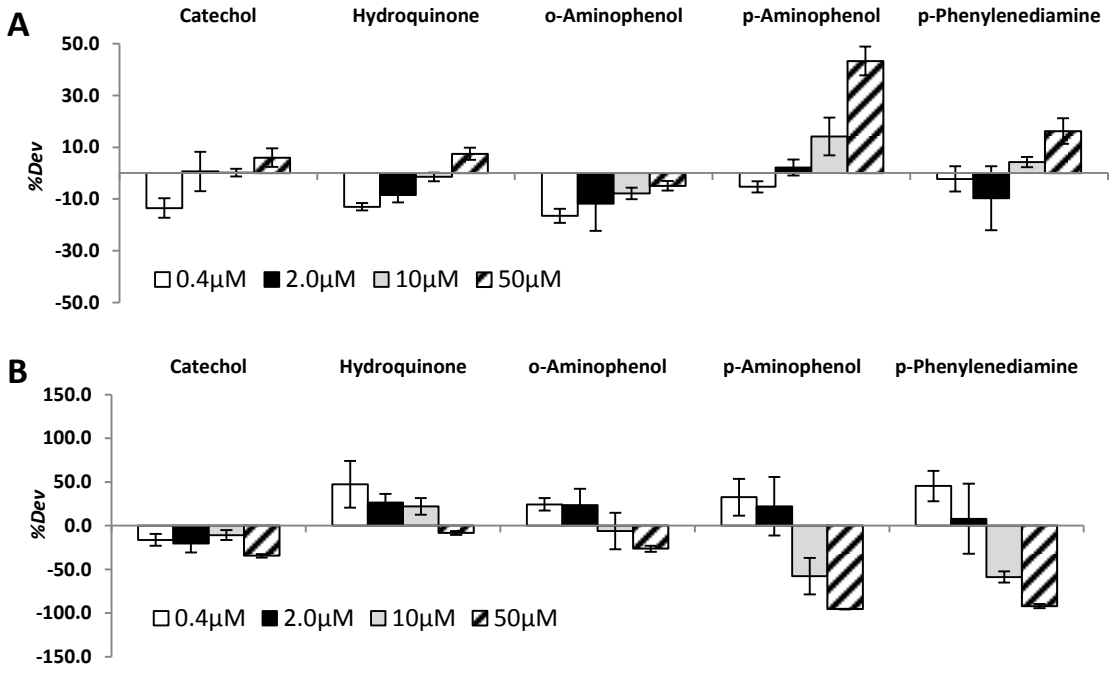

Figure 3.23 *%Dev* of **A**) $t_{F'_{MAX}}$ and **B**) F'_{MAX} from the control values calculated for catechol, hydroquinone, *o*-aminophenol, *p*-aminophenol and *p*-phenylenediamine from fitted kinetic ThT curves (± S.D., *n*=3).

maximum rate of *f*Aβ extension from 20 μM $A\beta_{1\text{-}40}$. All of the other compounds investigated increased F'_{MAX} at concentrations ≥ 2 μM, but at concentrations of 10 μM and higher, *o*-aminophenol, *p*-aminophenol, and *p*-phenylenediamine decrease the value of F'_{MAX}. The effect of slowing fibril extension is most pronounced for *p*-aminophenol and *p*-phenylenediamine. At an incubation concentration of 50 μM *p*-aminophenol and *p*-phenylenediamine the % deviation of the calculated F'_{MAX} is 96 ± 10% and 92 ± 28%, respectively, a two-fold decrease in F'_{MAX} of *f*Aβ extension. As with $t_{F'_{MAX}}$ the effect of these analogues on F'_{MAX} is concentration dependent. Generally speaking incubation concentrations of ≤ 2 μM decrease $t_{F'_{MAX}}$ and increase F'_{MAX}, whereas incubation concentrations of ≥ 10 μM increase $t_{F'_{MAX}}$ and decrease F'_{MAX}. The difference in the observed activity for these compounds at lower incubation concentrations (≤2 μM), as compared to higher incubation concentrations (≥ 10 μM) will be investigated further using the active synthetic analogues of *o*-aminophenol first presented in **Section 3.2.4**.

3.2.2.3 Synthetic Analogues of *o*-Aminophenol

3.2.2.3.1 IC_{50} Values for Inhibition of *f*Aβ Formation

Five synthetic analogues of *o*-aminophenol were further investigated via the kinetic ThT fibrillogenesis assay: GS-1044, GS-1045, GS-1047, GS-1048 and GS-1049 (refer to **Figure 3.8** for analogue structures). Each compound was incubated with 20 μM $A\beta_{1\text{-}40}$ at four concentrations (0.4 μM, 2 μM, 10 μM and 50 μM). 20 μM $A\beta_{1\text{-}40}$ in the absence of 3HAA served as the control. In **Figure 3.25** the fibrillization curves generated via the kinetic ThT fibrillogenesis assay are presented for GS-1044, GS-1047, GS-1048, GS-1045 and GS-1049. From the kinetic fibrillization curves values for *%Fib* were determined at 75 h (**Table 3.12**) and IC_{50} values for *f*Aβ inhibition were determined from the fitted dose response curves (**Figure 3.25**), and corrected with concurrently collected 3HAA controls (**Table 3.14**). With a corrected IC_{50} value of 194 ± 160 μM GS-1044 was approximately 40x less active than 3HAA; although this is a significant loss of activity, GS-1044 does possess antifibrillogenic activity, albeit weakly so. All of the other analogues derived from *o*-aminophenol which were surveyed retained excellent activity – comparable to or exceeding that of 3HAA. With a corrected IC_{50} value of 1.9 ± 1.1 μM GS-1049 has 2x improved potency over 3HAA and is the most potent of the 3HAA and *o*-aminophenol analogues run to date.

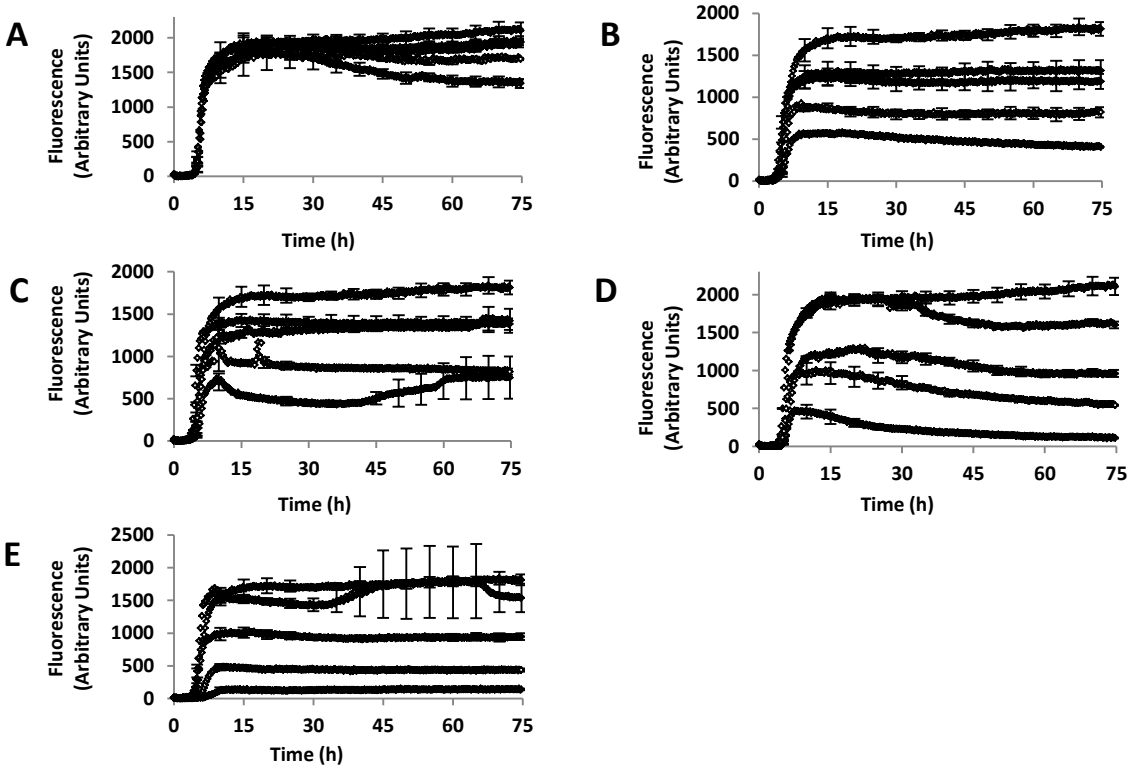

Figure 3.24 75 h kinetic ThT fluorescence curves of 20 µM Aβ1-40 in the absence (control) and presence of **A**) GS-1044, **B**) GS-1047, **C**) GS-1048, **D**) GS-1049 and **E**) GS-1045 (0.4 µM, 2 µM, 10 µM and 50 µM) (± S.D., *n*=3, for clarity error bars are only shown every 5 h).

Table 3.13 Values for *%Fib* as determined from the kinetic fibrillization curves obtained by ThT fluorescence measurements at 75 h for GS-1044, GS-1047, GS-1048 (**%Fib* at 40 h used), GS-1045 and GS-1049 (± S.D., *n*=3).

Concentration (µM)	*%Fib*					
	GS-1044	GS-1047	GS-1048*	GS-1045	GS-1049	
0	98.9 ± 5.4	98.6 ± 4.5	93.4 ± 3.0	98.9 ± 5.4	98.6 ± 4.5	
0.4	90.7 ± 1.8	71.6 ± 6.9	75.4 ± 4.9	75.1 ± 2.0	83.6 ± 11.8	
2	91.3 ± 3.8	64.6 ± 4.8	72.8 ± 1.8	45.1 ± 2.2	51.4 ± 2.8	
10	79.5 ± 1	44.6 ± 3.4	46.9 ± 1.6	25.4 ± 0.8	23.7 ± 1.4	
50	63 ± 3.2	22.1 ± 0.5	24.0 ± 2.1	5.2 ± 0.2	7.5 ± 0.8	

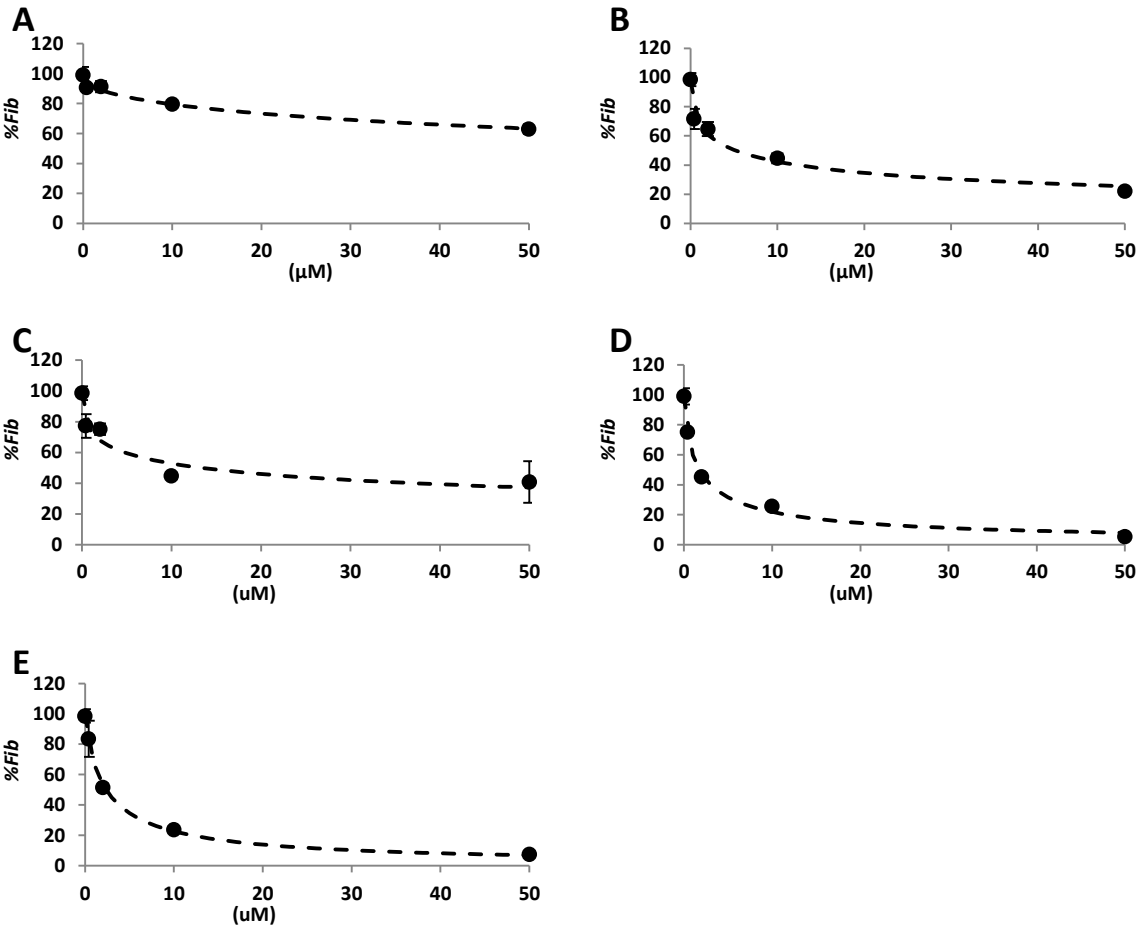

Figure 3.25 Fitted dose response curves (hashed lines) to *%Fib* values determined at 72 h (black circles, ± S.D., *n*=3) **A**) GS-1044, **B**) GS-1047, **C**) GS-1048, **D**) GS-1045 and **E**) GS-1049 from kinetic fluorescence measurements during the ThT fibrillogenesis assay for of 20 µM $A\beta_{1\text{-}40}$.

Table 3.14 Absolute and corrected IC_{50} values for inhibition of *f*Aβ formation (from 20 µM $A\beta_{1\text{-}40}$) by GS-1044, GS-1047, GS-1048 (**%Fib* at 40 h used), GS-1045 and GS-1049 as determined from *%Fib* data at 75 h from Kinetic fibrillization curves obtained by ThT fluorescence measurements during the ThT fibrillogenesis assay for of 20 µM $A\beta_{1\text{-}40}$.

Compound	IC_{50} (µM)	IC_{50} (3HAA Control) (uM)	ξ	Corrected IC_{50} (µM)
3HAA	-	-	-	**5.3 ± 1.5**
GS-1044	155 ± 57	4.2 ± 2.0	36.7 ± 28.4	**194 ± 160**
GS-1047	5.8 ± 2.1	6.7 ± 1.7	0.9 ± 0.5	**4.6 ± 3.1**
GS-1048*	7.4 ± 2.3	6.7 ± 1.7	1.1 ± 0.4	**5.8 ± 4.8**
GS-1045	1.8 ± 0.3	4.2 ± 2.0	0.4 ± 0.3	**2.2 ± 1.7**
GS-1049	2.4 ± 0.2	6.7 ± 1.7	0.4 ± 0.2	**1.9 ± 1.1**

3.2.2.3.2 Values of F'_{MAX} and $t_{F'_{MAX}}$ of *f*Aβ Formation

$t_{F'_{MAX}}$, and F'_{MAX}, of *f*Aβ formation of $A\beta_{1\text{-}40}$ was determined for the incubations of 20 μM $A\beta_{1\text{-}40}$ with GS-1044, GS-1047, GS-1048, GS-1045 and GS-1049 by fitting the triplicate data for the fibrillization curves presented in **Figure 3.25** The calculated values of $t_{F'_{MAX}}$, and F'_{MAX} for incubations of each compound (at all concentrations) as well as their respective controls are presented in **Table 3.15**, **Table 3.16** and **Figure 3.26** where $t_{F'_{MAX}}$ and F'_{MAX} are compared in terms of *%Dev* from their relative controls.

Table 3.15 Values of $t_{F'_{MAX}}$ calculated from fitted ThT fluorescence curves for GS-1044, GS-1047, GS-1048, GS-1045 and GS-1049 (± S.D., *n*=3).

Compound	[Compound] (μM)	$t_{F'MAX}$ (h)			Average (h)	*%Dev*
		Run 1	Run 2	Run 3		
GS-1044	0	6	6	5.8	5.9 ± 0.1	-
	0.4	5.3	6	5.5	5.6 ± 0.4	-5.2 ± 6.2
	2	5.7	5.4	5.7	5.6 ± 0.2	-5.0 ± 2.6
	10	5.8	5.6	5.5	5.6 ± 0.1	-4.9 ± 2.3
	50	5.9	6.3	5.6	5.9 ± 0.3	0.2 ± 5.5
GS-1047	0	5.2	6.9	5.4	5.8 ± 0.9	-
	0.4	5	4.3	5.5	4.9 ± 0.6	-15.5 ± 9.8
	2	4.7	5.6	5.4	5.2 ± 0.4	-10.5 ± 7.2
	10	5.5	6.2	5.9	5.9 ± 0.3	0.5 ± 5.7
	50	6	5.8	6	5.9 ± 0.1	1.7 ± 1.7
GS-1048	0	5.2	6.9	5.4	5.8 ± 0.9	-
	0.4	5.4	5.4	6	5.6 ± 0.4	-4.3 ± 6.1
	2	4.7	4.7	4.8	4.7 ± 0.1	-18.7 ± 1.6
	10	6.3	5.4	5.5	5.7 ± 0.5	-2.0 ± 08.5
	50	5.9	6.4	6	6.1 ± 0.3	4.9 ± 4.4
GS-1045	0	6	6	5.8	5.9 ± 0.1	-
	0.4	5.2	5.2	5.3	5.2 ± 0	-11.2 ± 0.3
	2	6.7	6.6	6.7	6.7 ± 0	13.2 ± 0.8
	10	5.6	5.8	5.6	5.7 ± 0.1	-3.6 ± 1.5
	50	6.1	6.1	6	6.1 ± 0.1	2.9 ± 0.9
GS-1049	0	5.2	6.9	5.4	5.8 ± 0.9	-
	0.4	5.4	5.4	5.3	5.4 ± 0.1	-7.6 ± 0.9
	2	5.5	5.5	5.7	5.5 ± 0.1	-5.1 ± 2.3
	10	6.8	7.5	6.4	6.9 ± 0.5	18.1 ± 9.0
	50	8.8	7.1	9.5	8.5 ± 1.2	45 ± 21

Table 3.16 Values of F'_{MAX} calculated from fitted ThT fluorescence curves for GS-1044, GS-1047, GS-1048, GS-1045 and GS-1049 (± S.D., *n*=3).

Compound	[Compound] (μM)	F'_{MAX} (ΔF/h)			Average (ΔF/h)		*%Dev*	
		Run 1	Run 2	Run 3				
GS-1044	0	1040.5	956.3	1090.2	1029 ± 67.7		-	
	0.4	983.9	933.1	1058.2	991.7 ± 62.9		-3.6 ±	6.1
	2	982.7	1013.7	1128.7	1041.7 ± 76.9		1.2 ±	7.5
	10	995.1	735.4	851.2	860.6 ± 130.1		-16 ±	13
	50	960.7	990	718.3	889.6 ± 149.1		-14 ±	14
GS-1047	0	1109.7	841.6	802.1	917.8 ± 167.4		-	
	0.4	567.2	669.5	760	665.6 ± 96.4		-28 ±	11
	2	479.7	481.8	600.1	520.6 ± 68.9		-43.3 ±	7.5
	10	424.2	471.7	609.4	501.8 ± 96.2		-45 ±	10
	50	242.7	230.5	201	224.7 ± 21.5		-75.7 ±	2.3
GS-1048	0	1109.7	841.6	802.1	917.8 ± 167.4		-	
	0.4	583.3	510.3	417.5	503.7 ± 83.1		-45.1 ±	9.1
	2	743.2	1002.5	798.3	848.0 ± 136.6		-8 ±	15
	10	661.3	1020.9	416.6	699.6 ± 304		-24 ±	33
	50	329.8	303.9	425.7	353.1 ± 64.2		-61.5 ±	7.0
GS-1045	0	1040.5	956.3	1090.2	1029 ± 67.7		-	
	0.4	962.5	1019.3	960.9	980.9 ± 33.3		-4.7 ±	0.2
	2	501	503.1	499.8	501.3 ± 1.7		-51.3 ±	0.2
	10	557.9	754.5	652.3	654.9 ± 98.3		-36.4 ±	5.5
	50	338.5	232.9	341.3	304.2 ± 61.8		-70.4 ±	14.3
GS-1049	0	1109.7	841.6	802.1	917.8 ± 167.4		-	
	0.4	1109.2	831.6	821.2	920.6 ± 163.4		0 ±	17
	2	409.5	714.7	606.7	577 ± 154.8		-37 ±	17
	10	150.7	216.7	287.3	218.3 ± 68.4		-76.2 ±	7.4
	50	45.8	46.2	45.2	45.7 ± 0.5		-95.0 ±	0.1

As observed with the analogues of 3HAA analyzed in **Section 3.2.2.2.1.** all of the analogues of *o*-aminophenol decrease lag time at concentrations $\leq$ 2 μM (with the exception of 2 μM GS-1045) resulting in negative *%Dev* of $t_{F'_{MAX}}$ from controls. At the highest concentration analyzed, 50 μM, all compounds have positive *%Dev* of $t_{F'_{MAX}}$ compared to controls. This effect was most pronounced for GS-1049 with a value for *%Dev* of $t_{F'_{MAX}}$ of 45 ± 6%, corresponding to a 2.7 h delay in *f*Aβ formation. This delay in fibril formation is significant larger than conferred

by all of the other analogues of *o*-aminophenol investigated (GS-1048 showed the next most prominent delay of just 0.3h).

In stark contrast to the previously analyzed analogues of 3HAA all analogues of *o*-aminophenol decreased F'_{MAX} at all of the incubation concentrations analyzed (with the exception of 2 µM GS-1044 and 0.4 µM GS-1049 where no change was observed). The observed values of *%Dev* of F'_{MAX} for GS-1044 varied only a slightly compared to the control. Generally speaking, for all other analogues increasing incubation concentration decreases F'_{MAX}. Despite substantial decreases in F'_{MAX} for GS-1047, GS-1048, GS-1045 and GS-1049 at 50 µM (-76 ± 7%, -62 ± 11%, -70 ± 14%, -95 ± 1%, respectively) an increase in $t_{F'_{MAX}}$ was only observed for GS-1049 at this concentration, indicating that decrease F'_{MAX} does not necessarily translate into an increase in $t_{F'_{MAX}}$; this results strongly suggests that GS-1049 is indeed interfering with Aβ nucleation.

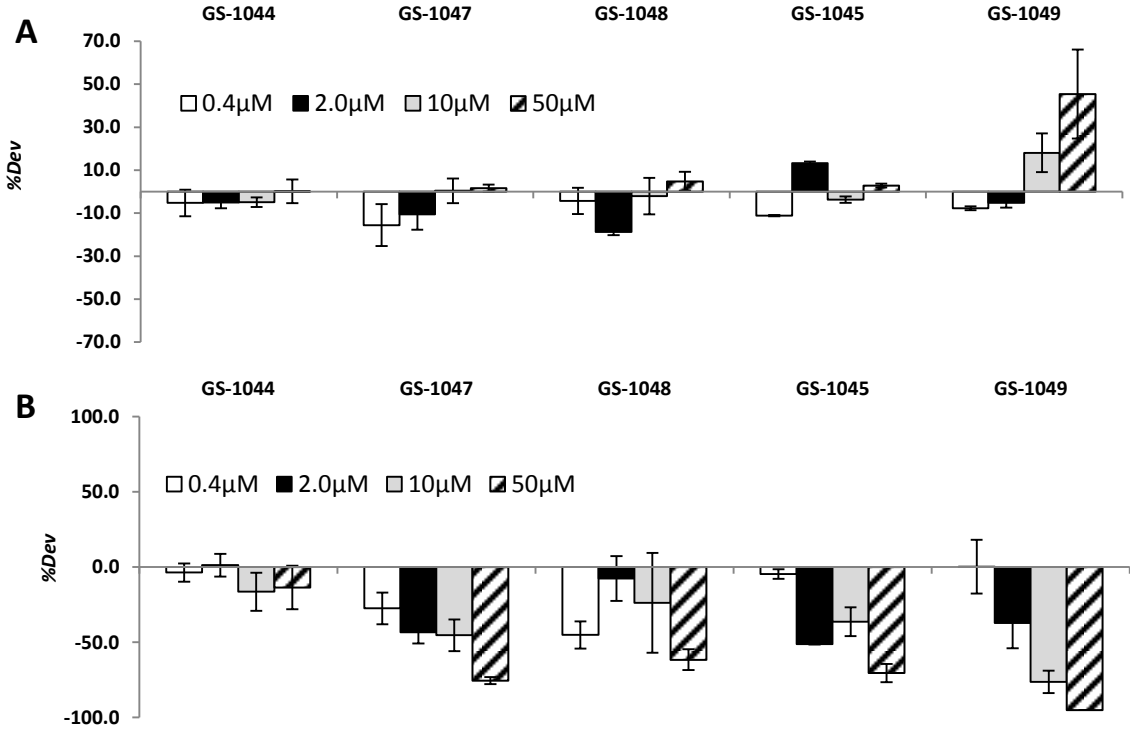

Figure 3.26 *%Dev* of **A**) $t_{F'_{MAX}}$ and **B**) F'_{MAX} from the control values calculated for GS-1044, GS-1047, GS-1048, GS-1045 and GS-1049 from fitted kinetic ThT curves (± S.D., *n*=3).

3.2.2.4 NCE-217

3.2.2.4.1 *IC*$_{50}$ Value for Inhibition of *f*Aβ Formation

NCE-217 is a unreported antiaggregant developed by Weaver and co-workers that is believed to interact with the HHQK motif of Aβ. NCE-217 consists of an indole-5-carboxylic acid ring linked at C-3 to a 2-napthol ring (**Figure 3.27**). The kinetic analysis of dose dependent

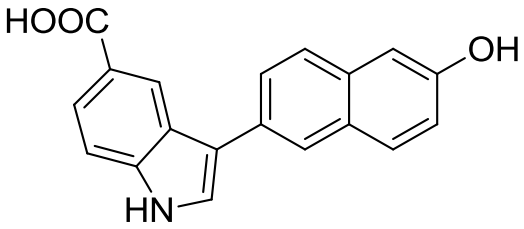

NCE-217

Figure 3.27 The structure of NCE-217, one of a series of potent bi-indole antifibrillogenic compounds developed by Weaver and coworkers.

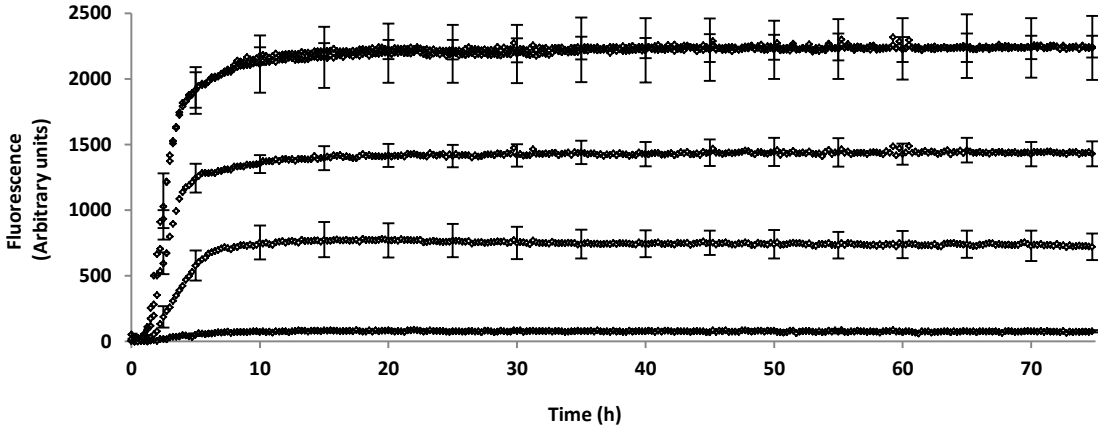

Figure 3.28 Kinetic ThT fluorescence curves of 20 μM $A\beta_{1-40}$ in the absence (control) and presence of NCE-217 (0.4 μM, 2 μM, 10 μM and 50 μM) (± S.D., *n*=3, for clarity error bars are only shown every 5 h).

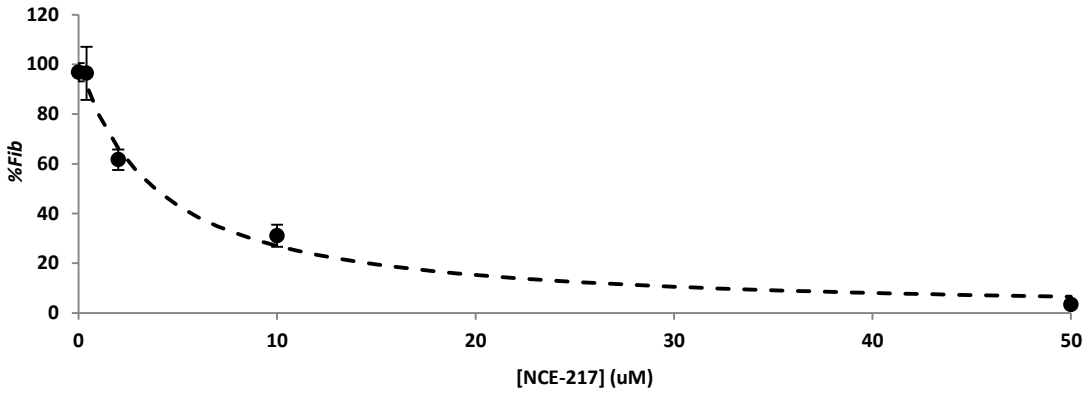

Figure 3.29 Fitted dose response curve (hashed line) to *%Fib* values determined at 75 h (black circles, ± S.D., *n*=3) for NCE-217 from kinetic fibrillization curves obtained by fluorescence measurements during the ThT fibrillogenesis assay of 20 µM $A\beta_{1\text{-}40}$ (± S.D., *n*=3).

Table 3.17 Corrected IC_{50} value for inhibition of *f*Aβ formation (from 20 µM Aβ) by NCE-217 as determined from *%Fib* data at 72 h from kinetic fibrillization curves obtained by ThT fluorescence measurements during the ThT fibrillogenesis assay for 20 µM $A\beta_{1\text{-}40}$.

Compound	IC_{50} (µM)	IC_{50} (3HAA Control) (µM)	ξ	Corrected IC_{50} (µM)
3HAA	-	-	-	**5.3 ± 1.5**
NCE-217	3.9 ± 1	20.9 ± 2.4	0.2 ± 0.1	**1 ± 0.5**

inhibition of *f*Aβ formation was conducted for comparison to 3HAA and the aminophenol analogues. Fibril formation of 20 µM $A\beta_{1\text{-}40}$ coincubated with NCE-217 at four concentrations, 0.4 µM, 2 µM, 10 µM and 50 µM, was assessed relative to $A\beta_{1\text{-}40}$ in the absence of compound. All incubations were done in triplicate in a 96-well plate. Fluorescence measurements were taken every 15 min over the course of 75 h. In **Figure 3.28** the fibrillization curves generated via the kinetic ThT fibrillogenesis assay are presented. From the kinetic fibrillization curves values for *%Fib* were determined at 75 h and the IC_{50} value for *f*Aβ inhibition was determined from the fitted dose response curves (**Figure 3.29**). From the fitted dose response curve an IC_{50} value for inhibition of *f*Aβ formation from 20 µM $A\beta_{1\text{-}40}$ was determined and corrected with a concurrently collected 3HAA control. With a corrected IC_{50} value of 1.0 ± 0.5µM NCE-217 is approximately 5x more active than 3HAA (**Table 3.17**).

3.2.2.4.2 Values of F'_{MAX} and $t_{F'_{MAX}}$ of *f*Aβ Formation

F'_{MAX} and $t_{F'_{MAX}}$ were determined by fitting the triplicate data for the fibrillization curves presented in **Figure 3.28** where 20 µM $A\beta_{1\text{-}40}$ was incubated alone (control) and with varying concentrations of NCE-217 (0.4 µM, 2 µM, 10 µM and 50 µM). The calculated $t_{F'_{MAX}}$, and F'_{MAX} for each of the triplicate curves are presented for incubations of 20 µM $A\beta_{1\text{-}40}$ with NCE-217 at each concentration as well as the control in **Table 3.18, Table 3.19** and **Figure 3.30** where $t_{F'_{MAX}}$ and F'_{MAX} are compared in terms of *%Dev* from the control.

NCE-217 increased $t_{F'_{MAX}}$ when incubated of 20 µM $A\beta_{1\text{-}40}$ in a dose dependent manner where higher concentrations of NCE-217 increased the $t_{F'_{MAX}}$. At the maximum incubation concentration of NCE-217 investigated, 50 µM, $t_{F'_{MAX}}$ was delayed by approximately 2.3 h, corresponding to a *%Dev* in $t_{F'_{MAX}}$ of 93 ± 10% by far the largest *%Dev* in $t_{F'_{MAX}}$ for any of

Table 3.18 Averaged values of $t_{F'_{MAX}}$ calculated from the general logistic curves fitted to fluorescence data collected via a kinetic ThT fibrillogenesis assay (± S.D., *n*=3).

[x] (µM)	$t_{F'MAX}$ (h)			Average (h)	*%Dev*
	Run 1	Run 2	Run 3		
0	2.8	2.2	2.4	2.4 ± 0.3	-
0.4	2.6	2.5	2.4	2.5 ± 0.1	3 ± 0.1
2	2.7	2.4	2.7	2.6 ± 0.2	6 ± 0.4
10	3.9	3.8	2.7	3.5 ± 0.7	42 ± 8
50	4.5	4.3	5.3	4.7 ± 0.5	93 ± 10

Table 3.19 Averaged values of F'_{MAX} of calculated from the general logistic curves fitted to fluorescence data collected via a kinetic ThT fibrillogenesis assay (± S.D., *n*=3).

[x] (µM)	F'_{MAX} (ΔF/h)			Average (ΔF/h)	*%Dev*
	Run 1	Run 2	Run 3		
0	822.1	1079.4	867.8	923.1 ± 137.2	-
0.4	1143	777.3	1125.1	1015.2 ± 206.1	10 ± 2
2	483.8	594.1	602.5	560.1 ± 66.2	-39 ± 5
10	156.4	245.2	265.5	222.4 ± 58	-76 ± 20
50	12.6	20.5	10.5	14.6 ± 5.3	-98 ± 36

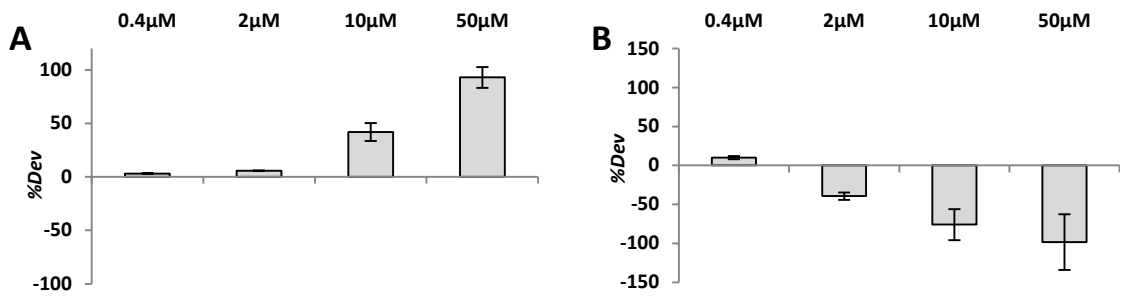

Figure 3.30 **A**) %Dev of $t_{F'_{MAX}}$ of *f*Aβ formation for incubations of 20 μM $Aβ_{1-40}$ with varying concentrations of NCE-217 from control ± S.D., *n*=3, and **B**) % deviation of F'_{MAX} of *f*Aβ formation for incubations of 20 μM $Aβ_{1-40}$ with varying concentrations of NCE-217 from control (± S.D., *n*=3).

the compounds investigated herein (GS-1049 was the next closest at 45 ± 6%). At an incubation concentration of 0.4 μM NCE-217 F'_{MAX} was slightly increased (*%Dev* 10 ± 2%); however, at incubation concentrations of 2.0 μM F'_{MAX} decreased with increasing NCE-217 concentration. At the highest incubation concentration investigated, 50 μM, NCE-217 decreased F'_{MAX} by 98 ± 36% as compared to the control.

3.3 An Assessment of Antioligomeric Activity

3.3.1 Positional Isomers of Catechol, Aminophenol and Phenylenediamine

Oligomers of $Aβ_{1-42}$ were prepared as described in **Section 6.4.2** and diluted to a final analysis concentration of 1 nM. 1 nM *o*$Aβ_{1-42}$ was incubated with a 10 μM solution of the three positional isomers of catechol, aminophenol and phenylenediamine overnight in a 96-well clear ELISA plate. Incubated solutions of *o*$Aβ_{1-42}$ with compound were then pipetted to another plate pre-adsorbed with 82E1 antibody for capture. Detection of *o*$Aβ_{1-42}$ was achieved by the addition of a *bio*-82E1 detection antibody followed by STP-HRP. TMB oxidation by HRP allowed for visualization of *o*$Aβ_{1-42}$. Due to the single-site assay format *o*$Aβ_{1-42}$ was selectively visualized by monitoring TMBD absorbance at 450 nm. The reported absorbances are the average of the three separate measurements conducted on incubations run in triplicate. For a more detail protocol used in the sandwich ELISA refer to **Section 6.4.3**.

The measured absorbances of captured *o*Aβ from overnight incubations with 10 μM solutions of resorcinol, *m*-aminophenol and *m*-phenylenediamine were all comparable to the

Table 3.20 Measured absorbance (450 nm) via the sandwich ELISA of captured *o*Aβ$_{1-42}$ from oligomer solutions (1nM *o*Aβ$_{1-42}$) incubated with the three positional isomers of catechol, aminophenol and phenylenediamine at a concentration of 10 µM (S.D., *n*=3).

Compound	A (450 nm)	A (450 nm) as % of Control
Blank	0.066 ± 0.001	-
Control	0.33 ± 0.02	**100 ± 6**
3HAA	0.17 ± 0.01	**41.6 ± 3.1**
***o*-Aminophenol**	0.07 ± 0.01	**0.27 ± 0.03**
***m*-Aminophenol**	0.31 ± 0.03	**94.0 ± 7.8**
***p*-Aminophenol**	0.40 ± 0.06	**128.5 ± 19.4**
Catechol	0.16 ± 0.01	**37.1 ± 1.6**
Resorcinol	0.35 ± 0.07	**110 ± 21**
Hydroquinone	0.07 ± 0.00	**1.8 ± 0.1**
***o*-Phenylenediamine**	0.25 ± 0.03	**69.6 ± 8.6**
***m*-Phenylenediamine**	0.33 ± 0.02	**102.9 ± 4.9**
***p*-Phenylenediamine**	0.15 ± 0.01	**32.1 ± 3.0**

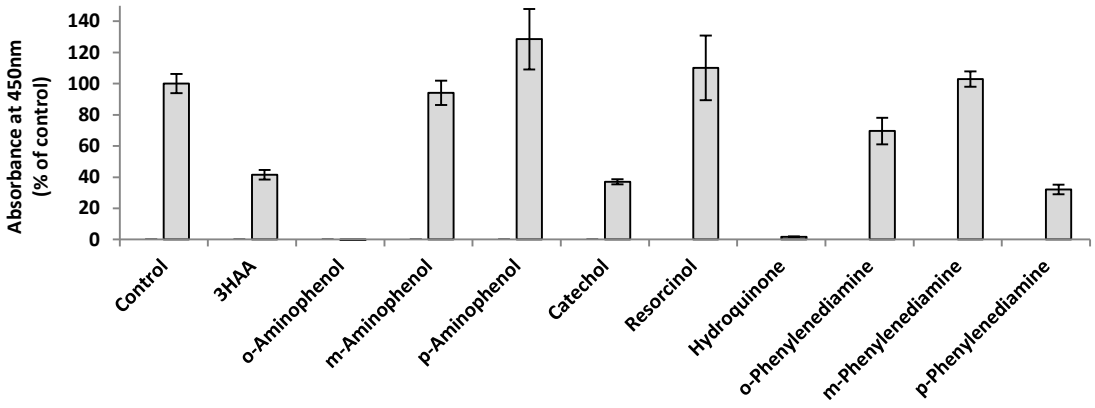

Figure 3.31 Measured absorbance (450 nm) via the sandwich ELISA of captured *o*Aβ$_{1-42}$ from oligomer solutions (1 nM *o*Aβ$_{1-42}$) incubated with the three positional isomers of catechol, aminophenol and phenylenediamine at a concentration of 10 µM (S.D., *n*=3).

control (**Table 3.20** and **Figure 3.31**) – these isomers were also the least active inhibitors of *f*Aβ formation. *o*-Aminophenol, catechol, hydroquinone and *p*-phenylenediamine, all of which are active inhibitors of *f*Aβ formation, effectively disassembled *o*Aβ. An absorbance measurement of 0% (relative to the control) indicate that overnight incubations of *o*Aβ with 10 µM solutions of

o-aminophenol and hydroquinone result in complete disassembly of oligomers. Interestingly, *p*-aminophenol, an active inhibitor of *f*Aβ formation does not dissociate preformed oligomers.

In the work described herein the two metrics measured for antiaggregant activity are: inhibition of *f*Aβ assembly and promotion of *o*Aβ disassembly. The positional isomers of catechol, aminophenol, and phenylenediamine discussed so far are either active as *f*Aβ inhibitors and *o*Aβ dissemblers, or effect neither process; intuitively this makes sense as the process of oligomerization and fibrillization are inherently linked. Interestingly however, compounds which possess excellent activity against *f*Aβ assembly may be inactive as disassemblers of *o*A. *p*-Aminophenol, an active inhibitor of *f*Aβ assembly, promoted *o*Aβ formation (129 ± 20%) (a similar result to many of the polyphenols analyzed in the preceding chapter); conversely, compounds which are inactive against *f*Aβ formation dissociated preformed *o*Aβ. *o*-Phenylenediamine, which is inactive against *f*Aβ formation, displayed moderate activity disassembling *o*Aβ. These results underscore the complexity of the aggregation process and imply that several mechanisms of action are likely at play.

3.3.2. Synthetic Analogues of *o*-Aminophenol

The antioligomeric activity of GS-1045, GS-1047, GS-1048 and GS-1049 was measured via a sandwich ELISA for comparison to 3HAA, following the same procedure as presented in **Section 2.3.1.1**. The measured absorbance of captured *o*Aβ form overnight incubation with 10 µM solutions of GS-1045 and GS-1047 were comparable to the control (**Table 3.21** and **Figure 3.32**); however, absorbance measurements of *o*Aβ incubated with GS-1048 and GS-1049 were increased relative to the control – suggesting not only that these analogues of *o*-aminophenol are ineffective as disassemblers of *o*Aβ, they promote further *o*Aβ formation.

Table 3.21 Measured absorbance (450 nm) via the sandwich ELISA of captured $oA\beta_{1\text{-}42}$ from oligomer solutions (1 nM $oA\beta_{1\text{-}42}$) incubated with GS-1045, GS-1047, GS-1048 and GS-1049 at a concentration of 10 µM (S.D., n=3).

Compound	A (450 nm)	A (450 nm) as % of Control
Control	0.33 ± 0.02	**100 ± 6**
GS-1045	0.37 ± 0.07	**116 ± 22**
GS-1047	0.32 ± 0.03	**97 ± 8**
GS-1048	0.41 ± 0.01	**134 ± 4**
GS-1049	0.54 ± 0.03	**182 ± 12**

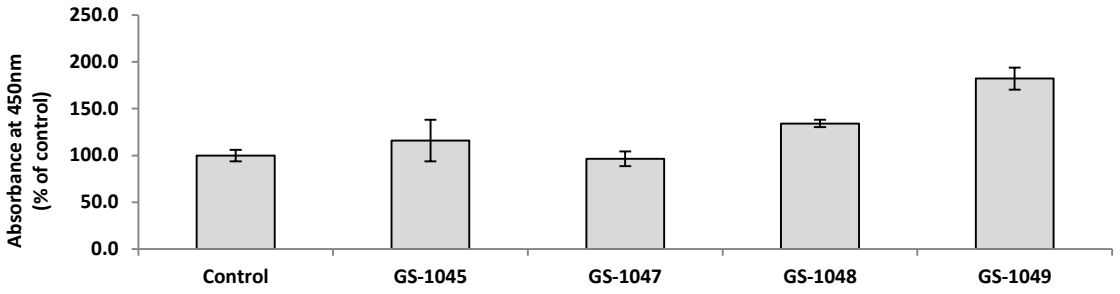

Figure 3.32 Measured absorbance (450 nm) via the sandwich ELISA of captured $oA\beta_{1-42}$ from oligomer solutions (1 nM $oA\beta_{1-42}$) incubated with GS-1045, GS-1047, GS-1048 and GS-1049 at a concentration of 10 µM (S.D., n=3).

3.4 The Successful Development of Novel Antiaggregants

A comprehensive assessment of several analogues of 3HAA has allowed for the elucidation of the aminophenol motif as the underlying functionality which confers the antiaggregant activity of 3HAA. The aminophenol motif is structurally similar to, but more active than, the catechol motif – a motif well known in the antiaggregant literature, as it is incorporated in a wide range of known antiaggregants. Both the *ortho*- and *para*-substituted isomers of catechol and aminophenol are active, however their respective *meta*-substituted isomers confer neither antifibrillogenic nor antioligomeric or activity; in addition to catechol, and aminophenol *p*-phenylenediamine has excellent antiaggregant activity, and is a scaffold that should be investigated in the development of novel Aβ antiaggregants.

Several analogues of *o*-aminophenol were developed using standard synthetic methods and resulted in discovery of four novel synthetic analogues of *o*-aminophenol that possessed improved antifibrillogenic activity, as compared to 3HAA. Interestingly, although the synthetic analogues of *o*-aminophenol investigated here were potent inhibitors of *f*Aβ formation, these compounds generally increased *o*Aβ formation in overnight incubations with preformed *o*Aβs and suggests a disparate mechanism of action than the plant-derived polyphenolic compounds investigated in **Chapter 2**. Considering the differences in activity, MM studies have been undertaken in an effort to elucidate the mechanism(s) by which these various classes of compounds interact with *m*Aβ and will be discussed in the following chapter.

Chapter 4: Insights into Mechanism of Action

Over the last two decades the antiaggregant activity of several novel classes of compounds has been rigorously characterized both *in vivo* and *in vitro*.[93,156,160,161] Due to their value as putative therapeutics Aβ antiaggregants remain an active area of research. However it remains that very little is known about the mechanism of action (MoA) of Aβ antiaggregants. Due to the amyloidogenic nature of Aβ protein crystallization is a challenge and a crystal structure of full length Aβ remains elusive;[161] this has confounded efforts to precisely determine the MoA of Aβ aggregation, although it is generally recognized that several intermediate structures precede the formation of toxic oligomers – though honing in on the active target presents a challenge.[90] The active motif(s) of antiaggregant interaction about Aβ are ill-defined – questions about their location remain.

Is there a single motif about Aβ at which all antiaggregants elicit their activity; furthermore, is this even possible given the structural variability inherent in the various classes of antiaggregants?

In the preceding chapters the antiaggregant activity of 3HAA and subsequently developed aminophenol analogues have been determined and directly compared to several known polyphenolic antiaggregants. These two classes of compounds both contain highly active antiaggregants of varying structural composition. The mode of interaction underpinning the observed activities for the aminophenols and polyphenols are investigated here using computational analysis. The preferred region of interaction about Aβ, as well as the preferred modes of interaction about those regions will be determined for molecules of each class and subsequently compared; in this way insight will be gained into the fundamental nature of the interaction of antiaggregants with Aβ. *In silico* methods in modern medicinal chemistry allow for the discovery and elucidation of potential binding motifs about proteins of therapeutic interest and will be applied here; these methods can be broadly split into two categories – quantum mechanics (QM) and molecular mechanics (MM).

4.1 Computational Methods in Medicinal Chemistry

4.1.1 Quantum Mechanics

QM uses quantum physics to calculate the properties of a molecule by explicitly considering the interaction of all electrons and nuclei within the system of analysis. QM is a powerful tool and can be used to explicitly calculate the energetics of various intramoleuclar and intermolecular interactions. Values such as molecular orbital energies, electrostatic potentials, transition-state geometries and energies as well as bond dissociation energies can be calculated with a high degree of accuracy. Despite the use of various approximations and the application of semi-empirical methods the application of QM remains computationally expensive even when analyzing the smallest systems; as such the application of quantum mechanics is limited to small molecules only.[162] Molecular mechanics is better suited for investigation of ligand binding to large molecular systems such as proteins or nucleic acids.

4.1.2 Molecular Mechanics

MM makes use of equations derived from the laws of classical physics to model atomic systems – it does not explicitly consider electrons. In essence, MM treats nuclei as a series of hard spheres connected by springs; in this way empirically derived forcefields may be used to model energy contributions of different aspects of molecular motion. In MM the Born-Oppenheimer approximation is applied – where energy changes only as a function of nuclear position and electrons are ignored; as such the calculated energies can be considered a function of the nuclear coordinates and are described by a potential energy surface.[162]

4.1.2.1 Force Fields

In MM the potential energy of a system is treated as a function of the atomic coordinates, as such the potential energy surface of a molecule can be described by a forcefield equation in the form:

$$E_{Total} = E_{Bonded} + E_{Non-Bonded}$$

Equation 4.1 The simplest form of a forcefield equation used to determine relative energies in MM calculations.

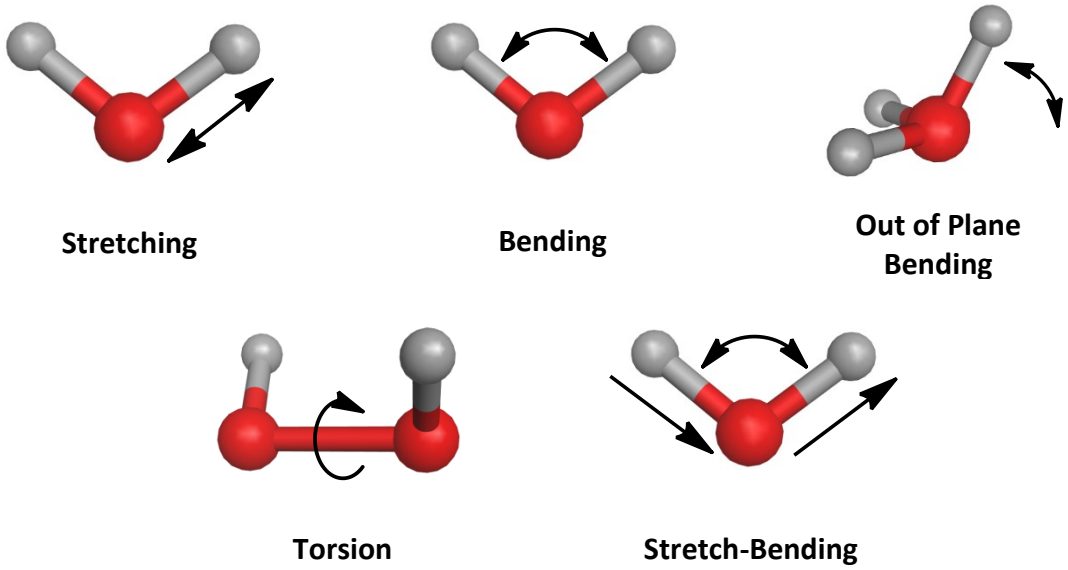

Figure 4.1 Examples of bonded atomic interactions accounted for in potential energy calculations by forcefields used in MM.

where the calculated potential energy of a molecular systems is the sum of all atomic interactions. Atomic interactions are either bonded or non-bonded. The bonded terms describe interactions between covalently linked atoms and include bond stretching, bending, out-of-plane bending and torsion – for optimal performance cross terms such as stretch-bending are included (**Figure 4.1**); non-bonded interactions describe long range non covalent interactions such as van der Waals and electrostatic forces and well as solvation energies.[162] The potential energy calculated for any molecular system, x, is the sum of the interatomic potentials for all bonded and non-bonded interactions considered in the applied forcefield:

$$E(x) = E_{str} + E_{bnd} + E_{stb} + E_{oop} + E_{tor} + E_{vdw} + E_{ele} + E_{sol}$$

Equation 4.2 Forcefield equation used to calculate the potential energy of a molecular system, x.

Equation 4.2 represents the generalized form of a forcefield used in MM simulations. Here, models for each of the considered interatomic potentials are parametric – that is, distributions about any term (such as bond length or angle) are described by a finite number of parameters. Energetic penalties are associated with the deviation of bonds and angles away from 'equilibrium' values. Take for example the energetic contribution due to bond stretching, E_{str}, within a molecular system, x. The interactions between all pairs of bonded atoms may be modeled using a harmonic potential derived from Hooke's law

$$E_{str(x)} = \sum_{Bonds} k_i\left(l_i - l_{i,0}\right)^2$$

Equation 4.3 Harmonic potential used to calculate the energetic contribution of bond stretching within a model molecular system, x.

where $E_{str(x)}$ is the sum total of energetic contributions of each bond in the molecular system, x. The energetic contribution of any bond, i, increases as bond length, l_i, deviates from the reference value, $l_{i,0}$. Accordingly, the determination of the energetic contribution of any bond within x requires that both $l_{i,0}$ and the force constant, k_i, are known. k_i and $l_{i,0}$ are parameters of the potential, $E_{str(x)}$, and are determined from experimental data and high-level quantum mechanical calculations. Parameters vary depending on the nuclei involved and their relative connectivity; as such, each potential contains a distinct set of parameters for interactions between different nuclei and different connectivities (*i*.e. C–C, C–O, C=O, or H–H). Values such as atomic mass, partial charge and van der Waals radius, as well as equilibrium values for bond length and bond angle are included in a typical parameter set.

MM has found application in a wide variety of applications for both small molecules and macromolecules such as nucleic acids and proteins; accordingly a number of forcefields are described in the literature. The functional form of potentials and parameters sets applied in any forcefield vary depending on the desired application, and are tailored to specific research objectives. A forcefield parameterized to accurately predict vibrational frequencies of covalent bonds will likely not model macromolecular events – such as protein folding – accurately (and vice versa). Selection of an appropriate forcefield is paramount in any research endeavor, and researchers must be diligent in defining their experimental objective. Here, the objective is to model potential binding interactions of a series of Aβ antiaggregants with a macromolecular receptor, Aβ. PFROSST is an all-atom forcefield parameterized for proteins, nucleic acids and small molecules. As such all MM calculated herein are conducted using the PFROSST forcefield, wherein AMBER *ff*10 parameters are used for macromolecules and parm@Frosst parameters are used for small molecules.[163] In PFROSST partial charges are dictionary-based for macromolecules and the AM1-BCC model applied for partial charges of small molecules.[164] As with all forcefields PFROSST is an empirically derived forcefield, and as such all computed energies have no meaning as absolute quantities. The computed energies, however, are still useful for comparison within a model system. The calculated ligand-protein interaction energies

within this model are determinant of the relative affinities of each ligand with the macromolecular receptor.

4.1.2.2. Energy Minimization

Energy minimization is the process whereby lowest energy state of a molecule is identified.[162] In MM the Born-Oppenheimer approximation is applied – where energy changes only as a function of nuclear position and electrons are ignored; as such the calculated energies can be considered a function of the nuclear coordinates and are described by a potential energy surface. Minimum values about the potential energy surface correspond to relatively stable molecular conformations. In the work described herein all molecules were energy minimized prior to analysis.

4.2. Experiment Design

4.2.1. Software

All MM calculations were conducted using the Molecular Operating Environment (MOE) software package (version 2013.0801, Chemical Computing Group, Montreal, Quebec, Canada).

4.2.2. Choice of Receptor Models

With only 39-43 AA residues Aβ lacks tertiary structure. In its monomeric form unaggregated Aβ has a secondary structure consisting of residues organized predominantly as α-helical or random coil substructures. Although certain regions about Aβ have a higher propensity to adopt specific conformations, the secondary structure of Aβ is dynamic and eludes absolute characterization. The objective of the *in silico* work described herein is to identify a potential binding motif for two classes of antiaggregants – one polyphenol-based and the other aminophenol-based. Considering Aβ's inherent lack of secondary structure it is likely that efforts to define antiaggregant interactions with Aβ are outside the purview of traditional ligand-receptor binding ideologies. Indeed several classes of active antiaggregants are known, and encompass series of structurally similar compounds which elicit their antiaggregant effect in a dose-dependent manner; still the traditional hand-in-glove or lock-in-key model of ligand-receptor interaction may not apply. The lack of a crystal structure and uncertainty in the absolute conformation of monomeric Aβ pose a significant challenge in modeling its interaction

with various antiaggregants. Modes of interaction for various antiaggregant molecules have been suggested, but still no consensus on an absolute motif has been reached.[111,158]

Advances in crystallographic methods have allowed for the structural elucidation of many proteins of therapeutic interest; as a result MM is used extensively in modern medicinal chemistry and has facilitated the discovery and refinement of binding motifs for a variety of receptors. Absolute structural information on Aβ-antiaggregant interactions under physiological conditions is scarce, and preclude the use of traditional *in silico* methodology wherein a well-defined receptor is screened against compounds of known therapeutic efficacy in an effort to elucidate potential binding motifs.

Previous studies indicated that a BBXB-type sequence of AA residues is shared among several amyloidogenic proteins and may represent a common motif for antiaggregant bonding. HHQK is the corresponding BBXB-type sequence about Aβ and may represent the center of interaction between for antiaggregants. Still, HHQK binding is experimentally unconfirmed, and further still the 3D structure of this potential motif during binding is unknown. A solution structure of antiaggregant-bound Aβ (at physiological conditions) could be used for traditional *in silico* ligand binding studies, as the 3D structure of the interacting AA would be well defined; however, no such structure exists for the antiaggregants investigated here. Solutions structures of Aβ obtained by NMR exist, but secondary structures vary (**Figure 4.2**). Changes in secondary structure – as observed in the various literature structures of Aβ – have a significant effect on the nature of observed receptor-ligand interaction, affecting both the AA residues involved as well as the types of interactions observed. Receptor conformation will inherently bias interactions towards specific AA residues, and as such arbitrarily choosing a receptor model may result in key interaction modes being missed altogether.

The antiaggregant docking study conducted here was completed using 9 structurally disparate receptor models. By using several structural models of Aβ each amino acid is assessed in a variety of conformations. Although structurally-based biases in binding certainly exist in each model assessed, by analyzing the aggregate data obtained for all receptors conformational influences can be mitigated as all AA are assessed in a variety of 3D structures.

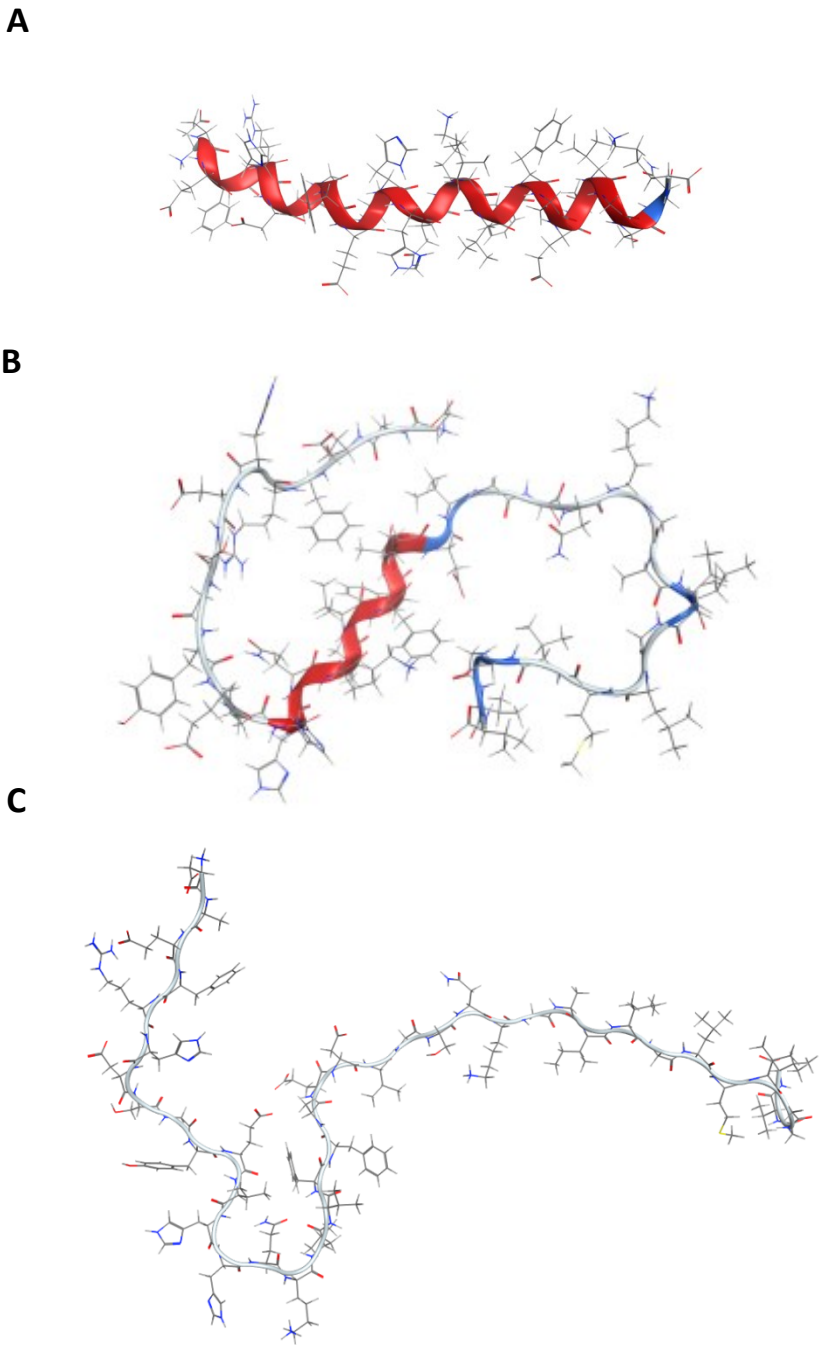

Figure 4.2 3D structures of Aβ models (identified by their PDB codes) **A**) 1AMB, **B**)2FLM and **C**)2M9R – 3 of 9 structures used in a *in silico* survey of antiaggregant aminophenol and polyphenol interactions with various isoforms of Aβ.[165–167]

Table 4.1 PDB codes of NMR structures used during *in silico* analyses of aminophenol and polyphenol antiaggregant binding to Aβ.

Isoform	PDB Code	Solvent Conditions
Aβ1-28	1AMB[165]	H_2O-D_2O (90:10) 450mM SDS
	1AMC[165]	H_2O-D_2O (90:10) 450mM SDS
Aβ1-40	1AML[168]	TFE-H_20 (40:60) 50mM potassium phosphate (pH 2.8)
	1BA4[169]	H2O-D2O (90:10) 100mM SDS (pH 5.1)
	2LFM[166]	H_2O-D_2O (93:7) 20mM phophate, 50mM NaCl
	2M9R[167]	DMSO
	2M9S[167]	DMSO
Aβ1-42	1IYT[170]	HFIP-H_2O (80:20) 1mM
	1Z0Q[171]	HFIP-H_2O (30:70) 1mM

The objective of the MM work presented here is not to define a 3D structure of a binding motif. The dynamic nature of Aβ structure may preclude the existence of a well-defined binding structure. The purpose of the MM work herein is twofold: first, to identify the AA residues about Aβ most likely to be involved in antiaggregant binding interactions; and second, to determine the nature of those interactions in an effort to gain insight into the molecular features which confer antiaggregant activity.

All of the surveyed structures were predominantly α-helical or random coil as this is the general structural composition of monomeric, unaggregated, Aβ.[171] In total 9 literature NMR solution structures of monomeric Aβ were assessed for ligand binding (**Table 4.1**). All Aβ structures were downloaded from the protein data bank (PDB).

4.2.3. Docking

4.2.3.1. Molecule Preparation

4.2.3.1.1. Aβ Receptors

Structural models of Aβ downloaded from PDB as protein database files (.pdb) were converted to MOE molecule files (.moe) and imported to MOE. All receptors were set to a protonation state according to physiological pH and were subsequently energy minimized prior to docking. An algorithm within MOE used to conduct the docking procedure allows for specific residues to be analyzed preferentially. This required that segment be defined in the sequence

Table 4.2 Residue composition of the segments screened for each of the three isoforms of Aβ analyzed.

Segment	Residues Docked		
	AB_{1-28}	AB_{1-40}	AB_{1-42}
1	1-6	1-6	1-6
2	4-9	4-9	4-9
3	7-12	7-12	7-12
4	10-15	10-15	10-15
5	13-18	13-18	13-18
6	16-21	16-21	16-21
7	19-24	19-24	19-24
8	22-28	22-27	22-27
9	-	25-30	25-30
10	-	28-33	28-33
11	-	31-36	31-36
12	-	34-40	34-39
13	-	-	37-42

editor found in MOE to be docked sequentially. To ensure complete coverage of each receptor sequence, the entirety of each sequence was docked in segments of 6 AA residues (with the exception of the 28 and 40 AA isoforms, where the final docked segment consisted of 7 amino acids. Consecutive segments overlapped by 3 AA residues (**Table 4.2**). Depending on the isoform of the model being docked, complete sequence coverage was achieved in 8-13 segments.

4.2.3.1.2. Antiaggregant Ligands

The antiaggregants to be surveyed were compiled into a MOE molecular database file (.mdb) and uploaded to MOE. All ligands were set to a protonation state according to physical pH (7.4) and were subsequently energy minimized prior to docking.

4.2.3.2. Docking Protocol

Docking was completed using the induced fit methodology native in the MOE docking algorithm. In MOE, the docking workflow begins with both a prepared receptor and a ligand database (**Figure 4.3**). Ligand placement is facilitated via a triangle matcher where ligand binding poses are generated by superposition of ligand atom triplets with triplets of receptor site points. Receptor site points are defined by the center positions of alpha spheres. Each iteration of

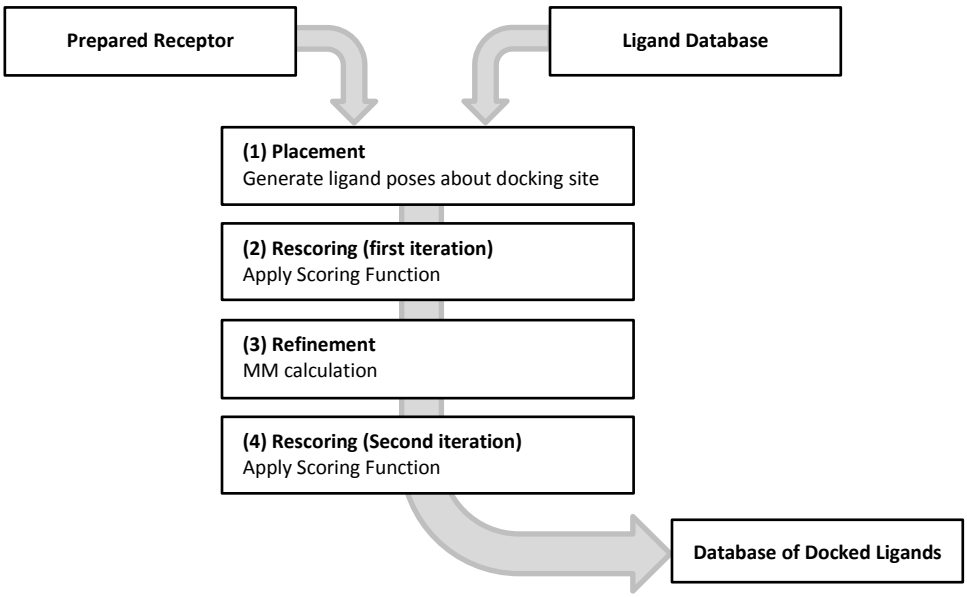

Figure 4.3 Stages of the docking algorithm in MOE.

ligand placement is randomized. A ligand conformation is randomly selected; random triplets of ligand atoms and alpha sphere centers are then used to determine the pose. The generated poses are assigned a score by the placement method; poses with favorable energies move on to the first iteration of rescoring which uses the London dG scoring function to estimate the free energy of binding from a given pose. Poses with favorable energies move on and are then refined by minimization using the PFROSST forcefield and move on to the second iteration of rescoring. This final iteration of rescoring uses the GBVI/WSA dG forcefield-based scoring function which estimates the free energy of biding of the ligand from a given pose. The docking protocol was set to retain a maximum of 30 favorable binding poses per ligand in the output database of favorable binding poses. The output databases for each segment of receptor screening (**Table 4.2**) for a particular receptor model were then combined for further analyses.

4.2.3.3. Selection of Poses for Further Analyses

Each antiaggregant ligand was docked along the entire sequence of each of the 9 PDB models of Aβ, resulting in thousands of stable interactions calculated for each ligand-receptor combination (**Table 4.3**). The position (relative to the receptor) and conformation of a receptor-bound ligand is referred to as a binding pose. During the docking procedure the free energy of binding of the ligand, ΔG, is calculated from a given pose. ΔG is the calculated in the final iteration of rescoring, and is given in units of kcal/mol. Negative values of ΔG indicate a

Table 4.3 The calculated stable protein-ligand interactions observed for each antiaggregant ligand with the 9 analyte receptor models of Aβ.

Compound	Number of Stable Protein-Ligand Interactions									
	1AMB	1AMC	1AML	1BA4	2FLM	2M9R	2M9S	1IYT	1Z09	Total
3HAA	185	176	264	264	277	299	274	299	293	***2331***
o-Aminophenol	122	125	246	242	257	265	231	213	265	***1966***
GS-1045	127	150	206	223	238	259	211	222	239	***1875***
GS-1047	141	165	216	222	239	225	214	227	233	***1882***
GS-1048	155	156	256	255	264	262	242	256	259	***2105***
GS-1049	149	164	253	260	277	273	251	246	284	***2157***
Rosmarinic Acid	206	206	328	323	326	327	326	351	355	***2748***
Epicatechin	147	155	247	249	229	247	267	250	259	***2050***
EGCG	193	189	311	304	298	315	311	327	338	***2586***
Quercetin	150	162	256	239	251	251	241	271	301	***2122***
Resveratrol	111	111	179	183	187	195	191	217	203	***1577***
Myricetin	155	165	253	259	247	247	245	260	274	***2105***
Kaempherol	140	144	237	225	232	224	231	254	262	***1949***
Morin	150	167	253	254	228	242	242	275	285	***2096***
Hesperetin	141	148	253	235	257	255	262	228	279	***2058***
Naringenin	136	129	221	186	212	210	235	235	221	***1785***
Luteolin	140	150	243	236	233	249	242	259	268	***2020***
Total	***2548***	***2662***	***4222***	***4159***	***4252***	***4345***	***4216***	***4390***	***4618***	**35412**

favorable interaction; the lower the value of ΔG the stronger the interaction. Since the work herein is focused on favorable binding interactions, 10 low energy poses were selected for each ligand with each receptor for further analysis. In the docking algorithm there is an option for automated removal of duplicate poses. The software considers poses to be duplicate if the same set of ligand-receptor atom pairs are involved in hydrogen-bond interactions or and the same set of ligand-receptor atom pairs are involved in hydrophobic interactions. Still, the output databases often contained series of poses with nearly identical poses. Take for example the three lowest energy poses of kaempferol binding to 1IYT presented in **Figure 4.4**. Provided for each pose is a 3D structure of the ligand-receptor interaction along with a diagram of the interaction. With energies of -4.7506 kcal/mol, -4.7481 kcal/mol and -4.7365 kcal/mol these three structures are essentially identical and were included in the database of output poses despite automated duplication removal enabled in the docking program; series of as many as 7 of such duplicates were encountered for all ligands. To ensure that a better sampling of interactions was analyzed, duplicates were therefore removed manually subsequent to analysis.

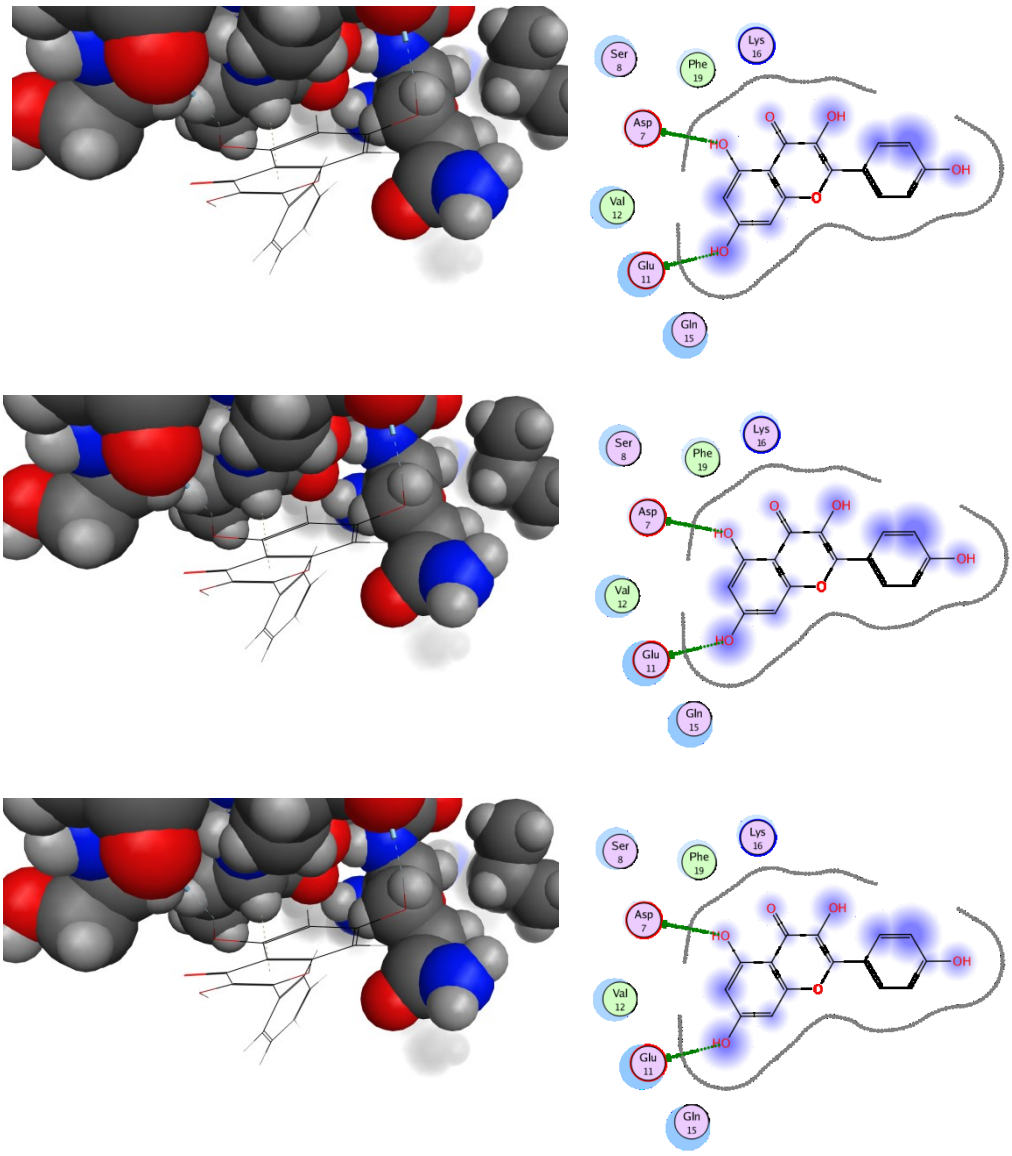

Figure 4.4 The three lowest energy poses of kaempferol binding to 1IYT.

4.2.3.4. Determination of Intermolecular Interactions of Selected Poses

The output databases obtained from the docking procedure contain coordinate data corresponding to the 3D structures of both the ligand and receptor generated for each pose. In the induced fit methodology employed in the docking procedure the receptor backbone atoms are fixed during refinement; however sidechains are free to move as such the 3D structure for each generated pose is unique. Structural data for both the receptor and ligand of a given pose were imported into MOE for analysis. Reports were generated for all favorable poses using the

ligand interaction function. Interaction data for each of the selected poses was collected and included the type of interaction as well as the AA involved in said interaction. The ligand interaction function will only explicitly report hydrogen-bonding, π-π, H-π, and cation-π interactions, and many of the analyzed binding poses contain no such interactions. When such was the case, the closest amino acid to each ring was determined by manual measurement. The AA with the closest carbon atom (or heteroatom) to each ring was identified and the interaction was said to be a van der Waals interaction (vdw) between the ring of the ligand and that AA. Accordingly, ligands with one ring system were assigned one vdw interaction, ligand with two rings were assigned two vdw interactions (each ring with its closest relative AA), and so forth. For polyphenols the 8 atom fused heterocyclic rings were treated as a single unit. To clarify, van der Waals interactions are involved in ***all*** ligand-protein interactions, but in the absence of any other interaction only vdw is at play. Assigning the vdw force to a specific AA residue(s) allows for the ligand position about the bound receptor to be noted.

4.3. Analysis of Antiaggregant Interactions

Interactions for the two classes of antiaggregants, polyphenol-based and *o*-aminophenol-based were examined to determine both the nature of the interactions and the amino acids involved in said interactions. In total 11 polyphenol-based antiaggregants (rosmarinic acid, epicatechin, EGCG, quercetin, resveratrol, myricetin, kaempferol, morin hesperetin, naringenin and luteolin) and 6 *o*-aminophenol-based (3HAA, *o*-aminophenol, GS-1045, GS-1047, GS-1048 and GS-1049) were subjected to *in silico* docking studies.

10 poses of all antiaggregants were selected for each receptor model of Aβ; this corresponds to 990 poses for the polyphenol-based antiaggregants and 540 poses for the *o*-aminophenol-based antiaggregants. Each binding poses was analyzed to determine the nature and strength of the interaction as well as the AA residue(s) involved. **Figure 4.5** shows the number of interactions counted for first 40 AA residues of Aβ with either polyphenol or *o*-aminophenol antiaggregants. In this figure only data from models at least 40 residues in length are included (1AML, 1BA4, 2LFM, 2M9R, 2M9S, 2M9R, 1IYT and 1Z0Q). Over these 7 receptor models 1305 interactions were observed for the polyphenols and 612 interactions were observed for the aminophenols. Both classes of antiaggregants showed a significant preference to interact with the first 28 residues of Aβ (89.3% and 84.0% of interactions for the polyphenols

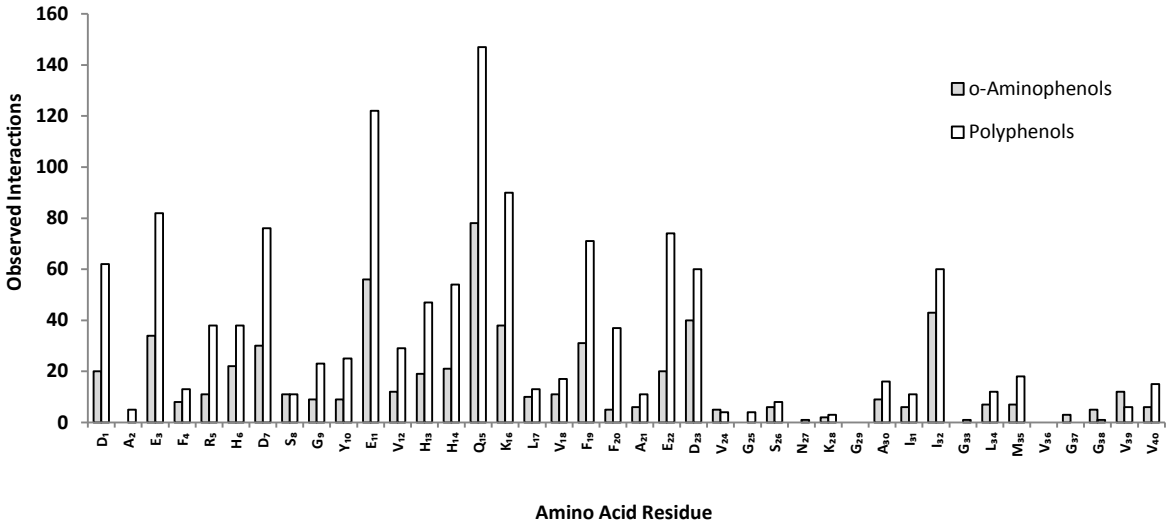

Figure 4.5 Rate of AA residue involvement with the first 40 AA residues of Aβ with 990 of the most favorable protein-ligand interactions of 11 polyphenols and 540 of the most favorable interactions of 6 aminophenols with Aβ models 1AML, 1BA4, 2LFM, 2M9R, 2M9S, 2M9R, 1IYT and 1Z0Q.

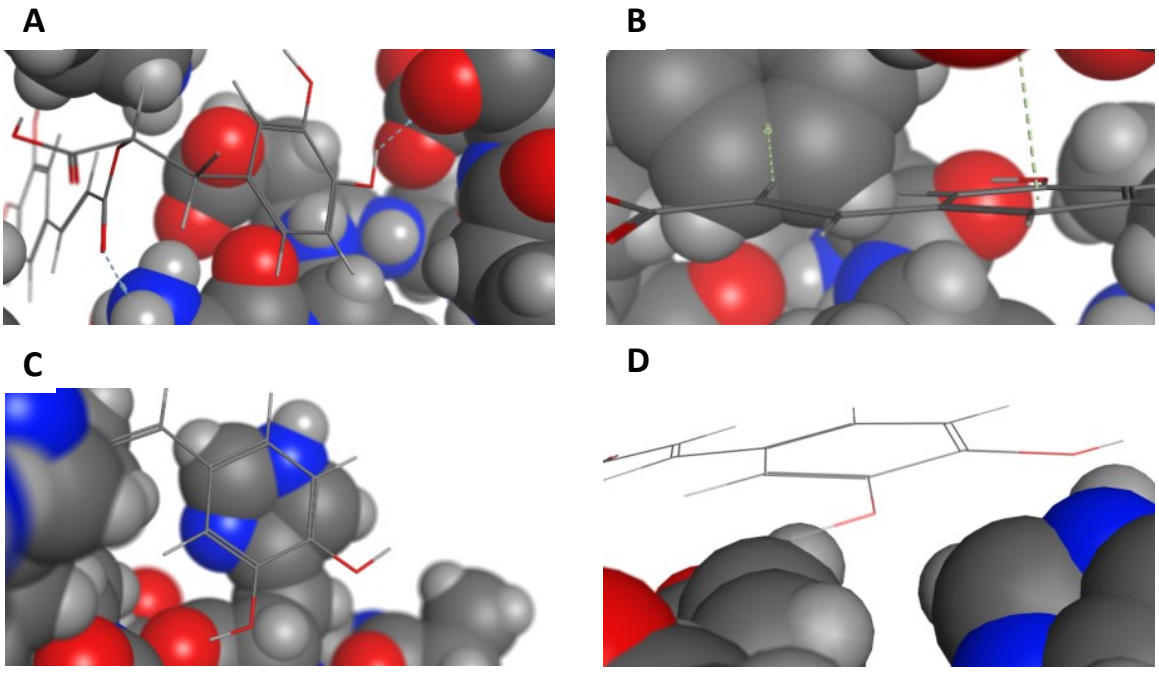

Figure 4.6 Rosmarinic acid interacts with Aβ via **A**) concurrent H^D and H^A interactions; **B**) concurrent H-π and π-H interactions; **C**) a π- π interaction and **D**) vdw interaction**.**

and aminophenols, respectively). The majority of binding interactions were observed within the first 28 residues for all the receptor models analyzed, with the exception of 1AML – as such only interactions with residues 1-28 of all receptor models were analyzed further. Interaction data for the 1AMB and 1AMC (models of $A\beta_{1-28}$) were subsequently included for further analysis.

6 modes of interaction were found to predominate in favorable binding poses (**Figure 4.6**): ligands were able to act as hydrogen-bond donors, forming hydrogen-bonds with either heteroatoms (denoted, H^D) or pi-systems (H-π) about Aβ; although less frequent, ligands were also able to act as hydrogen-bond acceptors having either their heteroatoms (H^A) or pi-systems (π-H) accept hydrogen-bonds from AA residues about Aβ; ligand aromatics were also able to interact via pi-pi stacking (π- π) with aromatic AA. In the absence of the aforementioned interactions binding was mediated per van der Waals interactions (vdw).

4.3.1. Polyphenols

4.3.1.1. Flavonoids

9 of the 11 polyphenols analyzed here belong to the flavonoid class of polyphenolic compounds. All flavonoids share the same core structure – a 15 carbon skeleton which consists of two phenyl rings one of which is fused to an oxygen-containing heterocyclic ring. The general structure is presented in **Figure 4.7A** (with ring designations and numbered carbons); the

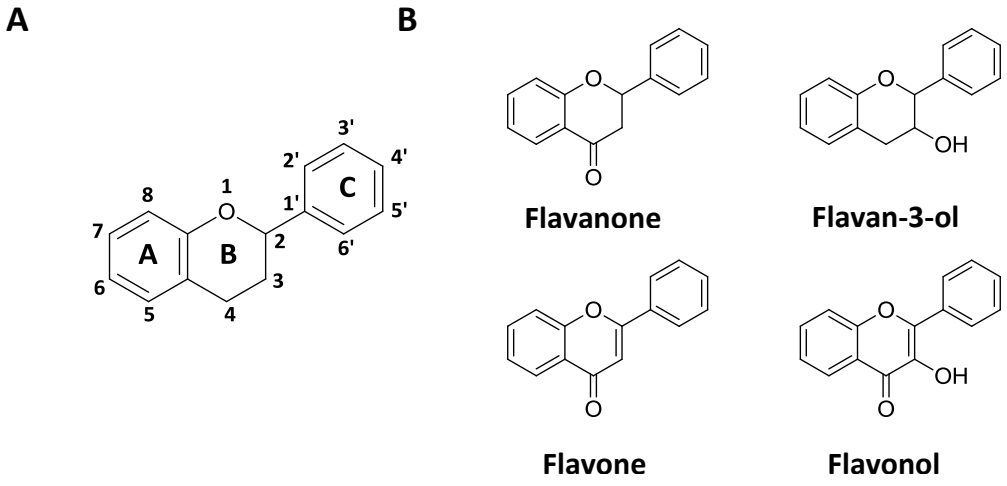

Figure 4.7 **A**) The general shared structure of flavonoids and **B**) the structures of 4 sub-classes of flavonoids analyzed for Aβ binding in the present study: flavan-3-ols, flavanones, flavonols and flavones.

structures of the 4 sub-classes of flavonoids analyzed here – flavan-3-ols, flavanones, flavonols and flavones are presented in **Figure 4.7B**. Compounds within specific classes differ in the number and placement of hydroxyl groups (or occasionally methyl esters, as in hesperetin).

The relative binding residues about Aβ and modes of interactions will be compared for the classes of flavonoids presented here. All of these compounds share comparable activity as inhibitors of *f*Aβ formation; however there are differences. Generally speaking flavonols show a modest improvement in efficacy relative to other classes of flavonoids.[172] Differences in activity amongst the various classes of flavonoids are likely structurally based and will be explored here; to this end, AA interactions (within the first 28 residues of Aβ) from the 90 poses selected for each flavonoid will be discussed in detail.

The data collected in the MM work presented here is an aggregate of data from docking experiments using several structurally unique models of Aβ. Each ligand is assessed for preferred AA residues as well as the types of interactions involved in binding. In the present discussion the distribution of AA residues involved in binding interactions with each compound will be referred to as the distribution profile of said compound; just the same, the types of interactions observed in binding for each compound will be referred to as the interaction profile.

4.3.1.1.1. Flavan-3-ols

Of the flavonoids analyzed two were flavan-3-ols, epicatechin and EGCG. The number of interactions observed at Aβ residues 1-28 is presented in **Figure 4.8** for both flavan-3-ols; interaction profiles are included for each flavonoid in this figure (presented as pie charts) and display the observed number of interactions by type (as a proportion of the total number of interactions observed).

128 interactions were observed for epicatechin and 20% of these occur at H_{13}, where the majority of π-π interactions take place (a trend of all the flavonoids analyzed). Binning the AA interaction count segments of 4 concurrent AA residues (**Figure 4.9**) shows that over a third of all observed interactions occur at HHQK (the most of any non-acid-containing 4 AA sequence) – indicating that this sequence is a favorable binding area. Both phenyl rings of epicatechin were able to engage in π-stacking with and did so with the majority of aromatic residues (no π-π

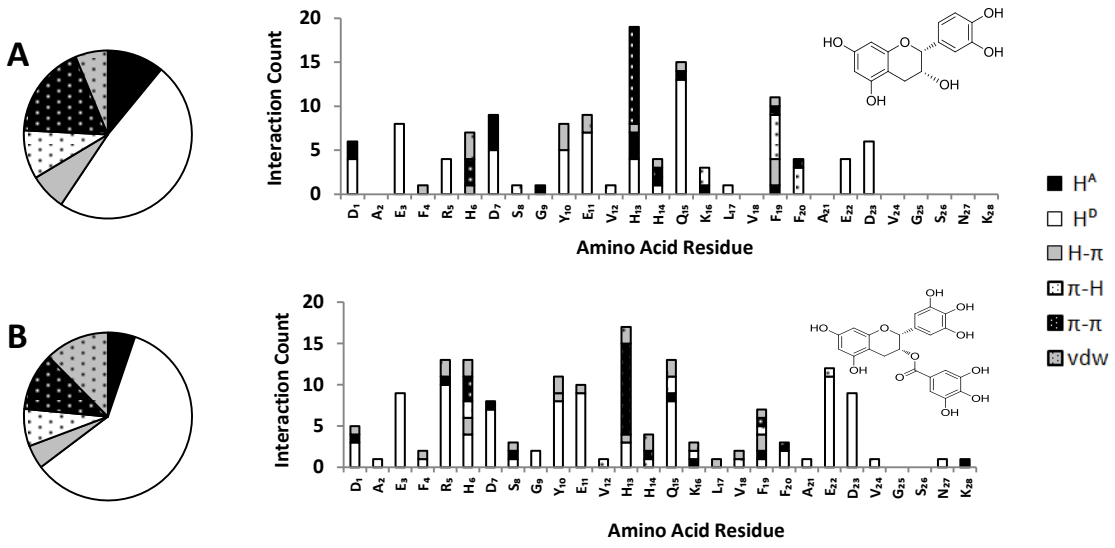

Figure 4.8 Interactions counts at Aβ AA residues 1-28 and interactions profiles for **A)** epicatechin and **B**) EGCG with the first 28 residues of Aβ.

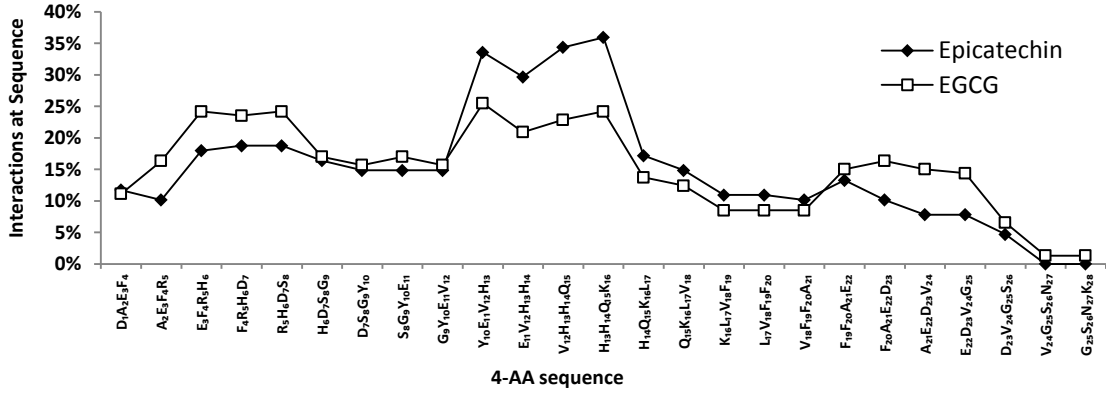

Figure 4.9 Distribution profiles of epicatechin and EGCG interactions within the first 28 residues of Aβ (interactions counts are binned in sections of 4 AA residues in length).

interactions were observed with Y_{10} and F_4). In addition to engaging AA via π-stacking both phenyl rings could accept hydrogen-bonds in the form of π-H type interactions; although these rings could also donate a hydrogen-bond and engage in H-π interactions, the vast majority of these interactions are mediated through hydrogens at the 4-position of the heterocyclic ring. H^A and H^D interactions are mediated through all aromatic hydroxyls as well as the alcohol at position 3 of the heterocyclic ring. H^A interactions comprised 11% of all observed interactions (the largest proportion for any of the flavonoids analyzed). The majority of observed interactions H^D interactions (48%) – typically with D and E residues.

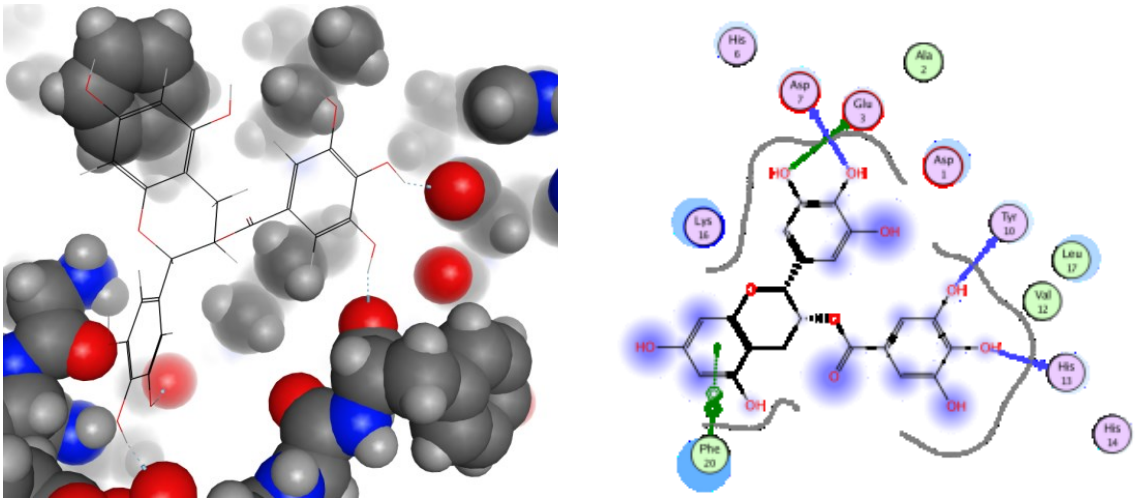

Figure 4.10 EGCG interacting with 1IYT via 4 concurrent H^D interactions and one π-π interaction.

EGCG is furnished with gallic acid ester on the alcohol at position 3 of the heterocyclic ring, the addition of which dramatically changed the interaction profile of EGCG. In total 153 interactions were observed – 25 more than epicatechin. Although a majority of interactions occur at H_{13}, the relative proportion is significantly less than observed with epicatechin (11.1% versus 20%), the relative proportion of interactions at D and E residues is concurrently increased relative to epicatechin. These changes are due to the gallic acid ester, which with three hydroxyl effectively increases the amount of intermolecular receptor-ligand interactions that can happen at once; this explains the increases in both total interactions as well as and proportion of H^D interactions observed. 91 unique H^D interactions were observed for EGCG, more than all other polyphenols analyzed here (flavonoids and otherwise). All of the flavonoids analyzed here often engaged in multiple H^D interactions simultaneously, but not usually to the degree of EGCG which formed the most extensive hydrogen-bond networks (**Figure 4.10**). As such EGCG bound D and E residues more often that the other flavonoids (excellent hydrogen-bond acceptors). Here, increased proportion of H^D interactions comes at the expense of all other types of interactions with the exception of vdw-type interactions which more than double compared to epicatechin.

4.3.1.1.2. Flavonols

Four flavonols were analyzed: quercetin, myricetin, kaempferol and morin. The number of interactions observed at Aβ residues 1-28 and interactions profiles are presented for all four flavonols in **Figure 4.11**. Although slightly higher, the number of interactions observed for each

of the flavonols was comparable to that observed for epicatechin (136, 134, 145 and 139 for quercetin, myricetin, kaempferol and morin, respectively). The distribution profiles of all the flavonols more closely resembles that of epicatechin than EGCG, however, systematic differences are observed. Similarly to epicatechin, the majority of flavonol interactions occur at $H_{13,}$ and D and E residues are favored, but flavonols tended to interact more frequently with aromatic residues; again HHQK is the most frequently interacted non-acid-containing segment (**Figure 4.12**). The interaction profiles are more or less conserved among the flavonols and these too are systematically different than that of epicatechin. Notable differences in interaction preferences are an increased propensity to interact via vdw or π-H interactions and a reduction in H-π and H^D interactions.

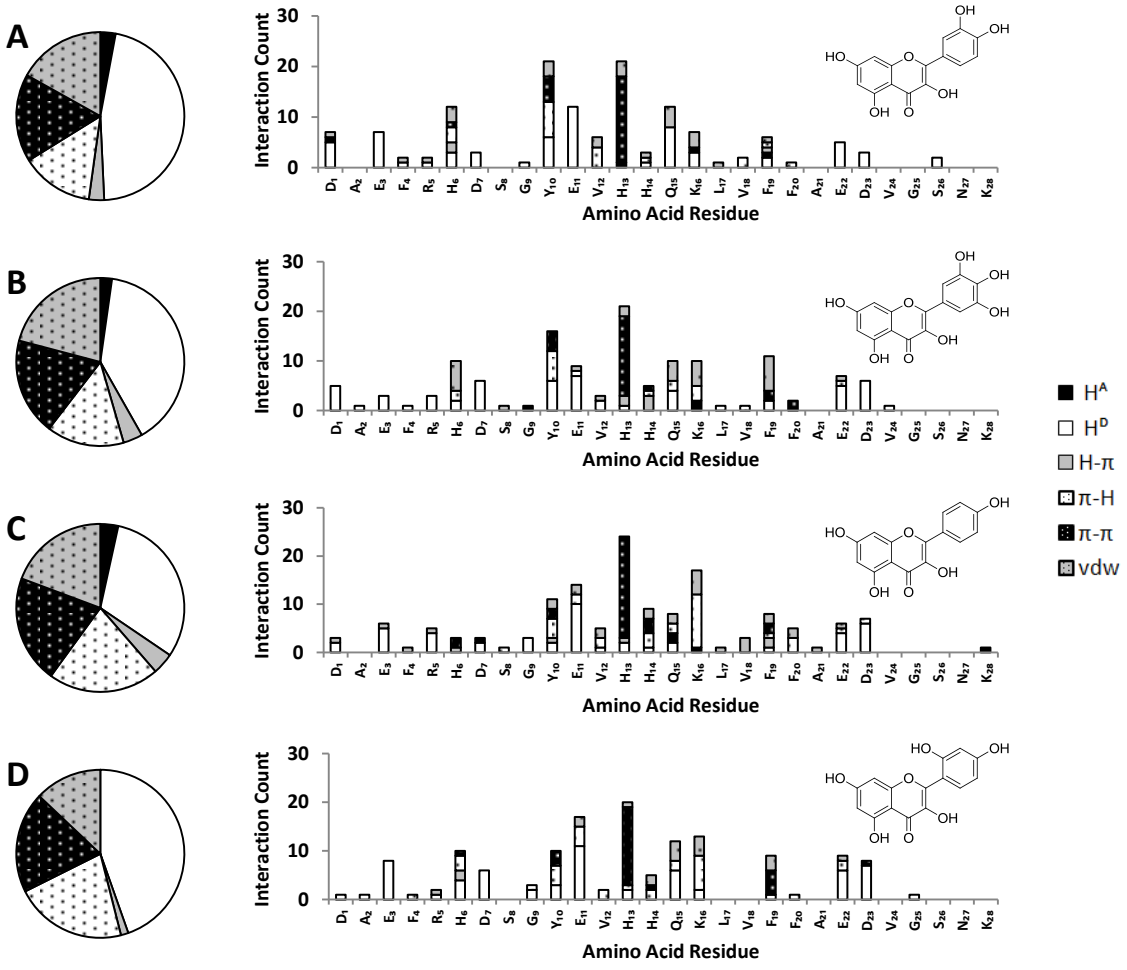

Figure 4.11 Interactions counts at Aβ AA residues 1-28 and interactions profiles for **A**) quercetin **B**) myricetin **C**) kaempferol and **D**) morin.

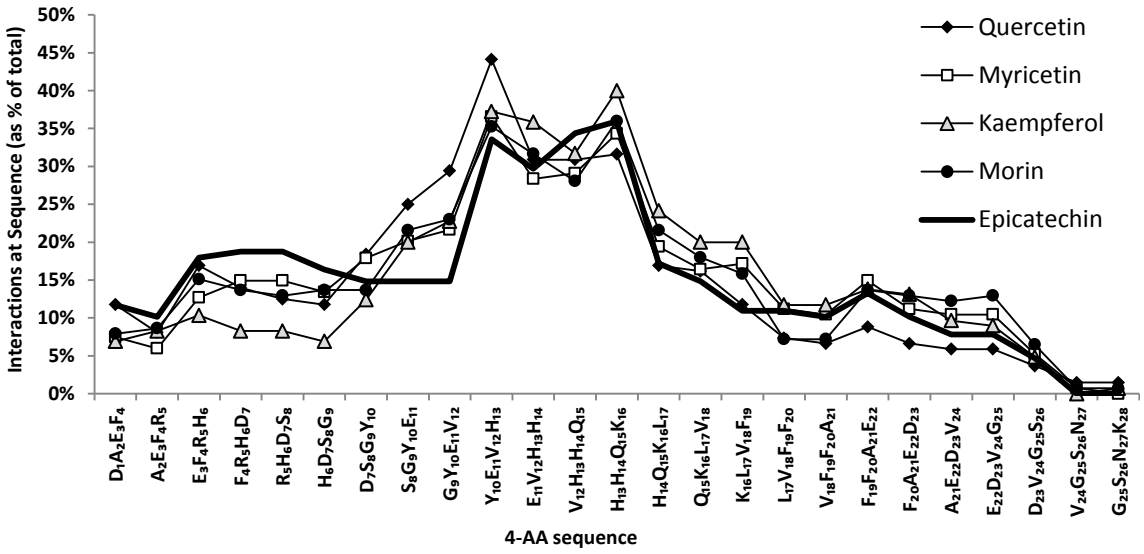

Figure 4.12 Distribution profiles of quercetin, myricetin, kaempferol and morin interactions within the first 28 residues of Aβ (interactions counts are binned in sections 4 AA residues in length). The distribution profile of epicatechin is presented as well for comparison (thick black line).

The changes in the interaction preferences of the flavonols are structurally based. Flavonols differ from epicatechin in three ways: aromatization of the heterocyclic ring, incorporation of a carbonyl at position 4 of the carbon skeleton; and the number and position of hydroxyls on the A ring of the flavonoid scaffold. Because the heterocyclic ring is aromatized, the flavonols have an extra ring that is able to participate in π-stacking; despite this, the proportion of observed π-π interactions does not change significantly in comparison to epicatechin (17%, 19%, 21% and 19% for quercetin, myricetin, kaempferol and morin respectively, versus 18% for epicatechin). As with epicatechin, flavonol π-stacking occurred predominantly with H_{13}, but unlike catechin they were also able to participate in π-π interactions with Y_{10} (again, no π-stacking were observed at F_4). The relative increase in π-H interactions is due flavonol incorporation of the aromatic heterocycle which is able to accept hydrogen-bonds in π-H type interactions; the decrease of H-π interactions is due to inclusion of a carbonyl at position 4 of the heterocyclic ring – these the hydrogens which typically mediate H-π interactions for epicatechin. H^D interactions were tended to make up a smaller proportion of all those observed for all flavonols when compared to epicatechin, due to of aromatization of the heterocyclic ring the enol at position 4 is in the plane of the heterocyclic ring for the flavonols. Approximately 20% of all H^D interactions observed for epicatechin were mediated

through this alcohol and moving it into the plane of the ring (as with the flavonols) reduces the relative amount of H^D interactions for this moiety.

4.3.1.1.3. Flavanones and Flavones

The observed interactions of two flavanones, naringenin and hesperetin, and one flavone, luteolin, were analyzed. The number of interactions observed at Aβ residues 1-28 and interactions profiles are presented for each compound in **Figure 4.13**. Although slightly higher again, the number of interactions observed for each of the flavonols was comparable to that observed for epicatechin (136, 135, and 139 for hesperetin, naringenin and luteolin, respectively).

The distribution profile of luteolin was very similar to that of epicatechin (**Figure 4.14**). The structure of luteolin more closely resembles that of the flavonols than epicatechin (aromatization of the heterocyclic ring, incorporation of a carbonyl at position 4 of the carbon skeleton) and accordingly the interaction profile shifts in much the same way as the flavonols

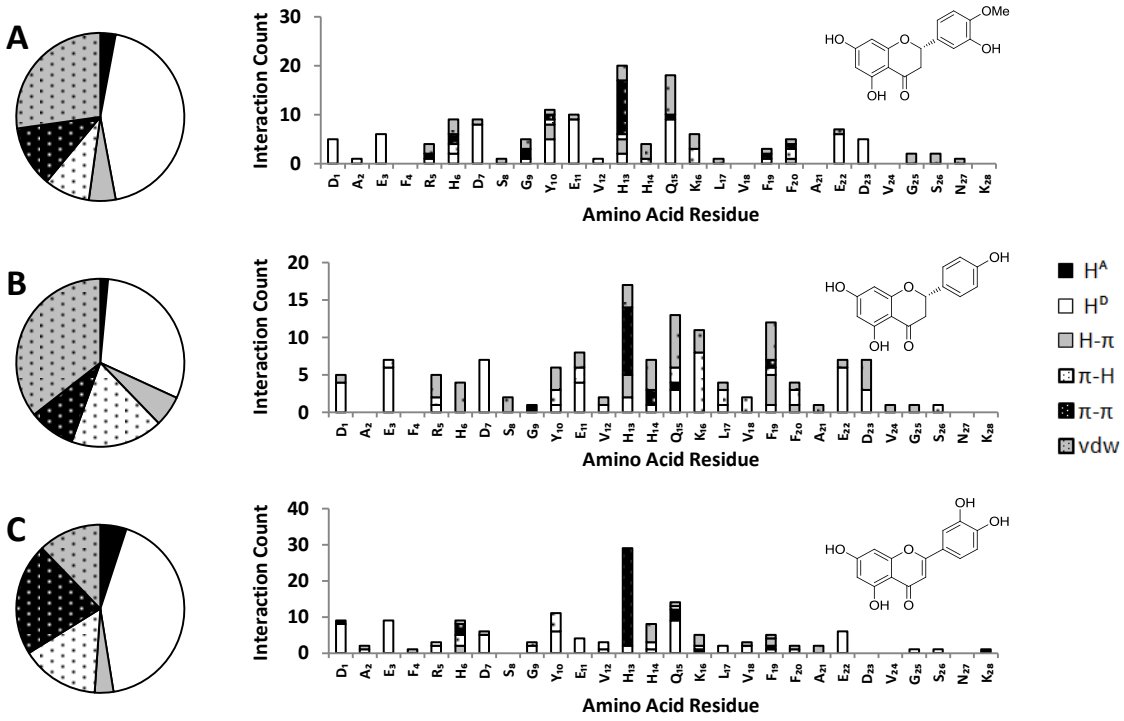

Figure 4.13 Interactions counts at Aβ AA residues 1-28 and interactions profiles for **A**) hesperidin **B**) naringenin and **C**) luteolin

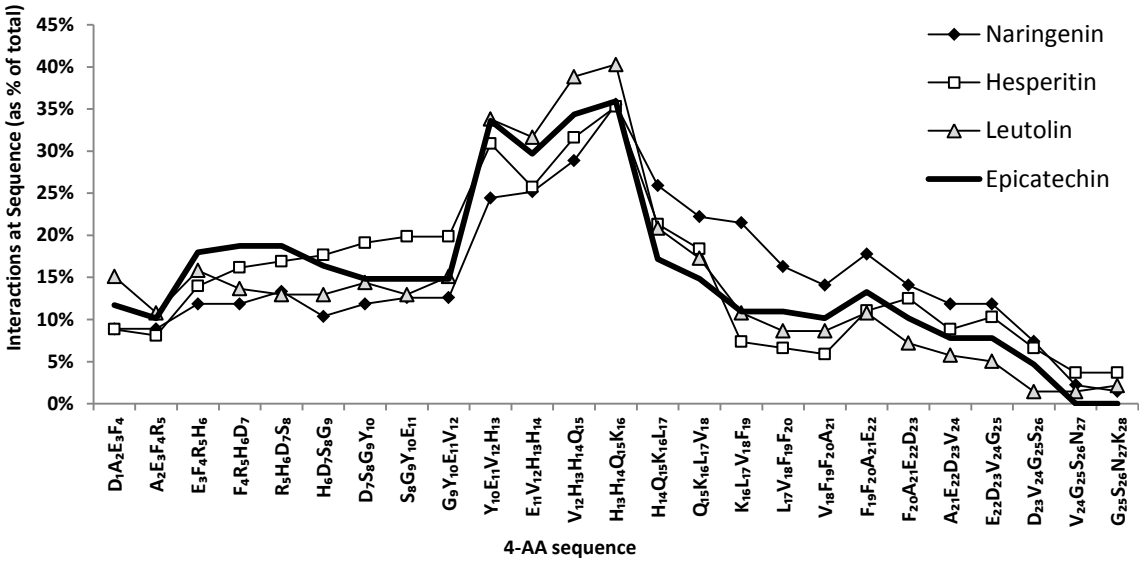

Figure 4.14 Distribution profiles of hesperetin, naringenin and leutolin interactions within the first 28 residues of Aβ (interactions counts are binned in sections 4 AA residues in length). The distribution profile of epicatechin is presented as well for comparison (thick black line).

when compared to epicatechin. An increased propensity to interact via vdw or π-H interactions and a reduction in H-π and H^D interactions are all observed. 42% of interactions were H^D interactions, lower than two of the flavonols, quercetin and morin (and lower still than epicatechin). The observed decrease in H^D interactions is due to outright replacement of the alcohol at position 3 by hydrogen which is unable to participate in H^D interactions. As with the flavonols aromatization of the heterocyclic ring both increases π-H and decreases H-π type interactions. The rate of π-π mediated interactions is consistent with both epicatechin and the flavonols.

The distribution of observed interactions for naringenin and hesperetin differed quite substantially among themselves, an interesting result considering that these two compounds are of the same class; comparatively, the flavonols all shared similar distributions in their interactions about Aβ. Further still, the distribution profiles of the observed reactions also differ substantially when comparing naringenin and hesperetin. The observed changes in both the interaction and distribution profile of these compounds reflects key structural changes when compared to epicatechin. With 4 hydroxyls and 1 alcohol epicatechin is able to form multiple concurrent H^D interactions, and furthermore the arrangement of these units about epicatechin allow for H^D interactions to occur in several unique arrangements (**Figure 4.15**). Both naringenin

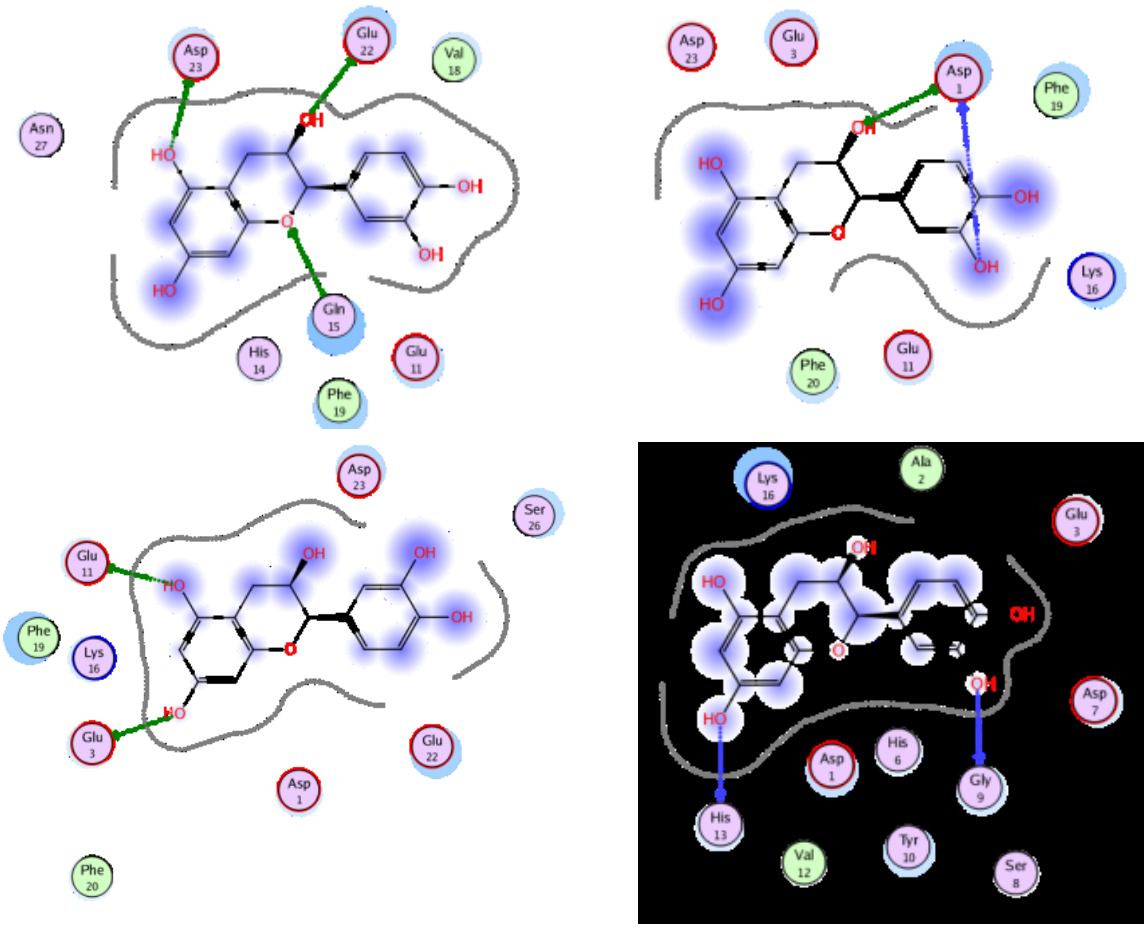

Figure 4.15 A selection of the many arrangements of multiple concurrent H^D interactions by Aβ-bound epicatechin.

and hesperetin have no alcohol at the 3 position about the heterocyclic ring; also removal of the hydroxyl at the 5' position and incorporation of a methyl ester at the 4' position are observed for naringenin and hesperetin, respectively. Both naringenin and hesperetin are still able to interact via H^D interactions, but these structural changes limit the possible arrangements of concurrent H^D interactions when binding Aβ, and as a consequence both compounds tend to interact more often through vdw-type interactions and explain the changes in distribution profiles. Hesperetin, with the incorporation of a hydrophobic methyl (the methyl ester at position 4') interacts more often about LVFFA, residues 11-21 of Aβ – this region of Aβ contains the majority of hydrophobic residues within the first 28 AA residues of Aβ. Naringenin tends to act by vdw-type interaction around AA residues more hydrophilic in nature – typically with residues 5-15 of Aβ. As for all of the flavonoids observed here the majority of interactions occur within the HHQK region of Aβ.

4.3.1.2. Other Polyphenols

In addition to the flavonoids two other polyphenol antiaggregants were analyzed: resveratrol and rosmarinic acid. The number of interactions observed at Aβ residues 1-28 and interaction profiles are presented for each compound in **Figure 4.16**. The number of interactions counted for rosmarinic acid (137) was significantly higher than resveratrol (101).

The distribution profile of resveratrol closely resembles that of the flavonoids. Although HHQK is the most frequented series of non-acid containing residues relative to the flavonoids interactions here decrease by approximately 10%. A closer look at the interaction profile of resveratrol (**Figure 4.17**) shows a significant decrease in π-stacking interactions relative to the

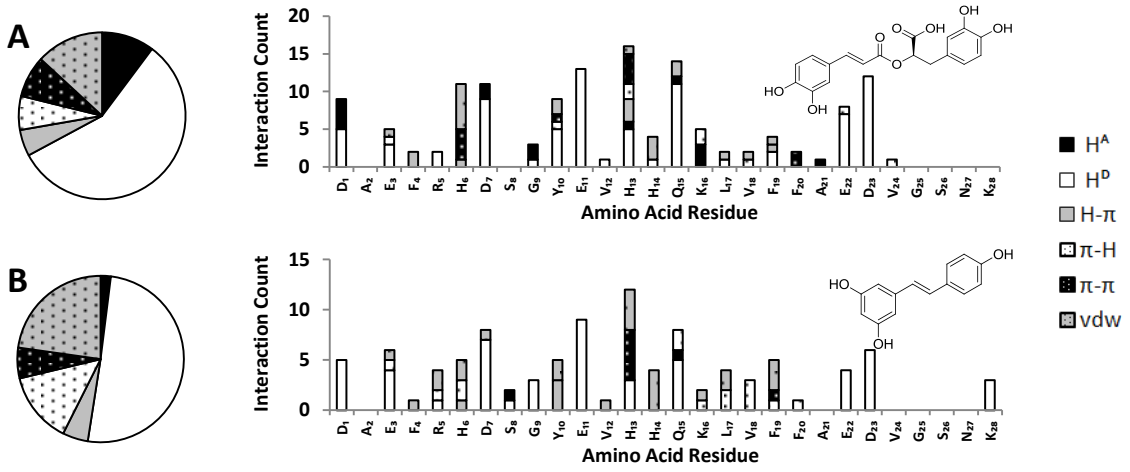

Figure 4.16 Interactions counts at Aβ AA residues 1-28 and interactions profiles for **A**) rosmarinic acid and **B**) resveratrol.

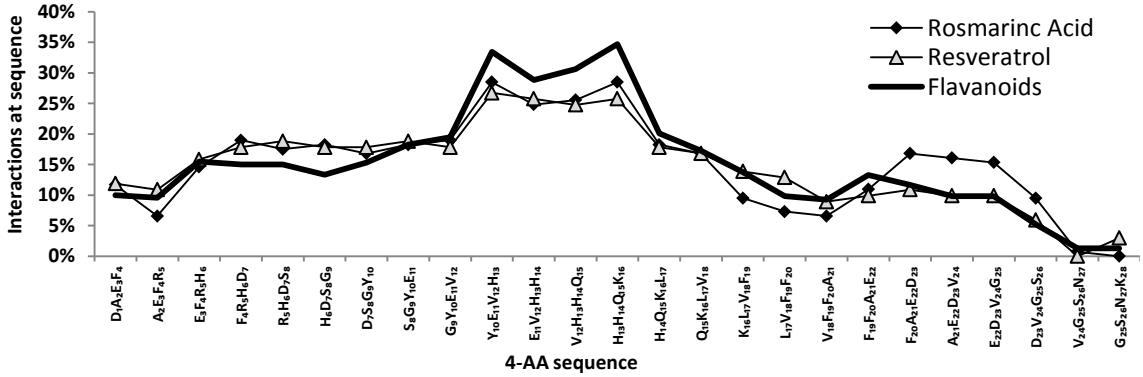

Figure 4.17 Distribution profiles of rosmarinic acid and resveratrol interactions within the first 28 residues of Aβ (interactions counts are binned in sections 4 AA residues in length). The average distribution profile of the flavonoids is presented as well for comparison (thick black line).

flavonoids (approximately 10%) which, in turn, decreases the number of π-π interactions observed at histidine residues. H^D interactions, on the other hand, increase by 10% (relative to the other flavonoids) and accordingly resveratrol was more likely to interact with D and E residues.

The structure of rosmarinic acid is vastly different than that of resveratrol and the flavonoids; however both the interaction profile and the distribution profile of interactions very closely resembles that of EGCG. Although rosmarinic acid has only 4 hydroxyls capable of forming (as compared to the 8 of EGCG) because of the flexibility afforded by the 6-atom linker between phenyl rings (**Figure 2.8**) the structure of rosmarinic is not as rigid as the flavonoids; as such rosmarinic acid may interact with Aβ in a variety of structural conformations in order to accommodate hydrogen-bonding. 59% of interactions conferred by rosmarinic acid were H^D interactions, comparable to the 57% of H^D interactions as observed with EGCG and a significant increase over the other flavonoids which on average interacted via H^D 41% of the time.

4.3.2. Aminophenols

4.4.2.1. 3HAA and *o*-Aminophenol

3HAA and *o*-aminophenol represent the structurally simplest of the aminophenol analogues investigated. The number of interactions observed at Aβ residues 1-28 and interaction profiles are presented for each compound in **Figure 4.18**. 119 interactions were observed for 3HAA within the first 28 residues of Aβ, and together H^D and H^A interactions made up 72% of these. H^D interactions were facilitated through either the amine or hydroxyl and occurred most frequently with E_{22} and D_{23}; H^A interactions were facilitated predominantly via the COOH (86%). Strictly hydrophobic interactions accounted for 17% of those observed; π-type interactions – namely π- π, π-H, and H- π interactions – together only accounted for 13% of all interactions observed. Although HHQK was again the 4-AA sequence at which the most interactions occur (25%) 3HAA does not exhibit a strong preference to bind in this region (**Figure 4.19**). 3HAA interactions were more homogeneously distributed about the sequence of Aβ than was observed for the polyphenolic antiaggregants. Generally sequences of AA which facilitated multiple concurrent H^D and/or H^A interactions were preferred.

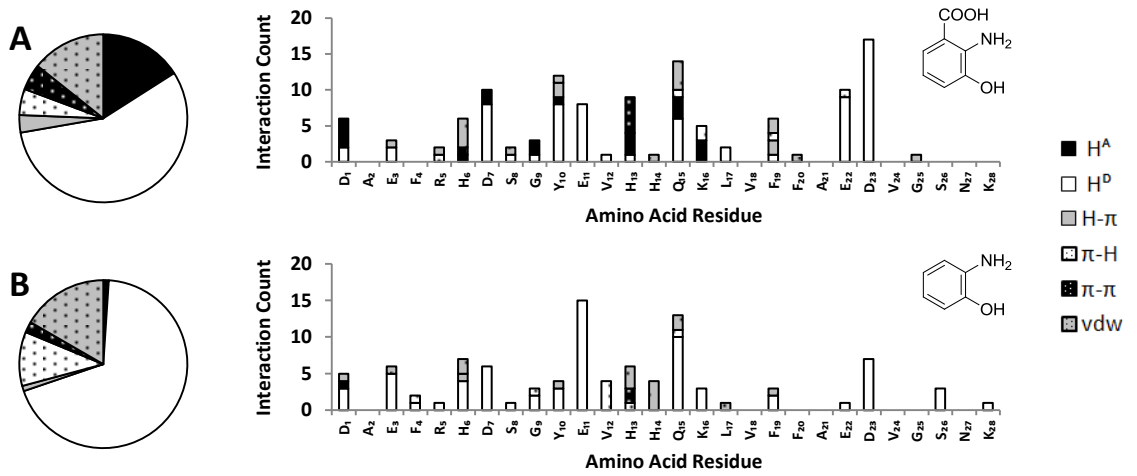

Figure 4.18 Interactions counts at Aβ AA residues 1-28 and interactions profiles for **A**) 3HAA and **B**) *o*-aminophenol.

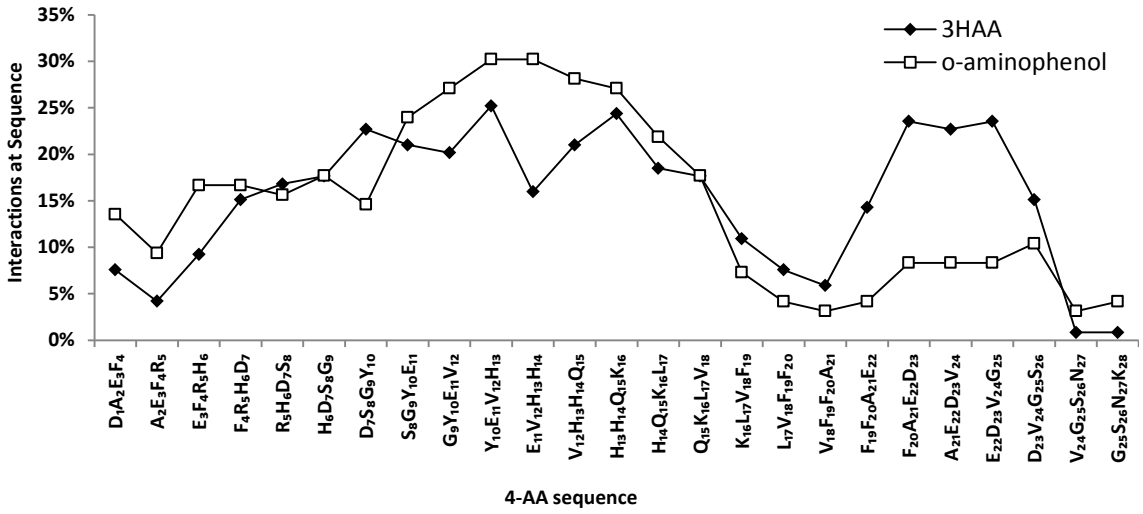

Figure 4.19 Distribution profiles of 3HAA and *o*-aminophenol interactions within the first 28 residues of Aβ (interactions counts are binned in sections 4 AA residues in length). The average distribution profile of the flavonoids is presented as well for comparison (thick black line).

96 interactions were observed for AP within the first 28 residues of Aβ – H^D interactions accounted for 69% of all those observed. H^D interactions were facilitated through either the amine or hydroxyl and occurred most frequently with E_{11} and Q_{15}. Only one H^A interaction was observed, a substantial decrease from 3HAA and a result of the absence of the COOH unit. As was observed with 3HAA, there is a substantial decrease in vdw, π- π, π-H, and H- π interactions (as compared to the polyphenol antiaggregants).

4.4.2.2. Synthetic Analogues of *o*-Aminophenol

Four synthetic analogues of *o*-aminophenol were analyzed: GS-1045, GS-1047, GS-1048 and GS-1049. The number of interactions observed at Aβ residues 1-28, interactions profiles, and structures are presented for all four analogues in **Figure 4.20**. The number of interactions observed for GS-1047 and GS-1048 (89 and 102, respectively) was comparable to *o*-aminophenol with 96.

GS-1047 and GS-1048 are methylated analogues of *o*-aminophenol – all three of these compounds contain only one aromatic ring, and as such the number of interactions observed for these compounds was significantly lower than those observed for all other antiaggregants analyzed in this survey. H^D interactions comprised the vast majority of those observed for

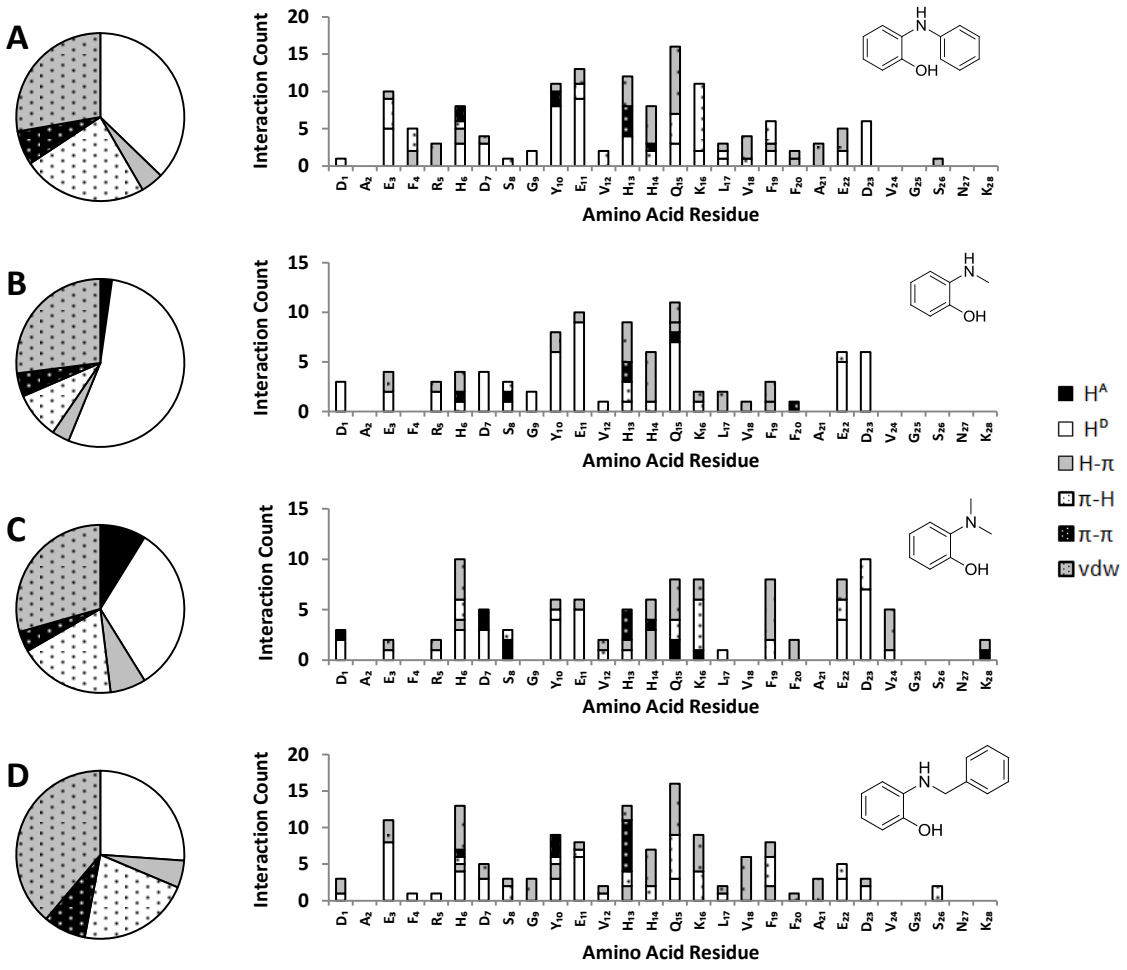

Figure 4.20 Interactions counts at Aβ AA residues 1-28 and interactions profiles for **A**) GS-1045 **B**) GS-1047 **C**) GS-1048 and **D**) GS-1049.

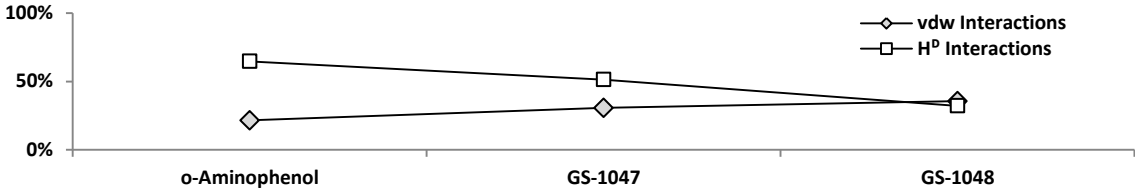

Figure 4.21 Proportion of hydrophobic interactions and H^D interactions observed for *o*-aminophenol and methylated analogues GS-1047 and GS-1048.

o-aminophenol, but the addition of one or two methyl groups about the amine (as with GS-1047 and GS-1048, respectively) significantly reduced the propensity to interact via H^D interactions and concurrently increased the amount of hydrophobic interactions observed (**Figure 4.21**). The increased propensity of GS-1047 and GS-1048 to interact via hydrophobic interactions resulted in a shift in the distribution profile of these compounds as they were less likely in interact with D and E residues via H^D interactions; instead the methylated analogues were more likely to interact via hydrophobic interactions about HHQK.

The number of interactions observed for GS-1047 and GS-1048 was significantly lower than the number of interactions observed for GS-1045 and GS-1049 (137 and 134, respectively). The amine of GS-1045 and GS-1049 are functionalized with a phenyl and benzyl ring, respectively, and as such these compounds were typically able to form more concurrent interactions during favorable binding poses. Proportionally, as compared to GS-1047 and GS-1048 (methylated analogues of *o*-aminophenol), GS-1045 and GS-1049 interacted with Aβ via π-stacking interactions twice as often; these compounds were also more likely to interact via π-H interactions and neither compound was observed to interact with Aβ via H^A interactions.

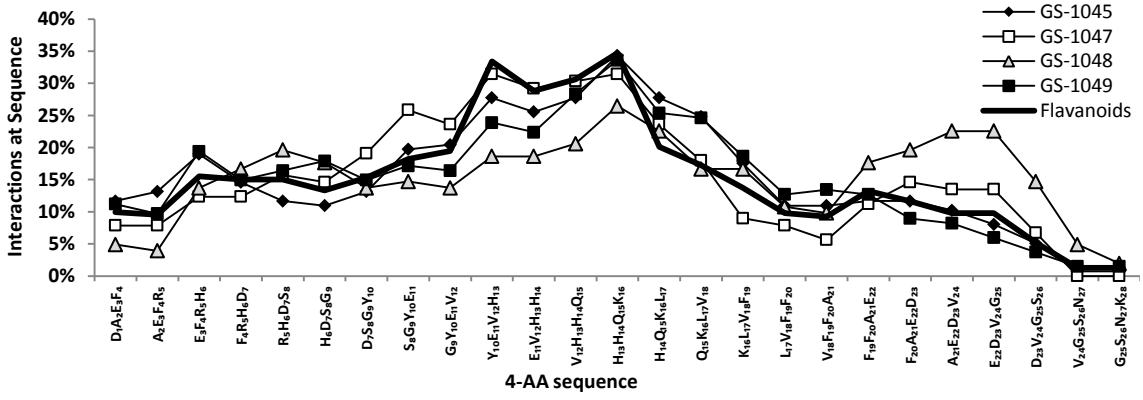

Figure 4.22 Distribution profiles of GS-1045, GS-1047, GS-1048 and GS-1049 interactions within the first 28 residues of Aβ (binned 4-AA sections. The average distribution profile of the flavonoids is presented as well for comparison (thick black line).

4.4. Aβ Residues Associated with Favorable Interactions

Taken together, the differences in the interaction profiles of *o*-aminophenol, GS-1047, GS-1048, GS-1045 and GS-1049 underscore the significant difference in interaction tendencies owing to simple structural modifications – as was also observed when comparing the flavonoids; however even in the face of differing interaction tendencies both the synthetic analogues of *o*-aminophenol and the polyphenols have a tendency to interact preferentially with the HHQK motif of Aβ (**Figure 4.22**) – a result suggesting the importance of this motif in antiaggregant interactions. Although HHQK may indeed play a prominent role in antiaggregant binding, the contributions of several key AA residues are noted and include π-stacking interactions with H_6 and Y_{10}, and H^D interactions with Q_{15} and D and E residues. To further probe the relative contributions of each AA residue to antiaggregant binding the interaction data for the polyphenol-based antiaggregants and aminophenol-based antiaggregants were pooled for further analysis.

4.4.1. Amino Acids

In **Figure 4.23A** the number of interactions observed at each AA about the first 28 residues of Aβ is presented; sorting the data by interactions at each type of AA as in figure **Figure 4.23B** it is apparent that interactions at H, D and E is preferred. Indeed these residues are the most active contributors to ligand binding and account for over half of all observed binding interactions (56.1%). Glutamine (Q), tyrosine (Y) and phenylalanine (F) are also major contributing AA and account for 25.6% of all interactions. The remaining 14 AA residues account for only 18.2% of all interactions and in themselves were not major contributors to antiaggregant binding.

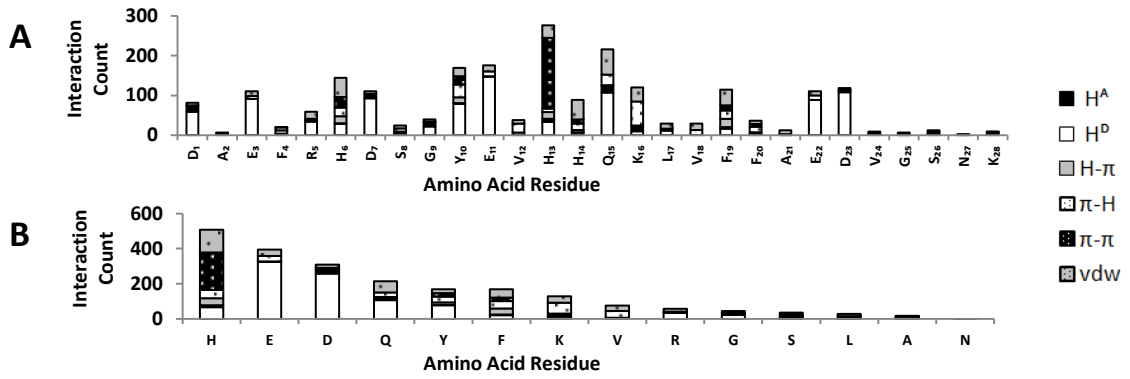

Figure 4.23 Counts for unique interactions involved in favorable polyphenol binding poses sorted by AA type.

4.4.1.1. Histidine and Tyrosine

A total of three histidines are contained within the first 28 residues of Aβ (H_6, H_{13}, and H_{14}) and these residues – along with Y_{10} – played a prominent role in antiaggregant binding. Interactions of Aβ-bound antiaggregants with H and Y residues accounted for almost a third of all interactions observed. Stabilization of bound antiaggregants was typically mediated through π-stacking interactions with H sidechains (83.6% of all π-π interactions), the vast majority of which were facilitated through H_{13} – by far, the most active single AA residue. Interestingly, π-π interactions of H_{13} to bound antiaggregants explicitly required an α-helical conformation. Of the 177 π-π interactions observed at H_{13} none occurred when H was in a random coil conformation, an important insight into the role of secondary structure in antiaggregant π-stacking interactions with H_{13}.

Arrangement of Aβ AA residues in an α-helical conformation results in the formation of 2 clefts (one on either side of H_{13}) which become favorable sites for interaction. One of these clefts is bordered by aromatic sidechains of H_6, Y_{10} and H_{13} and is a preferred site of ligand

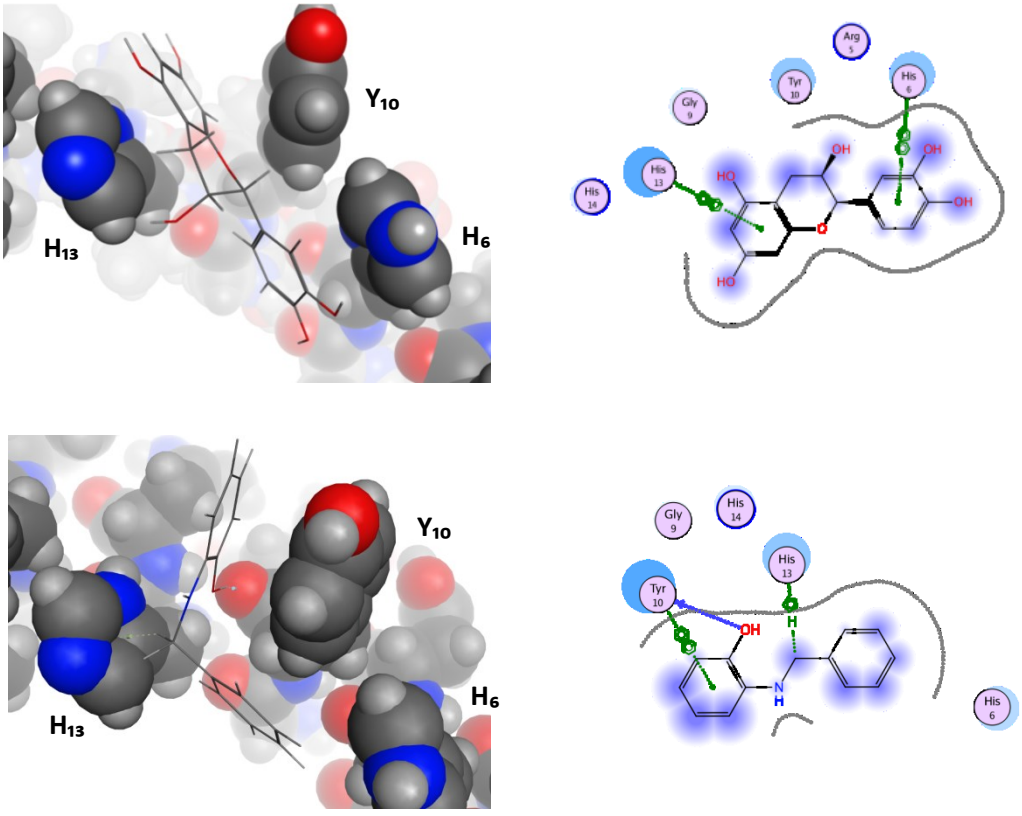

Figure 4.24 Epicatechin and GS-1049 bound to Aβ in the cleft formed by H_6, Y_{10} and H_{13}.

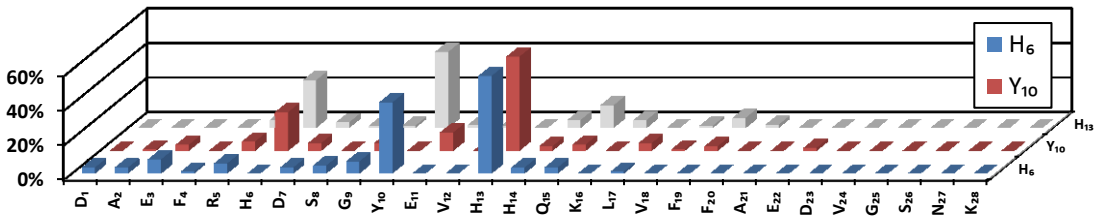

Figure 4.25 The distribution of partnered AA of ligand-bound H_6, Y_{10} and H_{13} in multiple-AA binding interactions.

interaction (**Figure 4.24**). When considering ligand interactions that involve more than one AA-residue, ligands that interact with H_{13} usually engage in concomitant interactions with Y_{10} or H_6 (44% and 28% of all multi-AA interactions at H_{13} involve Y_{10} or H_6, respectively); ligands engaged with H_{13} are further stabilized by various interactions with H_6 and Y_{10} – including hydrophobic, π-π, π-H, H-π, or H^A interactions. Here, H_6 and Y_{10} are considered partner AAs to H_{13} as ligands which interact with H_{13} overwhelming tend to do so simultaneously with either H_6 or Y_{10}. **Figure 4.25** shows the distribution of partner amino acids when ligands are bound to H_6, Y_{10} or H_{13}; multi-AA interactions of Aβ with ligands which involve any of these aromatic residues will, with a high rate of probability, involve either of the remaining aromatic residues.

4.4.1.2. Aspartic Acid, Glutamic Acid and Glutamine

Q, D and E all contain polar sidechains well suited to accepting hydrogen bonds. These residues played a significant role in mediating antiaggregant binding to Aβ, particularly the polyphenols. The first 28 AA of Aβ contain three of each D and E residues (D_1, D_7, D_{23}, E_1, E_3, and E_{23}) and one Q residue (Q_{15}). In total, interactions of Aβ-bound antiaggregants with Q, D and E residues accounted for 42.5% of all observed AA interactions, and furthermore these residues alone accounted for 71.7% of ligand H^D interactions.

Aβ-bound antiaggregants were often stabilized by an intricate network of hydrogen-bonds wherein ligands interact via H^D with several AAs concomitantly (**Figure 4.26**); Q, D and E residues were the key mediators of hydrogen-bonding networks. Unlike π-π interactions mediated by H_{13} there are no conformational requirements for H^D interactions – ligand stabilization by networks of hydrogen-bonding was observed regardless of the model of Aβ surveyed. Indeed H^D interactions are important contributors to ligand binding – 53.1% of binding poses analyzed contain at least one H^D interaction, and 13.6% of all binding poses contain two or more concurrent binding interactions. **Figure 4.27** shows the rate of involvement of each AA

residue in binding poses with at least 2 H^D interactions. Q, D and E residues were largely preferred in ligand binding poses involving multiple H^D interactions, typically contributing sidechain residues as hydrogen bond acceptors.

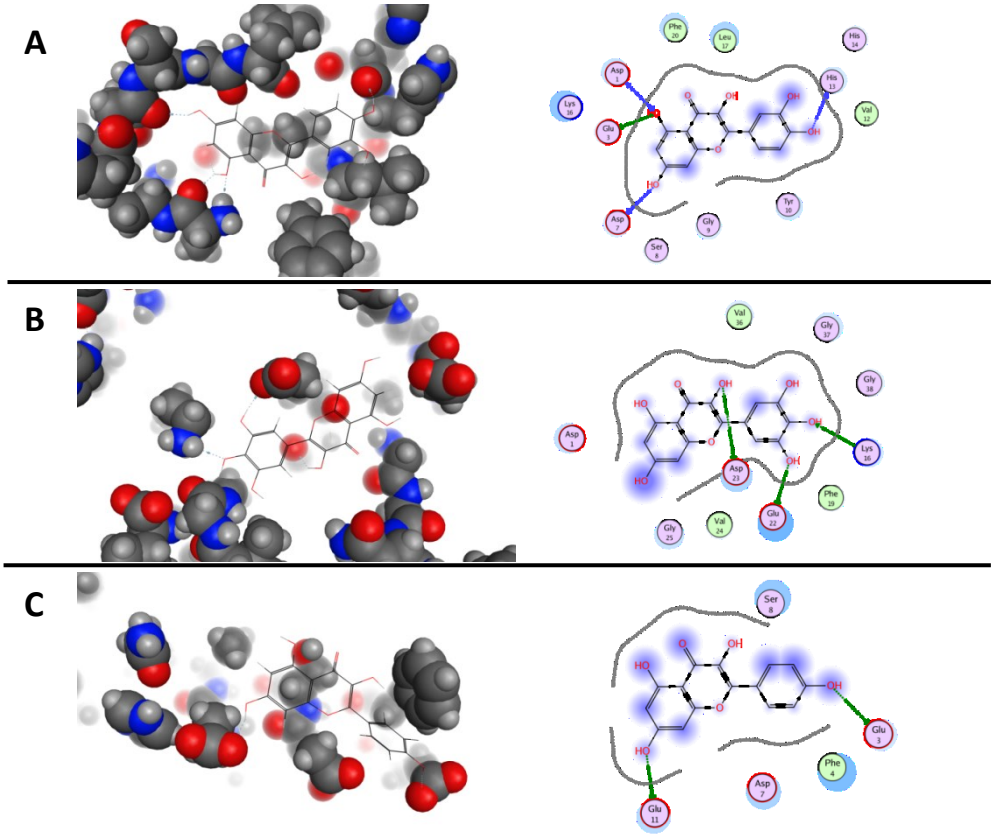

Figure 4.26 Typical Aβ binding of **A**) quercetin **B**) myricetin and **C**) kaempferol (receptor models 1ba4, 2lfm and 1amb, respectively) mediated through hydrogen-bond networks formed with multiple D and E residues.

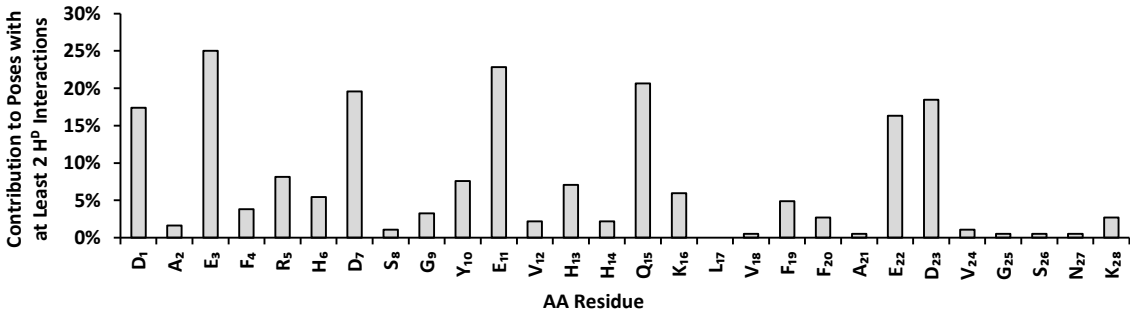

Figure 4.27 Proportion of binding poses, with at least 2 H^D interactions that involve AAs in the first 28 residues of Aβ.

4.4.2. HHQK

2160 unique AA interactions were observed within the first 28 residues of Aβ from the collection of analyzed polyphenol and aminophenol binding poses (**Table 4.4**); over half of these interactions occurred within the 10-AA sequence between Y_{10} and K_{16} of Aβ, and further still the majority of these interactions occurring within residues H_{13} and K_{16} – an interesting finding considering several classes of antiaggregants have their roots firmly embedded in the postulated motif. This result may seem unsurprising – after all HHQK contains H_{13} and Q_{15}, which with 276 and 215 interactions, respectively, are the two most active AA contributors to binding and as such have been discussed. The overwhelming majority of π-π interactions occur at H_{13} and with 107 observed H^D interactions at Q_{15} it was the third most active hydrogen-bond acceptor (behind D_{23} and E_{11} with 108 and 147 H^D interactions, respectively). Ignoring π-π and H^D interactions an even higher proportion of interactions occur at HHQK (**Figure 4.28**) – 37.9% of all H^A, π-π, H-π and π-H interactions.

From the *in silico* modeling conducted herein it is difficult to comment specifically on a structure or conformation about this motif, as the data collected are from docking experiments conducted on a multitude or receptor models; however it is clear that AA residues about HHQK are able to interact via a wide range of mechanisms, a fact which lends support to the notion that HHQK is indeed an excellent target for antiaggregant development.

Table 4.4 Percentage of observed AA interactions within residues GYEV (residues 9-12) and HHQK (residues 13-16) as compared to total interaction observed (residues 1-28).

Residues			AA Interactions	% (of Total)
D_1	-	K_{28}	2160	**100.0**
Y_{10}	-	F_{19}	1253	**52.1**
H_{13}	-	K_{16}	699	**32.8**

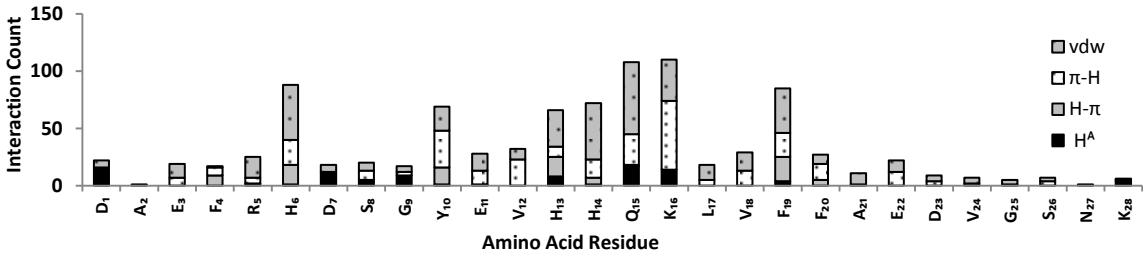

Figure 4.28 Counts of H^A, π-π, H-π and π-H interactions at Aβ AA residues 1-28.

4.5. Aβ Receptor Models Associated with Favorable Interactions

The energy of aminophenol and polyphenol binding poses were not equal among the receptor models analyzed. **Figure 4.29** shows the averaged ΔG of binding for the aminophenol and polyphenol antiaggregants with the various receptor models of Aβ – each point represents the average of 10 values and the data is presented as such for clarity. For both classes of compounds the order of preferred receptor models is more or less in agreement. The preferred receptor models for the aminophenols was in the order of 1AML > 2FLM > 1BA4 > 1Z0Q > 1AMB> 1AMC> 2M9S> 1IYT > 2M9R; for the polyphenols the order of preferred receptor models was 2FLM > 1AML > 1BA4 > 1AMB > 1Z0Q > 1AMC > 2M9S > 1IYT > 2M9R.

With a closer look at the 3D structures of the various receptor models key differences are noted between receptor models that are preferred versus those with less favorable binding interactions. 2FLM, 1AML and 1BA4 are the most preferred receptors and 2M9S, IYT and 2M9R are least preferred – 1AMB, 1AMC and 1Z0Q lie somewhere in between (**Figure 4.30** shows the structures of all receptor models used here). The most favorable receptors are typically those in which the 3D structure of the AA sequence results in the formation of geometric pockets about

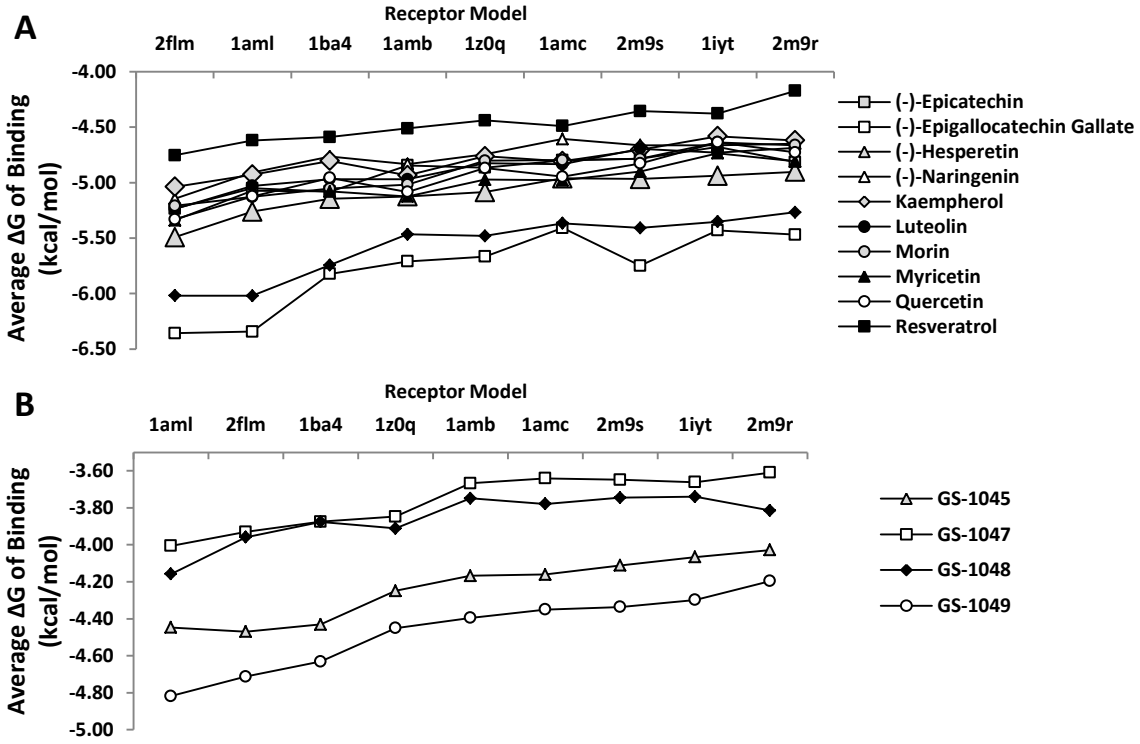

Figure 4.29 The average ΔG of binding of **A**) polyphenol antiaggregants and **B**) aminophenol antiaggregants with the various receptor models of Aβ.

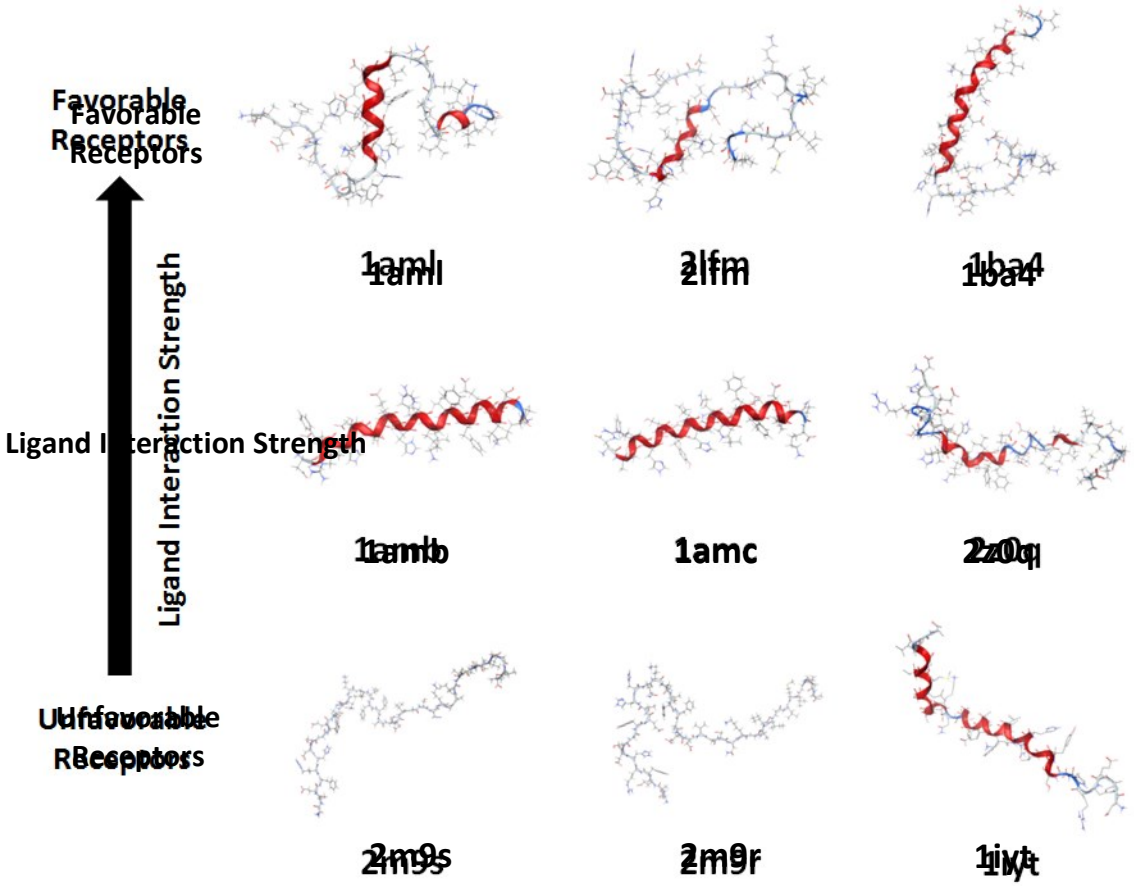

Figure 4.30 The 3D structures of all receptor models of Aβ used in the aminophenol and polyphenol ligand docking survey.

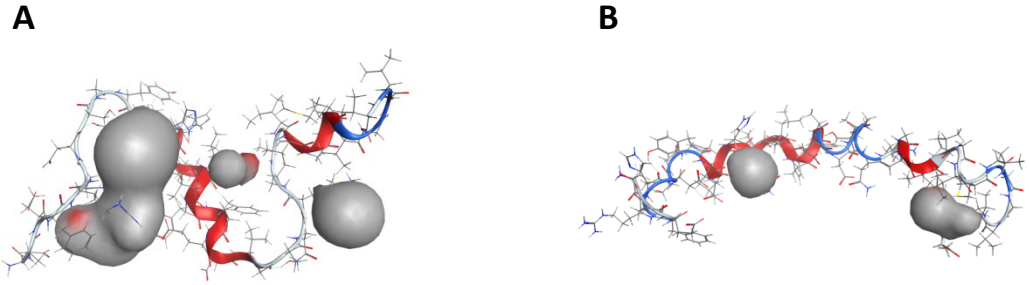

Figure 4.31 Geometric pockets about receptor models **A**) 1aml and **B**) 1z0q.

the receptor. These geometric pockets are buried sites in the receptor model which have limited solvent exposure but are also ligand accessible. The 'site finder' function of MOE allows for determination of geometric, ligand accessible, pockets in a receptor from its 3D coordinates. **Figure 4.31** shows the calculated pockets about the receptor models 1aml and 1z0q for comparison. MOE outputs the location of the pocket as well as the AA residues involved in the pocket (denoted pocket residues). The larger the geometric pocket about any particular model, the more pocket residues are involved; as such receptor models with fewer or smaller geometric pockets will contain fewer pocket residues.

To investigate the inherent link between observed ligand binding energy and the presence of receptor pockets the number of pocket residues was determined for each model of Aβ and are presented in **Table 4.5**.

Table 4.5 Pocket residues for each of the 9 receptor models.

Receptor	Pocket Residues (Repeat Residues Not Shown)	# of Pocket Residues
1amb	R_5, H_6, G_9, Y_{10}, H_{13} and H_{14}	6
1amc	none	0
1aml	D_1, A_2, E_3, F_4, R_5, H_6, D_7, S_8, Y_{10}, E_{11}, H_{14}, Q_{15}, L_{17}, V_{18}, F_{20}, A_{21}, E_{22}, G_{29}, A_{30}, I_{32}, N_{27}, K_{28}, G_{29}, I_{32}, G_{33} and V_{36}.	27
1ba4	D_1, E_3, E_{11}, K_{16}, F_{19} and F_{20}	6
1iyt	E_3, H_6, D_7, Y_{10}, K_{16}, L_{17}, F_{20}, A_{21} and V_{24}	9
1z0q	A_{30}, I_{31}, I_{32}, L_{34}, M_{35}, G_{38}, V_{39}, V_{40}, A_{42}, E_{11}, V_{12}, H_{14}, Q_{15} and V_{18}	14
2flm	D_1, A_2, E_3, F_4, R_5, H_6, D_7, S_8, G_9, Y_{10}, E_{11}, V_{12}, H_{13}, Q_{15}, K_{16}, V_{18}, A_{21}, E_{22}, D_{23}, V_{24}, G_{25}, S_{26}, N_{27} and V_{36}	26
2m9r	none	0
2m9s	G_9, Y_{10}, E_{11}, F_{19}, F_{20}, A_{21} and E_{22}	8

4.6. Mechanisms of Interaction

4.6.1. Polyphenols

990 polyphenol ligand binding poses were analyzed; during analysis the residues of interaction and types of interaction were determined for each pose. The majority of polyphenol binding poses contained at least one H^D interaction (556, 56.2%) – a significantly larger proportion than any other interaction, a testament to the importance of H^D interactions to Aβ polyphenol binding (**Figure 4.32A**). After H^D interactions vdw, π-H and π-π interactions were

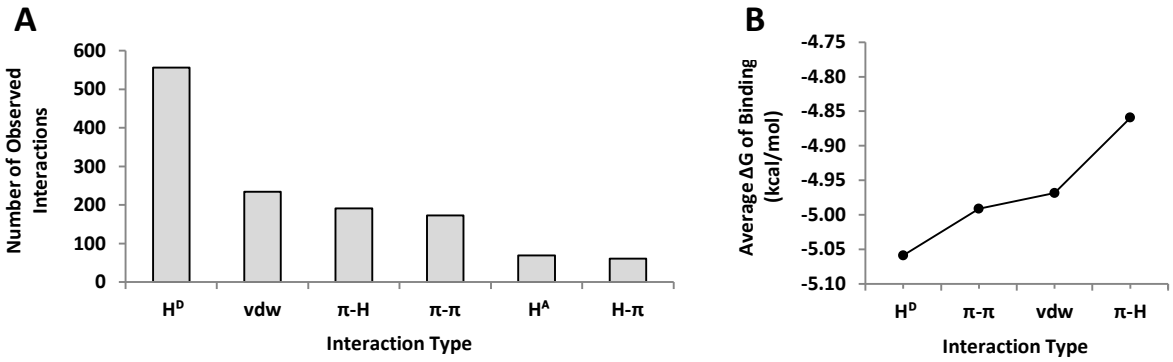

Figure 4.32 **A**) Number of each type of interaction observed within the set of analyzed polyphenol binding poses and **B**) The averaged ΔG of binding when H^D, π-π, vdw or π-H interactions are involved in ligand binding.

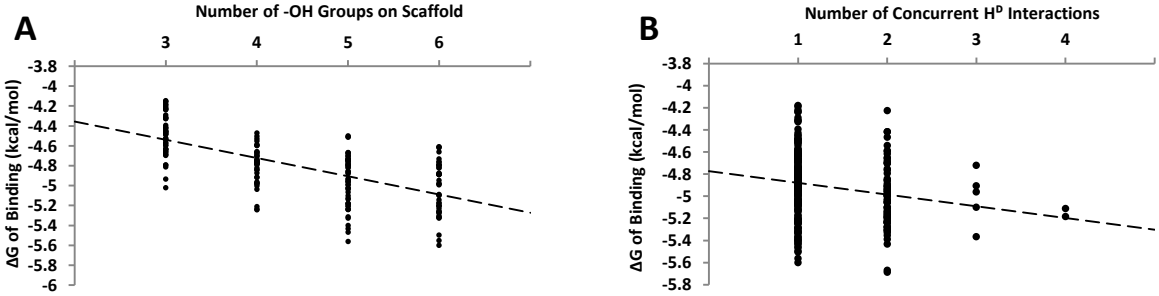

Figure 4.33 **A**) The ΔG of binding (when H^D interactions are contributing) sorted by the number of OH groups about the ligand scaffold and **B**) the ΔG of binding sorted by the number of contributing H^D interactions for the flavonoids and resveratrol.

most frequently observed and were incorporated in 23.6%, 19.3% and 17.4% of all interactions, respectively. Both H^A and H-π interactions were relatively infrequent and occurred in less than 7% of all observed interactions. The average ΔG of binding when the most frequently observed interactions are participating in a given pose is presented in **Figure 4.32B**. On average, the ΔG of binding is lowest in poses which incorporate H^D interactions; poses involving π-π or vdw interactions are slightly less energetically favorable than those involving H^D interactions. π-H interactions are the least energetically favorable and poses involving π-H interactions alone are typically higher in energy (resulting in a less stable binding interaction).

H^D interactions were the most important of any in conferring stable ligand binding poses. With the polyphenols binding stability is inherently linked to the number of groups capable of forming H^D interactions. Take for example the myricetin, quercetin, kaempferol and resveratrol – these ligands are all planar and of similar structure; the ΔG of binding for these ligands is on average lower when more enols or alcohols were incorporated into the structure

(**Figure 4.33A**). For the flavonoids and resveratrol the ΔG of binding also tended to decrease as the number of concurrent H^D interactions increased **Figure 4.33B**). H^D interactions were equally likely to occur regardless of structure – the observed counts of H^D interactions was equivalent for residues in an α-helical conformation or random coil conformation. As well there was no definitive correlation between the proportion of H^D interactions observed and the amount of pocket residues contained within the receptor model; this contrasts vdw interactions which tended to increase in number and energy favourability as the number of pocket residues increased (**Figure 4.34**). Indeed, vdw interactions were important in mediating polyphenol binding about Aβ, but in all receptor models (with the exception of 1aml) more H^D interactions were observed.

After H^D interactions, vdw and π-π interactions were the next most important in mediating polyphenol binding. π-π interactions are significant contributors to polyphenol binding to Aβ, however this process is extremely structurally dependent – 86.1% of all observed polyphenol π-π interactions occurred with receptors 1amb and 1amc. A random coil structure about H_{13} may well represent a viable motif for further investigation of polyphenol structure and propensity to form π-π interactions (**Figure 4.24**).

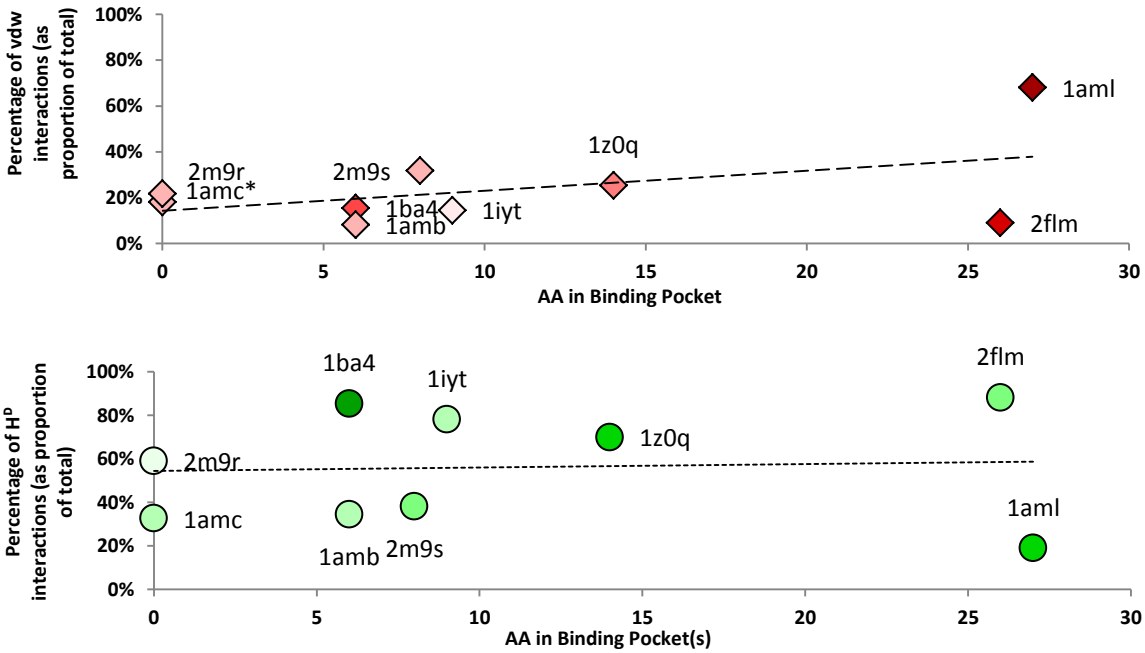

Figure 4.34 The relative percentage of vdw (red diamonds) and H^D interactions with each receptor model of Aβ; darker symbols represent a lower average value for the ΔG of binding for that particular interaction type (1aml has the most favorable vdw interaction, whereas 1ba4 has the most favorable H^D interactions on average).

4.6.2. Aminophenols

In total, 360 aminophenol binding poses were analyzed. As with the polyphenols H^D interactions represented the most observed interaction type, however the relative proportion of vdw and π-H interactions is significantly increased for the aminophenols and suggest that these interactions may play a larger role in ligand binding for this class of antiaggregant (**Figure 4.35A**). π-π, H-π and H^A interactions were observed in less than 8% of all interactions. π-H interactions occurred in a significant proportion of binding poses (24%) and these interactions typically had lower values for ΔG of binding indicating more stable ligand binding (**Figure 4.35B**); however it is interesting to note that of the 86 π-H interactions observed only 28 occurred on their own, the remaining 45 occurred in conjunction with an additional interaction (H^D, vdw, or π-π) indicating that π-H interactions in and of themselves are not responsible for ligand binding. π-H interactions are adjuvants to other interactions (particularly vdw, π-π and H^D interactions) and help decrease the overall ΔG of binding thereby increasing the stability of Aβ-bound ligands.

Although H^D interactions represented the most observed interaction type, on average the ΔG of binding for aminophenols interacting via H^D interactions was higher than when bound aminophenols interacted via either vdw or π-π interactions. The large proportion of poses which utilize H^D interactions indicate that these may well be a significant mediator of aminophenol binding; however it would seem that vdw type interactions are overall more important to aminophenol-Aβ complexation – this is in sharp contrast to the polyphenols. The relative proportion of π-π interactions is also sharply decreased relative to the polyphenols suggesting that these too are less important in mediating aminophenol binding.

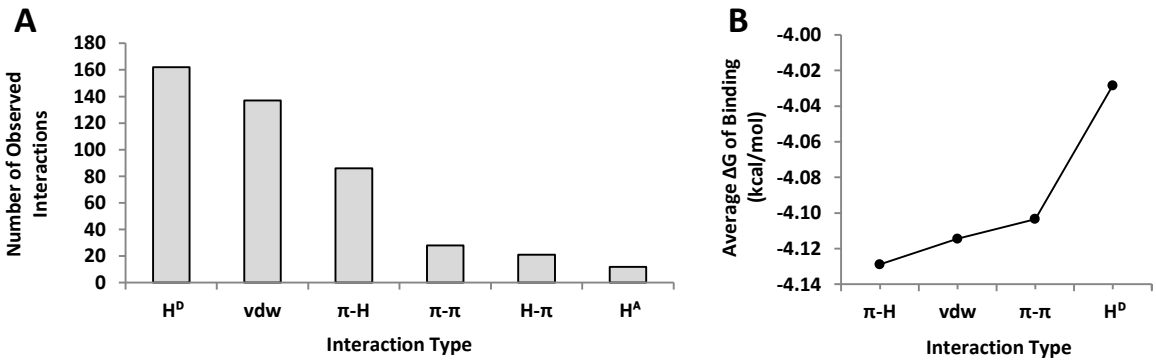

Figure 4.35 **A**) Number of each type of interaction observed within the set of analyzed aminophenol binding poses and **B**) The averaged ΔG of binding when H^D, π-π, vdw or π-H interactions are involved in ligand binding.

A high proportion of aminophenols interacted via vdw interactions only (38.0%). The structure of the Aβ receptor model significantly influenced the relative proportion of vdw interactions observed. Good linearity is observed between the proportion of vdw interactions observed for any model and the number of pocket residues in that model (**Figure 4.36**); furthermore the average ΔG of binding also generally increases as binding pocket size increases. Although the trend was somewhat observed for the polyphenols this relationship is much stronger for the aminophenols. 1aml and 2flm have large binding pockets and as such are involved in more vdw interactions with lower ΔG of binding. When analyzing the data for each of the models it is determined that as the proportion of vdw interactions increased the proportion of H^D interactions decreased. Indeed, with larger binding pockets, the ΔG of binding decreased for poses interacting via vdw interactions (**Figure 4.36**) – as vdw interactons become more favorable the relative proportion of H^D interactions decrease and, taken together, are a strong indicator that hydrophobic interactions play the most important role in aminophenol binding to Aβ.

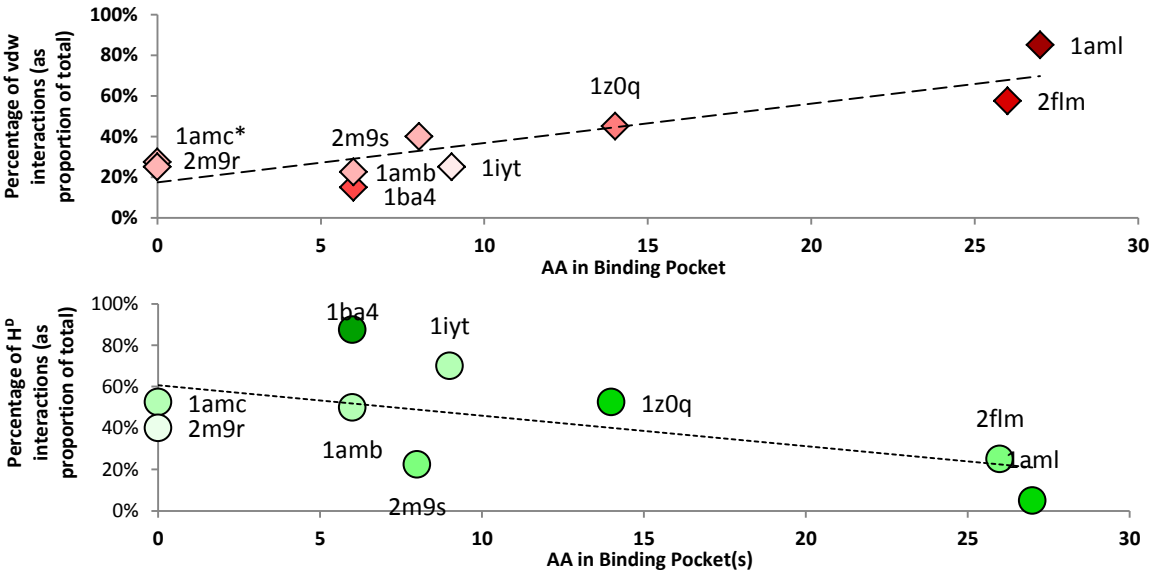

Figure 4.36 The relative percentage of vdw (red diamonds) and H^D interactions with each receptor model of Aβ; darker symbols represent a lower average value for the ΔG of binding for that particular interaction type (1aml has the most favorable vdw interaction, whereas 1ba4 has the most favorable H^D interactions on average).

Chapter 5: Aβ Binding

3HAA, *o*-aminophenol and the aminophenol analogues presented herein are excellent inhibitors of *f*Aβ formation, but the mechanism of action of these and other antiaggregants remains unclear. It is generally believed that *f*Aβ formation may proceed via several unique pathways. Association of *m*Aβ into higher order *o*Aβ is the first step of Aβ aggregation and these various species of *o*Aβ begin to adopt a conformation rich in β-sheets. *f*Aβ elongation may proceed via several disparate mechanisms whereby *f*Aβ extension may occur via incorporation of β-sheet rich *o*Aβs or alternatively by direct incorporation of *m*Aβs.

Because of the inherent complexity of *f*Aβ formation elucidation of a concise mechanism of action for antiaggregants remains a challenge. Several potential targets exist along the aggregation pathway of Aβ whereby antiaggregant compounds may elicit their effect. *m*Aβ, the various species of *o*Aβs and *f*Aβ are all potential targets for Aβ antiaggregants. Although scarce there have been reports of various antiaggregants interacting directly with *m*Aβ;[53,114,123,140,167] furthermore the MM studies conducted herein suggest that specific AA residues about Aβ may indeed represent areas of preferred antiaggregant binding. The activity of 3HAA and *o*-aminophenol observed via the sandwich ELISA experiments conducted here provide feasible evidence that these compound can indeed interact with *o*Aβ; however, no such activity was observed for the synthetic analogues of *o*-aminophenol. The antifibrillogenic activity of the synthetic analogues of *o*-aminophenol may be a result of ligand interactions with either *m*Aβ or fAβ although the biological assays conducted here to no provide insight into this detail. A series of nuclear magnetic resonance (NMR) spectroscopy experiments have been implemented to ascertain whether 3HAA or synthetic analogues of *o*-aminophenol are able to interact with *m*Aβ; to this end 3HAA and GS-1049, the most potent of the *o*-aminophenol analogues in the ThT fibrillogenesis assay were assessed for binding to Aβ and 10-AA truncations thereof. AnA was inactive in the ThT fibrillogenesis assay and was also investigated for comparison.

5.1 Nuclear Magnetic Resonance Spectroscopy

NMR is a powerful technique for measuring protein-ligand interactions and many specialized experiments have been developed to this end including saturation transfer difference spectroscopy (STD)[173] and diffusion ordered spectroscopy (DOSY);[174] these

spectroscopic techniques that may provide detailed insight into the mechanism of action of antiaggregants and will be reviewed in brief.

5.1.1 Diffusion Ordered Spectroscopy

Self-diffusion is the random translational motion of molecules driven by internal kinetic energy when the concentration gradient is equal to zero. The mass diffusivity or self-diffusion coefficient (*i.e.* the speed of random translational motion) is given by the Einstein-Stokes equation:

$$D = \frac{k_b T}{6\pi\eta r}$$

Equation 5.1 The Stokes-Einstein equation.

where k_b is Boltzmann's constant, T and η are the solution temperature and viscosity, respectively, and *r* is the Stokes-Einstein radius of the particle. The Stokes-Einstein radius of a solute is the radius of a hard sphere that diffuses at the same rate as that solute. By **Equation 5.1** the self-diffusion is inversely proportional to the Stokes-Einstein radius – solutes with a large Stokes-Einstein radius will self-diffuse more slowly than solutes with a comparatively smaller Stokes-Einstein radius; as such the translational motion of proteins in solution will be significantly slower than comparatively smaller ligands.

Using DOSY the self-diffusion coefficients may be determined for individual components of complex mixtures, given that these coefficients are sufficiently resolved. Consider for a moment a ligand forming a complex with a protein receptor: in its unbound state the ligand has a defined Stokes-Einstein radius, $r_{Unbound}$, but the Stokes-Einstien radius of the ligand effectively increases in the bound state (r_{Bound}) which results in a decrease in self-diffusion coefficient of the ligand; as such measurements of self-diffusion can be used to detect protein ligand complexation. A decrease in the measured self-diffusion coefficient of a ligand in the presence of a receptor is a good indication of complexation with said receptor.

The pulsed-field gradient method (PFG) of DOSY was introduced by Stejskal and Tanner in 1965 and is a simple method to determine the apparent self-diffusion coefficient, D_{APP}, of molecules using NMR.[174] In the pulsed-field gradient method after an initial 90° pulse (moving

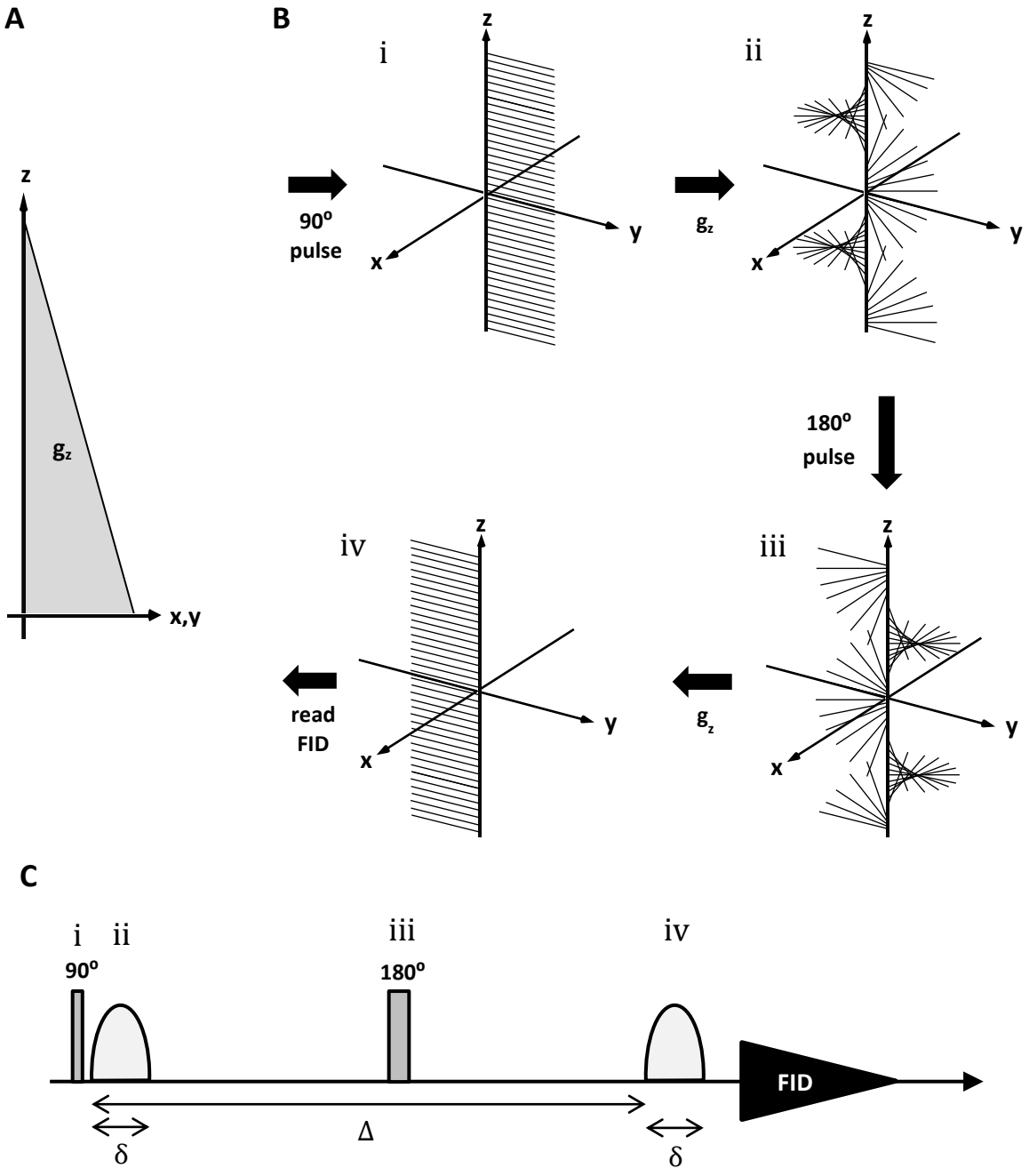

Figure 5.1 **A**) Schematic of gradient pulse, g_z. **B**) Schematic of spatial encoding of spin magnetization in the z-axis and **C**) the associated pulse sequence for a basic PFG DOSY experiment.

spins into the x-y plane) magnetization is spatially encoded in the z-direction with a gradient, g_z,(**Figure 5.1A**) for time, δ; the spins are allowed to precess before a 180° inversion pulse is applied. In the absence of diffusion a second gradient pulse after time, Δ, will rewind the

magnetization helix (**Figure 5.1B** and **C**). Translational motion in the z-direction causes a loss of coherence and therefore signal attenuation will be greater for compounds with larger values of D_{APP} (for any gradient, g_z).The intensity of the observed signals in a DOSY experiment is given by the function:

$$I = I_0 e^{-D_{APP}\gamma^2 g_z{}^2 \delta^2 \left(\frac{\Delta-\delta}{3}\right)}$$

Equation 5.2 Signal intensity as a function of DOSY parameters**.**

Here $\boldsymbol{I}_0$ is the signal intensity in the absence of an applied gradient and $\boldsymbol{I}$ is the signal intensity observed during the experimental pulse sequence. The observed intensity is a function of the gyromagnetic ratio, γ, the gradient strength, g_z, gradient application time, δ, diffusion time, Δ, and the $D_{APP.}$ Rearranging **Equation 5.2** we get:

$$\ln\left(\frac{I}{I_o}\right) = -D_{APP} g_z{}^2 \gamma^2 \delta^2 \left(\frac{\Delta-\delta}{3}\right)$$

Equation 5.3 Signal attenuation during a DOSY experiment.

Here the ratio of I and I_0 is the signal attenuation. During a PFG DOSY experiment δ, Δ are kept constant. Plotting the natural logarithm of the signal attenuation versus $g_z{}^2$ gives a linear plot of slope -D_{APP}.

5.1.2 Saturation Transfer Difference Spectroscopy

The STD-NMR experiment was introduced by Mayer and Meyer in 2001 and is a spectroscopic technique well suited to observing weak binding interactions between a protein and complexed ligand.[173] In short, STD-NMR experiments allows for determination of ligand binding by analyzing the difference between two spectra: so-called the *on-resonance* spectrum and *off*-resonance spectrum. First an on-resonance spectrum is collected in which an RF pulse is used to selectively saturate protein resonances. Spin diffusion allows for efficient intramolecular transfer of magnetization within the protein – leading to saturation of the entire protein (not only the directly saturated resonances). It is important that the RF pulse used to irradiate protein resonances is in a region devoid of any ligand signals; this ensures that saturation

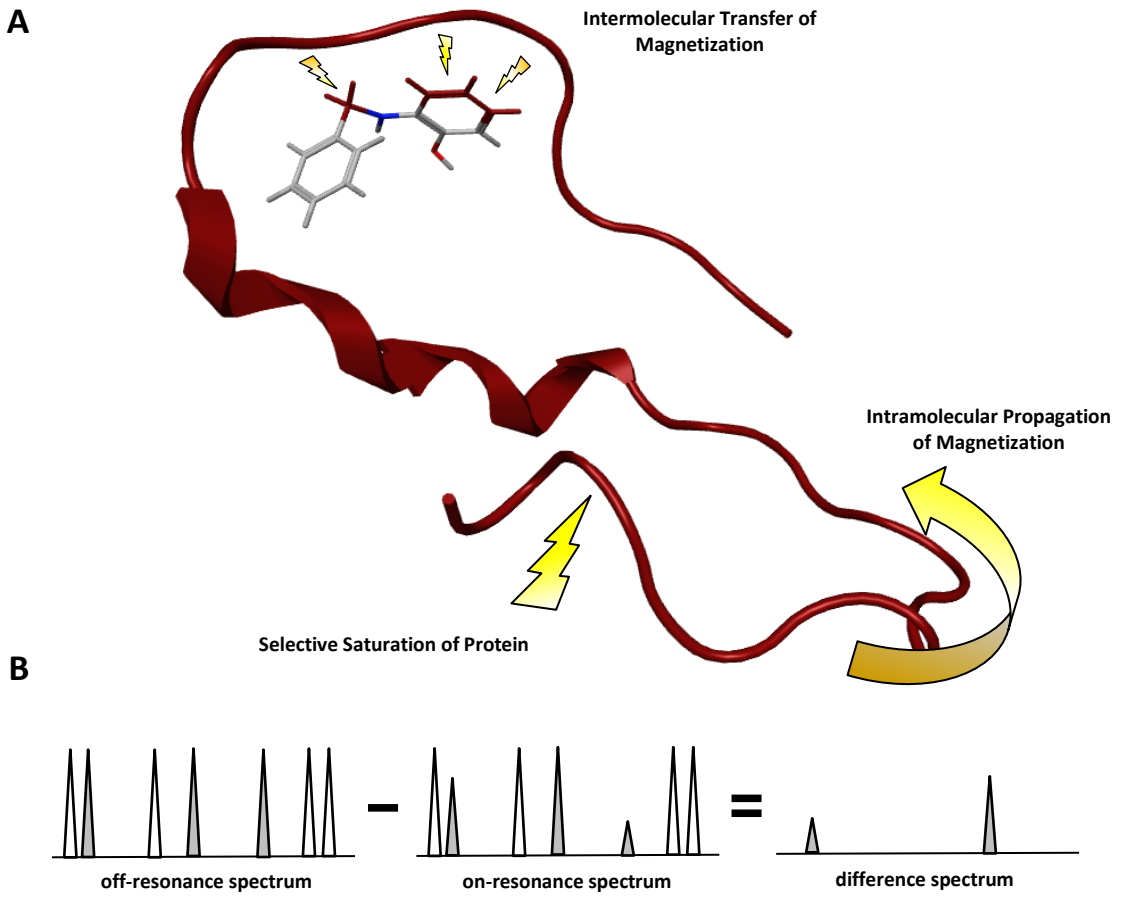

Figure 5.2 **A**) Saturation transfer from protein to ligand in an STD on-resonance experiement and **B**) subtraction of the on-resonance spectrum from an off-resonance spectrum gives a difference spectrum containing only ligand resonances of the binding ligand which receive saturation.

transfer is mediated through the protein and not from the RF pulse directly. Given a close enough proximity, magnetization is then transferred to binding regions of the ligand by intermolecular saturation transfer (**Figure 5.2A**), thereby resulting in a decrease in ligand signals intensities (due to a negative NOE build-up during relaxation). Second an off-resonance spectrum is obtained in which the saturation pulse is applied at a frequency clear of any protein or ligand resonances (typically at 30 ppm). Because there is no saturation transfer from protein to ligand during the off-resonance experiment there is no change in the intensity of ligand signals. Finally the on-resonance spectrum is subtracted from the off-resonance spectrum and the resulting difference spectrum will only contain ligand resonances involved in protein binding (**Figure 5.2B**).

5.2 Nuclear Magnetic Resonance Binding Studies

5.2.1. STD-NMR

5.2.1.1 $A\beta_{1-40}$

To assess whether 3HAA, AnA, and GS-1049 are able to bind $A\beta_{1-40}$ 3 mM solutions of each ligand were prepared containing 1 mM of freshly disaggregated $A\beta_{1-40}$. STD-NMR was run on each of the protein-ligand solutions in a H_2O-D_2O solution (9:1) buffered with PBS at 4°C (for a more detailed experimental, include pulse sequence parameters, please refer to **Section 6.3.1** of the methods chapter). In **Figure 5.3** the on-resonance, off-resonance and difference spectra are presented for 3HAA in the presence of $A\beta_{1-40}$. The three resonances of 3HAA are clearly visible in the difference spectrum and indicate a receptor interaction with $A\beta_{1-40}$; likewise GS-1049 resonances are visible in the difference spectrum obtained from a solution of GS-1049 in the presence of $A\beta_{1-40}$ (**Figure 5.4**). Compared to 3HAA and GS-1049, no AnA resonances are observed (with a s/n ≥ 1) in the STD experiment in the presence of $A\beta_{1-40}$ and indicate that AnA does not interact with the peptide in solution. STD experiments on 3 mM 3HAA, AnA or GS-1049 (in the absence of $A\beta_{1-40}$) show no resonances in the difference spectrum and indicate that

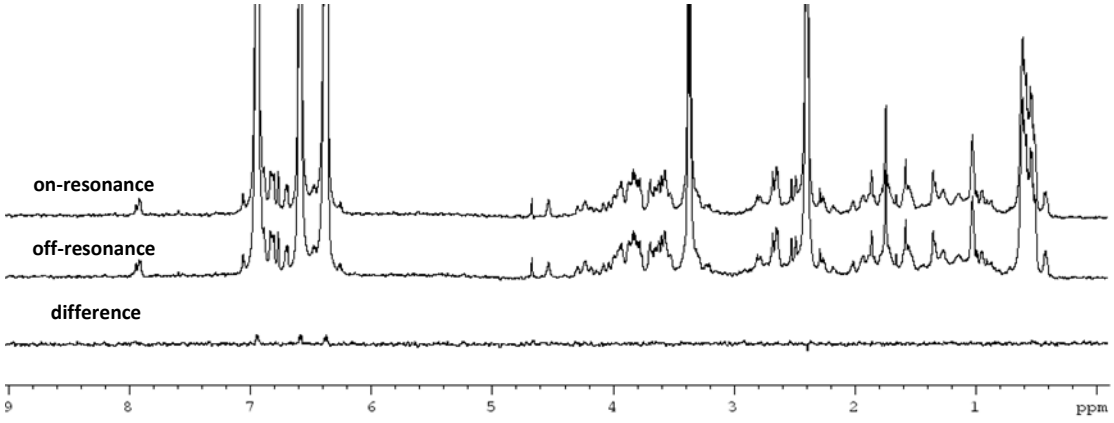

Figure 5.3 The on-resonance, off-resonance and difference spectra of 3mM 3HAA in solution with 1mM $A\beta_{1-40}$ in H_2O-D_2O solution (9:1) buffered with PBS at 4°C.

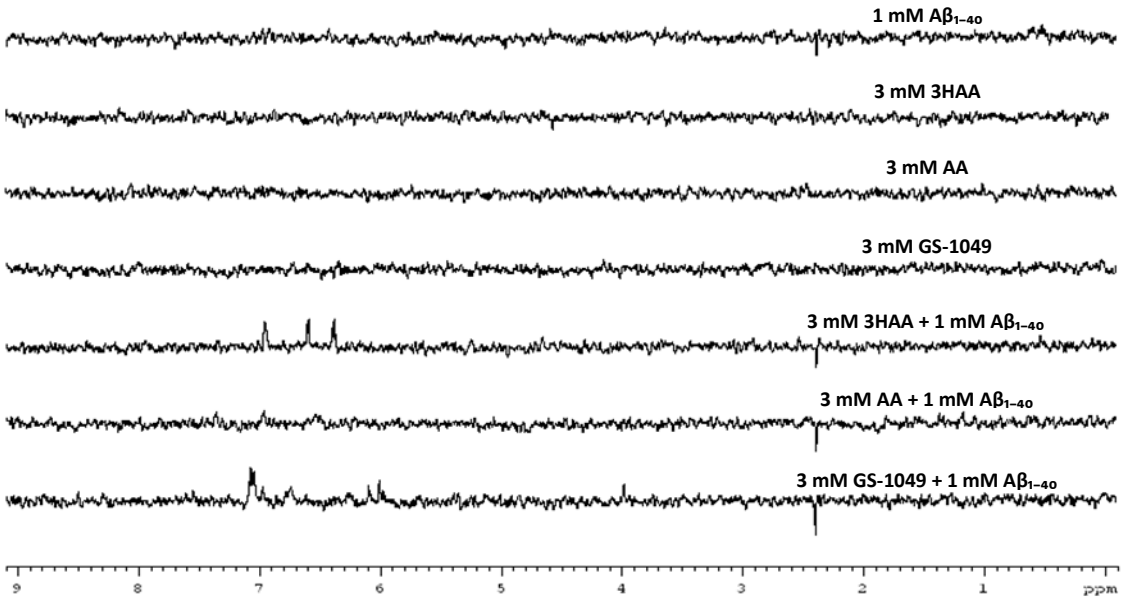

Figure 5.4 The difference spectra of 3mM 3HAA, AnA and GS-1049 in solution with 1mM $A\beta_{1-40}$ in H_2O-D_2O (9:1) buffered with PBS at 4°C, as well as difference spectra from equimolar solutions of each ligand (in the absence of $A\beta_{1-40}$) and $A\beta_{1-40}$ (in the absence of ligand).

saturation transfer is indeed facilitated through $A\beta_{1-40}$; likewise an STD experiment on 1mM $A\beta_{1-40}$ in the absence of ligand lack any observable resonances in the difference spectrum. Taken together these data indicate that both 3HAA and GS-1049 are able to interact with monomeric $A\beta_{1-40}$.

5.2.1.2 $A\beta_{1-10}$, $A\beta_{12-21}$ and $A\beta_{21-30}$

Initial MM studies have indicated that the majority of binding interactions occur within the first 23 residues of Aβ; these studies further indicate that biding interactions about HHQK are favored for the majority of antiaggregants analyzed. To assess whether specific regions of the Aβ are indeed preferred areas of interaction several peptides were synthesized for further NMR studies. 3 peptides were chosen for further study, each consisting of a 10-AA segment of the sequence of Aβ (**Table 5.1**). The three peptides chosen for study – $A\beta_{1-10}$, $A\beta_{12-21}$ and $A\beta_{21-30}$ – contain different structural elements and analyses of interactions with each will provide insight into AA residues which confer peptidc interactions with the ligands of investigation. $A\beta_{1-10}$ contains a mixture of aromatic residues and residues able to interact via as acceptors of ligand H^D interactions; $A\beta_{12-21}$ contains mainly aromatic and hydrophobic residues that interact

primarily via hydrophobic interactions; $A\beta_{21-30}$ contains no aromatics only residues able to interact via as acceptors of ligand H^D interactions as well as a few hydrophobic residues. Interaction preferences of the ligands with each of the peptides will provide further insight into potential mechanisms of ligand interaction.

3HAA, AnA, and GS-1049 were all assessed via STD for binding to $A\beta_{1-10}$, $A\beta_{12-21}$ and $A\beta_{21-30}$. Peptide-ligand solutions were prepared containing 3 mM ligand and 1 mM peptide (with exception of $A\beta_{12-21}$ which, due to limited solubility, was assessed at 0.5mM) in a H_2O-D_2O solution (9:1) buffered with PBS at 4^oC. Peptides were prepared using standard Fmoc chemistry and were at a minimum 97% pure by HPLC analysis (for more detailed experimentals please refer to **Section 6.1.3** of the methods chapter). The difference spectra for 3mM AnA with $A\beta_{1-40}$, $A\beta_{1-10}$, $A\beta_{12-21}$ and $A\beta_{21-30}$ are presented in **Figure 5.5**. No AA resonances are observed in difference spectra from STD analyses with any of the truncated 10-AA Aβ peptides – indicating again that AnA does not interact with any of these peptides in solution.

Preliminary STD experiments indicate that both 3HAA and GS-1049 are able to interact with monomeric $A\beta_{1-40}$. 3HAA interacted with neither $A\beta_{1-10}$ nor $A\beta_{21-30}$ – as indicated by no observable 3HAA resonances in the STD difference spectra (**Figure 5.6**).The difference spectrum of 3HAA with $A\beta_{12-21}$ indicates a positive binding interaction; however the signal is weaker than that observed in the difference spectrum with full length Aβ indicative of a weaker interaction. GS-1049 resonances were observable in the difference spectra of STD experiments with all three truncated Aβ peptides, although the observed resonances differed from peptide to peptide. The observed interaction was weakest with $A\beta_{21-30}$ although the resonance of the methylene hydrogen about the benzyl group of GS-1049 is observable. Interestingly aromatic resonances were observed in the difference spectra for GS-1049 with both $A\beta_{1-10}$ and $A\beta_{12-21}$ indicating that the aromatic residues of GS-1049 are in close proximity to these peptides during the observed binding interaction.

Table 5.1 Sequence AAs of $A\beta_{1-10}$, $A\beta_{12-21}$ and $A\beta_{21-30}$.

Peptide	Sequence
$A\beta_{1-10}$	DAEFRHDSGY
$A\beta_{12-21}$	VHHQKLVFFA
$A\beta_{21-30}$	AEDVGSNKAI

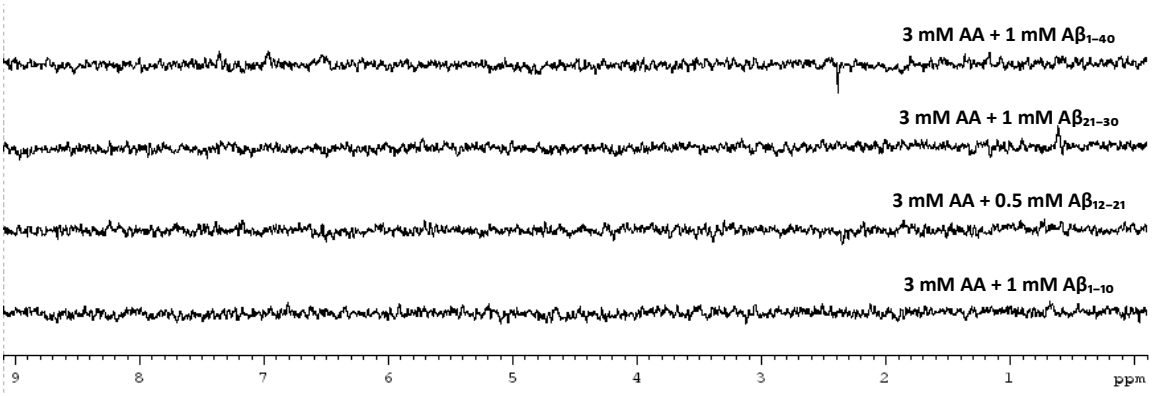

Figure 5.5 The difference spectra of 1 mM $A\beta_{1-40}$, 1 mM $A\beta_{1-10}$, 0.5 mM $A\beta_{12-21}$ and 1 mM $A\beta_{21-30}$ with 3mM AnA in H_2O-D_2O (9:1) buffered with PBS at 4^oC

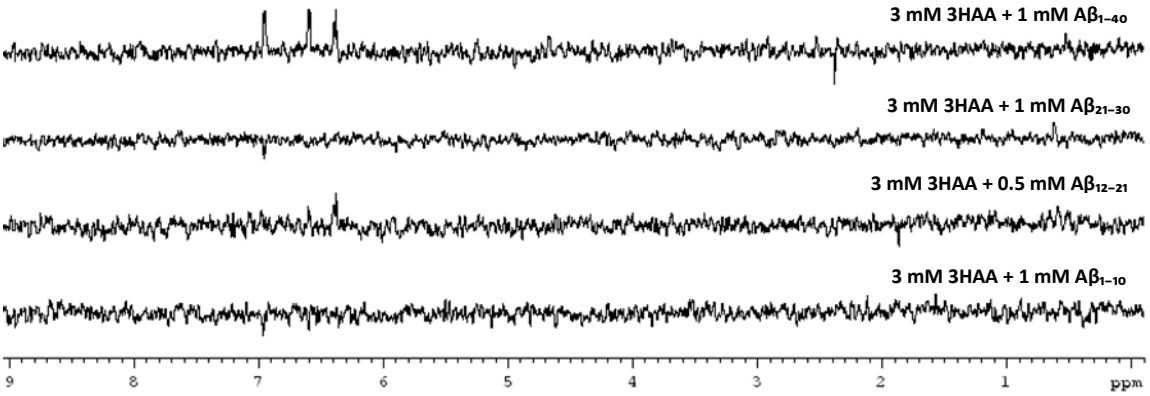

Figure 5.6 The difference spectra of 1 mM $A\beta_{1-40}$, 1 mM $A\beta_{1-10}$, 0.5 mM $A\beta_{12-21}$ and 1 mM $A\beta_{21-30}$ with 3mM 3HAA in H_2O-D_2O (9:1) buffered with PBS at 4^oC

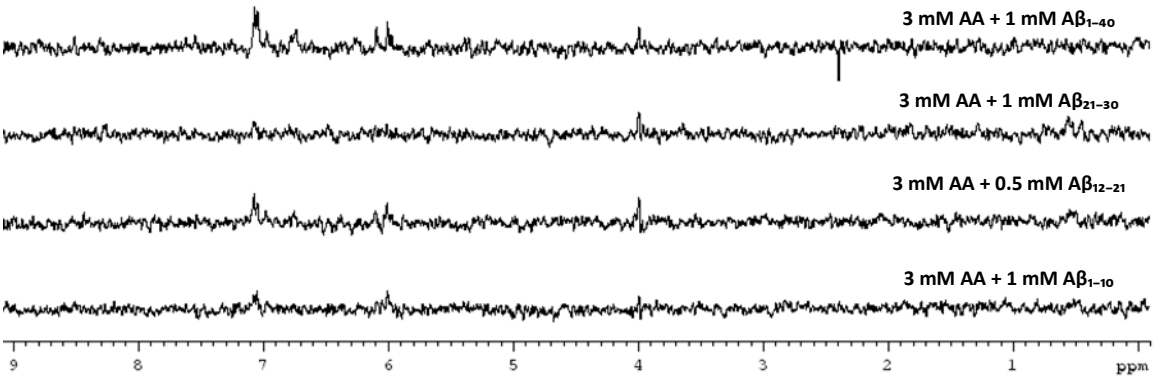

Figure 5.7 The difference spectra of 1 mM $A\beta_{1-40}$, 1 mM $A\beta_{1-10}$, 0.5 mM $A\beta_{12-21}$ and 1 mM $A\beta_{21-30}$ with 3mM GS-1049 in H_2O-D_2O (9:1) buffered with PBS at 4^oC

5.2.2 DOSY

To supplement the STD experimentation 3HAA, AnA and GS-1049 were further assessed for ligand binding using DOSY – GS-1045 was also assessed. 3 mM solutions of each ligand were prepared containing 1 mM peptide (with the exception of $A\beta_{12-21}$ which, due to limited solubility, was assessed at 0.5mM). DOSY was run on each of the peptide-ligand solutions in H_2O-D_2O (9:1) buffered with PBS at 4°C (for more a more detailed experimental please refer to **Section 6.3.2** of the methods chapter). In **Figure 5.8** a typical ^{1}H-NMR spectrum of a peptide-ligand experiment is presented. Here 3mM 3HAA is in solution with $A\beta_{21-30}$; a resonance due to water is observed at 4.7 ppm, the three resonances of 3HAA are downfield and peptide resonances are upfield.

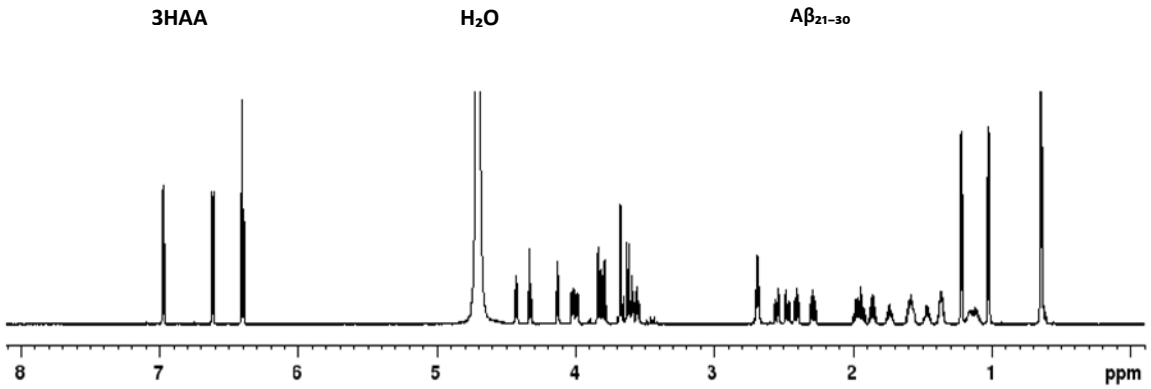

Figure 5.8 ^{1}H-NMR spectrum of a solution of 3 mM 3HAA containing 1 mM $A\beta_{21-30}$ in H_2O-D_2O (9:1) buffered with PBS at 4°C.

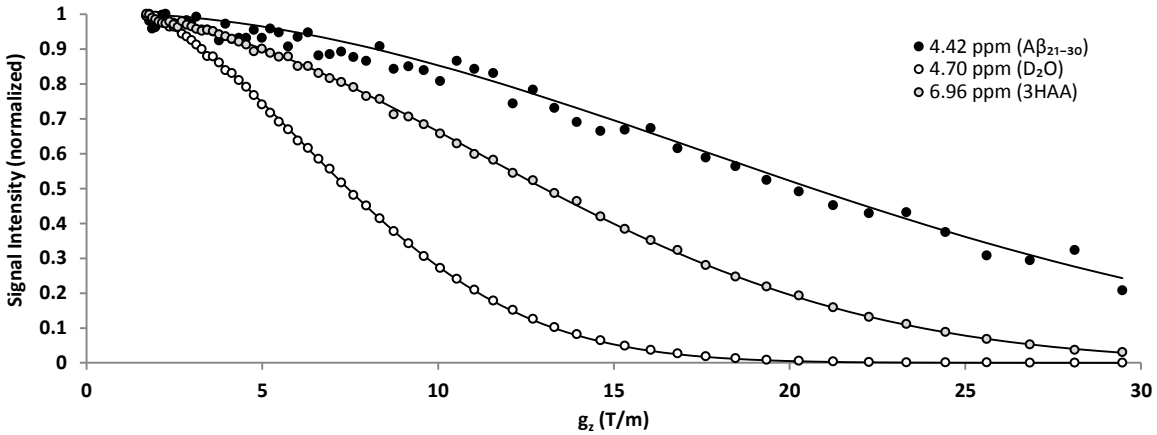

Figure 5.9 Signal intensity as a function of gradient strength, g_z, for a 3HAA resonance (6.96 ppm), a $A\beta_{21-30}$ resonance (4.42 ppm) and the water resonance (4.7 ppm), where the pulse gradients were incremented from 2 to 95% of the maximum gradient strength in a linear ramp in 64 steps.

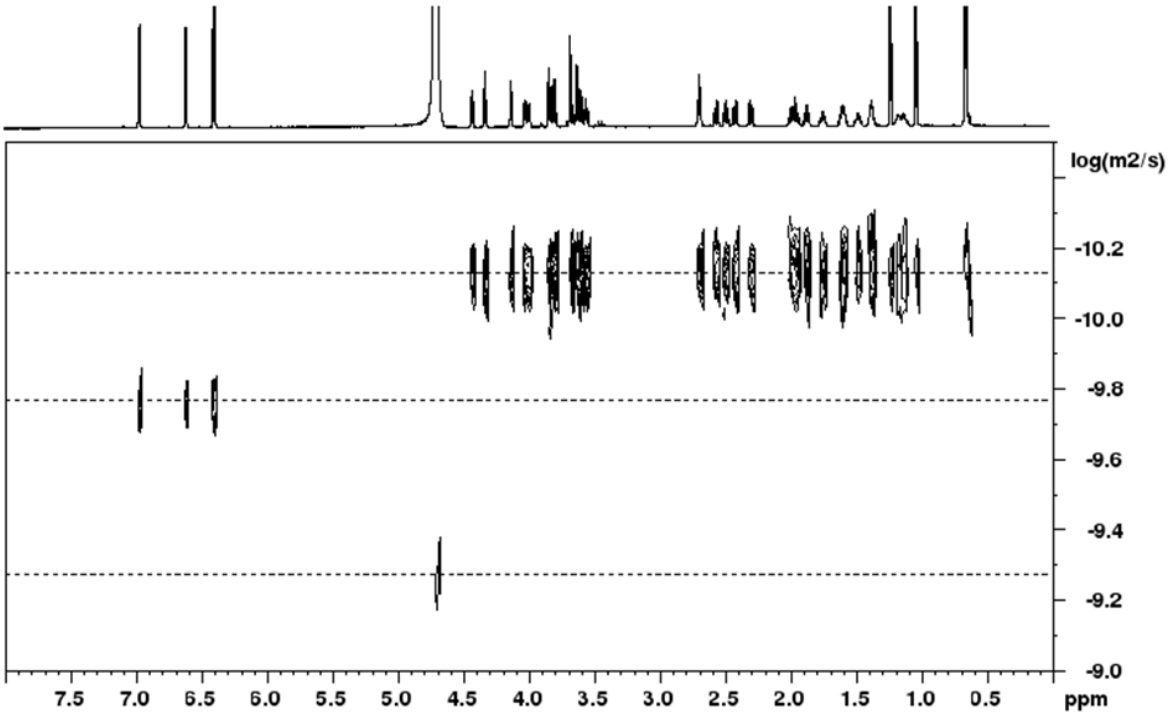

Figure 5.10 2D DOSY plot of a solution of 3 mM 3HAA containing 1 mM $A\beta_{21-30}$ in H_2O-D_2O (9:1) buffered with PBS at 4°C.

Diffusion coefficients for each of the resonances are determined individually by assessing signal attenuation as a function of gradient strength, g_z. The pulse gradients were incremented from 2 to 95% of the maximum gradient strength in a linear ramp in 64 steps. In **Figure 5.9** the signal intensity for a 3HAA resonance (6.96 ppm), a $A\beta_{21-30}$ resonance (4.42 ppm) and the water resonance (4.7 ppm) are presented as a function of gradient field strength. The observed intensity of the water resonance decreases the most rapidly with increasing gradient strength, a fact owing to its comparatively large self-diffusivity; signal attenuation is more gradual for the 3HAA and $A\beta_{21-30}$ resonances; $A\beta_{21-30}$ the largest of these three molecules has the smallest self-diffusivity and as such signal attenuation occurs more slowly than water and 3HAA. The signal intensity for each resonance in the spectrum may be analyzed as such and the diffusion coefficient determined for each. In **Figure 5.10** the resonances of this system are presented as a 2D plot with ^1H chemical shift (in ppm) on the x-axis and the logarithm of the diffusion coefficient on the y-axis, and clearly shows the difference in D_{APP} for each of the species in solution.

5.2.2.1 $A\beta_{1-10}$, $A\beta_{12-21}$ and $A\beta_{21-30}$

The D_{APP} was determined for each of the 10-AA Aβ peptides in the presence and absence of 3HAA, AnA, GS-1049 and GS-1045. If a peptide ligand binding interaction occurs this may be observed as an increase in the D_{APP} of the peptide. The measured D_{APP} of 1 mM $A\beta_{1-10}$, 0.5 mM $A\beta_{12-21}$ and 1 mM $A\beta_{21-30}$ are presented in **Table 5.2** and **Figure 5.1** for each peptide in the absence of ligand as well as in the presence of either 3HAA, AnA, GS-1049 or GS-1045 at a concentration of 3 mM. The D_{APP} was determined for each peptide resonances and averaged to give the D_{APP} of the peptide, error bars represent the S.D. of the averaged values. Although variation was observed in the absolute values of the measured D_{APP} of each peptide in the presence of ligand the differences were typically within the S.D. of the determined D_{APP}; this was true for all peptide ligand combinations with the exception of $A\beta_{21-30}$ in the presence of GS-1045 where a decrease in D_{APP} was seen that was outside of the S.D. of the peptide measured alone.

Table 5.2 The measured D_{APP} of $A\beta_{1-10}$, $A\beta_{12-21}$ and $A\beta_{21-30}$ in the absence and presence of 3 mM 3HAA, AnA, GS-1049 and GS-1045 in H_2O-D_2O (9:1) buffered with PBS at 4°C.

Ligand	$D_{Peptide}$ x 10^{-10} (m^2/s)			
	$A\beta_{1-10}$	$A\beta_{8-17}$	$A\beta_{12-21}$	$A\beta_{21-30}$
No Ligand	1.16 ± 0.10	1.13 ± 0.03	0.89 ± 0.24	1.34 ± 0.05
+ AnA	1.17 ± 0.09	1.13 ± 0.05	0.83 ± 0.28	1.26 ± 0.08
+ 3HAA	1.19 ± 0.07	1.10 ± 0.05	0.96 ± 0.13	1.24 ± 0.06
+ GS-1045	1.20 ± 0.07	1.11 ± 0.03	0.92 ± 0.19	1.22 ± 0.04
+ GS-1049	1.21 ± 0.06	1.12 ± 0.07	0.75 ± 0.31	1.26 ± 0.11

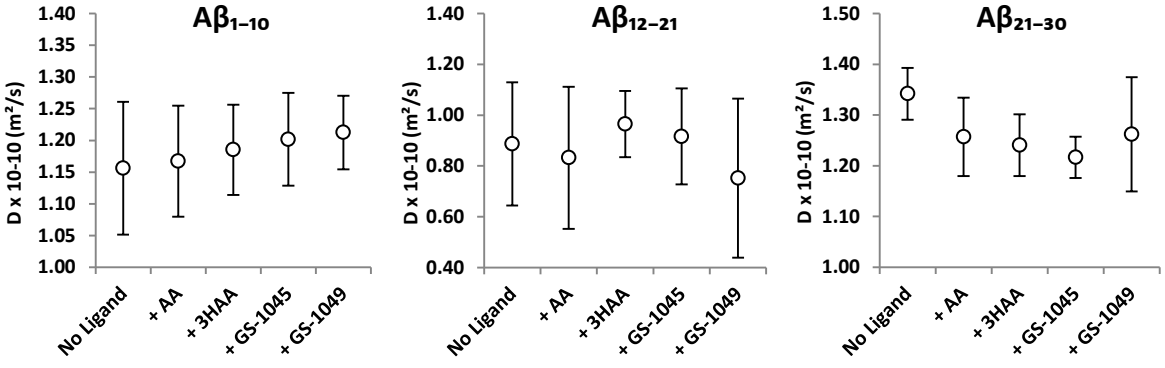

Figure 5.11 The measured D_{APP} of $A\beta_{1-10}$, $A\beta_{12-21}$ and $A\beta_{21-30}$ in the absence and presence of 3 mM 3HAA, AnA, GS-1049 and GS-1045 in H_2O-D_2O (9:1) buffered with PBS at 4°C. The D_{APP} was determined for all peptide resonances and averaged to give the D_{APP} of the peptide, error bars represent the S.D. of the averaged values.

5.2.2.1 3HAA, AnA, GS-1045 and GS-1049

The D_{APP} was determined for 3HAA, AnA, GS-1049 and GS-1045 the presence and absence of the three 10-AA Aβ peptides and are presented in **Table 5.3** and **Figure 5.12**. No significant change was observed in the D_{APP} for AnA or 3HAA; however changes were observed in the measured D_{APP} of GS-1045 and GS-1049 in the presence of the peptides. In the presence

Table 5.3 The measured D_{APP} of 3HAA, AA, GS-1049 and GS-1045 in the absence and presence of $A\beta_{1-10}$, $A\beta_{12-21}$ and $A\beta_{21-30}$ in H_2O-D_2O (9:1) buffered with PBS at 4°C.

Peptide	D_{Ligand} x 10^{-10} (m^2/s)			
	AA	3HAA	GS-1045	GS-1049
No Peptide	3.40 ± 0.03	2.94 ± 0.25	3.09 ± 0.05	2.88 ± 0.07
+ $A\beta_{1-10}$	3.42 ± 0.19	3.01 ± 0.38	2.96 ± 0.11	2.74 ± 0.07
+ $A\beta_{1-10}$	3.53 ± 0.07	3.16 ± 0.02	2.88 ± 0.03	2.86 ± 0.11
+ $A\beta_{12-21}$	3.41 ± 0.09	3.07 ± 0.17	2.87 ± 0.04	2.75 ± 0.04
+ $A\beta_{21-30}$	3.48 ± 0.08	3.17 ± 0.02	2.85 ± 0.03	2.80 ± 0.06

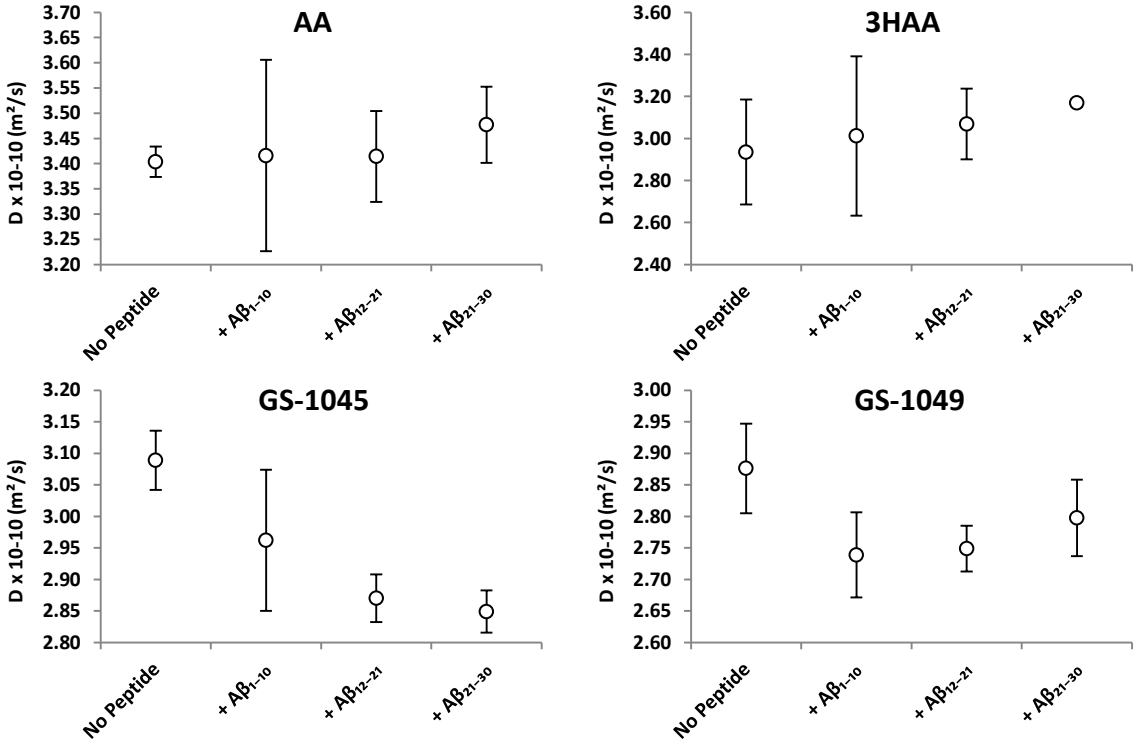

Figure 5.12 The measured D_{APP} of 3HAA, AA, GS-1049 and GS-1045 in the absence and presence of $A\beta_{1-10}$, $A\beta_{12-21}$ and $A\beta_{21-30}$ in H_2O-D_2O (9:1) buffered with PBS at 4°C. The D_{APP} was determined for each ligand resonance and averaged to give the D_{APP} of the ligand, error bars represent the S.D. of the averaged values.

of $A\beta_{12-21}$ and $A\beta_{21-30}$ the decrease in the measured D_{APP} of GS-1045 was outside of the measured D_{APP} of ligand alone; likewise in the presence of $A\beta_{1-10}$ and $A\beta_{21-30}$ the decrease in the measured D_{APP} of GS-1045 was outside of the measured D_{APP} of ligand alone. The measured decrease of D_{APP} of GS-1045 and GS-1049 in the presence of these peptides is a good indication of peptide ligand binding.

5.3 Evidence of Antiaggregant Binding to *m*Aβ

Using NMR spectroscopy, the peptide-ligand binding study conducted here are evidence of antiaggregant binding of monomeric $A\beta_{1-40}$. The STD and DOSY experiments suggest that 3HAA, GS-1045 and GS-1049 all directly associate with Aβ; however, using the methods outlined here, no evidence of binding was observed in peptide incubations with Ana, a compound which possesses neither antifibrillogenic nor antioligomeric activity. Only active antiaggregants were observed to interact with *m*Aβ; it is possible that interactions between these compounds and *m*Aβ may play a role in the observed antiaggregant activity.

Chapter 6: Methods

6.1 Peptide Synthesis

6.1.1 Chemicals

Dimethylformamide (DMF) and dichloromethane (DCM) were purchased from EMD Chemicals (Gibbstown, NJ). Fmoc-protected AAs, as well as the Fmoc-Ala-Wang and Fmoc-Tyr-Wang resins were purchased from either SynBioSci (Livermore, CA) or Novabiochem (Läufelfingen, Switzerland). o-benzotriazole-N,N,N',N'-tetramethyl-uronium-hexafluoro-phosphate (HBTU) was purchased from Aroz Technologies (Cincinnati, OH) Diisopropylethylamine (DIEA), triisopropylsilane (TIPS), and N-methyl-pyrrolidone (NMP) were purchased from Alfa Aesar (Ward Hill, MA). Piperazine, methy tert-butyl ether (MTBE) and 1-hydroxy-benzotriazole HOBt were purchased from Sigma-Aldrich (Oakville, ON). TFA was purchased from TFA, Chemicals (Gibbstown, NJ). Acetonitrile (MeCN) was purchased from VWR International (Mississauga, ON).

6.1.2 Synthesis

Peptides were synthesized using a CEM Liberty 12-channel automated microwave assisted peptide synthesizer – all coupling and deprotection steps were microwave assisted. The pre-loaded Fmoc-protected Wang resin was put in a reaction vessel washed three times with 10 mL of DMF, and then swollen in 50:50 DCM-DMF for 15 min (all resins were used at a 0.25 mM scale). The resin was Fmoc-deprotected using freshly prepared 20% piperizine v/v in DMF with 0.1% HOBt for 5 min. After deprotection the deprotection solution was drained and the resin washed four times with 7 mL of DMF. Sequential coupling of AAs was conducted by adding 2.5 mL of 20 mM Fmoc-AA in DMF, 0.5 mL of 35% DIEA v/v in NMP (activator base) and 1 mL of 0.5 M HOBt in DMF (Activator); the solution was mixed and microwave activated for 5 min. At the end of the coupling reaction the excess Fmoc-AA and reagents were drained and the resin washed four times with 7 mL of DMF. The newly affixed AA was then Fmoc-deprotected using freshly prepared 20% piperizine v/v in DMF with 0.1% HOBt for 5 min.

Once all AA residues have been coupled and deprotected the resin was again washed four times with 7 mL of DMF. The resin was removed from the reaction vessel and suction

filtered to remove DMF from the resin wash. The peptide-bound resin was then washed 5 times with 20 mL of DCM and again suction filtered to dryness. Once dry 15 mL of cleavage cocktail (95% TFA, 2.5% H_2O and 2.5% TIPS) was added allowed to react for 3-4 hours with intermittent stirring. The TFA cleavage cocktail was subsequently removed via suction filtration and -80^oC MTBE added to precipitate the cleaved peptide (20x volume). The precipitated crude peptide was allowed to settle and centrifuged (5 min, 3700 g) to form a pellet of crude peptide. The pellet was washed 3 more times with 20 mL of MTBE; each time followed by centrifugation and aspiration of the MTBE. Following the ether wash the crude material was dissolved in a minimal amount of deionized water and washed 3 more times with 5 mL of ether. The aqueous peptide solution was then frozen, lyophilized to dryness and kept at -80^oC until HPLC purification. All peptides were obtained with crude yields >90%.

6.1.3 Purification

Peptides were purified via reverse phase semipreparative HPLC using a Restek Ultra C18 reversed-phase column (5 µm, 100 Å, 21.2 x 150 mm) coupled to a Dionex Ultimate HPG-3200P semipreparative Pump. Binary solvent gradients at a constant flow rate of 20 mL/min were used for peptide purification and are presented in **Table 6.1** for $A\beta_{1-10}$, $A\beta_{12-21}$ and $A\beta_{21-30}$ (solvent A is 95:5 H_2O-MeCN with 0.05 % TFA and solvent B is 5:95 H_2O-MeCN with 0.05 % TFA). A Teledyne Isco Foxy Jr.® Fraction Collector was used to collect samples. Post-purification, peptide purity was assessed using a Dionex Ultimate 120 C18 reversed-phase column (5 µm, 120 Å, 4.6 x 150 mm) coupled to a Dionex Ultimate LPG-3400A Analytical Pump. In both cases a Dionex Ultimate VWD-3400 Variable Wavelength UV/Vis detector was used for detection of peptide at 280 nm. All peptides used for experimentation were ≥97% pure by HPLC peak area.

Table 6.1 Solvent gradients for semipreparative purification of $A\beta_{1-10}$, $A\beta_{12-21}$ and $A\beta_{21-30}$.

$A\beta_{1-10}$		$A\beta_{12-21}$		$A\beta_{21-30}$	
Time (min)	**%B**	**Time (min)**	**%B**	**Time (min)**	**%B**
0	0.0	0	0.0	0	0.0
1	0.0	1	0.0	1	0.0
10	17.9	18	30.0	5	2.2
12	100.0	20	100.0	6	100.0
14	100.0	22	100.0	7	100.0
16	0.0	24	0.0	8	0.0
20	0.0	28	0.0	12	0.0

6.2 Small-Molecule Synthesis

6.2.1 Chemicals

Dried solvents were purchased from EMD Chemicals (Gibbstown, NJ) and all other reagent and chemicals were purchase from either Sigma Aldrich (Oakville, ON) or VWR international (Mississauga, ON); all chemicals were used as received from the appropriate suppliers.

6.2.2 Synthesis

Unless otherwise noted all glassware was flame-dried and stored in an oven overnight, and was purged with argon and cooled before use. All reactions were carried out under an atmosphere or argon gas. Reactions were monitored by thin-layer chromatography (TLC) analysis. Dried solvents and all other chemicals were used as received from the appropriate suppliers. Flash chromatography (FC) was carried out on 44-63 μm silica gel (230-325 mesh).

6.2.2.1 GS-1031 and GS-1032

Catechol (2 g, 18.2 mmol), methyl iodide (3.22 g, 22.7 mmol) and finely divided K_2CO_3 (5.02 g, 36.3 mmol) were charged into a one neck round bottom flask, to which 50 mL of DMF was added. The mixture was heated to 60 ^{o}C and stirred overnight. Upon cooling, the mixture was diluted with water (150 mL), and extracted with EtOAc (2 x 100 mL). The organic layer was separated, washed with brine (100 mL), dried with Na_2SO_4, and concentrated *in vacuo*. The residue was purified with FC (10% EtOAc/Hex). Removal of solvent *in vacuo* yielded 2-methoxyphenol (GS-1031) (900 mg, 36%) and 1,2-dimethoxybenzene (GS-1032) (376 mg, 17%) as yellow oils. **GS-1031:** IR (neat) ν 3508, 3060, 3013, 2955, 2846, 1602, 1504, 1368, 1266, 1227, 1114, 1029, 919, 752 cm-1; ^{1}H-NMR (500 MHz, $CDCl_3$) δ 6.91-6.93 (m, 1H), 6.83-6.79 (m, 3H), 3.86 (s, 3H); ^{13}C-NMR (500 MHz, $CDCl_3$) δ 149.1, 147.7, 122.3, 121.0, 116.4, 112.9, 56.42. **GS-1032:** IR (nujol) ν 3068, 3001, 2951, 2838, 1724, 1590, 1504, 1465, 1333, 1255, 1130, 1033, 740 cm^{-1}; ^{1}H-NMR (500 MHz, $CDCl_3$) δ 6.98-6.92 (m, 4H), 3.84 (s, 6H); ^{13}C-NMR (500 MHz, $CDCl_3$) δ 150.7, 122.3, 113.3, 56.5; HRMS (ESI +) calcd for $C_8H_{10}O_2Na$ 161.0573, found 161.0565 $[M+Na]^+$.

6.2.2.2 GS-1033 and GS-1034

Catechol (1 g, 9.1 mmol), benzyl bromide (1.94 g, 11.4 mmol) and finely divided K_2CO_3 (2.51 g, 18.2 mmol) were charged into a one neck round bottom flask, to which 50 mL of ACN was added. With stirring the mixture was refluxed for overnight. Upon cooling, the mixture was diluted with water (150 mL), and extracted with EtOAc (2 x 100 mL). The organic layer was separated, washed with brine (200 mL), dried with Na_2SO_4, and concentrated *in vacuo*. The residue was purified with FC (15% EtOAc/Hex) to yield compound 2-(benzyloxy)phenol (GS-1033) (545 mg, 30%) as a yellow oil and 1,2-bis(benzyloxy)benzene (GS-1034) (791 mg, 30%) as a beige solid. **GS-1033:** IR (neat) ν 3528, 3064, 3037, 2939, 2877, 1602, 1509, 1266, 1224, 1119, 1009, 752 cm^{-1}; ^{1}H-NMR (500 MHz, $CDCl_3$) δ 7.48 (d, *J* = 7.5 Hz, 2H), 7.38 (t, *J* = 8, 2H), 7.31 (t, *J* = 7.5 Hz, 1H), 6.94 (dd, *J* = 1.5 Hz, 8 Hz, 1H), 6.86-6.80 (m, 2H), 6.75 (td, *J* = 1.5 Hz, 8 Hz, 2H), 5.15 (s, 2H); ^{13}C-NMR (500 MHz, $CDCl_3$) δ 148.2, 148.1, 138.9, 129.6, 129.0, 128.8, 122.8, 120.9, 116.8, 115.3, 72.0; HRMS (ESI +) calcd for $C_{13}H_{12}O_2Na$ 223.0730, found 223.0738 $[M+Na]^+$. **GS-1034:** IR (nujol) ν 2927, 2857, 1590, 1508, 1461, 1251, 1197, 1005, 752 cm^{-1}; ^{1}H-NMR (500 MHz, $CDCl_3$) δ 7.47 (d, *J* = 7.5 Hz, 4H), 7.38 (t, *J* = 8, 4H), 7.33 (t, *J* = 8 Hz, 2H), 7.04-7.07 (m, 2H), 6.91-6.93 (m, 2H), 5.14 (s, 4H); ^{13}C-NMR (500 MHz, $CDCl_3$) δ 150.5, 139.0, 129.6, 129.0, 128.9, 123.0, 116.8, 72.6; HRMS (ESI +) calcd for $C_{20}H_{18}O_2Na$ 313.1199, found 313.1197 $[M+Na]^+$.

6.2.2.3 GS-1035

2-methoxyphenol (0.27 g, 2.2 mmol), benzyl bromide (0.44 g, 2.6 mmol) and finely divided K_2CO_3 (0.60 g, 4.4 mmol) were charged into a one neck round bottom flask, to which 10 mL of ACN was added. The mixture, heated to 60 ^oC was stirred for 2.5 hr. Upon cooling, the mixture was diluted with water (40 mL), and extracted with EtOAc (2 x 50 mL). The organic layer was separated, washed with brine (50 mL), dried with Na_2SO_4, and concentrated *in vacuo*. The residue was purified with FC (5% EtOAc/Hex). Removal of solvent *in vacuo* yielded 1-benzyloxy-2-methoxybenzene (0.407 mg, 88%) as a yellow oil. IR (nujol) ν 3056, 3037, 2928, 2857, 1594, 1512, 1461, 1259, 1220, 1031, 744 cm^{-1}; ^{1}H-NMR (500 MHz, $CDCl_3$) δ 7.48 (d, *J* = 7.5 Hz, 2H), 7.41 (t, *J* = 7.5 Hz, 2H), 7.34 (t, *J* = 7.5 Hz, 1H), 6.99-6.93 (m, 3H), 6.91-6.87 (m, 1H); ^{13}C-NMR (500 MHz, $CDCl_3$) δ 149.9, 148.4, 137.5, 128.7, 128.0, 127.5, 121.6, 121.0, 114.4, 112.09, 71.18, 56.15; HRMS (ESI +) calcd for $C_{14}H_{14}O_2Na$ 237.0886, found 237.0880 $[M+Na]^+$.

6.2.2.4 GS-1036 and GS-1037

o-Anisidine (4 g, 32.5 mmol), methyl iodide (5.53 g, 39.0 mmol) and finely divided K_2CO_3 (4.93 g, 35.7 mmol) were charged into a one neck round bottom flask, to which 50 mL of DMF was added. The mixture was stirred overnight. At completion, the mixture was diluted with water (150 mL), and extracted with EtOAc (2 x 125 mL). The organic layer was separated, washed with brine (100 mL), dried with Na_2SO_4, and concentrated *in vacuo*. The residue was purified with FC (8% EtOAc/Hex). The purified compounds were taken up in DCM, and 1M HCl in MeOH was added dropwise. Removal of solvent *in vacuo* afforded 2-methoxy-N-methylaniline hydrochloride (GS-1036) (0.82 g, 15%) and compound 2-methoxy-N,N-dimethylaniline hydrochloride (GS-1037) (1.42 g, 24%) as white solids. **GS-1036:** IR (nujol) ν 2955, 2927, 2858, 2514, 2409, 1509, 1470, 1262, 1138, 1115, 1021, 783 cm^{-1}; ^{1}H-NMR (500 MHz, MeOD) δ 7.55 (td, *J* = 1.5 Hz, 7.5 Hz, 1H), 7.51 (dd, *J* = 2 Hz, 7.5 Hz, 1H), 7.31 (dd, *J* = 1 Hz, 8.5 Hz, 1H), 7.16 (td, *J* = 1 Hz, 8 Hz, 1H), 4.05 (s, 3H), 3.06 (s, 3H); ^{13}C-NMR (500 MHz, MeOD) δ 153.7, 132.6, 126.5, 124.1, 122.7, 114.05, 57.1, 36.8; HRMS (ESI +) calcd for $C_8H_{12}NO$ 138.0913, found 138.0918 $[M+H]^+$. **GS-1037:** IR (nujol) ν 2929, 2858, 2399, 1620, 1511, 1465, 1047 cm^{-1}; ^{1}H-NMR (500 MHz, MeOD) δ 7.75 (dd, *J* = 1.5 Hz, 8 Hz, 1H), 7.58 (td, *J* = 1.5 Hz, 7.5 Hz, 1H), 7.34 (dd, *J* = 1 Hz, 8.5 Hz, 1H), 7.22 (td, *J* = 1.5 Hz, 8 Hz, 1H), 4.08 (s, 3H), 3.31 (s, 6H); ^{13}C-NMR (500 MHz, MeOD) δ 152.6, 133.0, 131.9, 123.1, 122.0, 114.4, 57.3, 46.5. HRMS (ESI +) calcd for $C_9H_{14}NO$ 152.1070, found 152.1071 $[M+H]^+$.

6.2.2.5 GS-1038 and GS-1039

o-Anisidine (2 g, 16.2 mmol), benzyl bromide (3.05 g, 17.7 mmol) and finely divided K_2CO_3 (4.49 g, 32.5 mmol) were charged into a one neck round bottom flask, to which 50 mL of ACN was added. With stirring the mixture was refluxed for 4 hours. Upon cooling, the mixture was diluted with water (150 mL), and extracted with EtOAc (2 x 125 mL). The organic layer was separated, washed with brine (200 mL), dried with Na_2SO_4, and concentrated *in vacuo*. The residue was purified with FC (2.5% EtOAc/Hex). The purified compounds were taken up in DCM, and 1M HCl in MeOH was added dropwise. Removal of solvent *in vacuo* afforded N-benzyl-2-methoxyaniline hydrochloride (GS-1038) (1.63 g, 40%) and compound N,N-dibenzyl-2-methoxyaniline hydrochloride (GS-1039) (1.44 g, 30%) as white solids. **GS-1038:** IR (nujol) ν

2928, 2862, 2604, 2541, 2502, 2471, 1618, 1563, 1508, 1469, 1270, 763 cm^{-1}; ^{1}H-NMR (500 MHz, MeOD) δ 7.52 (td, *J* = 1.5 Hz, 7.5 Hz, 1H), 7.46-7.40 (m, 5H), 7.31 (dd, *J* = 1.5 Hz, 7.5 Hz, 1H), 7.26 (dd, *J* = 1 Hz, 8.5 Hz, 1H), 7.07 (td, *J* = 1.5 Hz, 7.5 Hz, 1H), 4.55 (s, 2H), 3.97 (s, 3H); ^{13}C-NMR (500 MHz, MeOD) δ 154.1, 132.7, 132.1, 131.8, 131.0, 130.1, 125.6, 124.3, 122.4, 114.0, 57.0, 55.9; HRMS (ESI +) calcd for $C_{14}H_{16}NO$ 214.1226, found 214.1226 $[M+H]^+$. **GS-1039:** IR (nujol) ν 2927, 2858, 2578, 1508, 1466, 1383, 1270, 1220, 1115, 1028 cm^{-1}; ^{1}H-NMR (500 MHz, MeOD) δ 7.68-7.64 (m, 4H), 7.45 (d, *J* = 8 Hz, 1H), 7.21-7.18 (m, 6H), 7.10 (td, *J* = 1.5 Hz, 8.5 Hz, 1H), 6.80 (d, *J* = 8 Hz, 1H), 6.57 (br, 1H), 5.07 (br, 2H), 4.76 (br, 2H), 4.09 (br, 3H); ^{13}C-NMR (500 MHz, MeOD) δ 152.6, 131.5, 131.0, 130.1, 129.6, 128.6, 124.1, 121.3, 111.8, 59.7, 55.9; HRMS (ESI +) calcd for $C_{21}H_{22}NO$ 304.1696, found 304.1702 $[M+H]^+$.

6.2.2.6 GS-1044

2-aminophenol (3 g, 27.5 mmol), was added to zinc oxide (1.12 g, 13.8 mmol) in formic acid (3.8 g, 82.5 mmol). The mixture was stirred at 70 ^{o}C for 1 hr. After cooling, the reaction was taken up in 20 mL of EtOAc, and was washed successively with H_2O (3 x 20 mL) and saturated $NaHCO_3$ (2 x 20 mL). After washing, the organic layer was concentrated *in vacuo*, taken up in hot H_2O (5 mL) and was filtered through cotton wool to yield white crystals (1.44 g, 48% yield). IR (nujol) ν 3380, 3107, 2927, 2856, 2748, 2620, 1660, 1594, 1535, 1461, 1383, 1282, 1216, 1103, 760 cm^{-1}; ^{1}H-NMR (500 MHz, DMSO-*d6*) δ 9.93 (s, 1H), 9.57 (s, 1H), 8.27 (d, *J* = 1.9 Hz, 1H), 8.02 (dd, *J* = 1.2 Hz, 8 Hz, 1H), 6.92 (td, *J* = 1.5 Hz, 7.5 Hz, 1H), 6.86 (dd, *J* = 1.5 Hz, 7 Hz, 1H), 6.76 (td, *J* = 1.5 Hz, 8 Hz, 1H); ^{13}C-NMR (500 MHz, $CDCl_3$) δ 160.0, 146.7, 126.0, 124.1, 120.7, 119.0, 115.0; HRMS (ESI +) calcd for $C_7H_7NO_2Na$ 160.0369, found 160.0364 $[M+Na]^+$.

6.2.2.7 GS-1046

o-Anisidine (2.0 g, 16.3 mmol), 2,4,6-triphenyl-1,3,5,2,4,6-trioxatriborinane-pyridine complex (6.4 g, 16.3 mmol) and triethylamine (5.90 g, 81.2 mmol) were taken up in DCM (100 mL). To this solution was added 4 Å molecular sieves (4.0 g) and copper acetate (5.89 g, 32.6 mmol). The solution was stirred, loosely capped, at 22 ^{o}C overnight. The reaction mixture was filtered and washed through celite, and washed successively with saturated ammonium chloride (3 x 100 mL) and brine (3 x 50 mL). The organic layer was separated, dried with Na_2SO_4, filtered, concentrated *in vacuo*. The residue purified with FC (5% EtOAc/Hex). The purified compound was taken up in 20 mL of DCM, and 6M HCl in MeOH was added dropwise with stirring. This

mixture was stirred at 22 ^{o}C for 1 hr. Removal of solvent *in vacuo* afforded 2-methoxy-N-phenylaniline hydrochloride (2.19 g, 57% yield) as a white solid. ^{1}H-NMR (500 MHz, DMSO-*d6*) δ 7.21-7.18 (m, 3H), 7.04 (dd, *J* = 2.5 Hz, 8.5 Hz, 2H), 7.00 (dd, *J* = 1.5 Hz, 8 Hz, 1H), 6.89 (td, *J* = 2 Hz, 7.5 Hz, 1H), 6.84 (td, *J* = 1.5 Hz, 7.5, 1H), 6.79 (t, *J* = 7 Hz, 1H); ^{13}C-NMR (500 MHz, DMSO-*d6*) δ 149.6, 143.8, 132.0, 128.9, 120.9, 120.6, 119.3, 117.0, 116.8, 111.5, 55.4; HRMS (ESI +) calcd for $C_{13}H_{14}NO^{+}$ 200.1070, found 200.1071 $[M+H]^{+}$.

6.2.2.8 GS-1045

2-methoxy-N-phenylaniline hydrochloride (0.63 g, 2.6 mmol) was taken up in 20 mL of DCM, cooled to 0 °C and stirred for 10 min. Boron tribromide (1.28 g, 5.1 mmol) was added dropwise, and the mixture was allowed to attain rt with stirring over the course of 2 h. MeOH (25 mL) was added to quench, and was allowed to stir for 30 min. The reaction mixture was neutralized with saturated $NaHCO_3$ (100 mL), and extracted with DCM (3 x 50mL). The combined organic layers were washed with brine (100 mL), dried with Na_2SO_4, and filtered. 6 M HCl (25mL) was added to the dried organic layers with stirring. Removal of solvent *in vacuo* afforded 2-(phenylamino)phenol hydrochloride (0.49 g, 83 % yield). IR (nujol) ν 3162, 2683, 2597, 2472, 1625, 1600, 1550, 1463, 1377, 1346, 761, 739 cm^{-1}; ^{1}H-NMR (500 MHz, DMSO-*d6*) δ 10.7-9.3 (br 2H), 7.19 (s, 1H), 7.16 (d, *J* = 8Hz, 2H), 7.00 (d, *J* = 7.5 Hz, 2H) 6.89, (dd, *J* = 1 Hz, 8Hz, 1H) 6.79-6.70 (m, 3H); ^{13}C-NMR (500 MHz, DMSO-*d6*) δ 148.2, 144.4, 130.5, 128.8, 121.5, 119.1, 118.8, 118.6, 116.1, 115.5; HRMS (ESI +) calcd for $C_{12}H_{12}NO^{+}$ 186.0913, found 186.0916 $[M+H]^{+}$.

6.2.2.9 GS-1047

2-methoxy-N-methylaniline hydrochloride (0.75 g, 4.3 mmol) was taken up in 20 mL of DCM, cooled to 0 °C and stirred for 10 min. Boron tribromide (1.62 g, 6.5 mmol) was added dropwise, and the mixture was allowed to attain rt with stirring overnight. MeOH (25 mL) was added to quench, and was allowed to stir for 30 min. The reaction mixture was neutralized with saturated $NaHCO_3$ (100 mL), and extracted with EtOAc (3 x 100mL). The combined organic layers were washed with brine (100 mL), dried with Na_2SO_4, and filtered. Removal of solvent *in vacuo* afforded 2-(methylamino)phenol (0.15 g, 28 % yield). ^{1}H-NMR (500 MHz, DMSO-*d6*) δ 11.03 (s, 1H), 10.79 (br, 2H), 7.51 (dd, *J* = 1 Hz, 7.5 Hz, 1H), 7.26 (td, *J* = 1.5Hz, 7.5 Hz, 1H), 7.13 (dd, *J* = 1.5 Hz, 8 Hz, 1H), 6.90 (td, *J* = 1 Hz, 7.5 Hz, 1H) 2.85 (s, 3H); ^{13}C-NMR (500 MHz, DMSO-*d6*) δ 150.5, 129.6, 124.9, 123.0, 119.5, 116.7, 39.7

6.2.2.10 GS-1048

2-methoxy-N,N-dimethylaniline hydrochloride (1.0 g, 5.3 mmol) was taken up in 20 mL of DCM, cooled to 0 °C and stirred for 10 min. Boron tribromide (2.00 g, 8.0 mmol) was added dropwise, and the mixture was allowed to attain rt with stirring overnight. MeOH (25 mL) was added to quench, and was allowed to stir for 30 min. The reaction mixture was neutralized with saturated $NaHCO_3$ (100 mL), and extracted with EtOAc (3 x 100mL). The combined organic layers were washed with brine (100 mL), dried with Na_2SO_4, and filtered. The residue was purified with FC (10% EtOAc/Hex). Removal of solvent *in vacuo* afforded 2-(methylamino)phenol (0.28 g, 38 % yield). IR (nujol) ν 3455, 3290, 2572, 1618, 1460, 1235, 1124, 949, 797, 702 cm^{-1}; ^{1}H-NMR (500 MHz, DMSO-*d6*) δ 7.18 (td, *J* = 1.5 Hz, 7.5 Hz, 1H), 7.02 (td, *J* = 2 Hz, 7.5 Hz, 1H), 6.89 (dd, *J* = 1.5 Hz, 7.5 Hz, 1H), 6.71 (dd, *J* = 2 Hz, 7.5 Hz, 1H) 3.04 (s, 6H); ^{13}C-NMR (500 MHz, $CDCl_3$) δ 145.4, 131.4, 128.2, 125.1, 122.9, 117.3, 46.7; HRMS (ESI +) calcd. for $C_8H_{12}NO^+$ 138.0913, found 138.0909 $[M+H]^+$.

6.2.2.11 GS-1049

N-benzyl-2-methoxyaniline hydrochloride (1.0 g, 4.0 mmol) was taken up in 20 mL of DCM, cooled to 0 °C and stirred for 10 min. Boron tribromide (1.5 g, 6.0 mmol) was added dropwise, and the mixture was allowed to attain rt with stirring overnight. MeOH (25 mL) was added to quench, and was allowed to stir for 30 min. The reaction mixture was neutralized with saturated $NaHCO_3$ (100 mL), and extracted with EtOAc (3 x 100 mL). The combined organic layers were washed with brine (100 mL), dried with Na_2SO_4, and filtered. Removal of solvent *in vacuo* afforded 2-(benzylamino)phenol (0.73 g, 92 % yield). IR (nujol) ν 3211, 2756, 1612, 1570, 1489, 1456, 1357, 1281, 1138, 792, 729 cm^{-1}; ^{1}H-NMR (500 MHz, MeOD) δ 7.49-7.24 (m, 5H), 7.35 (q, 1H), 6.93 (dd, *J* = 1 Hz, 8 Hz, 1H), 6.86 (dd, *J* – 1 Hz, 8 Hz, 1H), 6.84 (s, 1H), 4.59 (s, 2H); ^{13}C-NMR (500 MHz, MeOD) δ 160.5, 137.2, 132.2, 132.0, 131.6, 131.0, 130.3, 118.0, 114.7, 111.3, 57.1; HRMS (ESI +) calcd for $C_{13}H_{14}NO^+$ 200.1070, found 200.1079 $[M+H]^+$.

6.3 NMR

Peptide binding studies were implemented on a Bruker Avance-III 700 MHz spectrometer outfitted with a 1.7 mm TCI CryoProbe. Samples were prepared to a volume of 50 µL and were analyzed in 1.7 mm x 103.5 mm tubes (Z106462, Bruker Biospin Corporation, Billerica, MA) at a temperature of 4°C.

6.3.1 STD

STD data were acquired using a 1D STD pulse sequence with a spoil sequence to destroy unwanted magnetization (Bruker pulse sequence stddiffesgp.3). The 1D STD pulse sequence is: relaxation delay, presaturation pulse train, π/2-pulse and then acquisition. The pulse sequence uses selective presaturation of 50 Gaussian shaped pulses of 50 ms, with 1 ms delay prior to the to the π/2-pulse. Total saturation time was 2.50 s with a relaxation delay of 4.00 s. The on-resonance frequency was set to 3 ppm where there are no ligand ^{1}H resonances (only resonances for the peptides of investigation); the off-resonance frequency was set to 30 ppm. The data were recorded with 8 dummy scans and 256 scans with a spectral window of 11261.3 Hz.

6.3.2 DOSY

Diffusion measurements were performed using ^{1}H pulsed gradients (Bruker pulse sequence stebpgp1s). Pulse gradients g_z were incremented from 2 to 95% of the maximum gradient strength in a linear ramp in 64 steps. The intergradient delay, Δ, and gradient pulse duration, δ, were 200 ms and 1.5 ms respectively. The data were recorded with 4 dummy scans and 256 scans with a spectral window of 8417.5 Hz.

6.4 Biology

6.4.1 Chemicals

Rosmarinic acid, epicatechin, EGCG, quercetin, resveratrol, myricetin, curcumin, kaempferol, leutolin, naringenin, hesperetin and apigenin were purchased from Alfa Aesar (Ward Hill, MA, USA), all other assayed ligands as well as HFIP, DMSO, Tween® 20, $NaHCO_3$, NaOH, NaCl, bovine serum albumin (BSA), tetrabutylammonium borohydride, TMB, 30% H_2O_2 w/w, sulfuric acid and hydrochloric acid were purchased from Sigma Aldrich (Oakville, ON). PBS

tablets, N,N-dimethylacetamide, tris(hydroxymethyl)aminomethane (tris), citric acid (monohydrate), tribasic potassium citrate (monohydrate) and 0.2 µm syringe filters were purchased from VWR International (Mississauga, ON). $A\beta_{1-40}$ and $A\beta_{1-42}$ were purchased from Anaspec (Fremont, CA). Monoclonal Aβ (unmodified and biotinylated) 82E1 (AA 1-16) were purchased from Clontech Laboratories, Inc. (Mountain view, CA). Streptavidin-HRP was purchased from Rockland Immunochemicals (Gilbertsville, PA). 96-well plates were obtained from Costar (Cambridge, MA).

6.4.2 Preparation of *m*Aβ

1 mg $A\beta_{1-40}$ or $A\beta_{1-42}$ was dissolved by brief vortexing in 1 mL of HFIP and the solution ultrasonicated for 10 min. Subsequent to dissolution HFIP was removed with a stream of argon gas for 1 h; upon removal of HFIP the peptide was either used directly in NMR experiments or the ThT fibrillogenesis assay.

6.4.3 Sandwich ELISA

6.4.3.1 Preparation of Preformed *o*$A\beta_{1-42}$

1 mg of $A\beta_{1-42}$ was dissolved by brief vortexing in 1 mL of HFIP and the solution ultrasonicated for 10 min. 8 µL of the dissolved $A\beta_{1-42}$ was added to a 1.5 mL microcentrifuge tube. HFIP was removed with a gentle stream of argon gas, the peptide dissolved in 150 µL of trifluoroacetic (TFA), incubated at room temperature for 10 min. After removal of TFA with a gentel stream of argon gas a further 150 µL of HFIP was added to redissolve the peptide film and was then removed along with any residual TFA with a stream of argon gas. 1mL of DMSO was added to the subsequent film of disaggregated peptide to produce a 1.77 µM stock solution of $mA\beta_{1-42}$. After 10 minutes of incubation at room temperature in DMSO the disaggregated peptide was diluted 50-fold into PBS buffer (to facilitate the formation of oligomers) in a 50 mL tube to 35.4 nM. After 1 h at room temperature an equal volume of PBS buffer (VWR International, Mississauga, ON, Canada) with 0.6% v/v Tween® 20 (Sigma-Aldrich Canada Ltd., Oakville, ON, Canada) was added to stop oligomerization and stabilize formed oligomers. The 17.7 nM mixture of oligomeric and monomeric $A\beta_{1-42}$ was either used immediately or frozen in aliquots at -80^{o}C (in polypropylene) tubes for later use. Oligomers prepared in this manner have been shown to be > 70 kDa and are similar to Aβ oligomers from AD brain.[107]

6.4.3.2 Solutions

6.4.3.2.1 Coating Solution

84 mg of $NaHCO_3$ is dissolved in 10mL of ultrapure Milli-Q H_2O and pH adjusted to 9.6 with 10 M NaOH for a final concentration of 100 µM $NaHCO_3$.

6.4.3.2.2 Washing Solution

250 µL of Tween® 20 is dissolved in 500 mL of PBS buffer for a final concentration of 0.05 % Tween® 20 v/v.

6.4.3.2.3 Blocking Solution

0.4 g of bovine serum albumin (BSA) is dissolved in 40 mL of PBS buffer for a final concentration of 1.0 % BSA m/v.

6.4.3.2.4 Incubation Solution

75 µL of Tween® 20 is dissolved in 15 mL of blocking solution and the system diluted to 150 mL using PBS for a final concentration of 0.1 % BSA m/v and 0.05 % Tween® 20 v/v.

6.4.3.2.5 Substrate Solution

The substrate solution consists of two components which are prepared individually and mixed prior to use. Solution A consists of 7.3 mg of tetrabutylammonium borohydride and 98.5 mg TMB dissolved in 10 mL of dimethylacetamide (for final concretions of 8.2 mM and 41 mM, respectively); buffer B consists of 12.71 g of citric acid (monohydrate), 13.63 g of tribasic potassium citrate (monohydrate), and 174 µL of H_2O_2 dissolved in 500 mL of deionized H_2O (205 mM $K_3C_6H_5O_7$citrate, pH 4.0, 3.08 mM H_2O_2). 250 µL of solution A is added to 10 mL of buffer B and incubated at room temperature for 15 min before use.

6.4.3.3 Dissociation of Preformed oAβ_{1-42}

The 17.7 nM mixture of prepared oligomers was diluted to a final concentration 1.0 nM in PBS buffer, and pipeted in aliquots of 150 µL into wells of a polypropylene 96-well plate (flat-bottom, wide well, with 0.5mL well capacity). Analyte compounds in DMSO were subsequently

added to each well to the desired concentration in 0.5 µL of DMSO. The plate was sealed with a plastic sheet and incubated at room temperature with shaking at 300 rpm for 16-18 hours.

6.4.3.4 Preparation of Capture Antibody Plate

165 µL of 0.1 mg/mL 82E1 monoclonal antibody (Clontech Laboratories Inc., Mountain View, CA, USA) was added to 5.33 mL of coating solution and the resulting solution pipeted in 50 µL aliquots into the wells of a polypropylene 96-well plate (flat-bottom, wide well, with 0.5mL well capacity). The plate was sealed with a plastic sheet and refrigerated overnight. After 16 hours antibody solutions were discarded from the coated plate and well were subsequently washed in triplicate with 200 µL of washing solutions. After washing the plate is blocked by adding 250 µL of 1% BSA (m/v) in PBS to each well and incubating for 1 hour at room temperature; the plate is subsequently emptied of blocking solution and each well is again washed in triplicate with 200 µL of washing solution.

6.4.3.5 oAβ_{1-42} Detection

50 µL of each oAβ_{1-42}-ligand incubation is transferred to the capture plate; the plate was sealed with a plastic sheet and incubated at room temperature with shaking at 300 rpm for 2 hours. After incubation the plate was emptied of oAβ_{1-42}-ligand solutions and washed in triplicate with 200 µL of washing solution. 50 µL of 0.1 mg/mL biotin-82E1 monoclonal antibody was diluted to 5.00 mL in incubation solution and pipted in 50 µL aliquots into the capture plate; the plate was sealed with a plastic sheet and incubated at room temperature with shaking at 300 rpm for 2 hours, and subsequently emptied and washed in triplicate. 50 µL of 0.1 mg/mL streptavidin-HRP was diluted to 20 mL in incubation solution and pipted in 50 µL aliquots into the capture plate; the plate was sealed with a plastic sheet and incubated at room temperature (under foil) with shaking at 300 rpm for 1 hours, and subsequently emptied and washed in triplicate. 100 µL of substrate solution is added to each well; the plate was sealed with a plastic sheet and incubated at room temperature with shaking at 300 rpm for 15 minutes. After incubation with substrate solution 100 µL of 0.118 M sulfuric acid is added to each well and absorbances at 450 nm determined. All data were collected using a Tecan Genious plate reader.

6.4.4 Thioflavin T Fibrillogenesis Assay

6.4.4.1 Solutions

6.4.3.4.1 Tris Buffer (pH 9.6)

0.969 g of tris (crystalized free base) is dissolved in 400 mL of ultrapure Milli-Q H_2O (20 mM tris, pH 9.6).

6.4.3.4.2 Tris-HCl Buffer (pH 7.4)

3.5 g of NaCl is dissolved in 200 mL of 20 mM tris buffer (pH 9.6) and pH adjusted to 7.4 with concentrated HCl (20 mM tris, 300 mM NaCl, pH 7.4).

6.4.3.4.3 Tris-Buffered Thioflavin T Solution

5.1 mg of ThT is dissolved by brief vortexing and subsequent ultrasonication in 2 mL of 20 mM tris-HCl buffer (pH 7.4); 200 µL of the ThT solution is then diluted to 200 mL with to 200 mL of 20 mM tris-HCl buffer (pH 7.4) for a final concentration of 8 µM ThT.

6.4.4.2 *f*$A\beta_{1\text{-}40}$ Detection

1 mg of freshly disaggregated $A\beta_{1-40}$ is dissolved by brief vortexing in 1 mL of tris buffer (pH 9.6) – ultrasonication for at least 10 minutes is typically needed for complete dissolution. The 1 mL of dissolved *m*$A\beta_{1-40}$ is diluted to 3.4 mL with tris buffer (pH 9.6) and pH adjusted to 7.4 using concentrated HCl. After adjustment to physiological pH the *m*$A\beta_{1-40}$ solution is filtered using a 0.2 µM syringe filter and subsequently combined with 3.4 mL of tris-buffered ThT solution (pH 7.4) and yields a solution with *m*$A\beta_{1-40}$ and ThT present at concentrations of 20 µM and 8 µM, respectively. The buffered *m*$A\beta_{1-40}$-ThT solutions is pipeted in aliquots of 100 µL into wells of a 96-well black plate (flat-bottom, wide well, with 0.5mL well capacity). Analyte compounds in DMSO were subsequently added to each well to the desired concentration in 0.4 µL of DMSO (0.4 uL of DMSO with no compound was added to control samples). The plate was subsequently covered with a clear polypropylene lid, sealed with parafilm and incubated at 37 ^{o}C for the duration of the experiment. ThT fluorescence due to *f*$A\beta_{1-40}$ formation was monitored using 401 nm and 480 nm for excitation and emission wavelengths, respectively. All data were collected using a Tecan Genious plate reader.

6.4.4.3 *Determination of F'_{MAX} and $t_{F'_{MAX}}$*

The fluorescence curves obtained via the ThT fibrillogenesis assay are fit using **Equation 3.1** in an iterative procedure. In all figures fluorescence data is presented as values of ΔF which is achieved by subtracting F_{MIN} of the experiment from all experimental values of $F(t)$ (as per **Equation 2.2**) For the first iteration of curve fitting the entire data range (0 - 75 h) is fitted using **Equation 3.1** using the method of linear least squares (**Figure 6.1A**). After fitting $t_{F'_{MAX}}$ is determined for the first iteration fit ($t_{F'_{MAX(1)}}$). Subtracting the time at which F_{MIN} is observed, $t_{F_{MIN}}$, from $t_{F'_{MAX(1)}}$:

$$t_{F'_{MAX(1)}} - t_{F_{MIN}} = \Delta t_{(1)}$$

Equation 6.1 Time range used to define the second iteration of curve fitting.

gives the value, $\Delta t_{(1)}$, in hours which is used to determine the range of values used in the next iteration of curve fitting (**Figure 6.1B**). Subsequently, fluorescence data within the range $t_{F'_{MAX(1)}} \pm \Delta t_{(1)}$ are fitted again with **Equation 3.1** – this is the second iteration of curve fitting. $t_{F'_{MAX}}$ is then determined for the second iteration fit ($t_{F'_{MAX(2)}}$), as are $t_{F''_{MAX}}$ and $t_{F''_{MIN}}$ ($t_{F''_{MAX(2)}}$ and $t_{F''_{MIN(2)}}$, respectively). The difference of $t_{F''_{MIN(2)}}$ and $t_{F''_{MAX(2)}}$:

$$t_{F''_{MIN(2)}} - t_{F''_{MAX(2)}} = \Delta t_{(2)}$$

Equation 6.2 Time range used to define the third (and final) iteration of curve fitting.

gives the value, $\Delta t_{(2)}$, in hours which is used to determine the range of values used in the final iteration of curve fitting (**Figure 6.1B**). Fluorescence data within the range $t_{F'_{MAX(1)}} \pm (1.5\,x\,\Delta t_{(2)})$ are fitted then fitted – this is the third and final iteration of curve fitting. A comparison of the first, second and final iteration of curve fitting is shown in **Figure 6.1C** and the parameters used in the iterations of data fitting are given in **Table 6.2**. F'_{MAX} and $t_{F'_{MAX}}$ are determined for each of three data sets taken in triplicate. The determined values of F'_{MAX} and $t_{F'_{MAX}}$ are then averaged, such that errors for each value can then be included (± S.D.).

Table 6.2 Range of curve fits and fitting parameters used in the three iterations of the curve fitting procedure used to determine F'_{MAX} and $t_{F'_{MAX}}$ ($t_{F_{MIN}}$ denoted with *).

Iteration	*Fit Range (h)*	*Fitting Parameters*				$t_{F'MAX}$	$t_{F''MAX}$	$t_{F''MIN}$
		a	b	c	*d*			
1	0 - 75	1636	499	0.94	0	***6.6***	-	-
2	2.3* - 11	1373	46179	1.76	0	***6.09***	***5.34***	***6.84***
(Final)	3.9 - 8.3	1288	193499	2.03	0	-	-	-

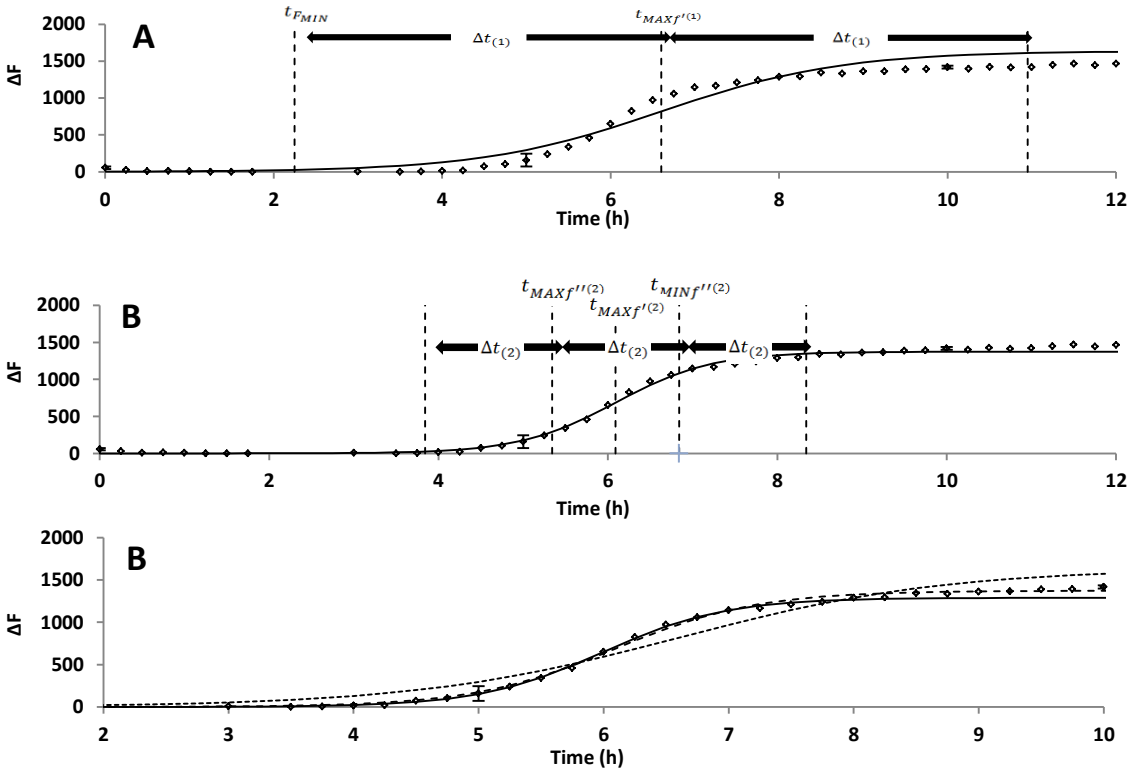

Figure 6.1 Enlargement of the region of a ThT fluorescence curve corresponding to the elongation phase *f*Aβ formation showing **A**) the first iteration of curve fitting using the general logistic equation along with $t_{F_{MIN}}$, $t_{F'_{MAX(1)}}$, and $\Delta t_{(1)}$ as well as **B**) the second iteration of curve fitting along with $t_{F'_{MAX(2)}}$, $t_{F''_{MIN(2)}}$, $t_{F''_{MAX(2)}}$ and $\Delta t_{(2)}$ and finally **C**) a comparison of the first, second and final iterations of curve fitting.

Chapter 7: Discussion & Future Directions

7.1 3HAA

7.1.1 Inhibition of Aβ Fibrillogenesis

Previously conducted CD studies suggested that 3HAA inhibited the formation of β-sheet containing species from freshly disaggregated *m*Aβ and as such the compound was investigated here for both antifibrillogenic and antioligomeric activity. Using the ThT fibrillogenesis assay it was shown that 3HAA inhibited *f*Aβ formation with an IC_{50} of 5.3 ± 1.5 μM. Although slightly less, the antifibrillogenic activity of 3HAA is of the same order of magnitude as a variety of polyphenols which are among the most potent small-molecule inhibitors of *f*Aβ formation presented in the literature and indicate that 3HAA is one of the most potent endogenous antiaggregants known.

7.1.2 The Aminophenol Motif of 3HAA Confers Antifibrillogenic Activity

3HAA contains one of each a carboxylic acid, an amine and a hydroxyl. To determine the functionality that confers the observed antifibrillogenic activity of 3HAA 6 analogues which contained one or two of the functional groups (substituted as in 3HAA) were assessed via the ThT antiaggregant assay (**Figure 3.1**). None of the monofunctionalized analogues were active inhibitors of *f*Aβ alone and indicate that the presence of a carboxylic acid, amine or hydroxyl alone does not confer antifibrillogenic activity. Of the difunctionalized analogues only *o*-aminophenol actively inhibited *f*Aβ formation in a dose-dependent manner and did so with an IC_{50} of 5.1 ± 3.6 μM which is a slight increase in antifibrillogenic activity compared to 3HAA.

Further studies investigating variations on the aminophenol motif subsequently determined that with an IC_{50} of 8.0 ± 6.7 μM catechol also possessed significant antifibrillogenic activity however *p*-phenylenediamine did not; additionally the *para*-isomers of these compounds were all active with IC_{50} values of 3.4 ± 1.8 μM, 15.2 ± 7.5 μM and 2.0 ± 0.9 μM for *o*-aminophenol, hydroquinone and *p*-phenylenediamine, respectively (**Table 3.10**). Interestingly, none of the *meta*-distributed analogues conferred substantial antifibrillogenic activity.

7.1.2.1 Catechol

Although the catechol moiety (2,3-disubstituted dihydroxyl) occurs in a wide variety of structurally unique antiaggregants (apomorphine, dopamine, dihydroxybenzoic acids, rosmarinic acid and flavonoids, to name a few)[53,105,107,158] (**Figure 3.7**) the antifibrillogenic activity of catechol or hydroquinone has not been presented in the literature. Given the structural diversity in catechol-containing antiaggregants it is very likely that the catechol moiety itself plays a fundamental role in conferring the observed antiaggregant activity of these compounds. Analogues of catechol investigated in the present study show that both hydroxyls must be present in order to confer activity; Indeed analogues of catechol in which one or both of the hydroxyls are substituted benzyl or methyl ethers (the structures of GS-1031, GS-1032, GS-1033, GS-1034 and GS-1035 are presented in **Figure 3.8**) are devoid of antiaggregant activity. The necessity for free hydroxyls to confer antifibrillogenic activity is a finding consistent with the results of a study by Lashuel and coworkers.[53] The study, in which apomorphine and derivatives thereof were investigated, showed that apomorphine potently inhibited *f*Aβ formation; however analogues in which the catechol moiety of apomorphine was methylated were rendered completely inactive (**Figure 7.1**).

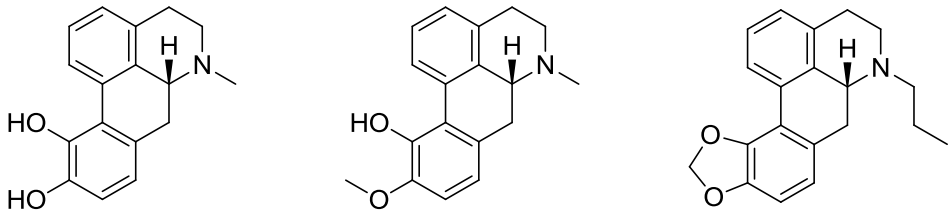

Figure 7.1 Structures of apomorphine, R(-)-apocodeine and M-121.

7.1.2.1 *o*-Aminophenol

In an exhaustive literature search only one mention of antiaggregants containing the aminophenol motif was found although no specific details are included.[93] Given the ubiquity of catechol-containing compounds in the antiaggregant literature *o*-aminophenol was selected for further analogue development. Several analogues of *o*-aminophenol were investigated in which the hydroxyl was replaced by either a methyl (*o*-anisidine), phenyl (*o*-phenoxyaniline) or benzyl ether (GS-1040) (**Figure 3.8**) a modification which resulted in complete abrogation of

antiaggregant activity. Unlike catechol the *o*-aminophenol motif is amenable to structural modifications by alkylation or arylation while retaining activity, so as long the hydroxyl group remains unaltered. Several analogues of *o*-aminophenol were synthesized in which the amine was altered, modified by either alkylation or arylation (**Figure 7.2**); with the exception of GS-1048 these compounds have improved potency in *f*Aβ inhibition relative to both 3HAA and *o*-aminophenol (IC_{50} values of *f*Aβ formation of 4.6 ± 3.1 μM, 2.2 ± 1.7 μM and 1.9 ± 1.1 μM for GS-1047, GS-1045 and GS-1049, respectively). The most significant gain in potency is observed for analogues which incorporate an aromatic ring about the amine of the aminophenol motif. Of all the analogues synthesized and assessed for antifibrillogenic activity GS-1049 was the most potent inhibitor of *f*Aβ formation; only the flavonoid myricetin and the synthetic bi-indole NCE-217 were more active than GS-1049 in this regard (IC_{50} values of *f*Aβ formation of 1.7 ± 0.9 μM and 1.0 ± 0.5 μM, respectively).

Given the excellent antifibrillogenic activity of the aminophenol analogues developed herein it is determined that this is a novel class of compounds worthy of further exploration. Thus far, the only aminophenol analogues which have undergone *in vitro* testing have been those which explore the effect of alkyl and aryl substitutions about the amine of the aminophenol moiety, and while these compounds have excellent activity the μM threshold in the observed μM potency has yet to be reached. This indeed is a lofty goal considering inhibitors of *f*Aβ formation have yet to be reported with activities in the nM range, although improved potency may be achieved through simple modifications of the current scaffold *o*-aminophenol scaffold. Prospective structures are given in **Figure 7.3**.

Given the propensity of these compounds to interact via hydrophobic interactions it is likely that increasing the hydrophobic character of future analogues may result in an increase in potency. This may be achieved through the addition of hydrophobic groups (such as methyl

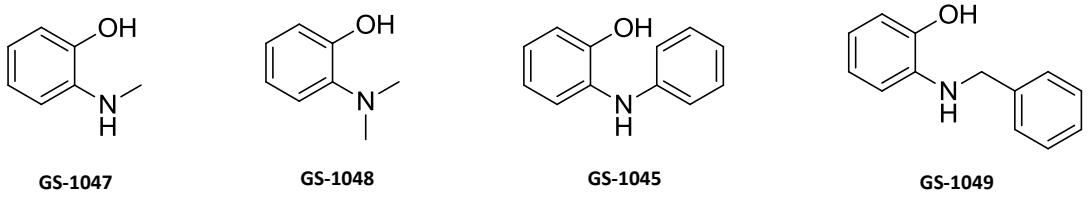

GS-1047 **GS-1048** **GS-1045** **GS-1049**

Figure 7.2 Analogues of *o*-aminophenol that actively inhibit *f*Aβ formation.

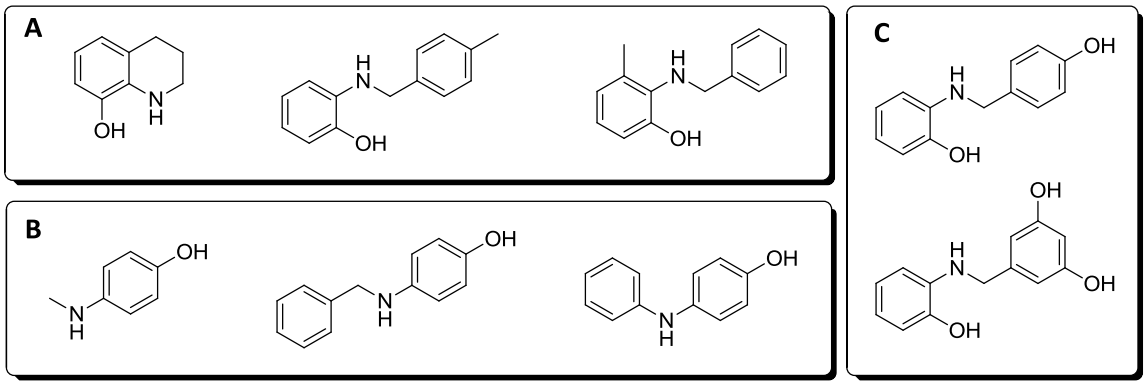

Figure 7.3 Analogues of the *o*-aminophenol antiaggregants proposed for future development which may have increased potency. Structural modifications which **A**) increase the hydrophobic character of analogues, **B**) incorporate the *p*-aminophenol scaffold and **C**) incorporate additional hydroxyl moieties may increase antifibrillogenic potency.

groups) about either the phenyl ring containing the aminophenol moiety or about the ring(s) affixed to the amine (**Figure 7.3A**). Alternatively, altering the substitution pattern about the *o*-aminophenol scaffold may also lead to improved activity, especially if one considers the improved potency of *p*-aminophenol relative to its *ortho*-distributed counterpart. Analogues which incorporate the *p*-aminophenol motif are certainly worth investigating further (**Figure 7.3B**). Finally, given the excellent activity of the polyphenol antiaggregants and the decidedly large role of H^D interactions in conferring antiaggregant activity further incorporation of hydroxyl moieties may serve to bolster activity (**Figure 7.3C**). Future analogues with increased antifibrillogenic potency may potentially be achieved by incorporating one or more of these structural modifications into future analogues.

7.2 Insights into Potential Mechanism(s) of Action

Through the course of the studies described in this thesis structurally distinct compounds were assessed for both their antifibrillogenic and antioligomeric activity against Aβ using *in vitro* biological assays; a variety of active compounds were investigated and include 3HAA, positional isomers of catechol, aminophenol and phenylenediamine, synthetic analogues of *o*-aminophenol and finally an assortment of plant-derived polyphenolic compounds. Using the ThT fibrillogenesis assay, *f*Aβ formation was monitored and a variety of compounds were shown to possess antifibrillogenic activity – *not a single compound* analyzed in the work described herein had the effect as to increase *f*Aβ formation. A modified sandwich ELISA

protocol determined that many active inhibitors of *f*Aβ formation were also shown to affect preformed soluble *o*Aβs but these results are not as straightforward. While most active inhibitors of *f*Aβ formation are also active modulators of *o*Aβs these compounds did not ubiquitously decrease measured *o*Aβs after overnight incubation – in many cases active inhibitors of *f*Aβ formation are shown to increase *o*Aβ formation. At first glance these disparate results may seem confounding and somewhat contradictory, but a deeper analysis may provide critical insight into the MoA of these various classes of antiaggregants.

7.2.1 Antifibrillogenic versus Antioligomeric Activity

Aggregation of Aβ is a complex process for which a complete mechanistic picture remains ill-defined. Although it is generally agreed that soluble *o*Aβs are the principle neurotoxic species in the aggregation process, some debate remains as to the role of *o*Aβs in the formation of *f*Aβs.[175] The discovery of new polyclonal antibodies such as the A11 and OC antibodies have shown that oligomers can be broadly categorized according to the secondary structure of their monomeric units. Both A11 and OC are epitope specific and recognize a generic backbone structure that is common to oligomeric state and independent of protein sequence;[176,177] these antibodies recognize *o*Aβs high in β-sheet content but do not recognize *m*Aβ, *f*Aβ or *o*Aβs lacking β-sheet content, so called Aβ-derived diffusible ligands (ADDLs). It is believed that oligomeric species which show immunoreactivity to A11 and OC are on-pathway species to *f*Aβ formation where these oligomers, high in β-sheet content, eventually are incorporated into growing *f*Aβs. A11 has been shown to reduce the toxicity of on-pathway oligomers in a transgenic murine model of AD and, as such, these are strongly implicated as a principle neurotoxic species.[175] On the other hand, ADDLs are the multimeric species implicated as off-pathway *o*Aβs; these off-pathway *o*Aβs have a different neurotoxic profile than their on-pathway counterparts.[178] In recent years, significant efforts in elucidating the mechanism of *f*Aβ formation have resulted in the identification of structurally disparate classes of oligomers, but even so, the connection between *o*Aβ formation and subsequent *f*Aβ formation is still poorly understood.

From the analyses conducted, it is determined that there is no correlation between antifibrillogenic activity and antioligomeric activity for any of the compounds investigated (Pearson's r of -0.075). In **Figure 7.4** the *%Fib* of all investigated compounds (at an incubation concentration of 10 μM) is compared to the absorbance at 450 nm due to the

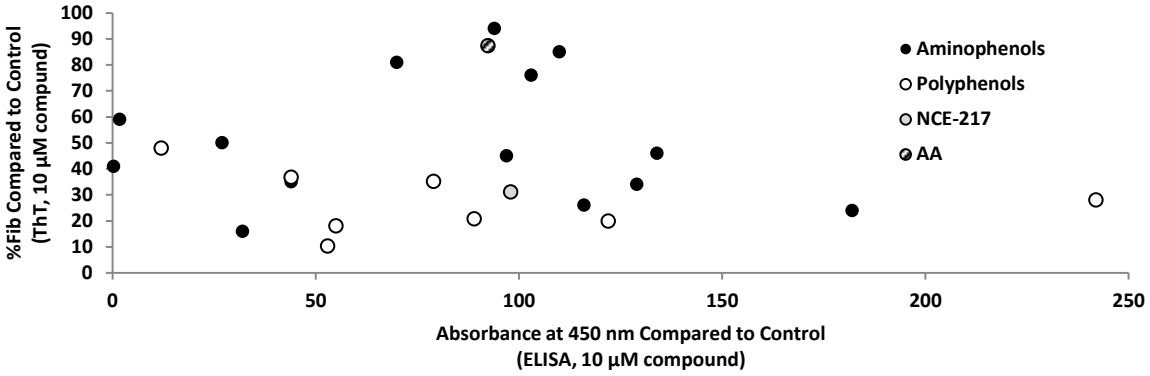

Figure 7.4 Antifibrillogenic activity of various antiaggregants versus their antioligomeric activity as determined at 10 µM incubations of compound with Aβ using the ThT fibrillogenesis assay and ELISA assay, respectively.

presence of oligomers after overnight incubation with compound (again, at an incubation concentration of 10 µM) as determined via ELISA (using the 82E1 antibody for detection). This result is in agreement with results published by Necula and coworkers who compared the antifibrillogenic activity of several antiaggregants to their antioligomeric acitivity.[175] The lack of a correlation between antifibrillogenic activity and antioligomeric activity strongly suggests that several mechanisms of action underlie the observed decrease in *f*Aβ formation due to the antiaggregants investigated here.

Within the aggregation pathway of Aβ the various intermediate species exist in a dynamic equilibrium (**Figure 1.8**). Slight perturbations in various equilibria within the pathway may have drastic effects on *f*Aβ formation. Compounds which decrease *o*Aβ formation could ultimately decrease *f*Aβ formation by stabilizing *m*Aβ – likely in an α-helical conformation. Studies have repeatedly suggested that formation of β-sheet containing oligomers occurs via random coil protein intermediates; also the majority of published CD data suggest that antifibrillogenic compounds stabilize structures high in α-helical character. Stabilizing Aβ in an α-helical form would serve to inhibit the transition of *m*Aβ to random coil structures which can thereafter incorporate into growing *o*Aβs and ultimately *f*Aβs (**Figure 7.5A**).

Compounds which increase *o*Aβ formation are similarly able to decrease *f*Aβ formation, and likely do so by shifting *m*Aβ oligomerization to off-pathway ADDLs. By pushing aggregation towards off-pathway assemblies the supply of *m*Aβ that may be incorporated into growing *o*Aβs and *f*Aβs is exasperated. Again, this may potentially be achieved through the stabilization of a structural form of *m*Aβ which would be preferentially incorporated into growing ADDLs. In the

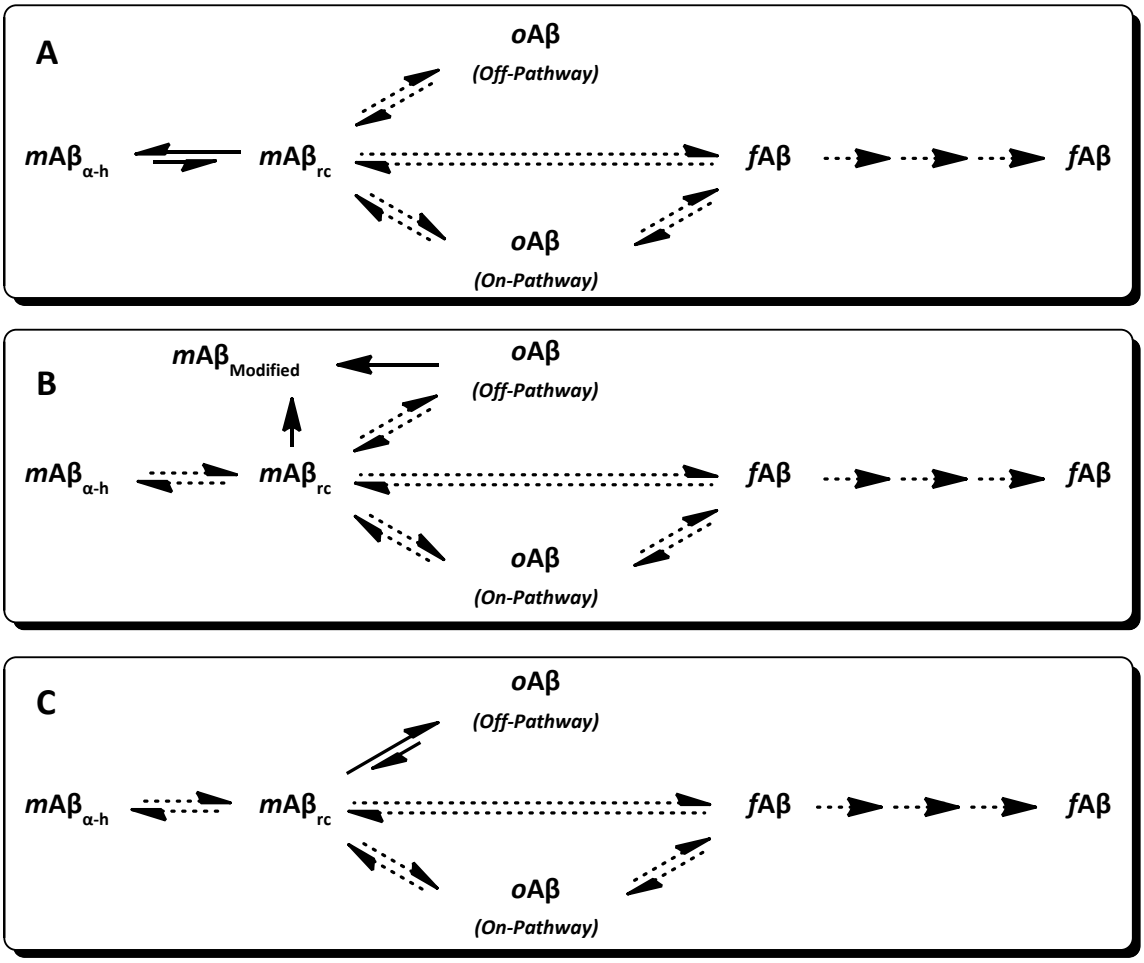

Figure 7.5 The antioligomeric activity of Aβ antiaggregants could potentially decrease *f*Aβ formation by several disparate mechanisms. **A**) Compounds which decrease *o*Aβ formation may do so by stabilization of α-helical *m*Aβs ($m\text{Aβ}_{\alpha\text{-h}}$) and would thereby preclude their incorporation into growing *o*Aβs and *f*Aβs through random coil intermediates ($m\text{Aβ}_{rc}$). **B**) Compounds which covalently modify *m*Aβs may render Aβ fibrillogenically inactive and would preclude their incorporation into growing *o*Aβs and *f*Aβs. **C**) Compounds which increase the formation of off-pathway ADDLs may deplete the supply of *m*Aβs which are eventually incorporated into on-pathway *o*Aβs and *f*Aβs.

study conducted here *o*Aβ detection was achieved using *bio*-82E1. Since the recognition element of this antibody is sequence specific, it does not distinguish between on-pathway and off-pathway assemblies. Future work utilizing polyclonal antibodies such as A11 or OC could be used to test the postulate that these compounds upregulate ADDL formation, as compounds which selectively promote these assemblies would concurrently decrease the formation of *o*Aβs detectable by epitope specific antibodies.

The sandwich ELISA assay employed in this thesis is a modified protocol developed by Levine and coworkers used to assess the effect of antiaggregant compounds on preformed oligomers of Aβ. This protocol uses *o*Aβ solutions prepared from freshly disaggregated *m*Aβ and contain a mixture of both *m*Aβ and *o*Aβ;[107] as such compounds incubated with *o*Aβ solution may decrease oligomer signal (relative to a control) indicating disassembly of *o*Aβ complexes, or conversely, incubated compounds may promote further oligomerization of *m*Aβs present in solution. Although all of the compounds analyzed potently inhibit *f*Aβ formation, these compounds disparately affected *o*Aβs, suggesting several mechanisms potentially underlie the observed antiaggregant activity of these compounds. Several structural trends are observed among the various classes of antiaggregants and may provide insight into their MoA.

7.2.1.1 Polyphenols

Incubations of several polyphenols with preformed *o*Aβs were analyzed using the sandwich ELISA assay (**Table 7.1**). Of all the polyphenols analyzed the flavanone luteolin was the only antiaggregant that did not affect *o*Aβs (relative to a control in the absence of compound); incubation of preformed oligomers with apigenin, the only other flavanone analyzed resulted in modest disassembly of *o*Aβs. The similar activity shared by the flavanones is a common trait of the polyphenols analyzed herein. For example, the four flavonols analyzed – kaempferol, quercetin, morin and myricetin – were all active disassemblers of preformed *o*Aβs although to varying degrees. Kaempferol, the most active initiator of *o*Aβ disassembly reduced observed *o*Aβs by almost 90% whereas myricetin, the least active of the flavonols, only reduced *o*Aβs by 10%. In addition, the flavonoids discussed thus far, the polyphenols EGCG, resveratrol and rosmarinic acid, also promoted *o*Aβ disassembly. Several structurally distinct and different compounds presented here show a propensity to initiate *o*Aβ disassembly. Although this experiment provides little insight into the mechanism of action, this could be a direct result of *m*Aβ stabilization via the active compounds. Such an interaction would effectively shift the *m*Aβ-*o*Aβ equilibrium towards *m*Aβs thereby reducing the *in vivo concentration of o*Aβs. There is a distinct possibility that these compounds may dissociate *o*Aβs via covalent modification of peptide AA residues. Indeed autoxidation of polyphenolic compounds is a well-known phenomenon, and the *o*-benzoquinone products are susceptible to nucleophilic attack via Michael addition or Schiff-base formation by basic amino acid sidechains. Covalent modification could potentially destabilize oligomers which subsequently dissociate into

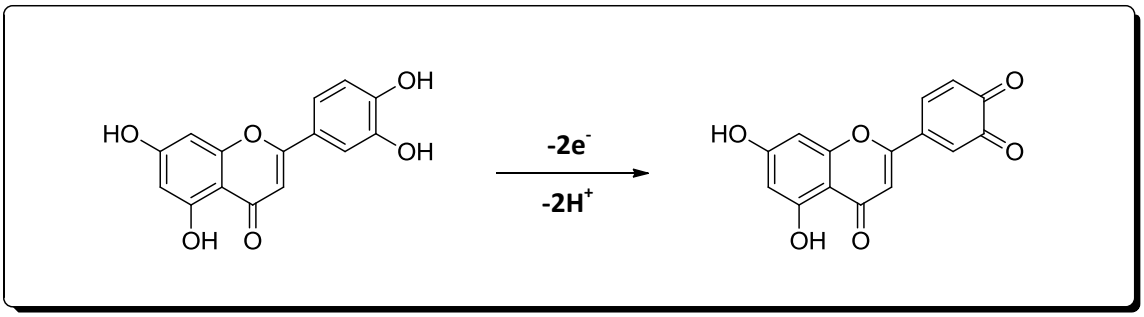

Figure 7.6 Autoxidation of quercetin into *o*-benzoquinone containing compound.

*m*Aβs. Several polyphenolic compounds were also observed to increase *o*Aβ formation relative to the control; this is a result that has not been reported in the literature to date and strongly suggests that several mechanisms underlie the observed activity of these compounds polyphenolic compounds. The flavan-3-ol epicatechin showed a modest increase in *o*Aβ formation relative to the control incubated in the absence of compound. Both flavanones that were analyzed increased oligomer signal by over 50% and indicate a significant increase in *o*Aβ formation. Interestingly epicatechin, naringenin and hesperetin all contain a non-aromatic C-ring which may constitute a structural motif with confers upregulated *o*Aβ formation; it is also noteworthy that curcumin, naringenin and hesperetin do not contain a vicinal diphenol moiety and therefore are unable to form benzoquinones adducts with Aβ. The compounds likely elicit their effect by stabilizing *m*Aβ in a conformation amenable to incorporation into growing *o*Aβs. As these compounds are all potent inhibitors of *f*Aβ formation it is likely that these compounds promote selective incorporation of *m*Aβs into ADDLs which are off-pathway assemblies of fibril formation.

Although both inhibitors and promoters of *o*Aβ were observed (with a wide range of potencies) the ELISA data presented here show that: 1) antifibrillogenic polyphenols likely inhibit *f*Aβ formation via several disparate mechanisms (perhaps concurrently), 2) compounds with similar scaffolds had similar effects on *o*Aβs (ie. *o*Aβ promotion versus *o*Aβ disassembly) 3) that compounds with similar functional group substitutions about their various scaffolds possessed similar activity regardless of whether the compounds acting to increase or decrease *o*Aβs.

7.2.1.2 3HAA and Analogues Thereof

Significant structural differences are observed between antifibrillogenic analogues of 3HAA which increase *in vitro o*Aβ formation compared to those which decrease *in vitro o*Aβ

formation. 3HAA, *o*-aminophenol, *o*-phenylenediamine, *p*-phenylenediamine, catechol and hydroquinone all decrease *o*Aβ formation; the structures of these compounds are similar to those which have been shown by Levine and coworkers to dissociate preformed oligomers – namely, 2,3-DHB, 3,4-DHB, 2,5-DHB and gallic acid (**Figure 7.7A**).[107] As with the polyphenol antiaggregants which disassembled preformed *o*Aβs, autoxidation of these analogues of 3HAA results in the formation of benzoquinones which may destabilize *o*Aβs via covalentl modification.

Three of the four synthetic analogues of *o*-aminophenol increased oligomerization: GS-1045, GS-1048, and GS-1049; interestingly, *p*-aminophenol also increased *o*Aβ formation, a surprising result as this compound is structurally similar to the analogues of 3HAA which inhibited *f*Aβ formation. It is worth noting that all of these compounds (with the exception of GS-1048 which contains dimethylaniline) are able to form *o*-quinoimines which would be able to react with Aβ to form covalent adducts.

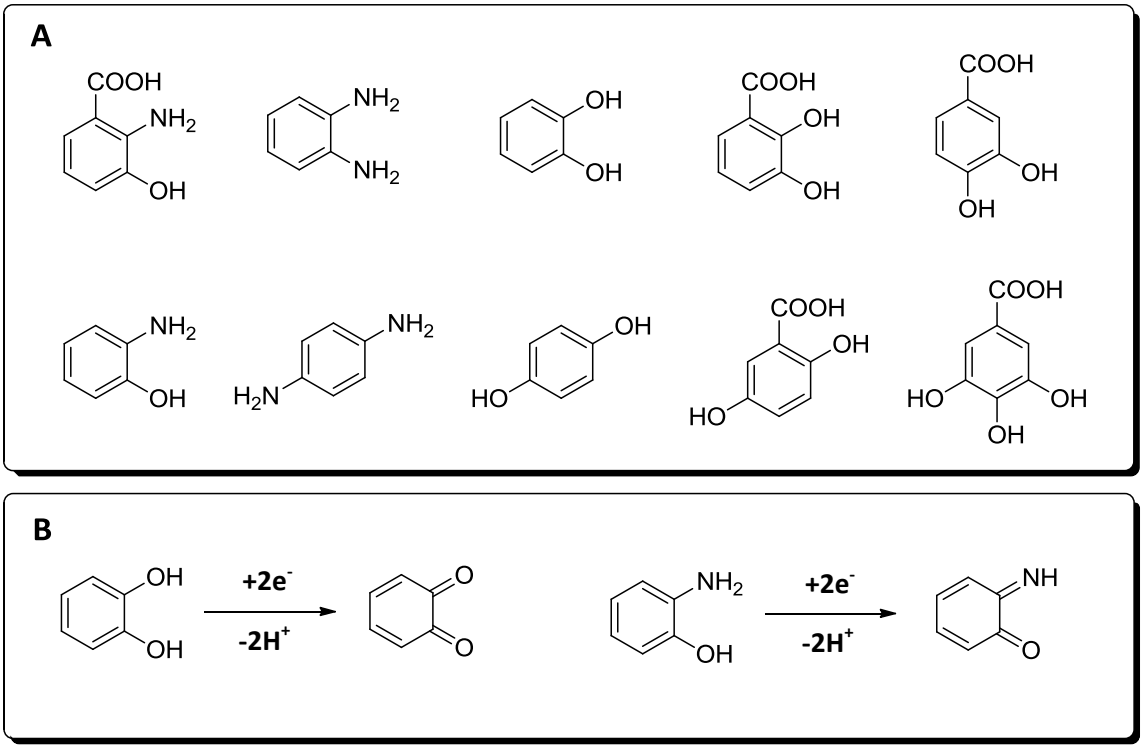

Figure 7.7 **A**) Structures of compounds that disassemble preformed *o*Aβ. **B**) Oxidation of catechol and *o*-aminophenol into the corresponding *o*-benzoquinone and *o*-quinoimine, respectively.

7.2.1.3 Assessment of Putative Mechanisms

The majority of the antifibrillogenic agents analyzed in this thesis efficiently disassembled preformed *o*Aβ. The observed decrease in preformed *o*Aβ elicited by these compounds can potentially be explained by two separate MoAs: the first (**Figure 7.5A**) proposes that the decrease in observed *o*Aβs is a result of stabilization of *m*Aβ – this would effectively shift the *m*Aβ-*o*Aβ equilibrium towards *m*Aβ thereby decreasing *o*Aβ; and the second proposes that covalent modifications of *o*Aβs (achieved through adduct formation of with benzoquinone oxidation products) results *o*Aβ destabilization and subsequent dissociation into *m*Aβs (**Figure 7.5C**).

Indeed several pieces of literature evidence provide a compelling argument for a MoA in which Aβ is covalently modified. The flavonoid baicalein is a flavonoid which potently inhibits α-synuclein fibrillogenesis and has been shown via electrospray mass spectrometric (ES-MS) to form protein-benzoquinone adducts with the protein.[179] This may explain why oxidized forms of rifampimicin, baicalein and other flavanoids more potently inhibit α-synuclein fibrillization than their non-oxidized counterparts[180,181] and why the antifibrillogenic activity of dopamine (and related vicinal diphenol analogues) is drastically reduced in the presence of a reducing agent;[53] however, results from a study by Levine and co-workers show no correlation between dissolution of preformed oligomers and activity as a reducing agent.[107]

Although there exists some literature evidence supporting a mechanism in which Aβ is covalently modified, the results of the work presented in this thesis may lend significant support to a mechanism of action whereby reduction *o*Aβ levels is achieved through stabilization of *m*Aβ. STD-NMR studies indicate that 3HAA and GS-1049 do interact with Aβ at physiological pH, a particularly important result as AnA (inactive as an inhibitor of *f*Aβ) does not show Aβ binding (**Figure 5.4**). All of the polyphenols are expected to interact with *m*Aβ more strongly than both 3HAA and GS-1049 considering the predicted interaction energies of the polyphenols with monomeric models of Aβ, as determined in the MM work described herein. Several models

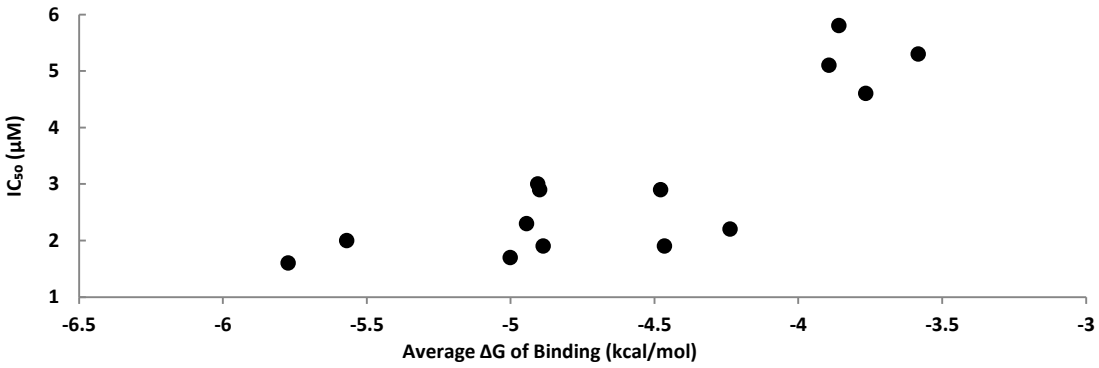

Figure 7.8 The average ΔG of binding (kcal/mol) for the polyphenolic antiaggregants, 3HAA, *o*-aminophenol and synthetic analogues thereof (GS-1045, GS-1047, GS-1048 and GS-1049) versus the observed IC_{50} of *f*Aβ inhibition as determined via the ThT fibrillogenesis assay.

were assessed for binding to all of these compounds, and the average ΔG of binding is considerably lower for the polyphenols in comparison to both 3HAA and GS-1049; furthermore, there is a high correlation between the expected binding energies of these compounds and the observed IC_{50} of *f*Aβ inhibition, as determined via the ThT fibrillogenesis assay (Pearson's *R* of 0.820) (**Figure 7.8**); taken together these results suggests that an interaction with *m*Aβ accounts somewhat for the observed antifibrillogenic activity of these compounds.

7.2.1.3.1 Polyphenols

π-π interactions are widely accepted as being the main contributor in the interaction of polyphenols with Aβ.[156,172] While the MM work conducted in **Chapter 4** supports the notion that π-stacking interactions are important mediators of polyphenol interactions with Aβ, it also suggests that the importance of H^D interactions has, to date, been largely overlooked. In the rigorous assessment of polyphenol binding to monomeric models of Aβ described in **Chapter 4**, it is found that H^D interactions are incorporated into stable binding interactions more often than π-π interactions; although this may be an artifact of the inherent structural specificity of π-π interactions, on average, H^D interactions were lower in energy. Given the potential importance of H^D interactions in mediating Aβ binding, this interaction should be considered when developing novel antiaggregants as groups which confer H^D interactions may increase compound potency.

7.2.1.3.2 Analogues of *o*-Aminophenol

The MM studies conducted indicate that the interaction profiles of 3HAA and *o*-aminophenol are significantly different from those of the synthetic analogues of *o*-aminophenol. H^D interactions tend to predominate in 3HAA and *o*-aminophenol binding to Aβ. GS-1045, GS-1047, GS-1048 and GS-1049 too interacted most often via H^D interactions, however π-π and vdw interactions tended to confer the most stable binding. The incorporation of additional ring systems in GS-1048 and GS-1049 results in significantly lower predicted values of ΔG of binding than GS-1047, GS-1048, *o*-Aminophenol and 3HAA; these lower values in ΔG of binding are closer to those observed for the polyphenols and suggest π-π interactions are important in conferring antifibrillogenic activity.

Clearly, there are differences in the interaction profiles when comparing the polyphenol antiaggregants to the various aminophenol antiaggregants, but overall trends in the interaction preferences of these compounds have provided a solid insight into a non-covalent MoA for *o*Aβ disassembly and will be discussed further.

7.2.1.3.3 Stabilization of Structurally Disparate Forms of Aβ

In general, 3HAA, *o*-aminophenol, and the polyphenols were more apt to interact with Aβ via H^D interactions than the synthetic analogues of *o*-aminophenol; the majority of these compounds also promoted *o*Aβ disassembly. Although it has been suggested that this is due to covalent modification of Aβ the MM work completed here indicates that the effect of various antiaggregants on *o*Aβ formation or dissolution may indeed be a result of these compounds stabilizing structurally disparate forms of Aβ. The proportion of H^D or vdw interactions observed for these compounds via MM analysis is be a strong indicator of whether they will promote *o*Aβ formation or disassemble preformed *o*Aβs.

There is an extremely strong correlation between the proportion of H^D bonding observed for a compound (in MM analyses) and the amount of oligomer in solution after overnight incubation with said compound (as determined via the ELISA assay)(Pearson's r of -0.837, if Kaempferol data is excluded)(**Figure 7.9A**). Compounds that interact with Aβ with a high proportion of H^D interactions tend to destabilize oligomers while compounds that interact

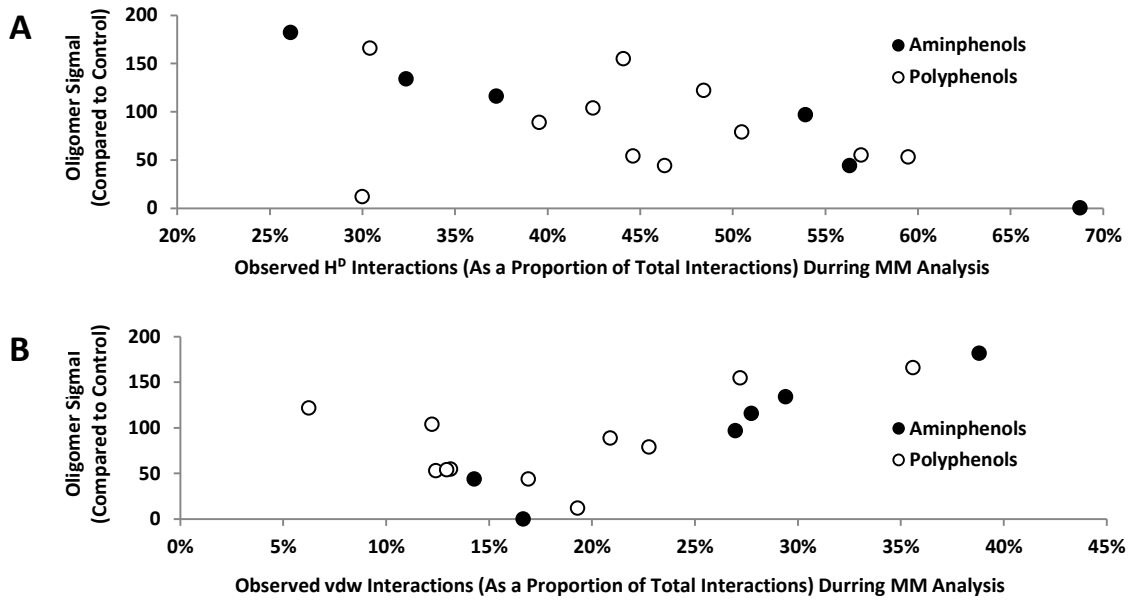

Figure 7.9 Signal due to oligomer formation compared **A**) to the proportion of H^D interactions and **B**) to the proportion of vdw interactions observed during MM analysis for the aminophenols and polyphenols.

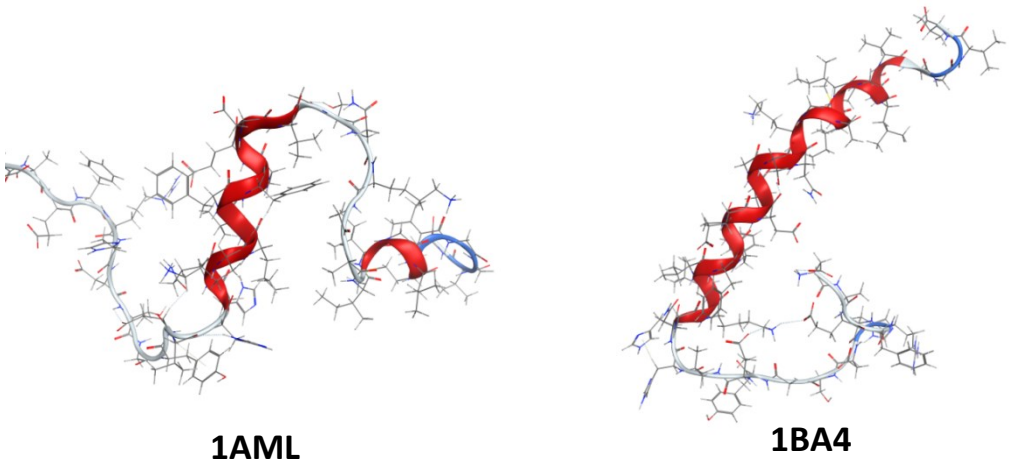

Figure 7.10 A comparison of *m*Aβ receptor models 1AML and 1BA4.

with a lower proportion of H^D interactions promote their formation. The proportion of observed vdw interactions observed also correlated well with the ELISA data. Compounds which interacted with a higher proportion of vdw interactions tended to promote *o*Aβ formation and those who interacted less often via vdw interactions tended to disassemble preformed *o*Aβs (**Figure 7.9B**). These differences in the interaction preferences of the various compounds may lead to preferred stabilization of different structural forms of Aβ. It is worth noting that receptor

models 1BA4 and 1AML were most likely to interact via H^D and vdw interactions, respectively, and may represent structural homologues to the various forms of Aβ differentially stabilized by these compounds. This observation opens up the possibility of a non-covalent MoA which may account for both in increase in *o*Aβs afforded by some antiaggregants and the promotion of *o*Aβ disassembly afforded by others. In this MoA disassembly of *o*Aβs may be the result of preferential stabilization of a form of Aβ that is incompatible with oligomer formation – therby driving the *m*Aβ-*o*Aβ equilibrium towards *m*Aβs; promotion of *o*Aβ formation may be the results of stabilization of a form of Aβ that is preferentially incorporated into off-pathway *o*Aβs. Both of these pathways would result in a decrease in *f*Aβ formation and neither would involve covalent modification of Aβ.

7.2.1.3.4 Agreement with the Nucleation-Dependent Polymerization Model

According the nucleation-dependent model of Aβ polymerization the rate of fibril extension is proportional to the concentration of *m*Aβ present in solution. During the analysis of the kinetic ThT data the maximum rate of *f*Aβ formation, F'_{MAX}, was determined for Aβ in the presence of several analogues of 3HAA including *o*-aminophenol and synthetic analogues thereof. Antiaggregants which were more active inhibitors of *f*Aβ formation also decreased the maximum rate of fibril formation (**Figure 7.11**). This suggests that these compounds do indeed decrease the concentration of *m*Aβ in solution that is able to incorporate into growing *f*Aβs, and is consistent with the nucleation-dependent polymerization model. By analyzing the $t_{F'_{MAX}}$ 4 compounds were shown to increase lag time: *p*-aminophenol and *p*-phenylenediamine, NCE-217, and GS-1049. Similar studies have suggested that this is due to inhibition of Aβ nucleation which delays *f*Aβ formation.[96,182] These compounds were the only one observed to increase lag time and suggest slightly different mechanisms of action.

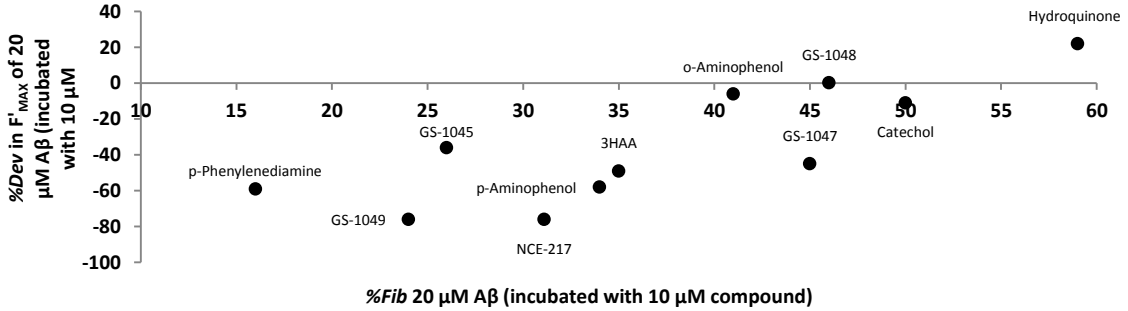

Figure 7.11 %Fib of 20 µM Aβ incubated with 10 µM compound compared to the observed F'_{MAX} at that concentration.

7.3 Future Experimental Work

In the studies conducted in this thesis, a combination of *in vitro* biological assays, NMR binding studies and MM work has provided significant insight into the MoA of two distinct classes of antiaggregant compounds – one aminophenol-based and the other polyphenol-based. The results obtained indicate that inhibition of *in vitro f*Aβ formation is achieved through several MoAs. Compounds which are potent inhibitors of *f*Aβ promotion may do so through distinct mechanisms and as such have various effects on *o*Aβ dissolution and assembly. At the heart of these disparate mechanisms lays a common feature: stabilization of various structural forms of *m*Aβ; however some literature evidence provide a compelling argument for a MoA in which Aβ is covalently modified by benzoquinone-type structures that may be formed due to autoxidation of various antiaggregants. Taken together, the evidence presented here indicates that varying mechanisms of action may underlie the observed antifibrillogenic activity of these compounds. In fact, there is a strong possibility that both mechanisms may be at play but in the absence of further evidence this is simply conjecture. Clearly, the combination of methods applied over the course of this thesis research has provided improved insight into the MoA of these compounds. Further development of these methods may allow for the subtleties of the MoA of Aβ antiaggregants to be fully understood.

Here only two classes of compounds have been investigated, but there are dozens of structurally unique classes of compounds that inhibit *f*Aβ formation.[93] The methods employed in this research should be applied to more classes of antifibrillogenic compounds in an effort to obtain a more complete picture MoA(s) that underlies their observed activity.

7.3.1 The Thioflavin T Fibrillogenesis Assay

The ThT fibrillogenesis assay is ubiquitously employed in published studies of antiaggregants and their development; however in all but a few cases only *%Fib* is analyzed in order to determine the relative IC_{50} values of *f*Aβ formation. The fitting methods applied in this research show that collection of kinetic ThT data may provide much more insight into the kinetics of *f*Aβ formation. Both the delay in *f*Aβ formation and the maximum rate of fibril formation can be determined by analyzing kinetic ThT fibrillogenesis assay data. By comparing the analyses of kinetic ThT data for the polyphenols and other structural classes of antiaggregants to the data collected for the aminophenols, further insight may be gained in the

role of structure in inhibiting Aβ nucleation; accordingly, all future ThT analyses should be collected as kinetic data.

7.3.2 ELISA

The sandwich ELISA protocol applied in this thesis has shown that the various antiaggregants have differing effects on *o*Aβ despite all being potent inhibitors of *f*Aβ formation. Here *o*Aβ detection has been facilitated using the 82E1 antibody. As 82E1 is a sequence specific antibody that detects AA residues 1-16 of Aβ it does not distinguish between off-pathway *o*Aβs and on-pathway *o*Aβs which are postulated to further associate into *f*Aβs. Although the preliminary ELISA work has given significant insight into the MoA of these compounds, future studies should also include epitope specific antibodies such as A11 and OC; in this way on-pathway and off-pathway *o*Aβs may be distinguished. By distinguishing between on-pathway and off-pathway oligomers the supposition that compounds which increase *o*Aβ formation can be confirmed as decreasing *f*Aβ formation through promotion of off-pathway ADDLs.

7.3.3 MM

Because no single structure of *m*Aβ has been implicated as a therapeutic target for the various classes of known antiaggregants a novel method was developed herein whereby analyte antiaggregants were assessed for binding to 9 models of *m*Aβ. The results of these studies indicate that there is an excellent correlation between the observed binding energies of analyte compounds and their antifibrillogenic activity; furthermore, the interaction preferences of these compounds correlates very well the effect of these compounds with regards to *o*Aβ dissolution and formation. It is likely that the methods utilized in this research may be used to predict compound effect on *o*Aβs; to confirm this assertion, these methods should be applied to other structural classes of antiaggregants. In addition, future MM work should include the other positional isomers of *o*-aminophenol as well as catechol and phenylenediamine (and positional isomers thereof).

7.3.4 NMR

The preliminary NMR work conducted in this thesis have shown that both 3HAA and GS-1049 are able to interact with *m*Aβ in solution and complement MM and *in vitro* assay results that suggest these compounds are able to stabilize pathologically inert species of *m*Aβ. Future

work using ^{13}C and ^{15}N labelled Aβ may be used to determine precisely how these compounds interact with *m*Aβ and would allow for specific AA residues involved in binding to be determined; these studies should be expanded to include multiple compounds from structurally diverse classes of antiaggregants to assess differences in Aβ binding. STD-NMR and DOSY were successfully applied to incubations of compounds with various 10-AA segments of Aβ and were able to distinguish differences in binding to various segments of the Aβ sequence. These results may indicate that the observed differences in binding are sequence specific, but these observed differences in binding may be due to specific AA residues incorporated into the peptide sequences; consequently, further studies using scrambled variants of the 10-AA peptides presented herein could be used to determine if the observed interactions are indeed sequence specific or are simply AA specific.

7.3.4 Other Experiments

Given the potential of these compounds to modify Aβ covalently, future studies should also explore this MoA in more detail. Incubations of Aβ with the compounds assessed herein as well as future analogues should be analyzed with ES-MS to determine whether Aβ has been covalently modified via benzoquinone-type structures which may potentially form *in situ*. As several of the compounds are known to be redox-active, the reducing potential of these compounds should be assessed to determine whether any correlation exists between the ability of compounds to form benzoquinone-type intermediates and their respective antiaggregant activity.

7.4 Conclusion

Aβ aggregation is an extremely complex process, the pathways for which have yet to be fully elucidated. The limited understanding of the MoA(s) by which antiaggregants elicit their effect has in large part stifled their development as putative AD therapeutics. 3HAA was shown here to be an excellent platform for the development of a novel class of *o*-aminophenol containing antiaggregants; these antiaggregants have excellent antifibrillogenic activity. By comparing the observed activity of these compounds with known antiaggregants it has been determined that the activity of the aminophenol-based antiaggregants is comparable with the most active compounds presented in the literature. Analogues of even higher activity may potentially be achieved by either incorporating additional hydroxyl or hydrophobic moieties or

moving to a scaffold based on *p*-aminophenol; these analogues should be pursued further and may lead to compounds with nM potency.

The combination of *in vitro* assays, MM work and NMR binding studies presented in this thesis has been used to clarify the MoA of the aminophenol-based antiaggregants as well as a variety of known polyphenol antiaggregants. Although the observed interactions that mediate Aβ binding differ amongst the various compounds it is clear that H^D, π-π and hydrophobic interactions all play a critical role in Aβ binding; subtleties in interaction preference of these compounds likely account for the differences in oligomeric and fibrillogenic activity. The results described indicate that *o*Aβ formation and *f*Aβ formation are inherently linked and have worked towards clarifying how they relate. The methodologies applied here are applicable to a wide range of structurally disparate classes of antiaggregants and if applied more ubiquitously should clarify the MoA(s) underlying Aβ aggregation.

The excellent activity of 3HAA is an important result considering it is a compound endogenous to the brain. The potent antioligomeric and antifibrillogenic activity of 3HAA raises the possibility that AD progression may be related to the absence of endogenous compounds which mediate disease progression. Although 3HAA has been identified here there are most certainly other compounds which may ameliorate disease progression that have yet to be discovered; as such further identification of endogenous compounds which inhibit the pathogenesis of AD may potentially lead to therapeutic interventions which may prevent AD progression.

Importantly, the results described in this thesis have shown a connection between what many have considered to be discrete pathways of aggregation, and furthermore suggest a common mechanism – stabilization of *m*Aβ. To date, antiaggregants that have progressed to clinical trials have done so on the basis of antifibrillogenic activity – and these trials have had disappointing results; some view these failures as evidence against the amyloid hypothesis of AD progression. It may be that candidate selection on the basis of *f*Aβ inhibition alone has led to the disappointing outcomes of clinical testing. Considering that different effects on *o*Aβ formation lead to the same result – the inhibition of *f*Aβ formation – future compounds selected for clinical testing should be rigorously assessed for their effect on *o*Aβ formation. It stands to reason that compounds that inhibit *f*Aβ formation by the different mechanism presented here may have significantly different effects in clinical testing.

Although it is clear that many questions are left to be addressed, such as what are the structures of *m*Aβs which are stabilized, and furthermore can conformational motifs about these putative targets be identified in order to facilitate rational drug development. Despite these questions the work presented here has somewhat clarified the MoA of these Aβ antiaggregants. By clarifying the complex mechanistic picture it is hoped that the insights presented here have provided a framework for further mechanistic studies that will encourage pharmaceutical research programmes to meaningfully assess the utility and therapeutic potential of Aβ antiaggregants.

References

1. Pender, R. World Alzheimer report 2014 dementia and risk reduction. (2014).

2. Selkoe, D. J. & Schenk, D. Alzheimer's disease: molecular understanding predicts amyloid-based therapeutics. *Annu. Rev. Pharmacol. Toxicol.* **43,** 545–584 (2003).

3. Wimo, a., Jonsson, L. & Winblad, B. An estimate of the worldwide prevalence and direct costs of dementia in 2003. *Dement. Geriatr. Cogn. Disord.* **21,** 175–181 (2006).

4. Brookmeyer, R., Johnson, E., Ziegler-Graham, K. & Arrighi, H. M. Forecasting the global burden of Alzheimer's disease. *Alzheimer's Dement.* **3,** 186–191 (2007).

5. Graeber, M. B., Kösel, S., Egensperger, R. Banati, R.B., Müller, U., Bise, K., Hoff, P., Möller, H. J., Fujisawa, K. & Mehraein, P. Rediscovery of the case described by Alois Alzheimer in 1911: historical, histological and molecular genetic analysis. *Neurogenetics* **1,** 73–80 (1997).

6. Katzman, R. The prevalence and malignancy of Alzheimer disease. A major killer. *Alzheimer's Dement.* **4,** 378–380 (2008).

7. Selkoe, D. J. Alzheimer's disease: genes, proteins, and therapy. *Physiol. Rev.* **81,** 741–767 (2001).

8. Masters, C. L., Simms, G., Weinman, N. A., Multhaup, G., McDonald, B. L. & Beyreuther, K. Amyloid plaque core protein in Alzheimer disease and Down syndrome. *Proc. Natl. Acad. Sci. U. S. A.* **82,** 4245–4249 (1985).

9. Wong, C. W., Quaranta, V. & Glenner, G. G. Neuritic plaques and cerebrovascular amyloid in Alzheimer disease are antigenically related. *Proc. Natl. Acad. Sci. U. S. A.* **82,** 8729–8732 (1985).

10. Kang, J., Lemaire, H. G., Unterbeck, A., Salbaum, J. M., Masters, C. L., Grzeschik, K. H., Multhaup, G., Beyreuther, K. & Müller-Hill, B. The precursor of Alzheimer's disease amyloid A4 protein resembles a cell-surface receptor. *Nature* **325,** 733–736 (1987).

11. Coria, F., Castaño, E. M. & Frangione, B. Brain amyloid in normal aging and cerebral amyloid angiopathy is antigenically related to Alzheimer's disease β-protein. *Am. J. Pathol.* **129,** 422–428 (1987).

12. Rocchi, A., Pellegrini, S., Siciliano, G. & Murri, L. Causative and susceptibility genes for Alzheimer's disease: A review. *Brain Res. Bull.* **61,** 1–24 (2003).

13. Martin, J. B. Molecular basis of the neurodegenerative disorders. *N. Engl. J. Med.* **25,** 1970–1980 (1999).

14. Mullan, M., Crawford, F., Axelman, K., Houlden, H. Lilius, L., Winblad, B. & Lannfelt, L. A pathogenic mutation for probable Alzheimer's disease in the APP gene at the N-terminus of β-amyloid. *Nat. Genet.* **1,** 345–347 (1992).

15. Goate, A., Chartier-Harlin, M. C., Mullan, M., Brown, J., Crawford, F., Fidani, L., Giuffra, L., Haynes, A., Irving, N., James, L., Manti, R., Newton, P., Rooke, K., Roques, P., Talbot, C., Pericak-Vance, M., Roses, A., Williamson, R., Rossor, M., Owen, M. & Hardy, J . Segregation of a missense mutation in the amyloid precursor protein. *Nature* **349,** 704–706 (1991).

16. Gómez-Isla, T., Price, J. L., McKeel Jr., D. W., Morris, J. C., Growdon, J. H. & Hyman, B. T. Profound loss of layer II entorhinal cortex neurons occurs in very mild Alzheimer's disease. *J. Neurosci.* **16,** 4491–4500 (1996).

17. Walsh, D. M. & Selkoe, D. J. Aβ oligomers - a decade of discovery. *J. Neurochem.* **101,** 1172–1184 (2007).

18. Hartley, D. M., Walsh, D. M., Ye, C. P., Vasquez, S., Vassilev, P. M., Teplow, D. B. & Selioe, D. J. Protofibrillar intermediates of amyloid β-protein induce acute electrophysiological changes and progressive neurotoxicity in cortical neurons. *J. Neurosci.* **19,** 8876–8884 (1999).

19. Lambert, M. P., Barlow, A. K., Chiromy, B. A., Edwards, C., Freed, R. Liosatos, M. Morgan, T. E., Rozovosky, I., Trommer, B., Viola, K. L., Wals, P., Zhang, C., Finch, C. E., Krafft, G. A. & Klien, W. L. Diffusible, nonfibrillar ligands derived from $A\beta_{1\text{-}42}$ are potent central nervous system neurotoxins. *Proc. Natl. Acad. Sci. U. S. A.* **95,** 6448–6453 (1998).

20. Townsend, M., Shankar, G. M., Mehta, T., Walsh, D. M. & Selkoe, D. J. Effects of secreted oligomers of amyloid beta-protein on hippocampal synaptic plasticity: a potent role for trimers. *J. Physiol.* **572,** 477–492 (2006).

21. Walsh, D. M., Klyubin, I., Shankart, G. M., Townsend, M., Fadeeva, J. V., Betts, V., Podlisny, M. B., Cleary, J. P., Ashe, K. M., Rowan, M. J. & Selkoe D. J. The role of cell-derived oligomers of Aβ in Alzheimer's disease and avenues for therapeutic intervention. *Biochem. Soc. Trans.* **33,** 1087–1090 (2005).

22. Enya, M. Morishima-Kawashima, M., Yoshimura, M., Shinkai, Y., Kusui, K. Khan, K., Games, D., Schenk, D., Sugihara, S., Yamaguchi, H. & Ihara, Y. Appearance of sodium dodecyl sulfate-stable amyloid beta-protein (Aβ) dimer in the cortex during aging. *Am. J. Pathol.* **154,** 271–279 (1999).

23. Funato, H., Enya, M., Yoshimura, M., Morishima-Kawashima, M. & Ihara, Y. Presence of sodium dodecyl sulfate-stable amyloid beta-protein dimers in the hippocampus CA1 not exhibiting neurofibrillary tangle formation. *Am. J. Pathol.* **155,** 23–28 (1999).

24. Rockwood, K. Size of the treatment effect on cognition of cholinesterase inhibition in Alzheimer's disease. *J. Neurol. Neurosurg. Psychiatry* **75,** 677–685 (2004).

25. Panza, F., Solfrizzi, V., Frisardi, V., Capurso, C., D'Introno, A., Colacicco, A. M., Vendemiale, G., Capurso, A. & Imbimbo, B. P. Disease-modifying approach to the treatment of alzheimer's disease. *Drugs Aging* **26,** 537–555 (2009).

26. Melnikova, I. Therapies for Alzheimer's disease. *Nat. Rev. Drug Discov.* **6,** 341–342 (2007).

27. Rammes, G., Rupprecht, R., Ferrari, U. & Zieglga, W. The N-methyl-d-aspartate receptor channel blockers memantine, receptor currents in cultured HEK-293 and N1E-115 cell systems in a non-competitive manner. *Neurosci. Lett.* **306,** 304–307 (2001).

28. Luo, Y. Bolon, B., Kahn, S., Bennett, B. D., Babu-Kahn, S., Denis, P., Fan, W., Kha, H., Zhang, J., Gong, Y., Martin, L., Louis, J. C., Yan, q., Richards, W. G., Citron, M. & Vassar, R. Mice deficient in BACE1, the Alzheimer's β-secretase, have normal phenotype and abolished β-amyloid generation. *Nat. Neurosci.* **4,** 231–232 (2001).

29. Willem, M., Garratt, A. N., Novak, B., Citron, M., Kaufmann, S., Rittger, A., DeStrooper, B., Saftig, P., Birchmeir, C. & Haass, C. Control of peripheral nerve myelination by the β-secretase BACE1. *Science* **314,** 664–666 (2006).

30. Howlett, D. R., Simmons, D. L., Dingwall, C. & Christie, G. In search of an enzyme: the β-secretase of Alzheimer's disease is an aspartic proteinase. *Trends Neurosci.* **23,** 565–570 (2000).

31. Brik, A. & Wong, C.-H. HIV-1 protease: mechanism and drug discovery. *Org. Biomol. Chem.* **1,** 5–14 (2003).

32. Suguna, K., Padlan, E. a, Smith, C. W., Carlson, W. D. & Davies, D. R. Binding of a reduced peptide inhibitor to the aspartic proteinase from Rhizopus chinensis: implications for a mechanism of action. *Proc. Natl. Acad. Sci. U. S. A.* **84,** 7009–7013 (1987).

33. Hong, L., Koelsch, G., Lin, X., Wu, S., Terzyan, S., Ghosh, A. K., Zhang, X. C. & Tang, J. Structure of the protease domain of memapsin 2 (β-secretase) complexed with inhibitor. *Science* **290,** 150–153 (2000).

34. Ghosh, A., Gemma, S. & Tang, J. β-Secretase as a therapeutic target for Alzheimer ' s disease. *Neurotherapeutics.* **5,** 399–408 (2008).

35. Jeon, S. Y., Bae, K., Seong, Y. H. & Song, K. S. Green tea catechins as a BACE1 (β-secretase) inhibitor. *Bioorganic Med. Chem. Lett.* **13,** 3905–3908 (2003).

36. Ghosh, A. K., Kumaragurbaran, N., Hong, L., Kulkarni, S., Xu, x., Miller, H. B.,Reddy, D. S.,Weerasna, V., Turner, R., Chang, W., Koelsch G. & Tang J. Potent memapsin 2 (β-secretase) inhibitors: design, synthesis, protein-ligand X-ray structure, and in vivo evaluation. *Bioorganic Med. Chem. Lett.* **18,** 1031–1036 (2008).

37. Wolfe, M. S. The γ-secretase complex : membrane-dmbedded proteolytic ensemble. *Biochemistry* **45,** 7931-7939 (2006).

38. Sherrington, R., Rogaev, E. I., Liang, Y., Rogaeva, E. A., Levesque, G., Ikeda, M., Chi, H., Lin, C., Li, G., Tsuda, T., Mar, L., Foncin, J.-F., Bruni, A. C., Montesi, M. P., Sorbi, S., Rainero, I., Pinessi, L., Nee, L., Chumakov, I., Pollen, D., Brookes, A., Sanseau, P., Polinsky, R. J., Wasco, W., Da Silva, H. A. R., Haines, J. L., Pericak-Vance, M. A., Tanzi, R. E., Roses, A. D., Frasher, P. E., Rommens, J. M. & St George-Hyslop, P. H. Cloning of a gene bearing missense mutations in early-onset familial Alzheimer's disease. *Nature* **375,** 754–760 (1995).

39. Tanzi, R. E. & Bertram, L. Twenty years of the Alzheimer's disease amyloid hypothesis: A genetic perspective. *Cell* **120,** 545–555 (2005).

40. Suzuki, N., Cheung, T. T., Cai, X.-D., Odaka, A., Otvos Jr, L., Eckman, C., Golde, T. E. & Younkin, S. G. An increased percentage of long amyloid beta protein secreted by familial amyloid-β protein precursor (beta APP717) mutants. *Science* **264,** 1336–1340 (1994).

41. Wong, P. C. *et al.* Presenilin 1 is required for Notch1 and DII1 expression in the paraxial mesoderm. *Nature* **387,** 288–292 (1997).

42. Herreman, A., Serneels, L., Annaert, W., Collen, D., Schoonjans, L. & De Strooper B. Total inactivation of gamma-secretase activity in presenilin-deficient embryonic stem cells. *Nat. Cell Biol.* **2,** 461–462 (2000).

43. Dovey, H. F., John, V. Anderson, J. P., Chen L. Z., *et al.* Functional gamma-secretase inhibitors reduce beta-amyloid peptide levels in brain. *J. Neurochem.* **76,** 173–181 (2001).

44. Basi, G. S., Hemphil, S., Brigham, E. F., Liao, A., *et al.* Amyloid precursor protein selective γ-secretase inhibitors for treatment of Alzheimer's disease. *Alzheimers. Res. Ther.* **2,** 36 (2010).

45. Martone, R. L., Zhou, H., Atchinson, K., Comery, T., *et al.* Begacestat (GSI-953): A novel, selective thiophene sulfonamide inhibitor of amyloid precursor protein γ-secretase for the treatment of alzheimer's disease. *Pharmacology* **331,** 598–608 (2009).

46. Henley, D. B., May, P. C., Dean, R. a & Siemers, E. R. Development of semagacestat (LY450139), a functional γ-secretase inhibitor, for the treatment of Alzheimer's disease. *Expert Opin. Pharmacother.* **10,** 1657–1664 (2009).

47. Imbimbo, B. P. Alzheimer's disease: γ-secretase inhibitors. *Drug Discov. Today Ther. Strateg.* **5,** 169–175 (2008).

48. Gounder, M. M. & Schwartz, G. K. Moving Forward, One Step at a Time. *J. Clin. Oncol.* **30,** 2291–2293 (2012).

49. Doody, R. S., Raman, R., Farlow, M., Iwatsubo, T., Vellas, B., Joffe, S., Kieburtz, K., He, F., Sun, X., Thomas, R. G., Aisen, P. S., Siemers, E., Sethuraman, G. & Mohs, R. A phase 3 trial of semagacestat for treatment of Alzheimer's disease. *N. Engl. J. Med.* **369,** 341–50 (2013).

50. Wolfe, M. S. Inhibition and modulation of γ-secretase for Alzheimer's disease. *Neurotherapeutics* **5,** 391–398 (2008).

51. Yaari, R., Kumar, S. & Tariot, P. N. Non-cholinergic drug development for Alzheimer's. *Expert Opin. Drug Discov.* **3,** 745–760 (2008).

52. Weggen, S., Eriksen, J. L., Das, P., Sagi, S. A., Wang, R., Pietrzik, C. U., Kang, D. E., Marquez-Sterling, N., Golde, T. E. & Koo, E. H. A subset of NSAIDs lower amyloidogenic Aβ42 independently of cyclooxygenase activity. *Nature* **414,** 212–216 (2001).

53. Lashuel, H. A., Hartley, D. M., Balakhaneh, D., Aggarwal, A., Teichberg S. & Callaway, D. J. E. New class of inhibitors of amyloid-beta fibril formation. Implications for the mechanism of pathogenesis in Alzheimer's disease. *J. Biol. Chem.* **277,** 42881–42890 (2002).

54. Eriksen, J. L., Sagi, S. A., Smith, T. E., Weggen, S., Das, P., McLendon, D. C., Ozols, V. V., Jessing, K. W., Koo, E. H. & Golde, T. E.. NSAIDs and enantiomers of flurbiprofen target γ-secretase and lower Aβ42 in vivo. *J. Clin. Invest.* **112,** 440–449 (2003).

55. Imbimbo, B. P., Hutter-Paier, B., Facchinetti, F., Cenacchi, V., Lanzilotta, A., Pizzi, M. & Windisch M. CHF5074, a novel γ-secretase modulator, attenuates brain β-amyloid pathology and learning deficit in a mouse model of Alzheimer's disease. *Br. J. Pharmacol.* **156,** 982–993 (2009).

56. Rockwood, K. kirkland, S., Hogan, D. B., MacKnight, C., Merry, h., Verreault, R., Wolfson, C. & McDowell, I. Use of lipid-lowering agents, indication bias, and the risk of dementia in community-dwelling elderly people. *Arch. Neurol.* **59,** 223–227 (2002).

57. Postina, R., Schroeder, A., Dewachter, E., Bohl, J., Schmitt, U., Kojro, E., Prinzen, C., Endres, K., Hiemke, C., Blessing, M., Flamez, P., Dequenne, A., Godauz, E., van Leuven, F. & Fahrenholz, F. A disintegrin-metalloproteinase prevents amyloid plaque formation and hippocampal defects in an Alzheimer disease mouse model. *J. Clin. Invest.* **113,** 1456–1464 (2004).

58. Kojro, E., Gimpl, G., Lammich, S., Marz, W. & Fahrenholz, F. Low cholesterol stimulates the nonamyloidogenic pathway by its effect on the α-secretase ADAM 10. *Proc. Natl. Acad. Sci. U. S. A.* **98,** 5815–5820 (2001).

59. Parvathy, S. Ehrilich, M., Pedrini, S., Refolo, L., Buxbaum, J. D., Bogush, A., Petanceska, S. & Grandy, S. Atorvastatin-induced activation of Alzheimer's β-secretase is resistant to standard inhibitors of protein phosphorylation-regulated ectodomain shedding. *J. Neurochem.* **90,** 1005–1010 (2004).

60. Pedrini, S., Carter, T. L., Prendergast, G., Petancoska, S., Ehrlich, M. E. & Gandy, S. Modulation of statin-activated shedding of Alzheimer APP ectodomain by ROCK. *PLoS Med.* **2,** 0069–0078 (2005).

61. Famer, D. & Crisby, M. Rosuvastatin reduces caspase-3 activity and up-regulates α-secretase in human neuroblastoma SH-SY5Y cells exposed to Aβ. *Neurosci. Lett.* **371,** 209–214 (2004).

62. Corder, E. H., Saunders, A. M., Strittmatter, W. J., Schmechel, D. E., Gaskell, P.C., Small, G. W., Roses, A. D., Haines, J. L. & Pericak-Vance, M. A. Gene dose of apolipoprotein E type 4 allele and the risk of Alzheimer's disease in late onset families. *Science.* **261,** 921–923 (1993).

63. Corder, E. H., Saunders, A. M., Risch, N. J., Strittmatter, W. J., Schmechel, D. E., Gaskell Jr., P. C., Rimmler, J. B., Locke, P. A., Conneally, P. M., Schmader, K. E., Small, G. W., Roses, A. D., Haines, J. L. & Pericak-Vance, M. A. Protective effect of apolipoprotein E type 2 allele for late onset Alzheimer's disease. *Nat. Genet.* **7,** 180–184 (1994).

64. Burns, M. P., Igbavboa, U., Wang, L., Gibson-Wood, L. & Duff, K. Cholesterol distribution, not total levels, correlate with altered amyloid precursor protein processing in statin-treated mice. *Neuromolecular Med.* **8,** 175–190 (2006).

65. Strittmatter, W. J. & Roses, a D. Apolipoprotein E and Alzheimer disease. *Proc. Natl. Acad. Sci. U. S. A.* **92,** 4725–4727 (1995).

66. Refolo, L. M., Pappolla, M. A., Malester, B., LaFrancois, J., Bryant-Thomas, T., Wang, R., Tint, G. S., Sambamurti, K. & Duff, K. Hypercholesterolemia accelerates the Alzheimer's amyloid pathology in a transgenic mouse model. *Neurobiol. Dis.* **7,** 321–331 (2000).

67. Vega, G. L., Weiner, M. F., Lipton, A. M., von Bergmann, K., Lütjohann, D., Moore, C. & Sverlik, D. Reduction in levels of 24S-hydroxycholesterol by statin treatment in patients with Alzheimer disease. *Arch. Neurol.* **60,** 510–515 (2003).

68. Wahrle, S. E., Parsadanian, M., Hartman, R. E., Bales, K. R., Paul, S. M. & Holtzmann, D. M. Deletion of Abca1 increases Aβ deposition in the PDAPP transgenic mouse model of Alzheimer disease. *J. Biol. Chem.* **280,** 43236–43242 (2005).

69. Simons, M., Keller, P., De Strooper, B., Beyreuther, K., Dotti, C. G. & Simons, K. Cholesterol depletion inhibits the generation of β-amyloid in hippocampal neurons. *Proc. Natl. Acad. Sci. U. S. A.* **95,** 6460–6464 (1998).

70. Fassbender, K., Simons, M., Bergmann, C., Stroick, M., Lütjohann, D., Keller, P., Runz, H., Kühl, Bertsch, T. B., von Bergmann, K., Hennerici, M., Beyreuther, K. & Hartmann, T. Simvastatin strongly reduces levels of Alzheimer's disease β-amyloid peptides Aβ42 and Aβ40 in vitro and in vivo. *Proc. Natl. Acad. Sci. U. S. A.* **98,** 5856–5861 (2001).

71. Locatelli, S., Lütjohann, D., Schmidr, H.-J., Otto, C., Beisiegel, U. & von Bergmann, K. Reduction of plasma 24S-hydroxycholesterol (cerebrosterol) levels using high-dosage simvastatin in patients with hypercholesterolemia: evidence that simvastatin affects cholesterol metabolism in the human brain. *Arch. Neurol.* **59,** 213–216 (2002).

72. Zandi, P. P., Sparks, L., Khachaturian, A. S., Tschanz, J., Norton, M., Steinberg, M., Welsh-Bohmer, K. A. & Breitner, C. S. Do statins reduce risk of incident dementia and Alzheimer disease? The Cache County Study. *Arch. Gen. Psychiatry* **62,** 217–224 (2005).

73. Li, G., Higdon, R., Kukull, W. A., Peskind, E., Van Valen Moore, K., Tsuang, D., van Belle, G., McCormick, W., Bowen, J. D., Teri, L., Schellenberg, G. D. & Larson, E. B. Statin therapy and risk of dementia in the elderly: a community-based prospective cohort study. *Neurology* **63,** 1624–1628 (2004).

74. Schenk, D., Barbour, R., Dunn, W., Gordon, G., Grajeda, G., Hu, K., Huang, J., Johnson-Wood, K., Khan, K., Kholodenko, D., Lee, M., Liao, Z., Lieberburg, I., Motter, R., Mutter, L., Soriano, F., Shopp, G., Vasquez, N., Vandevert, C., Walker, S., Wogulis, M., Yednock, T., Games, D. & Seubert, P. Immunization with amyloid-beta attenuates Alzheimer-disease-like pathology in the PDAPP mouse. *Nature* **400,** 173–177 (1999).

75. Duff, K. Curing amyloidosis: Will it work in humans? *Trends Neurosci.* **22,** 485–486 (1999).

76. Janus, C., Pearson, J., McLaurin, J., Mathews, P. M., Jiang, Y., Schmidt, S. D., Chishti, M. A., Horne, P., Heslin, D., French, J., Mount, H. T. J., Nixon, R. A., Mercken, M., Bergeron, C., Fraser, P. E., St George-Hyslop, P. & Westaway, D. Aβ peptide immunization reduces behavioural impairment and plaques in a model of Alzheimer's disease. *Nature* **408,** 979–982 (2000).

77. Weiner, H. L., Lemere, C. A., Maron, R., Spooner, E. T., Grenfell, T. J., Mori, C., Issazadeh, S., Hancock, W. W. & Selkoe, D. J. Nasal administration of amyloid-β peptide decreases cerebral amyloid burden in a mouse model of Alzheimer's disease. *Ann. Neurol.* **48,** 567–579 (2000).

78. Morgan, D., Diamond, D. M., Gottschall, P. E., Ugen, K. E., Dickey, C., Hardy, J., Duff, K., Jantzen, P., DiCarlo, G., Wilcock, D., Connor, K., Hatcher, J., Hope, C., Gordon, M. & Arendash, G. W. Aβ peptide vaccination prevents memory loss in an animal model of Alzheimer's disease. *Nature* **408,** 982–985 (2000).

79. Poduslo, J. F., Curran, G. L., Kumar, A., Frangione, B. & Soto, C. β-Sheet Breaker Peptide Inhibitor of Alzheimer's Amyloidogenesis with Increased Blood – Brain Barrier Permeability and Resistance to Proteolytic Degradation in Plasma. *J. Neurbiology* (1999).

80. Schenk, D. B., Seubert, P. & Lieberburg, I. β-peptide immunization. *Neurol. Rev.* **57,** 934–936 (2000).

81. Birmingham, K. & Frantz, S. Promising drug is victim of bad business. *Nat. Med.* **8,** 199–200 (2002).

82. Winblad, B., Andreasen, N., Minthon, L., Floesser, A., Imbert, G., Dumortier, T., Maguire, R. P., Blennow, K., LuNMDArk, J., Staufenbiel, M., Orgogozo, J.-M. & Graf, A. Safety, tolerability, and antibody response of active Aβ immunotherapy with CAD106 in patients with Alzheimer's disease: Randomised, double-blind, placebo-controlled, first-in-human study. *Lancet Neurol.* **11,** 597–604 (2012).

83. Woodhouse, A., Dickson, T. C. & Vickers, J. C. Vaccination strategies for Alzheimer's disease: A new hope? *Drugs Aging* **24,** 107–119 (2007).

84. Doody, R. S., Thomas, R. G., Farlow, M., Iwatsubo, T., Vellas, B., Joffe, S., Kieburtz, K., Raman, R., Sun, X., Aisen, P. S., Siemers, E., Liu-Seifert, H. & Mohs, R. Phase 3 trials of solanezumab for mild-to-moderate Alzheimer's disease. *N. Engl. J. Med.* **370,** 311–21 (2014).

85. Salloway, S., Sperling, R., Fox, N. C., Blennow, K., Klunk, W., Raskind, M., Sabbagh, M., Honig, L. S., Porsteinsson, A. P., Ferris, S., Reichert, M., Ketter, N., Nejadnik, B., Guenzler, V., Miloslavsky, M., Wang, D., Lu, Y., Lull, J., Tudor, L. C., Liu, E., gruNMDAn, M., Yuen, E., Black, R. & Brashear, H. R. Two phase 3 trials of bapineuzumab in mild-to-moderate Alzheimer's disease. *N. Engl. J. Med.* **370,** 322–33 (2014).

86. Bunnage, M. E. Getting pharmaceutical R&D back on target. *Nat. Chem. Biol.* **7,** 335–339 (2011).

87. Soto, C., Castano, E. M., Frangione, B. & Inestrosa, N. C. The α-helical to β-strand transition in the amino-terminal fragment of the amyloid β-peptide modulates amyloid formation. *J. Biol. Chem.* **270,** 3063-3067 (1995).

88. Lambert, M. P., Viola, K. L., Chromy, B. A., Chang, L. Morgan, T. E., Yu, J., Venton, D. L., Krafft, G. A., Finch, C. E. & Klein, W. L. Vaccination with soluble Aβ oligomers generates toxicity-neutralizing antibodies. *J. Neurochem.* **79,** 595–605 (2001).

89. Stroud, J. C., Liu, C., Teng, P. K. & Eisenberg, D. Toxic fibrillar oligomers of amyloid-β have cross-β structure. *Proc. Natl. Acad. Sci.* **109,** 7717–7722 (2012).

90. LeVine, H. Small molecule inhibitors of Aβ assembly. *Amyloid* **14,** 185–197 (2007).

91. Wetzel, R. Kinetics and thermodynamics of amyloid fibril assembly. *Acc. Chem. Res.* **39,** 671–679 (2006).

92. Ahmed, M., Davis, J., Aucoin, D., Sato, T., Ahuja, S., Aimoto, S., Elliott, J. I., van Nostrand, W. E. & Smith, S. O. Structural conversion of neurotoxic amyloid-β(1-42) oligomers to fibrils. *Nat. Struct. Mol. Biol.* **17,** 561–567 (2010).

93. Torok, B., Bag, S., Sarkar, M., Dasgupta, S. & Torok, M. Structural features of small molecule amyloid-β self-assembly inhibitors. *Curr. Bioact. Compd.* **9,** 37–63 (2013).

94. Tjernberg, L. O., Näslund, J., Lindqvist, F., Johansson, J., Karlström, A. R., Thyberg, J., Terenius, L. & Nordstedt, C. Arrest of β-amyloid fibril formation by a pentapeptide ligand. *J. Biol. Chem.* **271,** 8545–8548 (1996).

95. Hetényi, C., Szabó, Z., Klement, É., Datki, Z., Körtvélyesi, T., Zarándi, M. & Penke, B. Pentapeptide amides interfere with the aggregation of β-amyloid peptide of Alzheimer's disease. *Biochem. Biophys. Res. Commun.* **292,** 931–6 (2002).

96. Findeis, M. A., Musso, G. M., Arico-Muendel, C. C., Benjamin, H. W., Hundal, A. M., Lee, J.-J., Chin, J., Kelley, M., Wakefield, J., Hayward, N. J. & Molineaux, S. M. Modified-peptide inhibitors of amyloid β-peptide polymerization. *Biochemistry* **38,** 6791–6800 (1999).

97. Ghanta, J., Shen, C. L., Kiessling, L. L. & Murphy, R. M. A strategy for designing inhibitors of β-amyloid toxicity. *J. Biol. Chem.* **271,** 29525–29528 (1996).

98. Soto, C., Sigurdsson, E. M., Morelli, L., Kumar, R. A., Castaño, E. M. & Frangione, B. β-sheet breaker peptides inhibit fibrillogenesis in a rat brain model of amyloidosis: Implications for Alzheimer's therapy. *Nat. Med.* **4,** 822-826 (1998).

99. Permanne, B., Adessi, C., Saborio, G. P., Fraga, S., Frossard, M.-J., van Dorpe, J., Dewachter, I., Banks, W. A., van Leuven, F. & Soto, C. Reduction of amyloid load and cerebral damage in a transgenic mouse model of Alzheimer's disease by treatment with a β-sheet breaker peptide 1. *FASEB J.* **16,** 860–862 (2002).

100. Gordon, D. J. & Meredith, S. C. Probing the Role of Backbone Hydrogen Bonding in β-Amyloid Fibrils with Inhibitor Peptides Containing Ester Bonds at Alternate Positions. *Biochemistry* **42,** 475–485 (2003).

101. Gordon, D. J., Tappe, R. & Meredith, S. C. Design and characterization of a membrane permeable N -methyl amino acid-containing peptide that inhibits Aβ1–40 fibrillogenesis. *J. Pept. Res.* **60,** 37–55 (2002).

102. Hughes, E., Burke, R. M. & Doig, a J. Inhibition of toxicity in the β-amyloid peptide fragment Aβ25-35 using N-methylated derivatives: a general strategy to prevent amyloid formation. *J. Biol. Chem.* **275,** 25109–15 (2000).

103. Kokkoni, N., Stott, K., Amijee, H., Mason, J. M. & Doig, A. J. N-methylated peptide inhibitors of β-amyloid aggregation and toxicity. Optimization of the inhibitor structure. *Biochemistry* **45,** 9906–9918 (2006).

104. Tjernberg, L. O., Lilliehöök, C., Callaway, D. J. E., Näslund, J., Hahne, S., Thyberg, J., Terenius, L. & Nordstedt, C. Controlling amyloid beta-peptide fibril formation with protease-stable ligands. *J. Biol. Chem.* **272,** 12601–12605 (1997).

105. Ono, K., Yoshiike, U., Takashima, A., Hasgawa, K., Naiki, H. & Yamada, M. Potent anti-amyloidogenic and fibril-destabilizing effects of polyphenols in vitro: implications for the prevention and therapeutics of Alzheimer's disease. *J. Neurochem.* **87,** 172–181 (2003).

106. Ono, K. & Yamada, M. Antioxidant compounds have potent anti-fibrillogenic and fibril-destabilizing effects for α-synuclein fibrils in vitro. *J. Neurochem.* **97,** 105–15 (2006).

107. Levine, H., Lampe, L., Abdelmoti, L. & Augelli-szafran, C. E. Dihydroxybenzoic acid isomers differentially dissociate soluble biotinyl-Aβ(1-42) oligomers. *Biochemistry.* **51,** 307-315 (2012).

108. Ono, K., Hasegawa, K., Naiki, H. & Yamada, M. Anti-amyloidogenic activity of tannic acid and its activity to destabilize Alzheimer's β-amyloid fibrils in vitro. *Biochim. Biophys. Acta* **1690,** 193–202 (2004).

109. Ono, K., Hasegawa, K., Naiki, H. & Yamada, M. Curcumin has potent anti-amyloidogenic effects for alzheimer's β-amyloid fibrils in vitro. *J. Neurscience Res.* **75,** 742–750 (2004).

110. Ono, K., hasegawa, K., Yoshiike, Y., Takashima, A., Yamada, M. & Naiki, H. Nordihydroguaiaretic acid potently breaks down pre-formed Alzheimer's β-amyloid fibrils in vitro. *J. Neurochem.* **81,** 434–440 (2002).

111. Ono, K., Hirohata, M. & Yamada, M. Ferulic acid destabilizes preformed β-amyloid fibrils in vitro. *Biochem. Biophys. Res. Commun.* **336,** 444–9 (2005).

112. Marambaud, P., Zhao, H. & Davies, P. Resveratrol promotes clearance of Alzheimer's disease amyloid-β peptides. *J. Biol. Chem.* **280,** 37377–37382 (2005).

113. Pappolla, M., Bozner, P., Soto, C., Shao, H., Robakis, N. K., Zagorski, M., Frangione, B. & Ghiso, J. Inhibition of Alzheimer β-fibrillogenesis by melatonin. *J. Biol. Chem.* **273,** 7185–7189 (1998).

114. Moore, S. A., Huckerby, T. N., Gibson, G. L., Fullwood, N. J., Surnbull, S., Tabner, B. J., El-Agnaf, O. A. M. & Allsop, D. Both the D-(+)- and L-(-)-enantiomers of nicotine Inhibit Aβ aggregation and cytotoxicity. *Biochemistry* **43,** 819–826 (2004).

115. Zeng, H., Zhang, Y., Peng, L.-J., Shao, H., Menon, N. K., Yang, J., Salomon, A. R., Freidland, R. P. & Zagorskim, M. G. Nicotine and amyloid formation. *Biol. Psychiatry* **49,** 248–257 (2001).

116. Ono, K., Yoshiikem Y., Takashima, A., Hasegawa, K., Naiki, H. & Yamada, M. Vitamin A exhibits potent antiamyloidogenic and fibril-destabilizing effects in vitro. *Exp. Neurol.* **189,** 380–92 (2004).

117. Ono, K. & Yamada, M. Vitamin A potently destabilizes preformed α-synuclein fibrils in vitro: implications for Lewy body diseases. *Neurobiol. Dis.* **25,** 446–54 (2007).

118. Ono, K., Hirohata, M. & Yamada, M. α-lipoic acid exhibits anti-amyloidogenicity for β-amyloid fibrils in vitro. *Biochem. Biophys. Res. Commun.* **341,** 1046–52 (2006).

119. Forloni, G., Colombo, L., Girola, L., Tagliavini, F. & Salmona, M. Anti-amyloidogenic activity of tetracyclines: studies in vitro. *FEBS Lett.* **487,** 404–407 (2001).

120. Howlett, D. R., George, A. R., Owen, D. E., Ward, R. V & Markwell, R. E. Common structural features determine the effectiveness of carvedilol, daunomycin and rolitetracycline as inhibitors of β-amyloid fibril formation. *Biochem. J.* **343,** 419–423 (1999).

121. Pollack, S. J., Sadler, I. I. J., Hawtin, S. R., Tailor, V. J. & Shearman, M. S. Sulfated glycosaminoglycans and dyes attenuate the nerotoxiceffects of β-amyloid in rat PC12 cells. *Neurosci. Lett.* **184,** 113–116 (1995).

122. Naiki, H., Hasegawa, K., Yamaguchi, I., Nakamura, H. & Gejyo, F. Apolipoprotein E and antioxidants Have different mechanisms of inhibiting Alzheimer's β-amyloid fibril formation in vitro. *Biochemistry* **37,** 17882–17889 (1998).

123. Naiki, H., Gejyo, F. & Nakakuki, K. Concentration-dependent inhibitory effects of apolipoprotein E on Alzheimer' s β-amyloid fibril formation in vitro. *Biochemistry* **36,** 6243–6250 (1997).

124. Monji, A., Tashiro, K., Yoshida, I., Hayashi, Y. & Tashiro, N. Laminin inhibits $A\beta_{40}$ fibril formation promoted by apolipoprotein E4 in vitro. *Brain Res.* **796,** 171–175 (1998).

125. Monji, A., Tashiro, K., Yoshida, I. & Kaname, H. Laminin inhibits both Aβ40 and Aβ42 fibril formation but does not affect Aβ40 or Aβ42-induced cytotoxicity in PC12 cells. *Neurosci. Lett.* **266,** 85–88 (1999).

126. Hirohata, M., Ono, K., Naiki, H. & Yamada, M. Non-steroidal anti-inflammatory drugs have anti-amyloidogenic effects for Alzheimer's β-amyloid fibrils in vitro. *Neuropharmacology* **49,** 1088–99 (2005).

127. Hirohata, M., Ono, K., Morinaga, A. & Yamada, M. Non-steroidal anti-inflammatory drugs have potent anti-fibrillogenic and fibril-destabilizing effects for α-synuclein fibrils in vitro. *Neuropharmacology* **54,** 620–7 (2008).

128. Thomas, T., Nadackal, T. G. & Thomas, K. Aspirin and non-steroidal anti-inflammatory drugs inhibit amyloid-β aggregation. *Neuroreport* **12,** 3263–3267 (2001).

129. Nakagami, Y., Nishimura, S., Murasugi, T., Kaneko, I., Meguro, M., Maurumoto, S., Kogen, H., Koyama, K. & Oda, T. A novel β-sheet breaker, RS-0406, reverses amyloid β-induced cytotoxicity and impairment of long-term potentiation in vitro. *Br. J. Pharmacol.* **137,** 676-682 (2002).

130. Klunk, W. E., Debnath, M. L., Koros, A. M. C. & Pettegrew, J. W. Chrysamine-G, a lipophilic analogue of congo red, inhibits Aβ-induced toxicity in PC12 cells. *Life Sci.* **63,** 1807–1814 (1998).

131. Pollack, S. J., Sadler, I. I. J., Hawtin, S. R., Tailor, V. J. & Shearman, M. S. Sulfonated dyes attenuate the toxic effects of β-amyloid in a structure-specific fashion. *Neurosci. Lett.* **197,** 211–214 (1995).

132. Klunk, W. E., Jacob, R. F. & Mason, R. P. Quantifying amyloid β-peptide (Aβ) aggregation using the congo red-Aβ (CR–Aβ) spectrophotometric assay. *Anal. Biochem.* **266,** 66–76 (1999).

133. Kung, M.-P., Hou, C., Zhuang, Z.-P., Skovronsky, D. & Kung, H. F. Binding of two potential imaging agents targeting amyloid plaques in postmortem brain tissues of patients with Alzheimer's disease. *Brain Res.* **1025,** 98–105 (2004).

134. Zhuang, Z.-P., Kung, M.-P., Skovronsky, D. M., Gur, T. L., Plössl, K., Trojanowskim J. Q., Lee, V. M.-Y. & Kung, H. F. Radioiodinated styrylbenzenes and thioflavins as probes for amyloid. *J. Med. Chem.* **44,** 1905–1914 (2001).

135. Bohrmann, B., Adrian, M., Dubochet, J., Kruner, P., Müller, F., Huber, W., Nordstedt, C. & Döbeli, H. Self-assembly of β-amyloid (42) is retarded by small molecular ligands at the stage of structural intermediates. *J. Struct. Biol.* **130,** 232–46 (2000).

136. Chyan, Y.-J., Poeggeler, B., Omar, R. A., Chain, D. G., Frangione, B., Ghiso, J. & Pappolla, M. A. Potent neuroprotective properties against the Alzheimer β-amyloid by an endogenous melatonin-related Indole structure, indole-3-propionic acid. *J. Biol. Chem.* **274,** 21937–21942 (1999).

137. Bendheim, P. E., Poeggeler, B., Neria, E., Ziv, V., Pappolla, M. A. & Chain, D. G. Development of indole-3-propionic acid (OXIGON^{TM}) for Alzheimer's disease. *J. Mol. Neurosci.* **19,** 213–217 (2002).

138. Cohen, T., Frydman-Marom, A., Rechter, M. & Gazit, E. Inhibition of amyloid fibril formation and cytotoxicity by hydroxyindole. *Biochemistry* **45,** 4727–4735 (2006).

139. Reixach, N., Crooks, E., Ostresh, J. M., Houghten, R. A. & Blondelle, S. E. Inhibition of β-amyloid-induced neurotoxicity by imidazopyridoindoles derived from a synthetic combinatorial library. *J. Struct. Biol.* **130,** 247–58 (2000).

140. Török, M., Abid, M., Mhadgut, S. C. & Török, B. Organofluorine inhibitors of amyloid-β fibrillogenesis. *Biochemistry* **45,** 5377–83 (2006).

141. Wood, S. J., MacKenzie, L., Maleeff, B., Hurle, M. R. & Wetzel, R. Selective inhibition of Aβ fibril formation. *J. Biol. Chem.* **271,** 4086–4092 (1996).

142. Iii, H. L., Ding, Q., Walker, J. A., Voss, R. S. & Augelli-, C. E. Clioquinol and other hydroxyquinoline derivatives inhibit Aβ(1-42) assembly. *Neurosci. Lett.* **465,** 99–103 (2009).

143. Simons, L. J., Carprathe, B. W., Callahan, M., Graham, J. M., Kimura, T., Lai, Y., Levine, H., Lipinski, W., Sakkab, A. T., Tasaki, Y., Walker, L. C., Yasunaga, T., Ye, Y., Zhuang, N. & Augelli-Szafran, C. E. The synthesis and structure-activity relationship of substituted N-phenyl anthranilic acid analogs as amyloid aggregation inhibitors. *Bioorganic Med. Chem. Lett.* **19,** 654–657 (2009).

144. Rzepecki, P., Gallmeier, H., Geib, N., Cernovska, K. & Ko, B. New heterocyclic β-sheet ligands with peptidic recognition. *J. Org. Chem.* **69,** 5168–5178 (2004).

145. Rzepecki, P., Nagel-Steger, L., Feuerstein, S., Linne, U., Molt, O., Zadmard, R., Aschermann, K., Wehner, M., Schrader, T. & Riesner, D. Prevention of Alzheimer's disease-associated Aβ aggregation by rationally designed nonpeptidic β-sheet ligands. *J. Biol. Chem.* **279,** 47497–505 (2004).

146. McLaurin, J., Franklin, T., Chakrabartty, A. & Fraser, P. E. Phosphatidylinositol and inositol involvement in Alzheimer amyloid-β growth and arrest. *J. Mol. Biol.* **278,** 183–194 (1998).

147. Gervais, F., Paquette, J., Morissette, C., Krzywkowski, P., Yu., Azzi, M., Lacombe, D., Kong, X., Aman, A., Laurin, J., Szarek, W. A. & Tremblay, P. Targeting soluble Aβ peptide with Tramiprosate for the treatment of brain amyloidosis. *Neurobiol. Aging* **28,** 537–547 (2007).

148. Giuffrida, M. L., Caraci, F., Pignataro, B., Cataldo, S., De Bona, P., Vruno, V., Molinaro, G., Papalardo, G., Messina, A., Palmigiano, A., Garozzo, D., Nicoletti, F., Rizzarelli, E. & Copani, A. β-amyloid monomers are neuroprotective. *J. Neurosci.* **29,** 10582–10587 (2009).

149. Soscia, S. J., Kirby, J. E., Washicosky, K. J., Tucker, S. M., Ingelsson, M., Hyman, B., Burton, M. A., Goldstein, L. E., Suong, S., Tanzi, R. E. & Moir, R. D. The Alzheimer's disease-associated amyloid β-protein is an antimicrobial peptide. *PLoS One* **5,** 1–10 (2010).

150. Stephenson, V. C., Heyding, R. A. & Weaver, D. F. The 'promiscuous drug concept' with applications to Alzheimer's disease. *FEBS Lett.* **579,** 1338–1342 (2005).

151. Lipinski, C. a, Lombardo, F., Dominy, B. W. & Feeney, P. J. Experimental and computational approaches to estimate solubility and permeability in drug discovery and development. *Adv. Drug Deliv. Rev.* **46,** 3–26 (2001).

152. Hann, M. M. & Oprea, T. I. Pursuing the leadlikeness concept in pharmaceutical research. *Curr. Opin. Chem. Biol.* **8,** 255–263 (2004).

153. Sulatskaya, A. I., Kuznetsova, I. M. & Turoverov, K. K. Interaction of thioflavin T with amyloid fibrils: stoichiometry and affinity of dye binding, absorption spectra of bound dye. *J. Phys. Chem. B* **115,** 11519–24 (2011).

154. LeVine, H. Thioflavine T interaction with synthetic Alzheimer's disease β-amyloid peptides: detection of amyloid aggregation in solution. *Protein Sci.* **2,** 404–410 (1993).

155. Jameson, L. P., Smith, N. W. & Dzyuba, S. V. Dye-binding assays for evaluation of the effects of small molecule inhibitors on amyloid (Aβ) self-assembly. *ACS Chem. Neurosci.* **3,** 807–819 (2012).

156. Porat, Y., Abramowitz, A. & Gazit, E. Inhibition of amyloid fibril formation by polyphenols: structural similarity and aromatic interactions as a common inhibition mechanism. *Chem. Biol. Drug Des.* **67,** 27–37 (2006).

157. Martin, T. L., Mufson, E. J. & Mesulam, M. M. The light side of horseradish peroxidase histochemistry. *J. Histochem. Cytochem.* **32,** 1554 (1984).

158. Conway, K. A., Rochet, J. & Bieganski, R. M. Kinetic stabilization of the α-synuclein protofibril by a dopamine-α-synuclein adduct. *Science.* **294,** 1346–1350 (2001).

159. Wang, C.-C., Huang, H.-B., Tsay, H.-J., Shiao M.-S., Wu, W.-J. W., Cheng, Y.-C. & Lin, T.-H. Characterization of Aβ aggregation mechanism probed by congo red. *J. Biomol. Struct. Dyn.* **30,** 160–9 (2012).

160. Findeis, M. A. Approaches to discovery and characterization of inhibitors of amyloid β-peptide polymerization. *Biochim. Biophys. Acta* **1502,** 76–84 (2000).

161. Soto, C. Plaque busters: strategies to inhibit amyloid formation in Alzheimer's disease. *Mol. Med. Today* **5,** 343–350 (1999).

162. Leach, A. R. *Molecular modelling: principles and applications*. (Prentice Hall, 2001).

163. Cornell, W. D., Cieplak, P., Bayly, C. I., Gould, I. R., Merz, K. M., Ferguson, D. M., Spellmeyer, D. C., Fox, T., Caldwall, J. W. & Kollman, P. A. A second generation force field for the simulation of proteins, nucleic acids, and organic molecules. *J. Am. Chem. Soc.* **117,** 5179–5197 (1995).

164. Jakalian, A., Jack, D. B. & Bayly, C. I. Fast, efficient generation of high-quality atomic charges. AM1-BCC model: II. Parameterization and validation. *J. Comput. Chem.* **23,** 1623–1641 (2002).

165. Talafous, J., Marcinowski, K. J., Klopman, G. & Zagorski, M. G. Solution structure of residues 1-28 of the amyloid β-peptide. *Biochemistry* **33,** 7788–7796 (1994).

166. Vivekanandan, S., Brender, J. R., Lee, S. Y. & Ramamoorthy, A. A partially folded structure of amyloid-beta(1-40) in an aqueous environment. *Biochem. Biophys. Res. Commun.* **411,** 312–316 (2011).

167. Richard, T., Papastamoulis, Y., Pierre, W. T. & Monti, J. P. 3D NMR structure of a complex between the amyloid beta peptide (1-40) and the polyphenol ε-viniferin glucoside: Implications in Alzheimer's disease. *Biochim. Biophys. Acta - Gen. Subj.* **1830,** 5068–5074 (2013).

168. Sticht, H., Bayer, P., Willbold, D., Dames, S., Hilbich, C., Beyreuther, K., Frank, R. W. & Rösch, P. Structure of Amyloid A4-(1-40)-peptide of Alzheimer's disease. *Eur. J. Biochem.* **233,** 293–298 (1995).

169. Coles, M., Bicknell, W., Watson, R. a., Fairlie, D. P. & Craik, D. J. Solution structure of amyloid β-peptide(1-40) in a water-micelle environment. Is the membrane-spanning domain where we think it is? *Biochemistry* **37,** 11064–11077 (1998).

170. Crescenzi, O., Tomaselli, S., Guerrini, R., Salvadori, S., D'Ursi, A. M., Temussi, P. A. & Picone, D. Solution structure of the Alzheimer amyloid β-peptide (1-42) in an apolar microenvironment: similarity with a virus fusion domain. *Eur. J. Biochem.* **269,** 5642–5648 (2002).

171. Tomaselli, S., Esposito, V., Vangone, P., van Nuland, N. A. J., Bonvin, A. M. J. J., Guerrini, R., Tancredi, T., Temussi, P. A. & Picone, D. The α-to-β conformational transition of Alzheimer's Aβ-(1-42) peptide in aqueous media is reversible: A step by step conformational analysis suggests the location of β conformation seeding. *ChemBioChem* **7,** 257–267 (2006).

172. Lakey-Beitia, J., Berrocal, R., Rao, K. S. & Durant, A. a. Polyphenols as therapeutic molecules in Alzheimer's disease through modulating amyloid pathways. *Mol. Neurobiol.* (2014). doi:10.1007/s12035-014-8722-9 (e-published ahead of print)

173. Mayer, M. & Meyer, B. Group epitope mapping by saturation transfer difference NMR to identify segments of a ligand in direct contact with a protein receptor. *J. Am. Chem. Soc.* **123,** 6108–6117 (2001).

174. Stejskal, E. O. & Tanner, J. E. Spin diffusion measurements: spin echoes in the presence of a time-dependent field gradient. *J. Chem. Phys.* **42,** 5 (1965).

175. Necula, M., Kayed, R., Milton, S. & Glabe, C. G. Small molecule inhibitors of aggregation indicate that amyloid β oligomerization and fibrillization pathways are independent and distinct. *J. Biol. Chem.* **282,** 10311–10324 (2007).

176. Kayed, R., Head, E., Thompson, J. L., McIntire, T. M., Milton, S. C., Cotman, C. W. and Glabe, C. G. Common structure of soluble amyloid oligomers implies common mechanism of pathogenesis. *Science.* **300,** 486–489 (2003).

177. Glabe, C. G. Conformation-dependent antibodies target diseases of protein misfolding. *Trends Biochem. Sci.* **29,** 542–547 (2004).

178. Deshpande, A., Mina, E., Glabe, C. & Busciglio, J. Different conformations of amyloid beta induce neurotoxicity by distinct mechanisms in human cortical neurons. *J. Neurosci.* **26,** 6011–6018 (2006).

179. Zhu, M., Rajamani, S., Kaylor, J., Han, S., Zhou, F. & Fink, A. L. The flavonoid baicalein inhibits fibrillation of α-synuclein and disaggregates existing fibrils. *J. Biol. Chem.* **279,** 26846–26857 (2004).

180. Li, J., Zhu, M., Rajamani, S., Uversky, V. N. & Fink, A. L. Rifampicin Inhibits α-Synuclein Fibrillation and Disaggregates Fibrils. *Chem. Biol.* **11,** 1513–1521 (2004).

181. Loureiro, J. A., Rocha, S. & Pereira, M. D. C. Charged surfactants induce a non-fibrillar aggregation pathway of amyloid-beta peptide. *J. Pept. Sci.* **19,** 581–587 (2013).

Appendix A: NMR Spectra

GS-1031

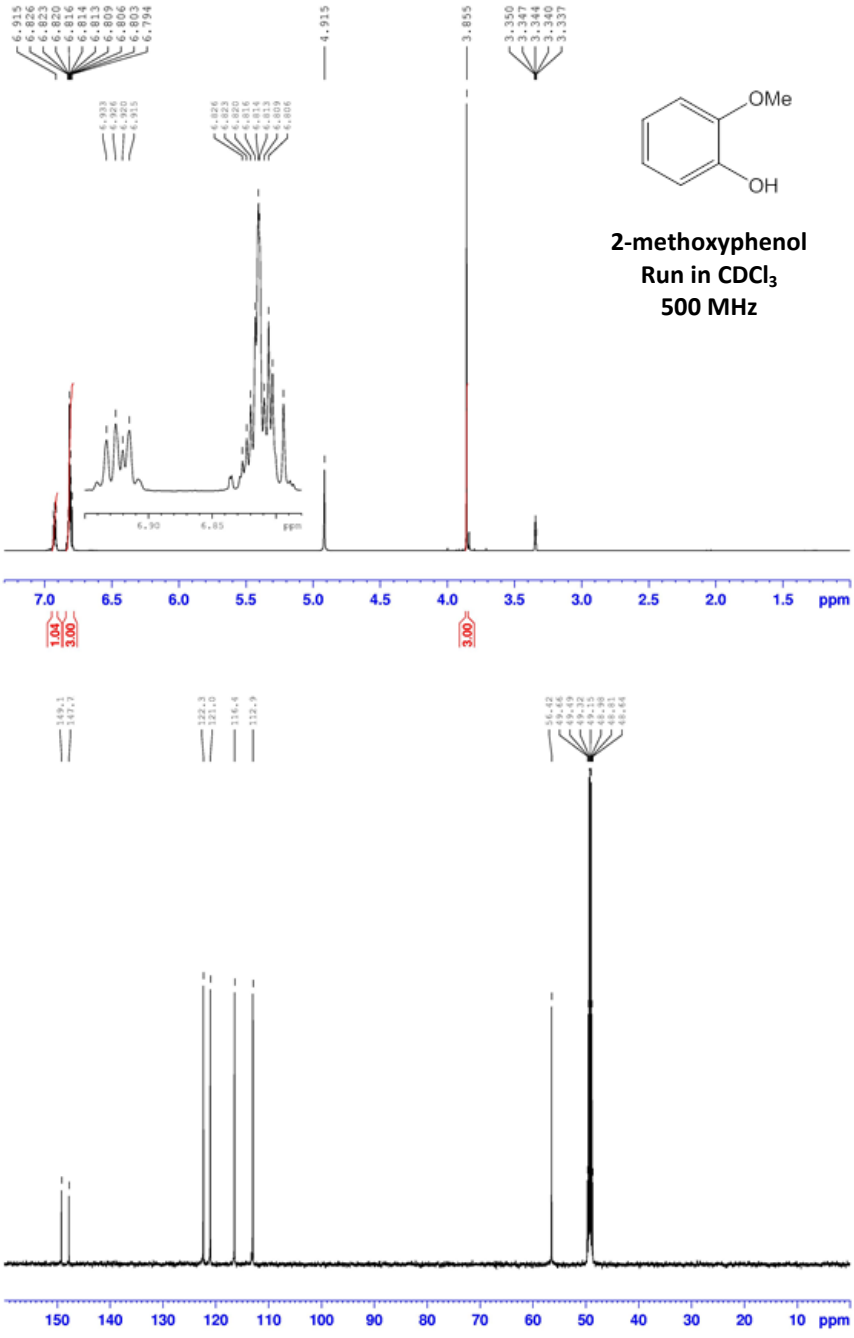

GS-1032

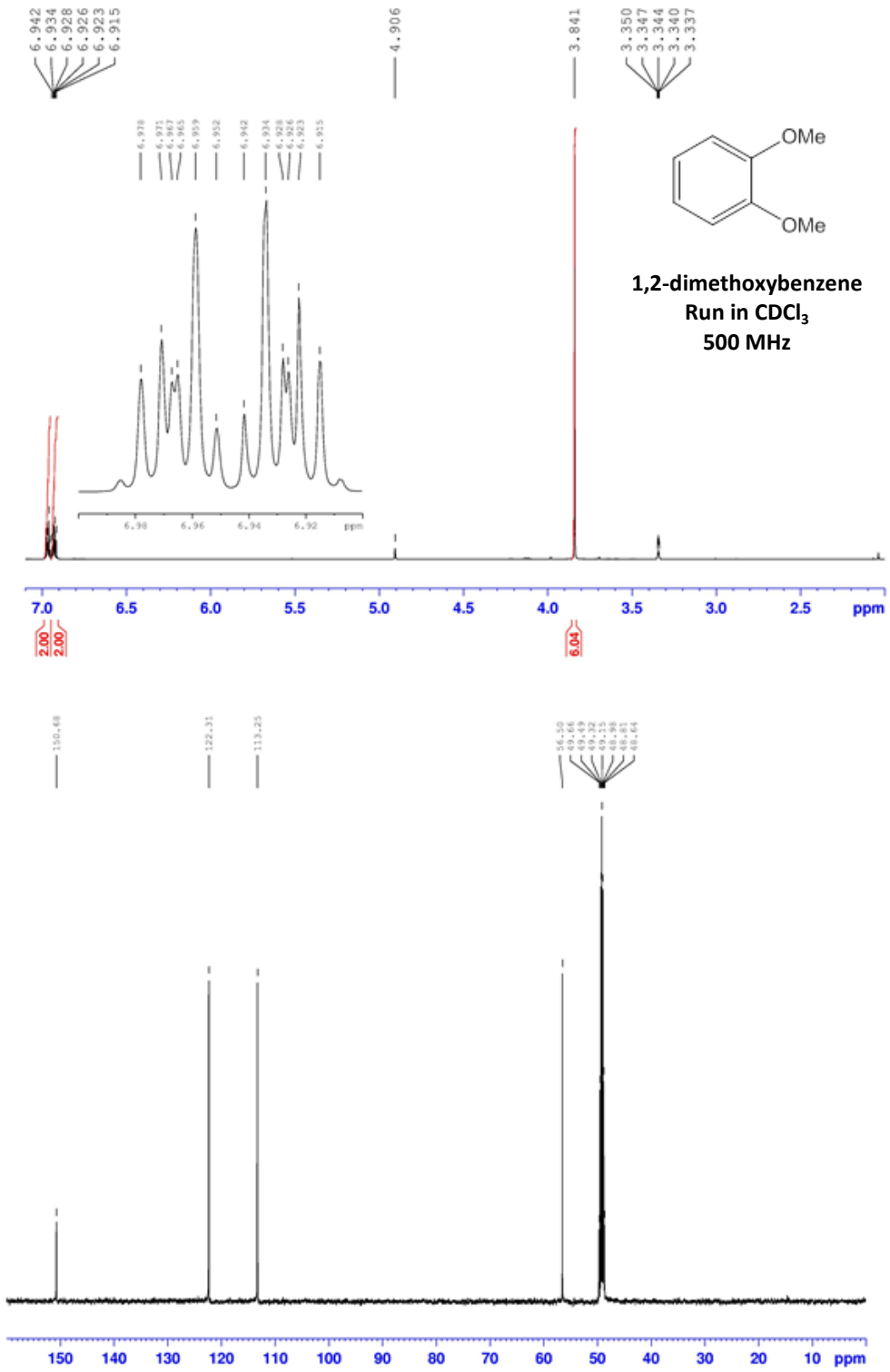
6.942
6.934
6.928
6.926
6.923
6.915
4.906
3.841
3.350
3.347
3.344
3.340
3.337
OMe
OMe
1,2-dimethoxybenzene
Run in CDCl3
500 MHz
7.0
6.5
6.0
5.5
5.0
4.5
4.0
3.5
3.0
2.5
ppm
2.00
2.00
6.04
150.68
122.31
113.25
56.50
150
140
130
120
110
100
90
80
70
60
50
40
30
20
10
ppm

GS-1033

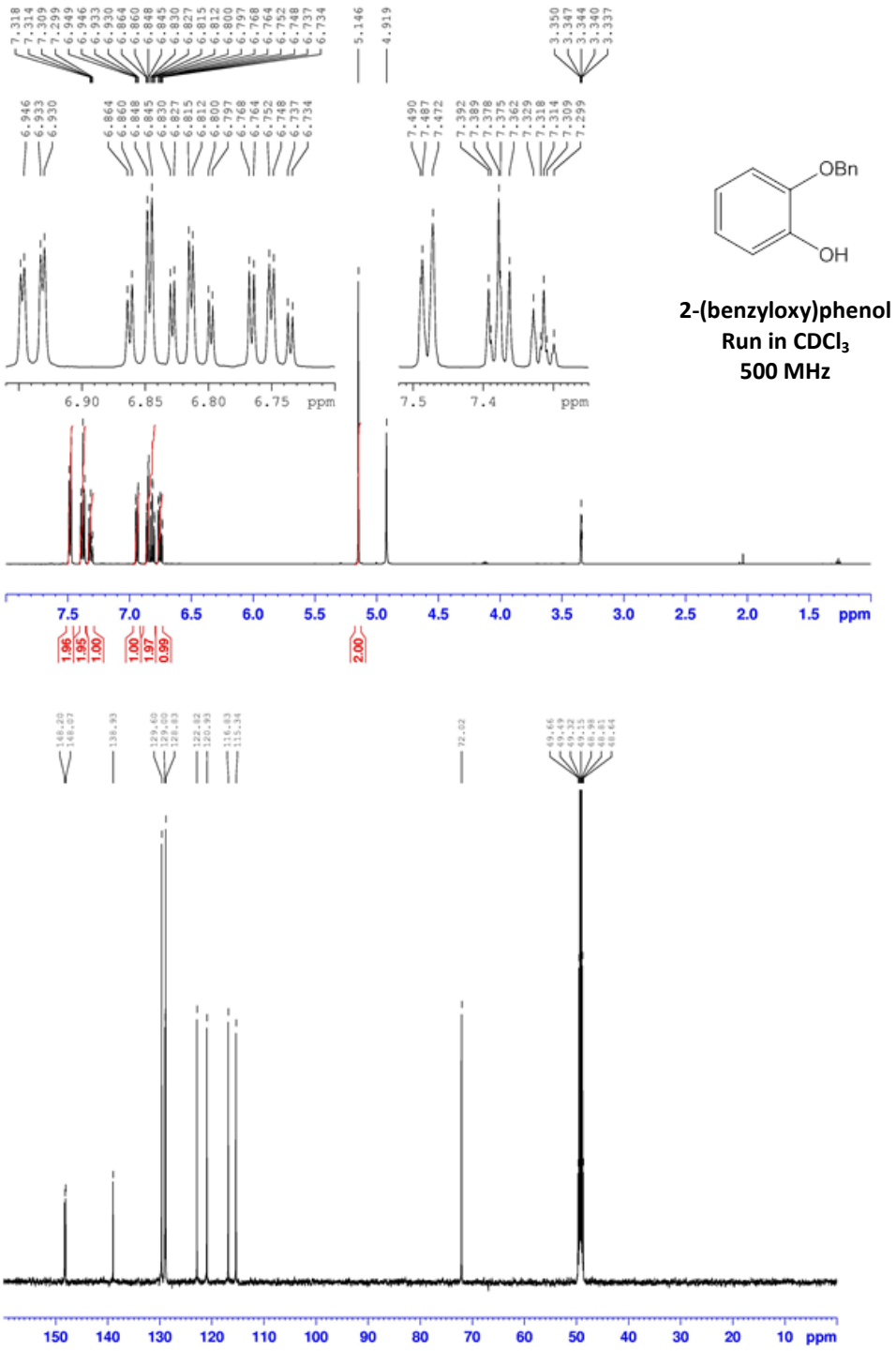

GS-1034

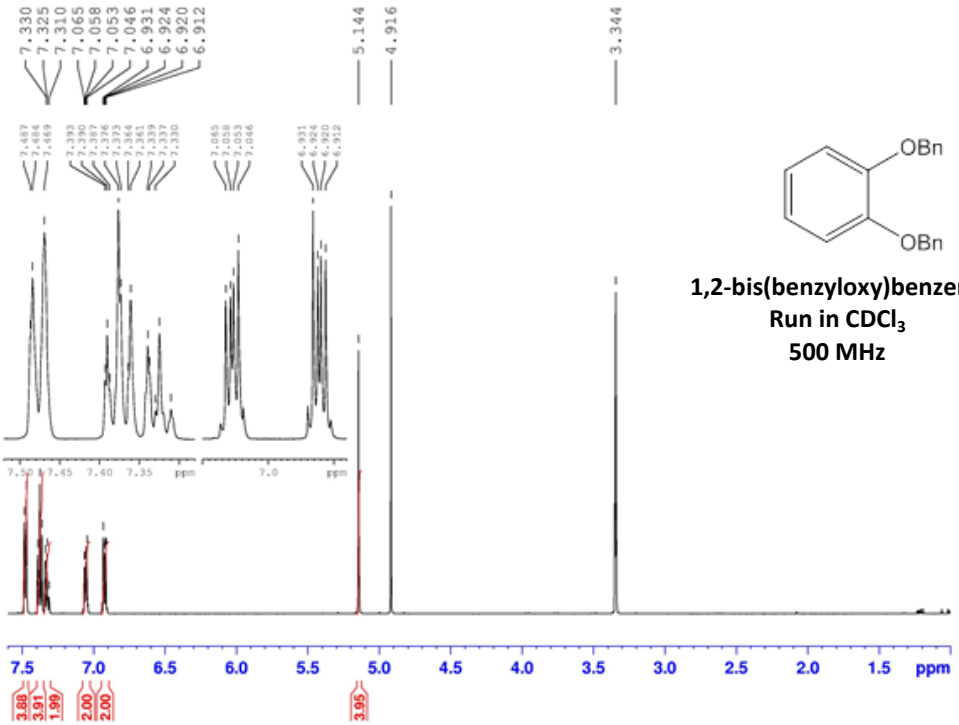

1,2-bis(benzyloxy)benzene
Run in $CDCl_3$
500 MHz

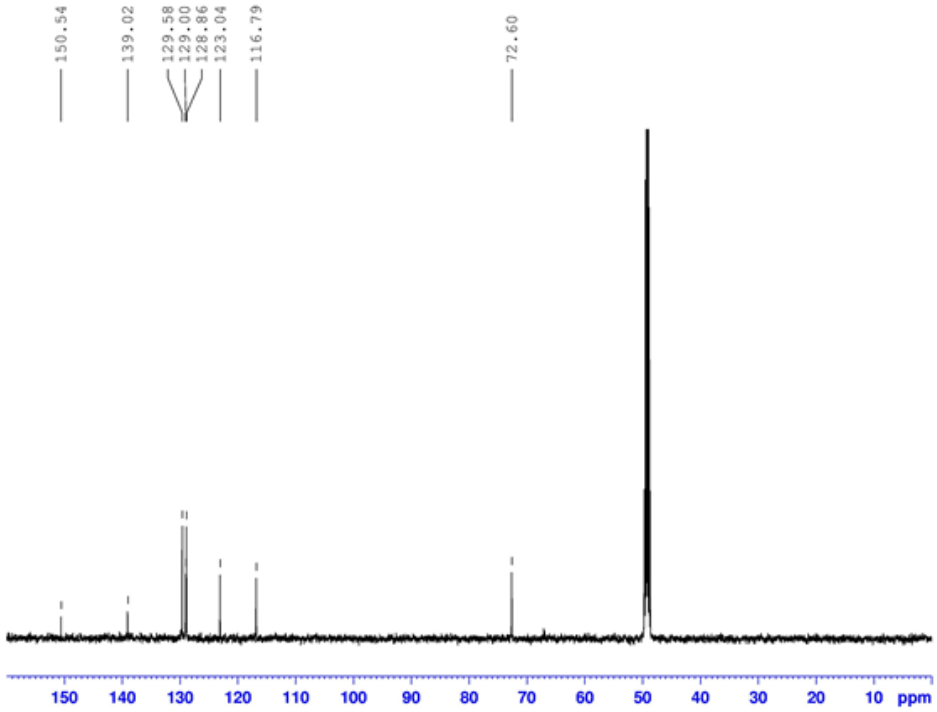

GS-1035

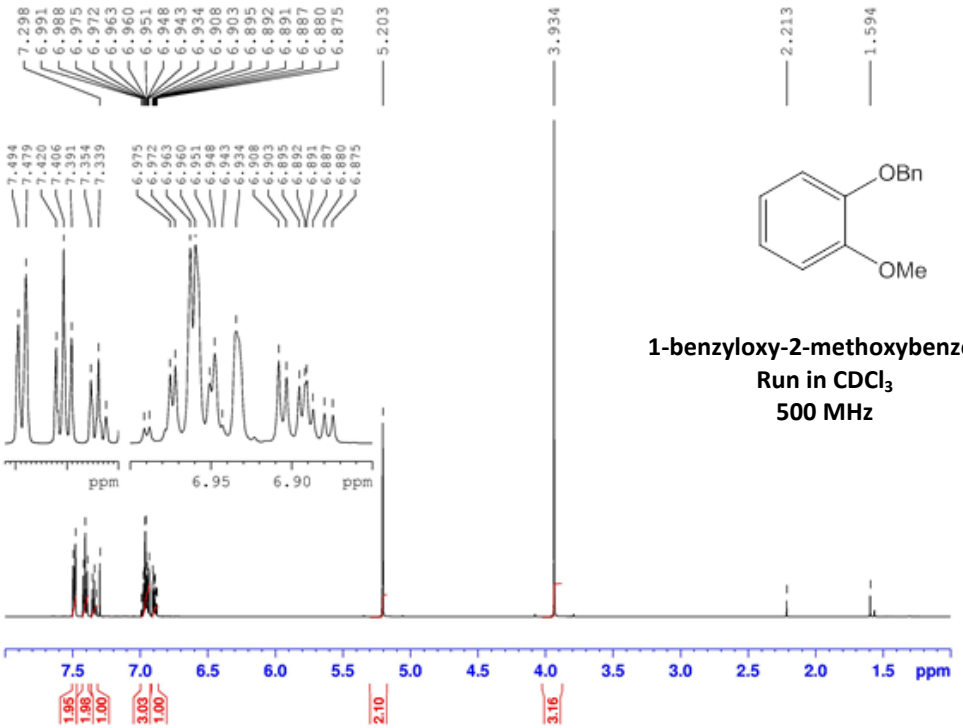

1-benzyloxy-2-methoxybenzene
Run in $CDCl_3$
500 MHz

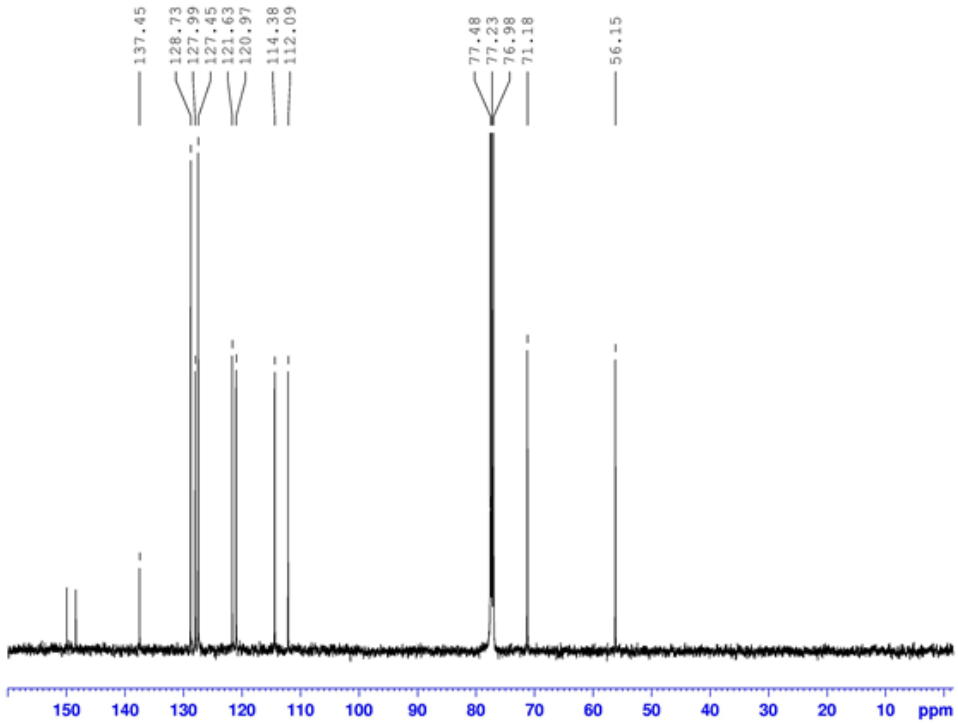

GS-1036

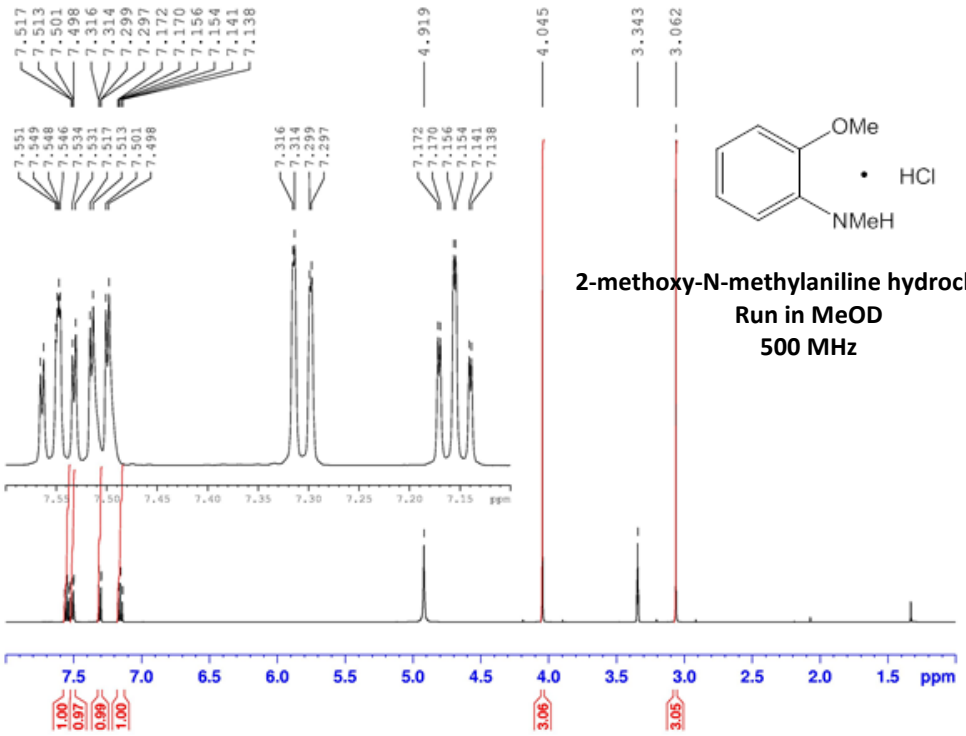

2-methoxy-N-methylaniline hydrochloride
Run in MeOD
500 MHz

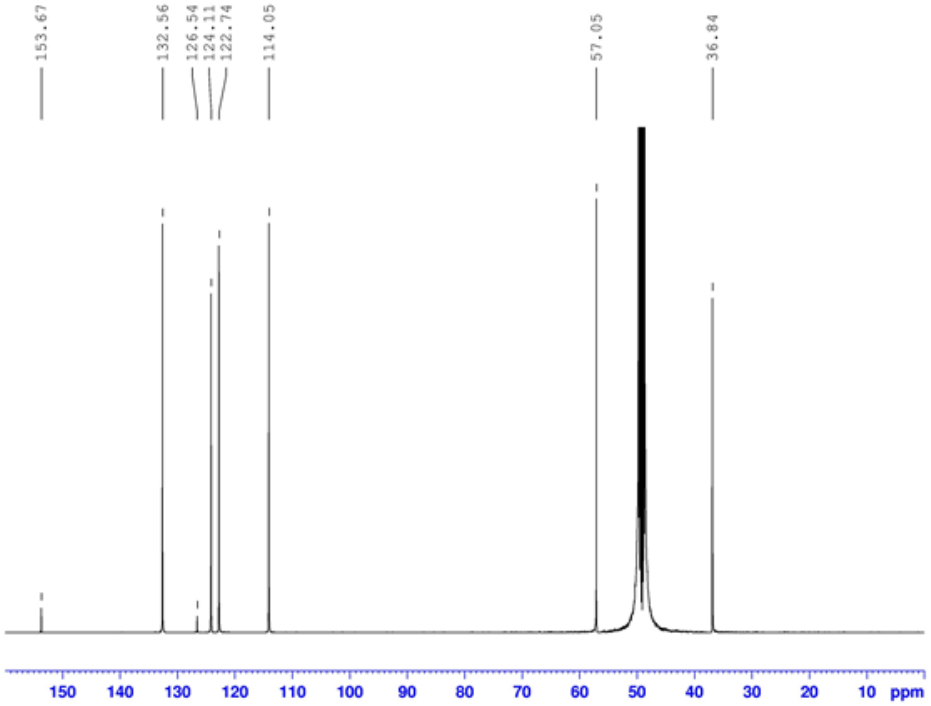

GS-1037

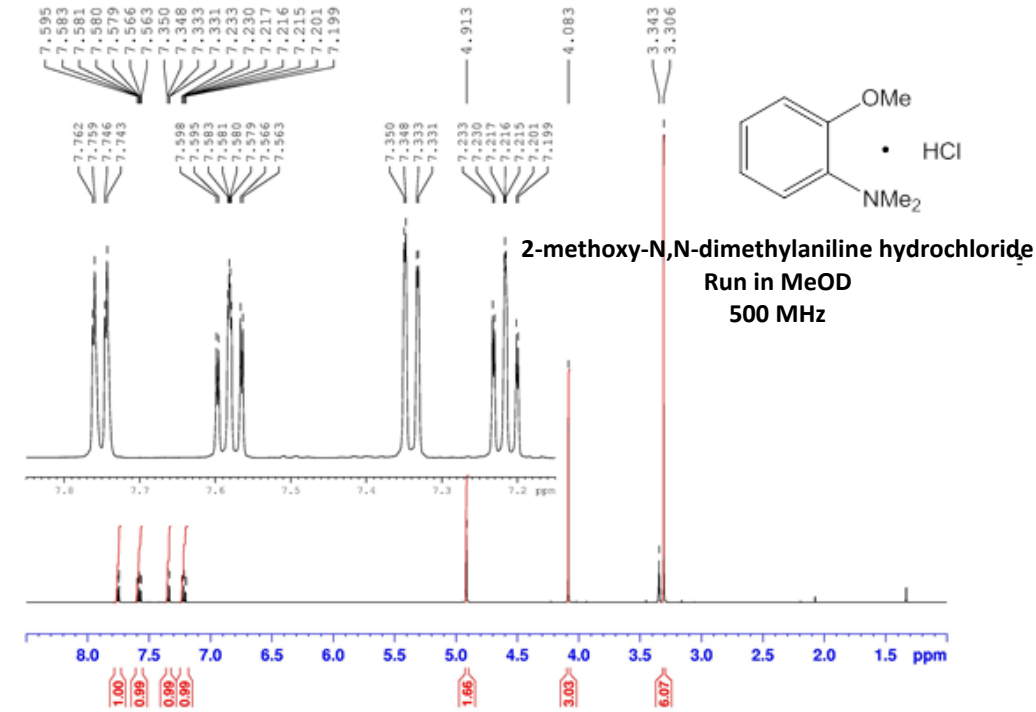
OMe
HCl
NMe2
2-methoxy-N,N-dimethylaniline hydrochloride
Run in MeOD
500 MHz

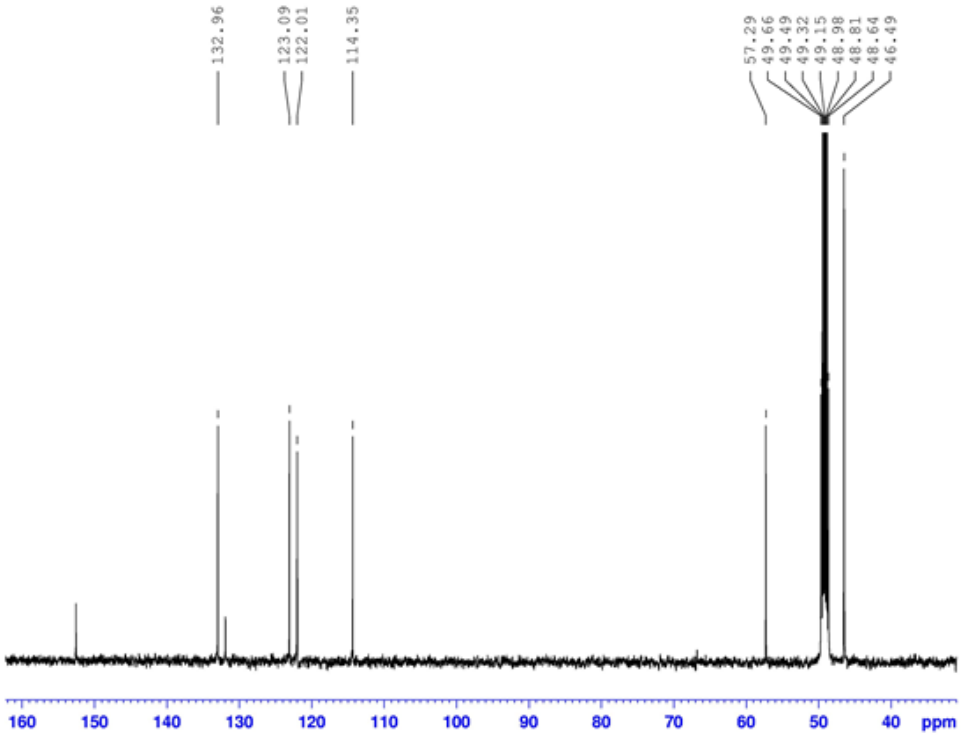

GS-1038

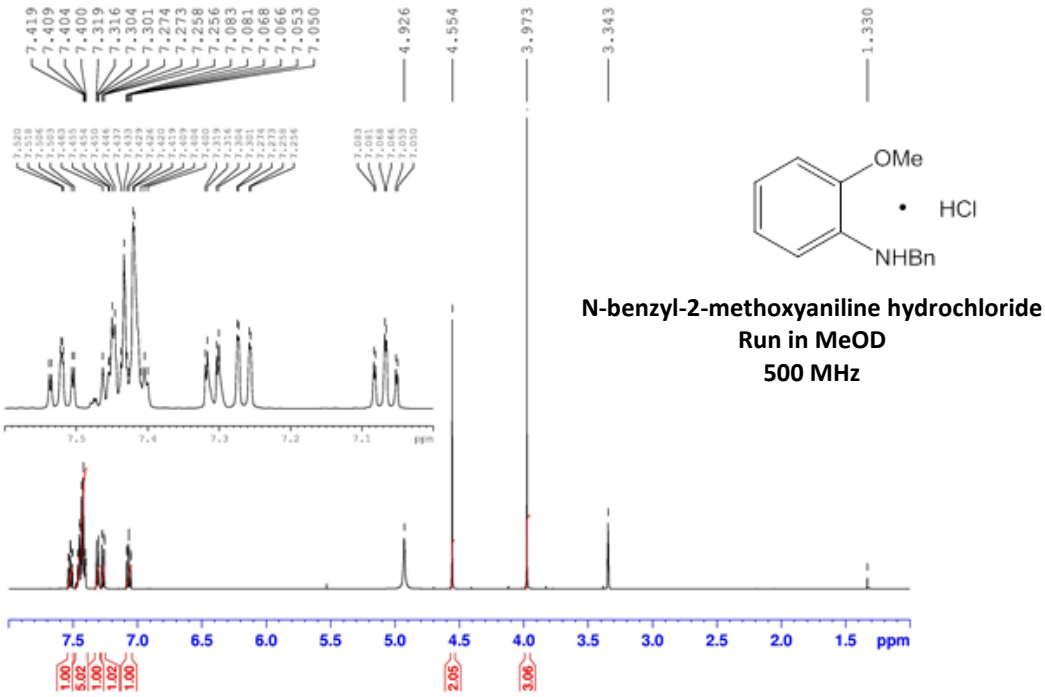

N-benzyl-2-methoxyaniline hydrochloride
Run in MeOD
500 MHz

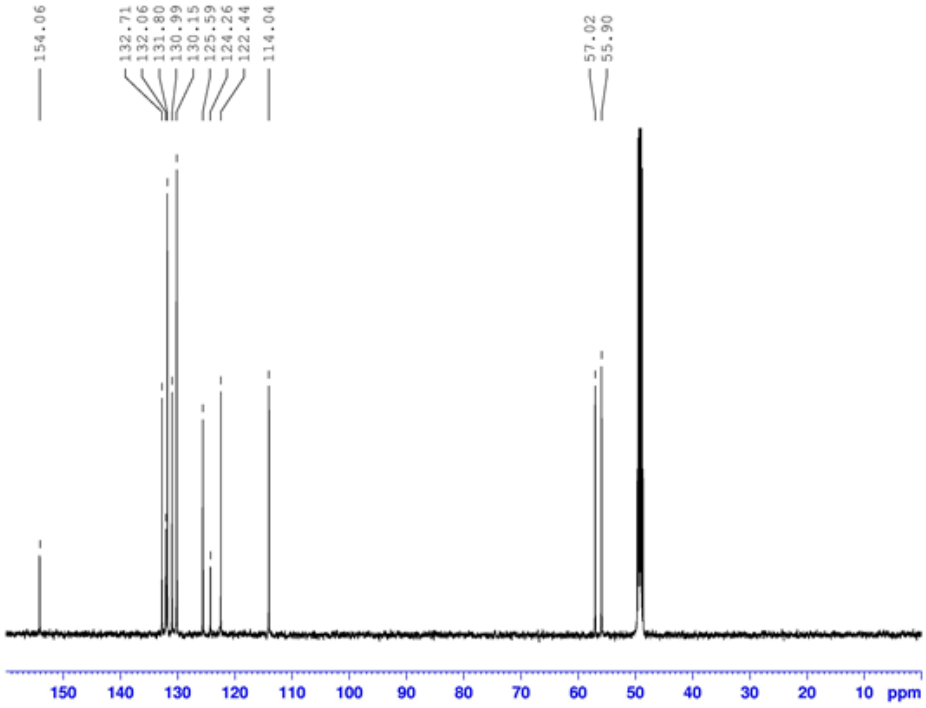

GS-1039

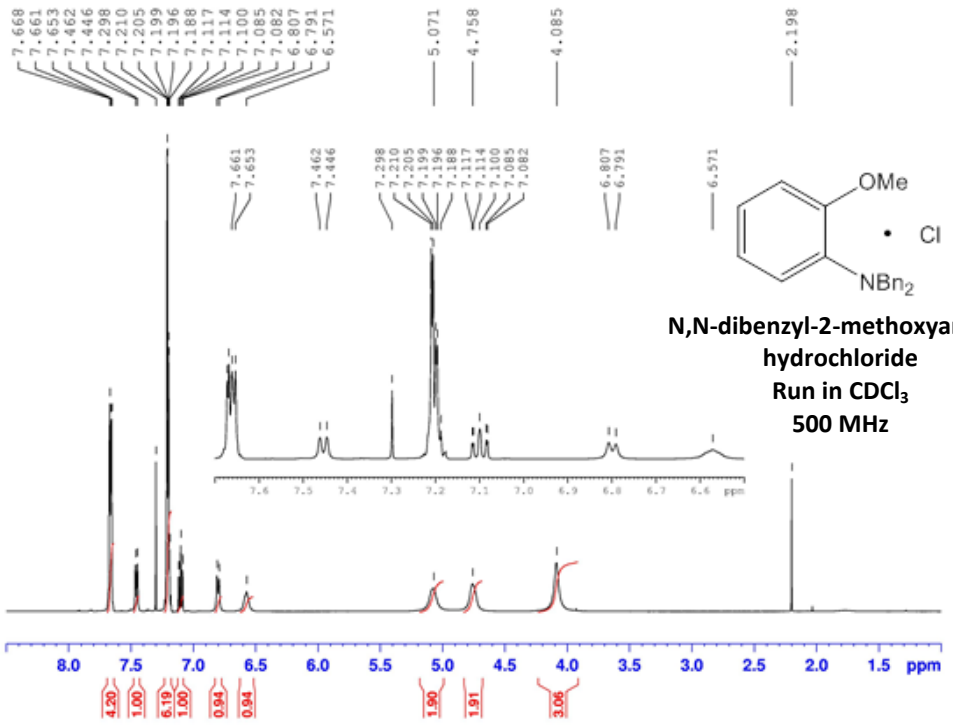

N,N-dibenzyl-2-methoxyaniline hydrochloride
Run in $CDCl_3$
500 MHz

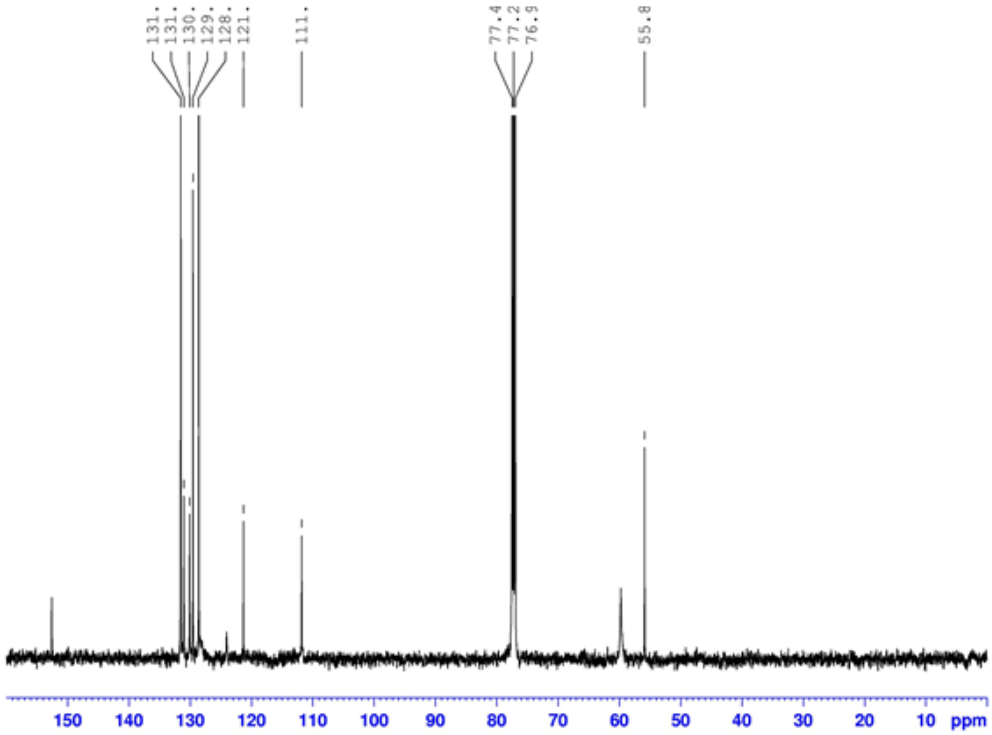

GS-1044

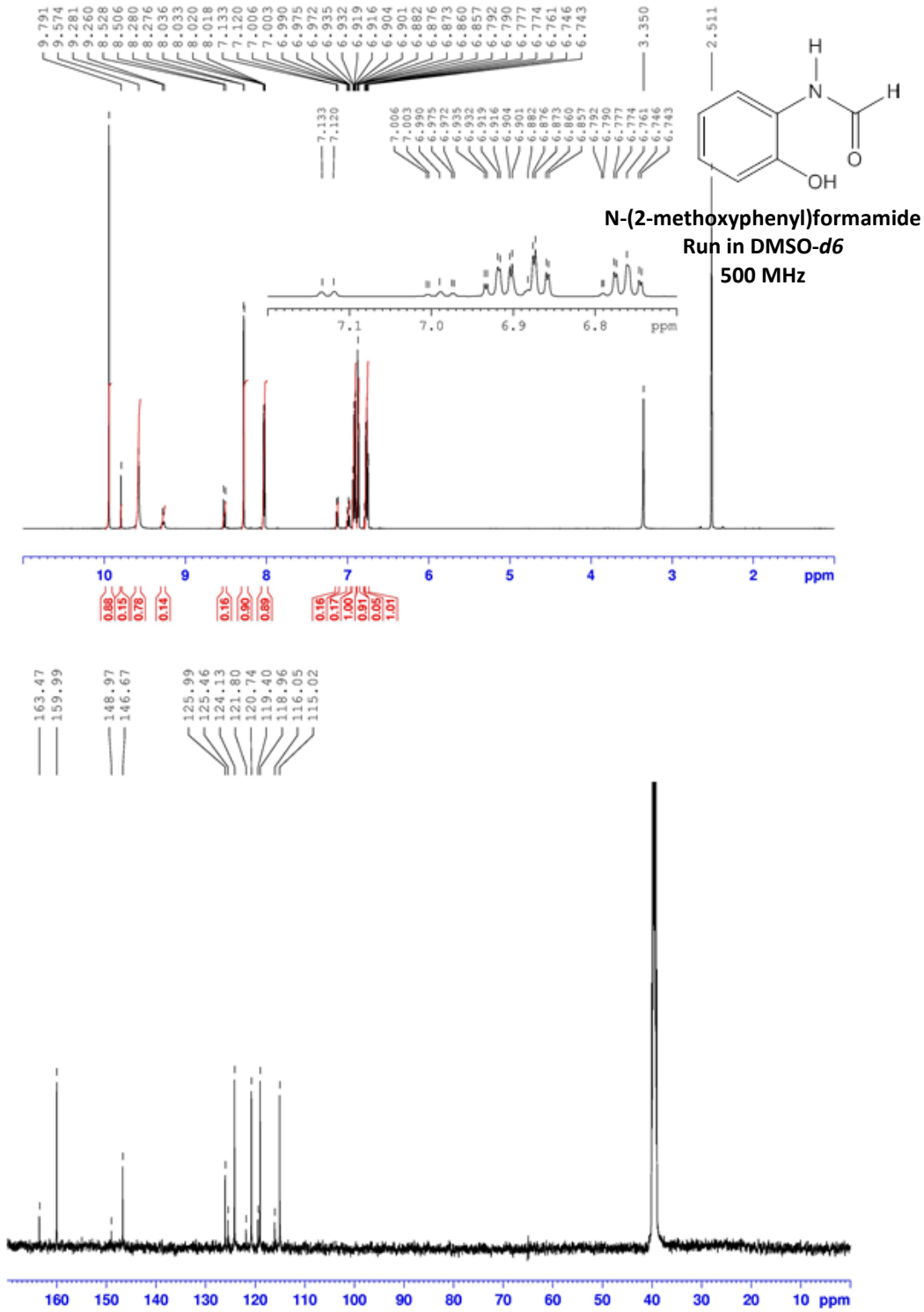
9.791
9.574
9.281
9.260
8.528
8.506
8.280
8.276
8.036
8.033
8.020
8.018
7.133
7.120
7.006
7.003
6.990
6.975
6.972
6.935
6.932
6.919
6.916
6.904
6.901
6.882
6.876
6.873
6.860
6.857
6.792
6.790
6.777
6.774
6.761
6.746
6.743
3.350
2.511
H
N
H
O
OH
N-(2-methoxyphenyl)formamide
Run in DMSO-d6
500 MHz
7.1
7.0
6.9
6.8
ppm
10
9
8
7
6
5
4
3
2
ppm
0.88
0.15
0.78
0.14
0.16
0.90
0.89
0.16
0.17
1.00
0.91
0.05
1.01
163.47
159.99
148.97
146.67
125.99
125.46
124.13
121.80
120.74
119.40
118.96
116.05
115.02
160
150
140
130
120
110
100
90
80
70
60
50
40
30
20
10 ppm

GS-1045

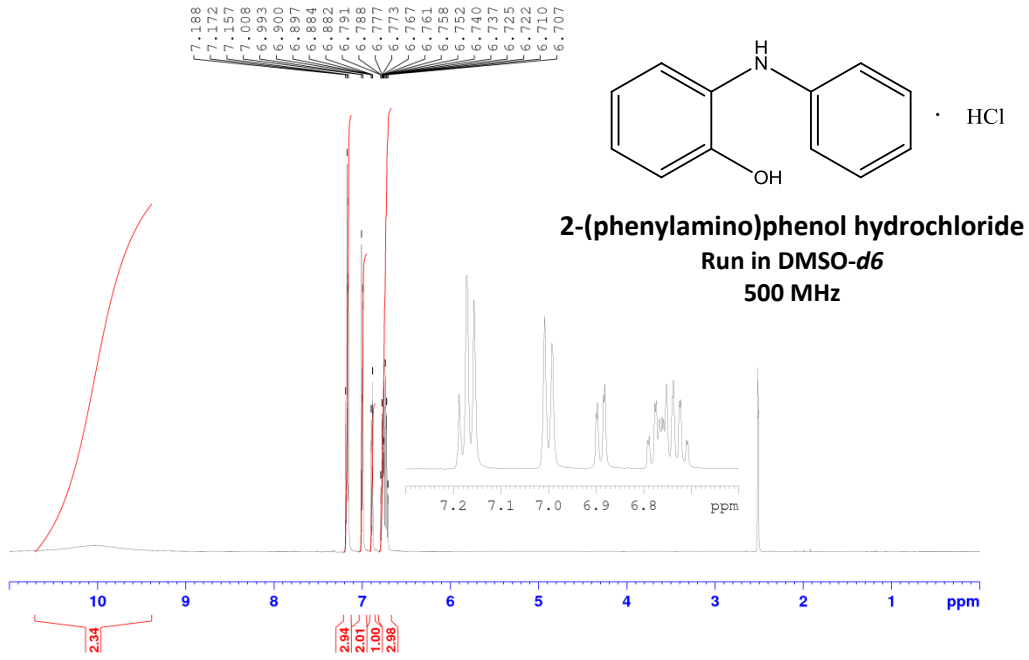
7.188
7.172
7.157
7.008
6.993
6.900
6.897
6.884
6.882
6.791
6.788
6.777
6.773
6.767
6.761
6.758
6.752
6.740
6.737
6.725
6.722
6.710
6.707
H
N
OH
· HCl
2-(phenylamino)phenol hydrochloride
Run in DMSO-d6
500 MHz
7.2 7.1 7.0 6.9 6.8 ppm
10 9 8 7 6 5 4 3 2 1 ppm
2.34
2.94
2.01
1.00
2.98

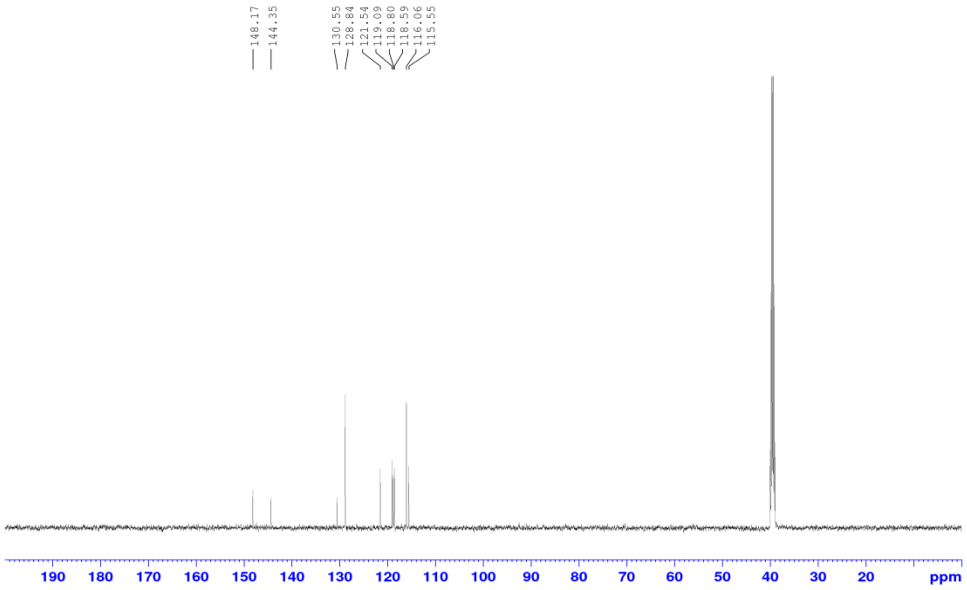
148.17
144.35
130.55
128.84
121.54
119.09
118.80
118.59
116.06
115.55
190 180 170 160 150 140 130 120 110 100 90 80 70 60 50 40 30 20 ppm

GS-1046

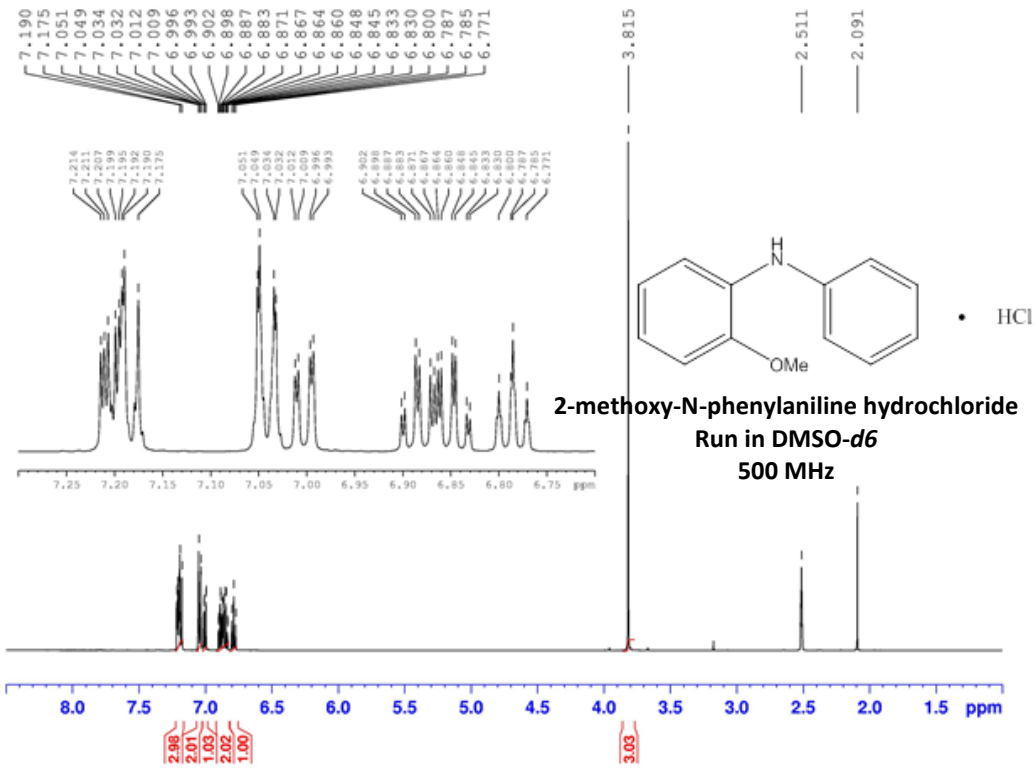

2-methoxy-N-phenylaniline hydrochloride
Run in DMSO-*d6*
500 MHz

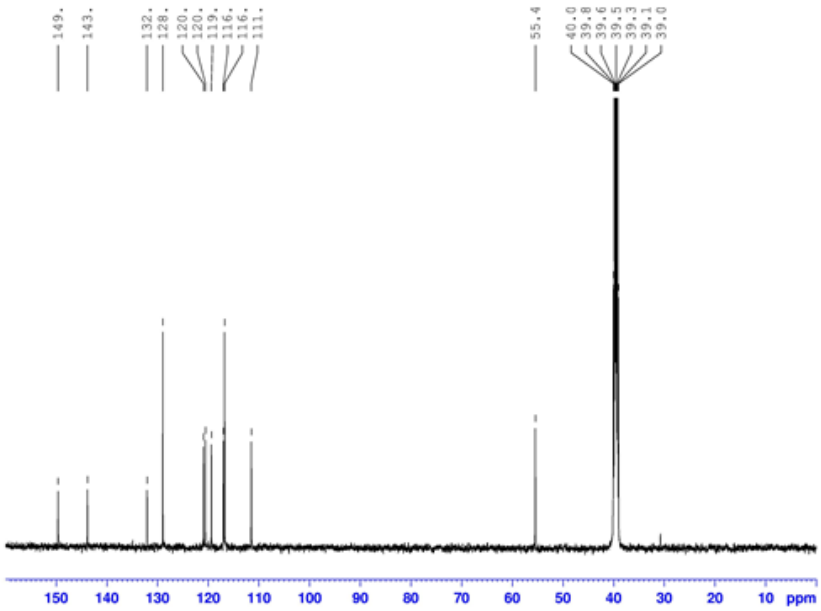

GS-1047

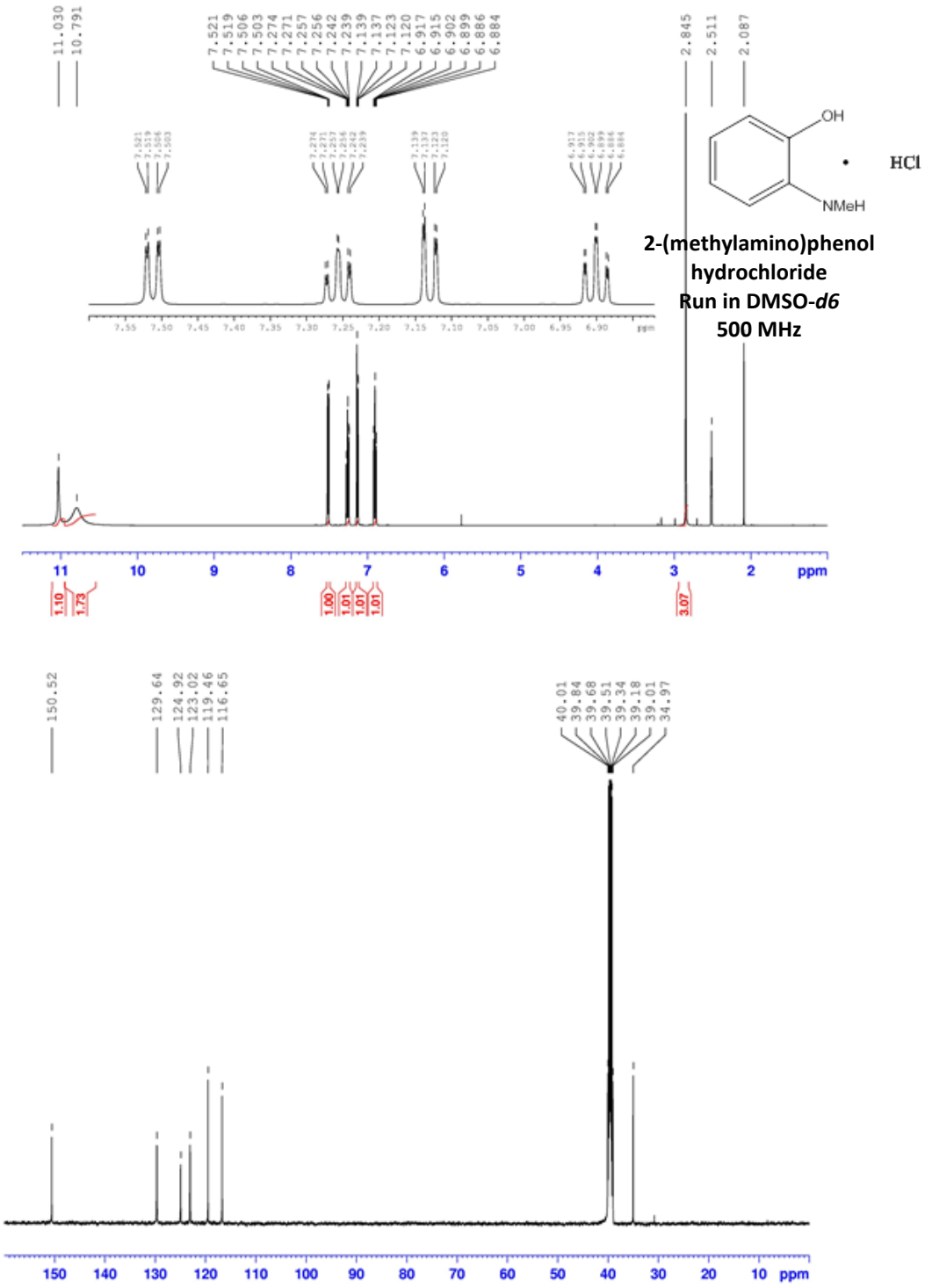
11.030
10.791
7.521
7.519
7.506
7.503
7.274
7.271
7.257
7.256
7.242
7.239
7.139
7.137
7.123
7.120
6.917
6.915
6.902
6.899
6.886
6.884
2.845
2.511
2.087
OH
NMeH
HCl
2-(methylamino)phenol
hydrochloride
Run in DMSO-*d6*
500 MHz
ppm
150.52
129.64
124.92
123.02
119.46
116.65
40.01
39.84
39.68
39.51
39.34
39.18
39.01
34.97

GS-1048

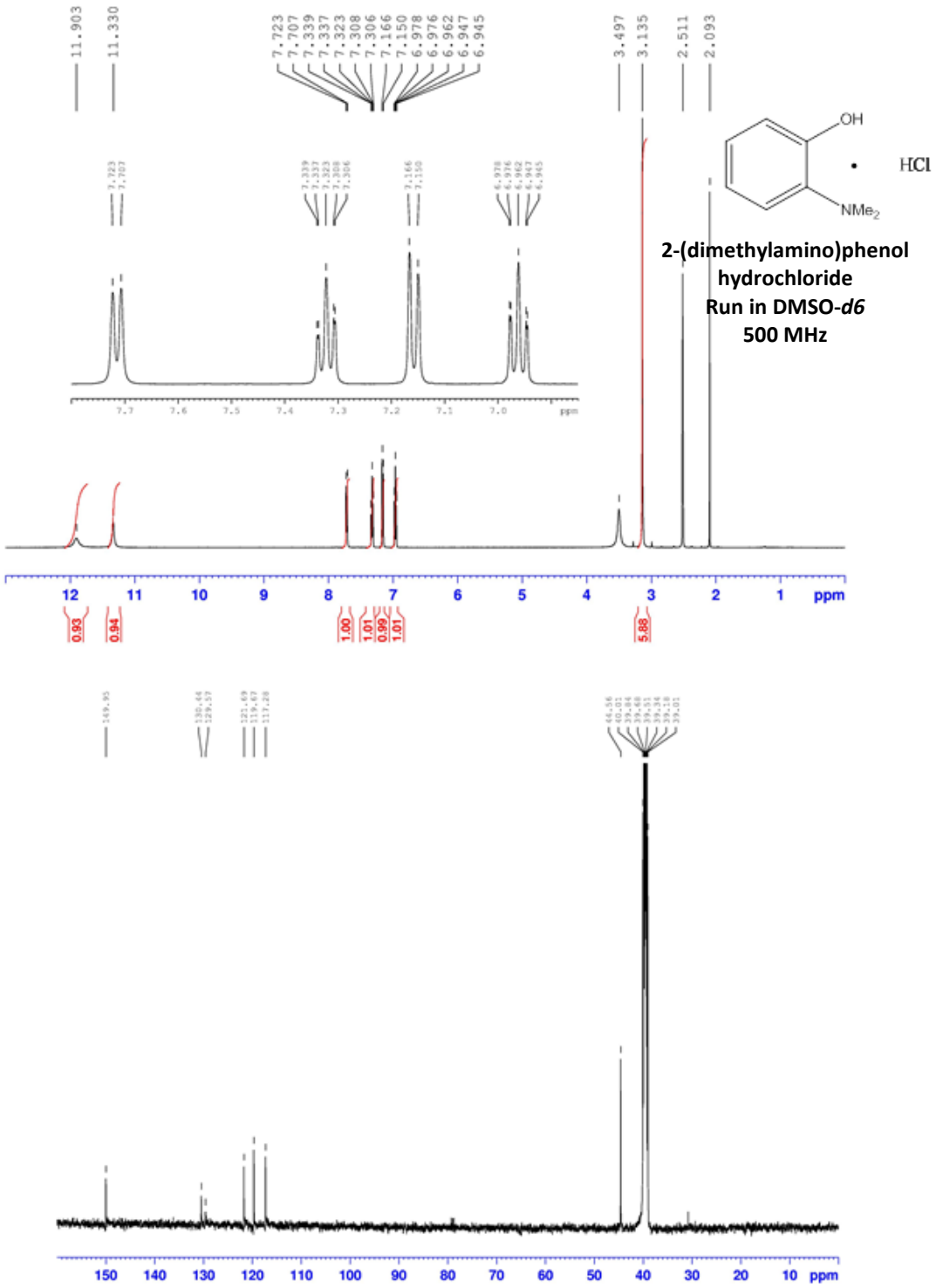
11.903
11.330
7.723
7.707
7.339
7.337
7.323
7.308
7.306
7.166
7.150
6.978
6.976
6.962
6.947
6.945
3.497
3.135
2.511
2.093
OH
HCl
NMe2
2-(dimethylamino)phenol
hydrochloride
Run in DMSO-d6
500 MHz
12
11
10
9
8
7
6
5
4
3
2
1
ppm
0.93
0.94
1.00
1.01
0.99
1.01
5.88
150
140
130
120
110
100
90
80
70
60
50
40
30
20
10
ppm

GS-1049

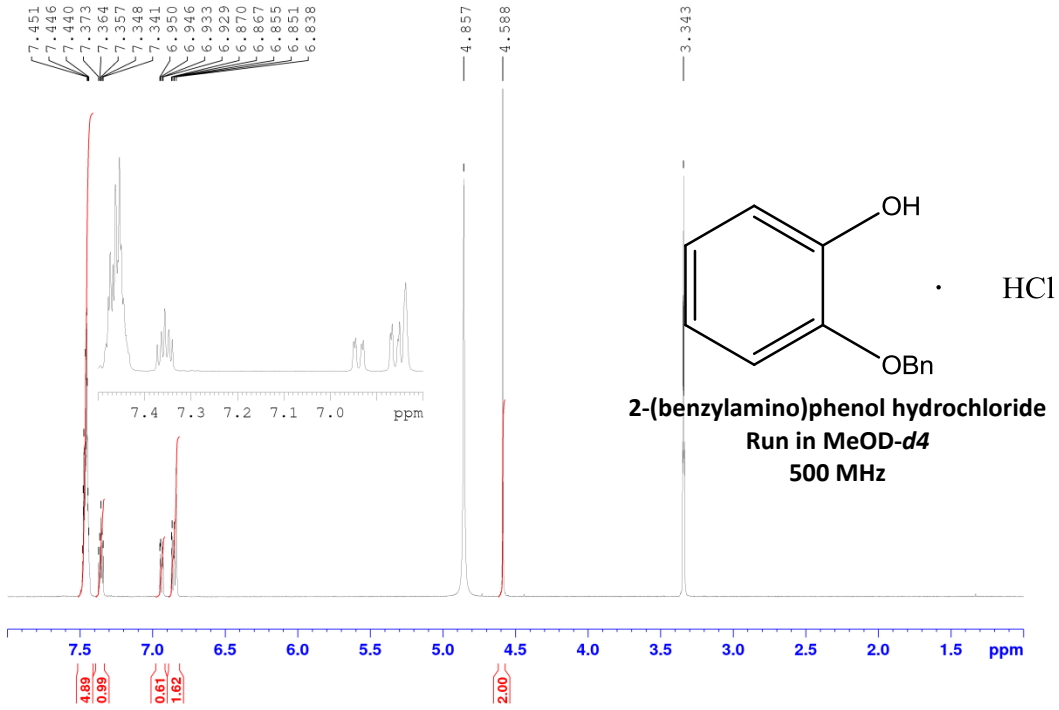

2-(benzylamino)phenol hydrochloride
Run in MeOD-*d4*
500 MHz

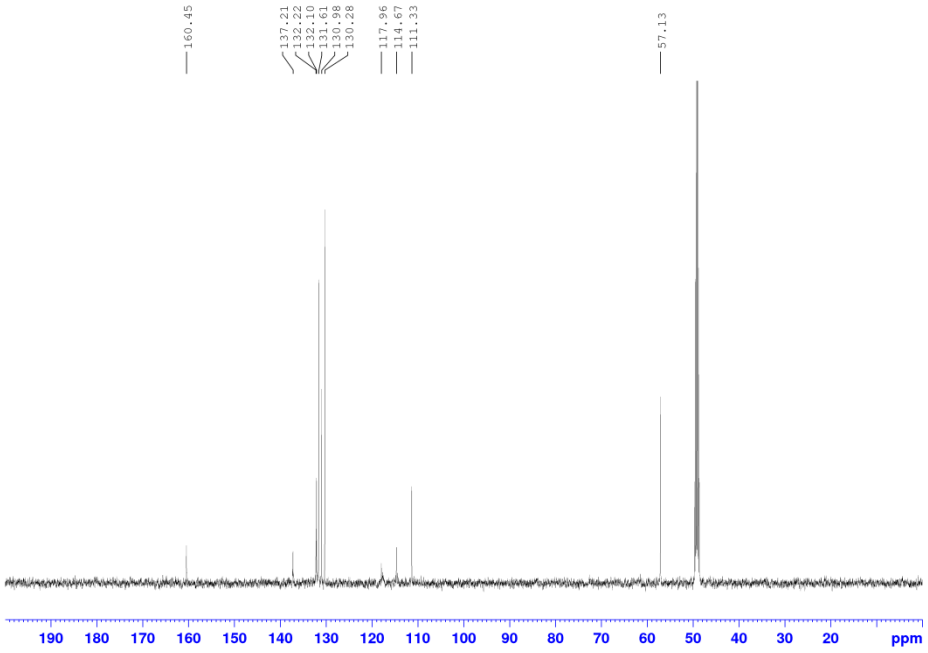

Appendix B: Copyright Permission

Gmail by Google

Gord Simms <gordon.a.simms@gmail.com>

AUTHOR Reuse of Full Text for Thesis/Disertation

2 messages

Gordon Simms <gordon.a.simms@gmail.com> Sun, Mar 8, 2015 at 1:01 PM
To: RightsLink@wiley.com

Hello,

My name is Gordon Simms and I am writing this for permission to reuse full text of my publication

Carter, M. D., Simms, G. a, & Weaver, D. F. (2010). The development of new therapeutics for Alzheimer's disease. *Clinical Pharmacology and Therapeutics*, *88*(4), 475–486. doi:10.1038/clpt.2010.165

for inclusion in my thesis.

Thank you very much.

Gordon

--
Gordon A. Simms
PhD Candidate, Department of Chemistry
Dalhousie University
1459 Oxford Street
Dalhousie University
Halifax, NS B3H 4R2

Wiley Global Permissions <permissions@wiley.com> Mon, Mar 9, 2015 at 3:51 PM
To: Gordon Simms <gordon.a.simms@gmail.com>

Dear Gordon:

Thank you for your request.

Permission is granted for you to use the material requested for your thesis/dissertation subject to the usual acknowledgements and on the understanding that you will reapply for permission if you wish to distribute or publish your thesis/dissertation commercially.

The terms of the journal's copyright transfer agreement (CTA) allow authors to self-archive submitted and accepted versions of articles on their own personal website, in a company/institutional repository or archive, and in approved not-for-profit subject-based repositories. Self-archiving of the accepted version is subject to an embargo.

You can read more about our policies on this here: http://olabout.wiley.com/WileyCDA/Section/id-820227.html

Sincerely,

Paulette Goldweber

Associate Manager, Permissions

Wiley

pgoldweb@wiley.com
T +1 201-748-8765

F +1 201-748-6008

111 River Street, MS 4-02

Hoboken, NJ 07030-5774

U.S.
permissions@wiley.com

WILEY

From: Gordon Simms [mailto:gordon.a.simms@gmail.com]
Sent: Sunday, March 08, 2015 12:01 PM
To: RightsLink
Subject: AUTHOR Reuse of Full Text for Thesis/Disertation

[Quoted text hidden]